The Dissertation Committee for Yu-Jeng Lin Certifies that this is the approved version of the following dissertation:

Modeling Advanced Flash Stripper for Carbon Dioxide Capture Using Aqueous Amines

Committee:

Gary T. Rochelle, Supervisor

Michael Baldea

Eric Chen

Gyeong S. Hwang

David Miller

Modeling Advanced Flash Stripper for Carbon Dioxide Capture Using Aqueous Amines

by

Yu-Jeng Lin, B.S., M.S.

Dissertation

Presented to the Faculty of the Graduate School of

The University of Texas at Austin

in Partial Fulfillment

of the Requirements

for the Degree of

DOCTOR OF PHILOSOPHY

THE UNIVERSITY OF TEXAS AT AUSTIN

August 2016

To my parents

Acknowledgements

Most importantly I would like to thank Mom and Dad. Pursuing Ph.D. abroad could be much tougher without your love and encouragement. You were always there supporting every decision I made. Thank you for giving us everything you have and make our life better. I would not be the person I am today without you.

I would like to thank my advisor, Dr. Gary Rochelle for this incredible journey. This work cannot be done without your consistent advising and encouragement. I am so lucky to have the best mentor who is brilliant, motivating, patient and thoughtful. The patience you have and the tremendous amount of time you spend on your everty student make me want to become a better mentor when it comes to teaching. Your passion and dedication to the work and the people you love while having a well work-life balance become a role model I want to follow. Every weekly meeting with you was always inspiring and motivated me to become a better engineer. I had the best learning experience of my life.

I also appreciate my advisors in National Tsing Hua University, Dr. Shi-Shang Jang and Dr. Shan-Hill Wong who encouraged me to step outside the comfort zone and meet the smartest people in the world. Thank you Maeve for editing all of the progress reports and helping me improve my writing skill. Those feedback is especially valuable for international students.

I have learned so much from all of my current and previous groupmates not just technical knowledge but also the way you approach and solve problems. Joining as the same class year and the same group, Di is a perfect company to discuss qualifying exam, course work and inevitably carbon capture. Tarun Madan was a great mentor who set great examples on modeling work when I came in as a first-year. The previous work by

David Van Wagener and Babatunde Oyenekan is an essential foundation of this work. It was always enjoyable to have discussions with my groupmates, Peter Frailie, Lynn Li, Brent Sherman, Matt Walters, Nathan Fine, Darshan Sachde, Eric Chen, Yang Du, Omkar Namjoshi, Steven Fulk, Matt Beaudry, Yue Zhang, Kent Fischer, Ye Yuan, and Junyuan Ding. Thank you for extending my vision and reminding me what I can do better. I am grateful to have my friends whom I've known since college, Jerry, Island, Helen, Kaif, and Ke-Hsun. Every trip we had always refreshed me and made me able to come back to work with full of energy and memory. It's been a memorable journey with all of your participation.

Modeling Advanced Flash Stripper for Carbon Dioxide Capture Using Aqueous Amines

Yu-Jeng Lin, Ph.D.

The University of Texas at Austin, 2016

Supervisor: Gary T. Rochelle

The intensive energy use is the major obstacle to deployment of CO_2 capture. Alternative stripper configurations is one of the most promising ways to reduce the energy consumption of CO_2 regeneration and compression. The advanced flash stripper (AFS) proposed in this work provides the best energy performance among other alternatives.

A systematic irreversibility analysis was performed instead of examining all the possible alternatives. The overhead condenser and the cross exchanger were identified the major sources of lost work that causes process inefficiencies. The AFS reduces the reboiler duty by 16% and the total equivalent work by 11% compared to the simple stripper using aqueous piperazine. The AFS was demonstrated in a 0.2 MW equivalent pilot plant and showed over 25% of heat duty reduction compared to previous campaigns, achieving 2.1 GJ/tonne CO_2 of heat duty and 32 kJ/mol CO_2 of total equivalent work. The proposed bypass control strategy was successfully demonstrated and minimized the reboiler duty.

Approximate stripper models (ASM) were developed to generalize the effect of solvent properties on energy performance and guide solvent selections. High heat of absorption can increase partial pressure of CO_2 at elevated temperature and has potential to reduce compression work and stripping steam heat. The optimum heat of absorption was quantified as 70–125 kJ/mol CO_2 at various conditions, which is generally higher than

existing amines with 60–80 kJ/mol. The energy performance of AFS is not sensitive to the heat of absorption.

A techno-economic analysis with process optimization that minimizes the annualized regeneration cost was performed to demonstrate the profitability of the AFS. The AFS reduces the annualized regeneration cost by 13% and the major savings come from the reduction of the OPEX, which counts for over 70% of the regeneration cost. The compressor and the cross exchanger are the major components of the CAPEX. The optimum lean loading is around 0.22 mol CO_2/mol alkalinity for PZ but is flat between 0.18 and 0.24 with less than 1% difference.

The AFS was demonstrated as a flexible system that can be applied to a wide range of solvent properties and operating conditions while still maintaining remarkable energy performance. Further improvement of energy efficiency by process modifications is expected to be marginal. Increasing solvent capacity will give the most energy and cost reduction in the future.

Table of Contents

List of Tables

List of Figures

Chapter 1: Introduction

1.1 CO_2 CAPTURE FROM COAL-FIRED POWER PLANTS

The coal-fired power plant is the major source of anthropogenic carbon emissions (Figure 1.1) (EPA, 2015b). Coal-fired plants accounts for 77% of the emissions from electricity generation and 31% of total fossil-fuel combustions in the U.S. in 2013. Regulatory actions have been taken by the Environmental Protection Agency (EPA) to reduce carbon emissions. The Clean Power Plan requires each state to propose a comprehensive plan to reduce overall CO_2 emissions by 10–50% before 2030 (EPA, 2015a). Those states generate more electricity from coal-fired power plants will have higher target to achieve. Emission limits have been set as 1400 and 1000 lb/MWh-gross for new-built coal-fired and natural gas-fired power plants while the average emission rates are around 1800 and 800 lb/MWh, respectively. The regulation will force the power sectors to add carbon capture and sequestration (CCS) technology to the coal-fired power plant or shift to other low-carbon power generation such as natural gas firing and renewable energy.

Coal is still considered the largest share (34%) of total electricity generation in 2040 because of its abundance and low price compared to other alternatives (EIA, 2015). CCS is projected to contribute 14% of carbon reduction through 2050, and coal-fired power plants will be the largest single application with 2/3 of them equipped with CCS (IEA, 2013). The actual scenario will depend on how cost-competitive the CCS can be and the demonstration for commercial plants.

Figure 1.2 shows post-combustion CO_2 capture for coal-fired plants. The CO_2 in the flue gas will be separated by the capture process and compressed up to 150 bar for further storage and enhanced oil recovery (EOR).

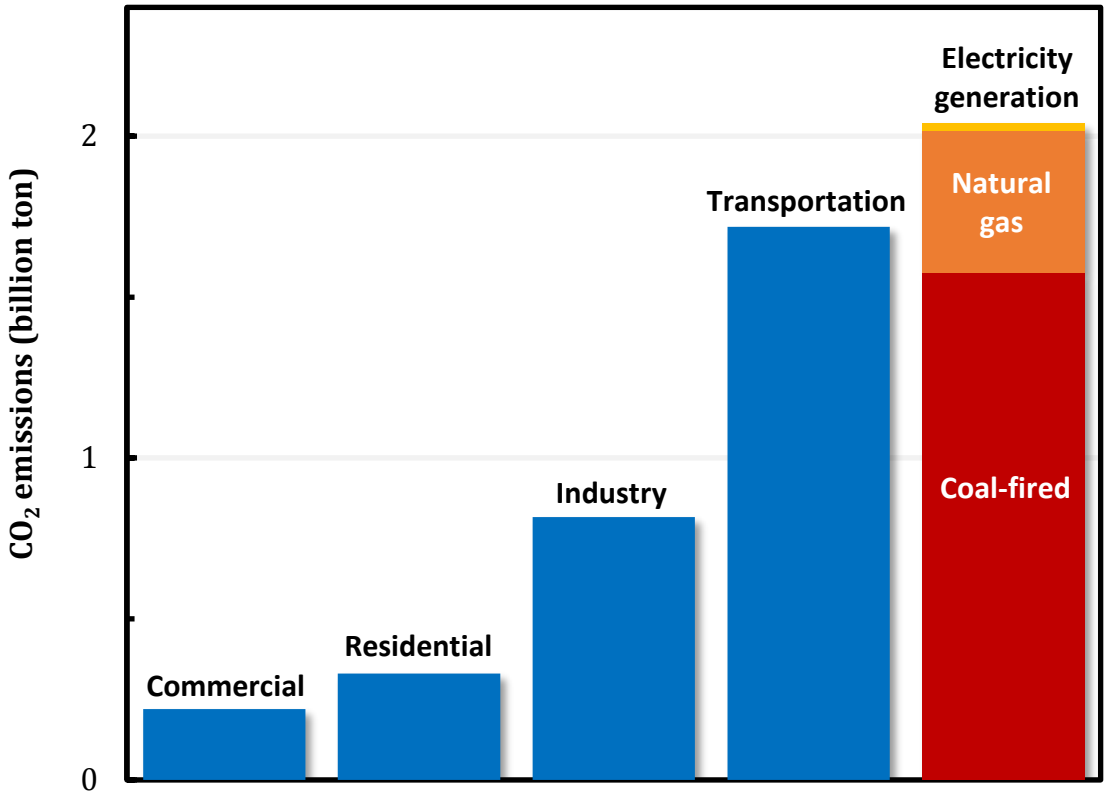

Figure 1.1: 2013 U.S. CO_2 Emissions from fossil fuel combustion by sector (replotted from Figure ES-6 in EPA report, 2015).

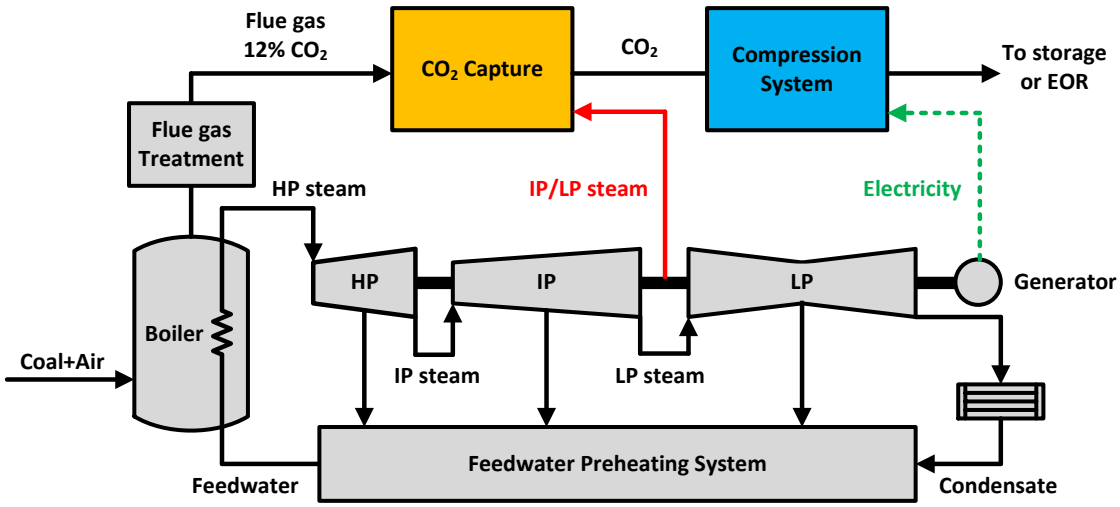

Figure 1.2: Post-combustion CO_2 capture from coal-fired power plant.

1.2 AMINE SCRUBBING PROCESS

Amine scrubbing is considered the most mature technology for CO_2 capture and has been successfully applied to two commercial-scale coal-fired power plants (Hirata et al., 2014; Stéphenne, 2014). A typical amine scrubbing process includes an absorber, a stripper, and a cross exchanger (Figure 1.3). Desulfurized flue gas is contacted with the aqueous amine in the absorber to remove 90% of the CO_2. The rich solvent carrying the CO_2 from the bottom of the absorber is sent to the stripper and heated for CO_2 regeneration. After condensing the water, the purified CO_2 will be sent to the multi-stage compressor.

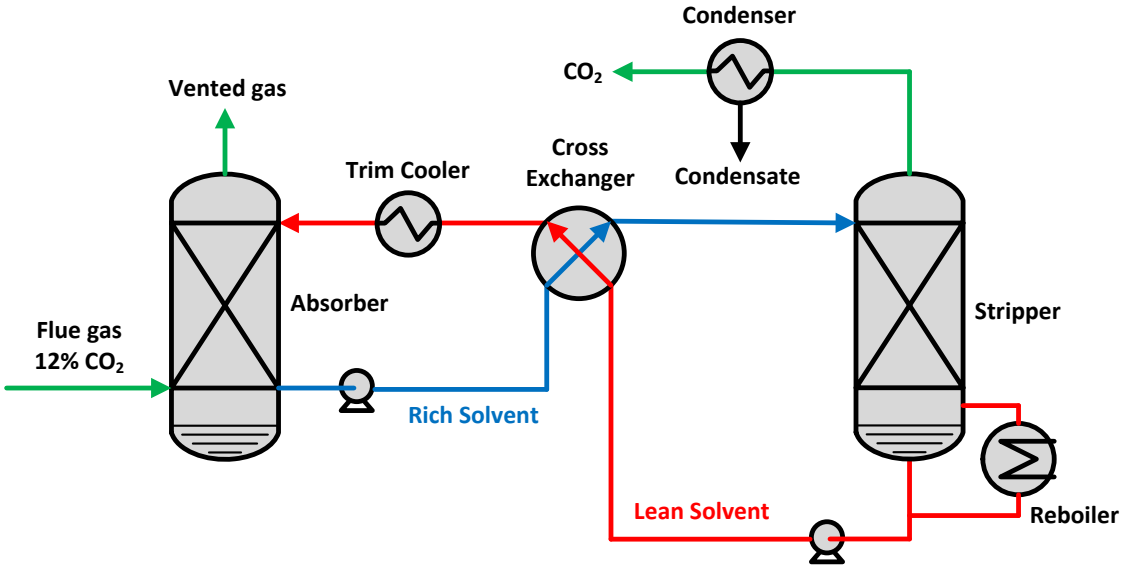

Figure 1.3: Amine scrubbing process.

1.3 Energy use for CO_2 regeneration

The intensive energy consumption is the major obstacle to deployment of CO_2 capture (Rochelle, 2009). CO_2 regeneration requires heat duty, which is usually supplied by extracting the steam from the crossover pipe between the intermediate and low pressure turbines in the power plant. Other major energy requirements include the pump work and CO_2 compression work. Implementing CO_2 capture incurs a 20–30% penalty on electricity output for a typical coal-fired power plant (Aroonwilas et al., 2007; Oexmann, 2011; Romeo et al., 2008). The reboiler duty provides heat of CO_2 desorption, heat of stripping steam, and sensible heat.

- Heat of CO_2 desorption

Absorbing CO_2 by aqueous amines is exothermic. Regenerating CO_2 needs to reverse the reactions by providing heat to the rich solvent, so the heat of absorption (ΔH_{abs}) determines the least amount of heat duty requirement for CO_2 stripping. The heat of absorption is dependent on solvent and which type of reactions dominates. Amine can

react with CO_2 via carbamate and bicarbonate formation reactions. CO_2 absorption dominated by carbamate formation (primary and secondary amines) usually gives a higher heat of absorption than bicarbonate formation (tertiary amines) (I. Kim et al., 2011).

The heat of absorption can be expressed using Equation 1.1 from Lewis and Randall (Equation XVIII.9) (Lewis et al., 1923). Equation 1.2 integrates the partial pressure of CO_2 (P^*_{CO2}) from a reference temperature (T_{ref}) to the operating temperature (T). The P^*_{CO2} at elevated temperature will increase with heat of absorption and results in a high stripper pressure.

$$\Delta H_{abs} = -R\left[\frac{\partial ln f_{CO_2}}{\partial\left(\frac{1}{T}\right)}\right]_{P,x} \approx -R\left[\frac{\partial ln P^*_{CO_2}}{\partial\left(\frac{1}{T}\right)}\right]_{P,x} \quad (1.1)$$

$$\frac{{P_{CO_2}}^*(T)}{{P_{CO_2}}^*(T_{ref})} = exp\left[\frac{\Delta H_{abs}}{R}\left(\frac{1}{T_{ref}} - \frac{1}{T}\right)\right] \quad (1.2)$$

- Heat of stripping steam

When the rich solvent is heated in the reboiler, water is vaporized and generate steam for stripping, which ultimately is condensed in the overhead condenser. Analogous to the heat of absorption, the latent heat of water vaporization determines the partial pressure of water in the stripper as shown in Equation 1.3.

$$\Delta H_{vap} = -R\left[\frac{\partial ln P^*_{H_2O}}{\partial\left(\frac{1}{T}\right)}\right]_{P,x} \quad (1.3)$$

The difference between the heat of absorption and the heat of water vaporization determines the selectivity between CO_2 and the water vapor as shown in Equation 1.4. The heat of absorption is typically greater than the heat of vaporization (around 40 kJ/mol H_2O).

$$\frac{{P_{CO_2}}^*(T)}{{P_{H_2O}}^*(T)} = \frac{{P_{H_2O}}^*(T_{ref})}{{P_{CO_2}}^*(T_{ref})} exp\left[\left(\frac{\Delta H_{abs} - \Delta H_{vap}}{R}\right)\left(\frac{1}{T_{ref}} - \frac{1}{T}\right)\right] \quad (1.4)$$

- Sensible heat

The sensible heat is needed to heat the rich solvent from the absorber to the reboiler temperature. The cross exchanger preheats the rich solvent by recovering enthalpy from the hot lean solvent. The sensible heat requirement will be dependent on the solvent rate and the cross exchanger performance.

1.4 PRIOR WORK OF ALTERNATIVE STRIPPERS

Alternative strippers have been proposed to reduce the energy use for CO_2 capture. Previous work on stripping process evaluation are summarized in Table 1.1. Most work compared the energy performance by modeling alternative processes using conventional solvent monoethanolamine (MEA). Rochelle's research group have extended the evaluation to the advanced solvent piperazine (PZ) and used total equivalent work (W_{eq}) to estimate the overall energy performance. Previous work approached the best configuration by screening various alternatives. This work will apply the irreversibility analysis to understand where the process inefficiencies come from and how much room still left to be improved.

Table 1.1: Prior work on alternative strippers.

Author/year	Solvent	Simulation Tool	Experiment Demonstration	Performance Indicator	Economic Analysis
(Chang et al., 2005)	DGA/MDEA	Aspen Plus®	N/A	Heat duty	No
(Oyenekan et al., 2007)	K^+/PZ MDEA/PZ	Aspen Custom Modeler®	N/A	W_{eq}	No
(Jassim et al., 2006)	MEA	Aspen Plus®	N/A	W_{eq}	No
(Tobiesen et al., 2006)	MEA	In-house code	N/A	Heat duty	No
(Van Wagener, 2011)	PZ	Aspen Plus®	Pilot-scale	W_{eq}	No
(Le Moullec et al., 2011)	MEA	Aspen Plus®	N/A	W_{eq}	No
(Karimi et al., 2011)	MEA	Unisim®	N/A	W_{eq}	Yes
(Knudsen et al., 2011)	MEA	N/A	Pilot-scale	Heat duty	No
(Fernandez et al., 2012)	MEA	Aspen Plus®	N/A	W_{eq}	Yes
(Ahn et al., 2013)	MEA	Unisim®	N/A	W_{eq}	No
(Madan, 2013)	PZ	Aspen Plus®	N/A	W_{eq}	No
(Fang et al., 2014)	MEA	N/A	Lab-scale	Heat duty	No
(Jung et al., 2015)	MEA	Aspen Plus®	N/A	W_{eq}	Yes
(Liang et al., 2015)	MEA	ProMax®	N/A	W_{eq}	No
(Higgins et al., 2015)	MEA	Aspen Plus®	N/A	Heat duty	No
(Stec et al., 2015)	MEA	N/A	Pilot-scale	Heat duty	No
This work	**PZ generic solvent**	**Aspen Plus® Approximate model**	**Pilot-scale**	**Updated W_{eq}**	**Yes**

1.4.1 Solvent selections

The energy improvement by alternative stripper configurations is also dependent on the amine solvents used. There are four important solvent properties that have significance on energy performance.

- Absorption rate

The absorption rate determines the packing requirement in the absorber and the CO_2 rich loading, which affects not only the solvent capacity but also the mass transfer driving force in the stripper. Higher absorption rate is always beneficial.

- Heat of desorption

As discussed in Section 1.3, the heat of desorption must be provided by the reboiler to regenerate CO_2 and it also affects the partial pressure of CO_2 at stripper temperature. Higher partial pressure of CO_2 can reduce compression work and improve the selectivity between CO_2 and water vapor.

- CO_2 capacity

The CO_2 capacity is defined as the amount of CO_2 can be carried per unit weight of solvent (mol CO_2/ kg solvent). It is solvent-specific and dependent on the difference of the operating lean and rich loadings. A solvent with greater CO_2 capacity needs less solvent circulated to reach a certain removal rate and can reduce sensible heat requirement.

- Thermal stability

A thermally stable solvent can be operated at a relatively higher temperature, which contributes to a higher CO_2 partial pressure while avoiding significant degradation.

Concentrated PZ has been characterized and regarded as a new standard solvent for CO_2 capture (Rochelle et al., 2011). Table 1.2 compares the solvent properties with MEA. PZ has almost twice absorption rate and capacity and is more thermally stable than

MEA. The downsides of PZ are the higher viscosity and the precipitation limits at lean loading and low temperature.

Most of this work will use PZ as solvent to demonstrate the stripper performance. The viscosity and precipitation issues will be considered by using a lower concentration of PZ. To generalize the effect of solvent properties on the stripper configurations, approximate stripper models using generic solvent will be developed.

Table 1.2: Comparisons of solvent properties of MEA and PZ.

Property	**7 m MEA**	**8 m PZ**
Absorption rate[a] (10^{-7}mol/s-Pa-m^2)	4.3	18.5
Capacity[b] (mol CO_2/mol alkalinity)	0.5	0.86
T_{max}[c] (°C)	122	163
Heat of absorption[d] (kJ/mol)	72	67
Viscosity[e] (cP)	3	10.8
Solid precipitation[f]	No	Yes

[a] Average liquid side mass transfer rate between 0.5 and 5 kPa of P^*_{CO2} at 40 °C (Dugas, 2009)
[b] Difference of lean and rich loading between 0.5 and 5 kPa of P^*_{CO2} at 40 °C (Dugas, 2009)
[c] Corresponds to 2% amine loss per week (Davis, 2009; Freeman, 2011)
[d] Differential heat of absorption at 1.5 kPa of P^*_{CO2} (Li, Voice, et al., 2013)
[e] Average between 0.5 and 5 kPa of P^*_{CO2} at 40 °C (Amundsen et al., 2009; Freeman et al., 2011)

1.4.2 Quantifying energy performance

Some of the previous work used heat duty to indicate the energy performance without considering the electricity loss is dependent on the steam temperature and other energy contributors. Also, the reported energy reduction was compared at arbitrary operating conditions and design specifications. In this work, total equivalent work will be used to evaluate the overall energy performance with updated heat-to-work conversion efficiency and compressor configuration that reflect current state-of-art. A thorough

analysis at a wide range of operating conditions and design specifications will be conducted.

1.4.3 Demonstration of operability and profitability

Previous work were limited in process simulation without considering potential increase in process complexities and capital cost for the alternative strippers. Demonstrating the operability and profitability is essential to scaling up to commercial plants in the future. This work will test the proposed configuration in a pilot-scale experiment in order to demonstrate the energy performance and operability. A rigorous techno-economic analysis will be performed for a commercial-scale plant in order to justify potential cost benefit. An optimum design that minimizes the overall regeneration cost will be provided.

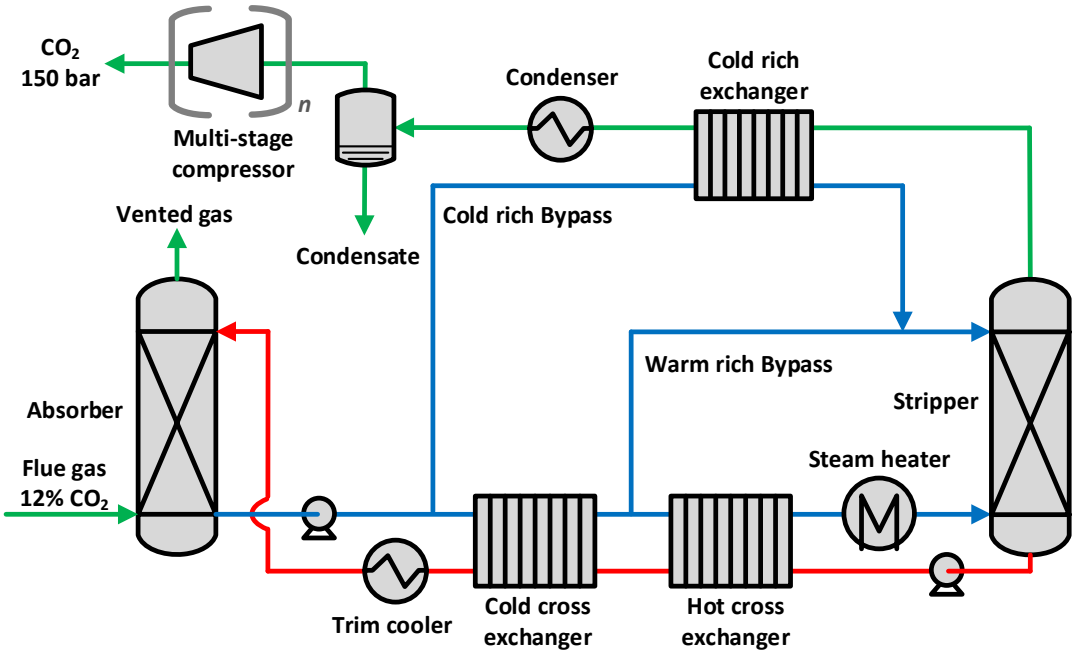

Figure 1.4: Advanced flash stripper.

1.5 RESEARCH SCOPE

This work will simulate the stripping and compression process in Aspen Plus® using an in-house built model "Independence" for PZ (Frailie, 2014). The absorber is out of the scope. The best stripper configuration, the advanced flash stripper proposed in this work is shown in Figure 1.4. The research scope will include:

- Quantify minimum work and lost work using exergy analysis.
- Propose new stripper configurations based on the irreversibility analysis.
- Evaluate energy performance of alternative strippers with updated equivalent work and compression work calculations.
- Identify important operating parameters and design specifications by sensitivity analyses.
- Demonstrate the operability and performance of the advanced flash stripper in the pilot plant at the UT Austin.
- Validate the Independence model using the pilot plant data and further explore optimum design using the validated model.
- Develop approximate stripper models that can predict the energy performance for amine screening and generic solvent study.
- Quantify the effect solvent properties and investigate the interactions with alternative stripper configurations.
- Reduce the cost of the lean/rich solvent cross exchanger by designing at optimum temperature approach and pressure drop.
- Perform techno-economic analysis including capital and energy cost for the advanced flash stripper.
- Explore the optimum operating lean loading and process specifications that minimizes the regeneration cost.

Chapter 2: Modeling Methods

2.1 STRIPPER MODELING IN ASPEN PLUS®

Simulation results were obtained from Aspen Plus® version 7.3. The Electrolyte Non-Random Two-Liquid (e-NRTL) property method is used to describe the CO_2-amine-H_2O chemistry accounting for the non-ideality in the aqueous electrolyte system (C. C. Chen et al., 1982, 2004). For the gas-liquid contactor, Aspen Plus® RateSep™ provides a rigorous rate-based model for heat and mass transfer using a non-equilibrium approach, applying two-film theory. The application of the rate-based model to the amine scrubbing process has offered accurate prediction against pilot plant data (Zhang et al., 2009).

Piperazine (PZ) will be primarily used as solvent in this work. Concentrated PZ has been demonstrated as an advanced solvent that has higher reaction rate and CO_2 capacity and is more thermally stable than MEA (Dugas, 2009). It can be used up to 150 ºC without significant thermal degradation (Freeman, 2011). The thermodynamic model used in this work is "Independence", which was built in-house and rigorously regressed in Aspen Plus® with experimental data including amine volatility, heat capacity, CO_2 solubility, and amine pK_a over a range of amine concentration and CO_2 loading. Details of model development can be found in previous work (Frailie, 2014). Equilibrium reactions are used in the stripper due to the relatively higher operating temperature. The reaction set is shown in Equation 2.1.

$$PZ + CO_2 + PZ \rightleftharpoons PZH^+ + PZCOO^- \quad (2.1a)$$

$$PZCOO^- + CO_2 + PZCOO^- \rightleftharpoons PZH^+ + PZ(COO)_2{}^{2-} \quad (2.1b)$$

$$PZCOO^- + CO_2 + H_2O \rightleftharpoons H^+PZCOO^- + HCO_3^- \quad (2.1c)$$

$$PZ + H^+PZCOO^- \rightleftharpoons PZH^+ + PZCOO^- \quad (2.1d)$$

CO_2 loading is defined as mole of total CO_2 per mole of alkalinity. Equation 2.2 is a calculation example for PZ, which has two moles equivalent alkalinity for every mole of amine.

$$CO_2\ loading\left(\frac{mol}{mol}\right) = \frac{[CO_2]+[HCO_3^-]+[PZCOO^-]+[H^+PZCOO^-]+2\times[PZ(COO)_2{}^{2-}]}{2\times([PZ]+[PZCOO^-]+[PZ(COO)_2{}^{2-}]+[PZH^+]+[H^+PZCOO^-])} \quad (2.2)$$

For the stripper modeling, CO_2 solubility data is the most important data input, which will be used to predict the equilibrium partial pressure of CO_2 (P^*_{CO2}) at high temperature 120–150 °C and lean loading conditions. The predicted P^*_{CO2} will affect the stripper pressure and the amount of stripping steam produced.

Figure 2.1 shows the partial pressure of CO_2 with predicted by Independence with varied CO_2 loading and compares with experimental data (Xu, 2011). The predicted P^*_{CO2} tends to underestimate at temperature above 150 °C. However, the measured P^*_{CO2} data at high temperature can be scatter even at the same CO_2 loading. The model will be extrapolated when the CO_2 loading is below 0.25 (mol CO_2/mol alkalinity) because of lacking of data.

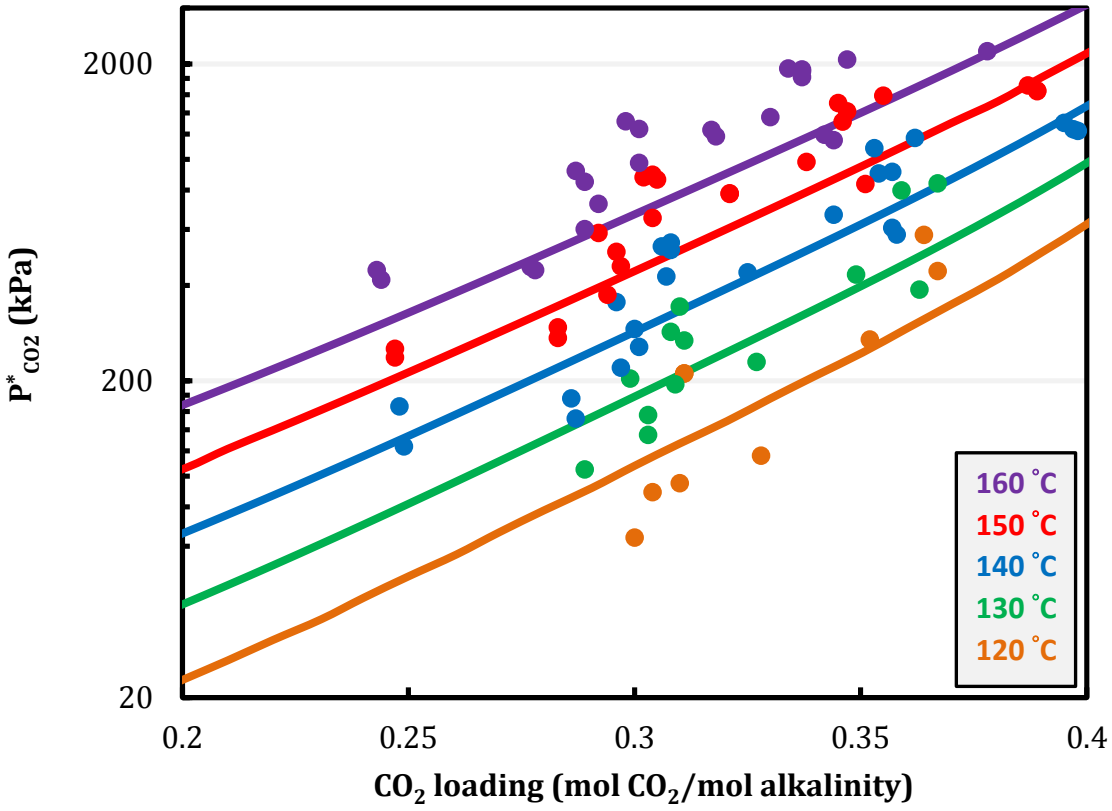

Figure 2.1: CO_2 solubility at high temperature for 8 m PZ; lines: predicted by Independence; points: experiment data (Xu, 2011).

2.2 CALCULATING HEAT EXCHANGER LMTD

This work uses a rigorous way to calculate the log mean temperature difference (LMTD, ΔT_{LM}) for heat exchangers that have two-phase flows. Previous work forced the rich solvent stream to stay in liquid phase and calculated the LMTD by inlet and outlet temperatures when heater blocks were used to simulate the cross exchanger (Van Wagener, 2011). The calculated LMTD could be under-predicted. In this work, the LMTD is obtained by integrating the temperature profile using the HeatX block instead of relying solely on inlet/outlet temperatures using Equation 2.3. The temperature profile is split into 100 segments with equal exchanger duty. The Q_i and $\Delta T_{LM,i}$ are exchanger duty and

LMTD of each segment, respectively. When the segment is small enough the $\Delta T_{LM,i}$ can be calculated by inlet/outlet temperature assuming the temperature profile is linear.

$$\Delta T_{LM} = \frac{\sum_{i=1}^{n} Q_i}{\sum_{i=1}^{n} \frac{Q_i}{\Delta T_{LM,i}}} \tag{2.3}$$

When the configuration has two cross exchangers in order to extract warm rich solvent from between, the average LMTD ($\Delta T_{LM,avg}$) will be calculated by Equation 2.4, which weights the LMTD of each exchanger ($\Delta T_{LM,1}$ and $\Delta T_{LM,2}$) by their exchanger duties (Q_1 and Q_2). The average LMTD will be specified.

$$\Delta T_{LM,avg} = \frac{Q_1 + Q_2}{\frac{Q_1}{\Delta T_{LM,1}} + \frac{Q_2}{\Delta T_{LM,2}}} \tag{2.4}$$

2.3 TOTAL EQUIVALENT WORK

The total equivalent work is a more useful metric of overall energy use than reboiler duty alone. As Equation 2.5 shows, the total equivalent work consists of pump work (W_{pump}), compression work (W_{comp}), and heat duty work (W_{heat}). Heat duty work is obtained by converting the reboiler duty to electricity using Equation 2.6 by multiplying the Carnot cycle efficiency and the steam turbine efficiency ($\eta_{stm\text{-}tb}$). The $T_{stm,sat}$ is the saturation temperature of heating steam extracted from the power plant and the sink temperature (T_{sink}) is assumed as 313.15 K (40 °C). The isentropic efficiency of the steam turbine system is set to a typical value of 90% (Bhatt, 2011; Bhatt et al., 1999). The pump work is required to pressurize the rich solvent from atmospheric pressure to the stripper pressure (P_{strp}) as calculated using Equation 2.7. It assumes that the pump efficiency (η_p) is 65%. The calculation of compression work will be discussed in Section 2.5.

$$W_{eq} = W_{heat} + W_{pump} + W_{comp} \tag{2.5}$$

$$W_{heat} = \eta_{stm-tb} \left(\frac{T_{stm,sat} - T_{sink}}{T_{stm,sat}} \right) Q_{reb} \tag{2.6}$$

$$W_{pump} = \frac{\dot{V}_{rich}(P_{strp} - 1\ bar)}{\eta_p} \quad (2.7)$$

2.4 HEAT-TO-ELECTRICITY EFFICIENCY

The Carnot cycle efficiency used in Equation 2.6 simplifies the conversion of heat duty to electricity without integrating the CO_2 capture process with the entire power plant. The accuracy will be examined by comparing the heat-to-electricity efficiency (W_{heat}/Q_{reb}) with a steam cycle simulated in Aspen Plus®. Steam power plants are operated via Rankine cycle to avoid compression and expansion of two-phase flow. Figure 2.2 shows the steam cycle of a typical coal-fired power plant. The steam from the last stage of low pressure turbine is totally condensed to water, pumped to high pressure, and then heated up to above saturation temperature by the preheating system and the boiler.

A supercritical power plant integrated with CO_2 capture described in DOE Case 10 (2010) is selected as the reference steam cycle. The steam flow rates, outlet pressure of each steam turbine, and the preheating system are reproduced in the simulations. All the steam turbines are assumed as 90% isentropic efficiency to be consistent with Equation 2.6. The steam after the last LP turbine will be condensed at 40 °C. The outlet temperature of each heat exchanger in the feedwater preheating system will be maintained by manipulating the preheating steam flow rate at each temperature level.

The steam extracted between the IP and LP turbines is superheated and will be de-superheated by recycling a portion of the reboiler condensate so the sensible heat of the steam vapor will not be wasted. The reboiler condensate can either go to the condenser or the deaerator to return back to the steam cycle.

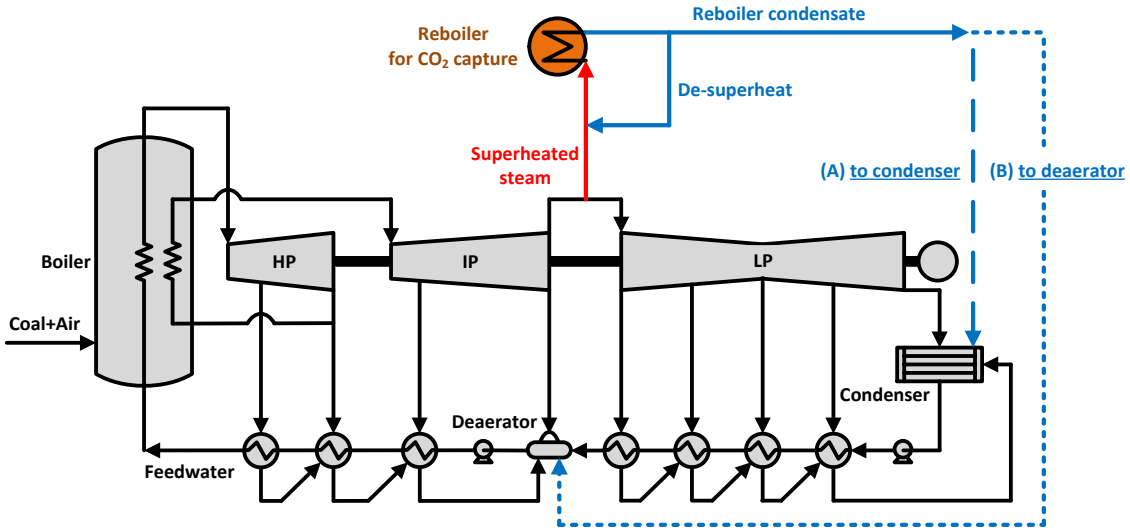

Figure 2.2: Steam cycle integrated with CO_2 regeneration.

Figure 2.3 compares the heat-to-electricity efficiency obtained from the steam cycle simulations and Equation 2.6 at various steam saturation temperature. The outlet pressure of the IP turbine was adjusted to satisfy each specified saturation temperature. The effect of condensate return locations are compared. If the condensate is returned to the condenser rather than the deaerator, the heat-to-electricity efficiency will increase 0.03–0.05, which is equivalent to 11–16% increase of electricity loss because of rejecting the sensible heat into the condenser.

The heat-to-electricity efficiency using Equation 2.6 is 0.01 lower than the actual steam cycle at 155 °C, which implies the electricity loss is underestimated by 3%. The difference becomes more significant with increasing steam temperature. The discrepancy comes from the use of the saturation temperature to represent the steam temperature. The extracted steam is superheated and is potentially more valuable. An average temperature that weights steam temperatures by their enthalpies should be more indicative. The amount of latent heat of saturated steam decreases with increasing saturation temperature.

Less contribution of enthalpy at saturation temperature makes the average steam temperature shift away from the saturation temperature.

Generally Equation 2.6 can reasonably predict the equivalent electricity loss and the trend with varied steam temperature.

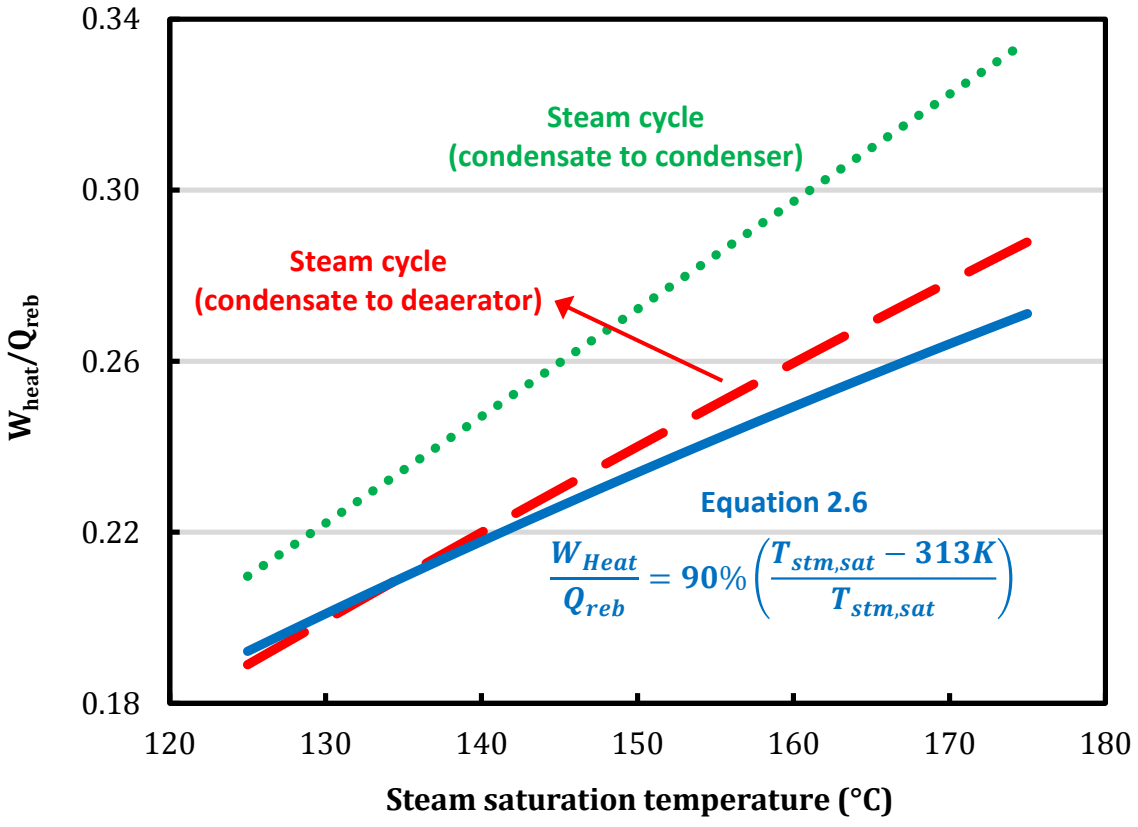

Figure 2.3: Heat-to-electricity efficiency at various steam saturation temperature.

2.5 MULTI-STAGE COMPRESSOR

In this work, the configuration and efficiency of the multi-stage compressor will be updated from previous work to reflect current state-of-art. Van Wagener (2011) proposed a correlation of compression work for CO_2 capture by regressing data from Aspen Plus®. The multi-stage compressor train employed the compressors with 72% polytropic efficiency, the intercoolers at 40 °C and water knock-out drums between stages.

2.5.1 Characteristics of CO_2 compression

The inlet pressure of the compressor train is determined by the stripper pressure, which is dependent on the operating lean loading and reboiler temperature. To sequester the CO_2 underground, the target pressure of the compressor has to be at least above its supercritical pressure, 74 bar, to avoid two-phase flow. To replace the pressure loss during transportation, 0.4–0.5 bar/km is required. In this work, the target pressure is set at 150 bar, which has been used as a standard. (NETL, 2010). When the CO_2 is in the supercritical phase such that its density is similar to liquid, the difference between a pump and a compressor for the compression task disappears and becomes a question of density rather than phase. The supercritical pump is suggested for the last stage when the density is above 500 kg/m^3 (Bergamini et al., 2011).

To decrease the pipeline diameter, aftercooling can be applied to increase CO_2 density and reduce volumetric flow rate (Moore et al., 2008). The aftercooler that cools CO_2 is employed before the supercritical pump to attain a density suitable for pumping and to reduce the pump work from reduced volumetric flow rate. As shown in Figure 2.4, the density increases dramatically around the critical region. The aftercooling temperature is specified as 30 °C to obtain the major density increase.

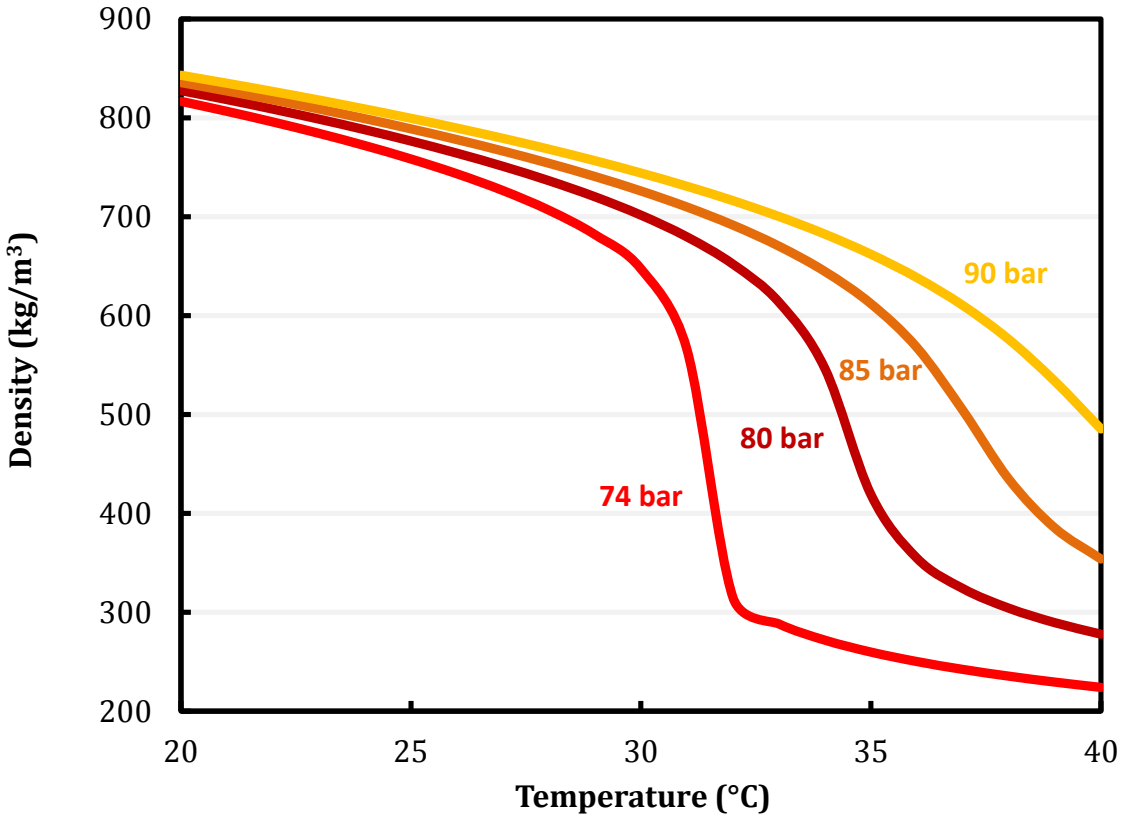

Figure 2.4: Density of supercritical CO_2 with varied temperature.

2.5.2 Updated multi-stage compressor configuration

Three types of compressor are typically used in industry: reciprocating, axial, and centrifugal. The reciprocating compressor provides a wide range of pressure ratio but can only accommodate inlet volume flow rate up to 7000 ft^3/min. The axial compressor has high capacity but lower pressure ratio (1.05–1.2). The pressure ratio and capacity of a centrifugal compressor is between that of a reciprocating and axial compressor. For a coal-fired power plant with 593 MW gross output, the CO_2 volume flow rate is around 140,000 ft^3/min at 1 bar inlet pressure. A centrifugal compressor with intermediate pressure ratio and large capacity has been suggested for CO_2 capture (Suri, 2007). The maximum pressure ratio is specified as 2 due to the relatively higher molecular weight.

The configuration shown in Figure 2.5 will be simulated in Aspen Plus®. The multi-stage compressor will compress the CO_2 from the stripper pressure to 76 bar that includes 2 bar of net positive suction head (NPSH), and the supercritical pump will pressurize the supercritical CO_2 to 150 bar. It assumes no pressure drop in the intercoolers. The polytropic efficiency of compressors is also updated to 86% (NETL, 2010). The supercritical pump efficiency is assumed as 65%. The specifications are shown in Table 2.1.

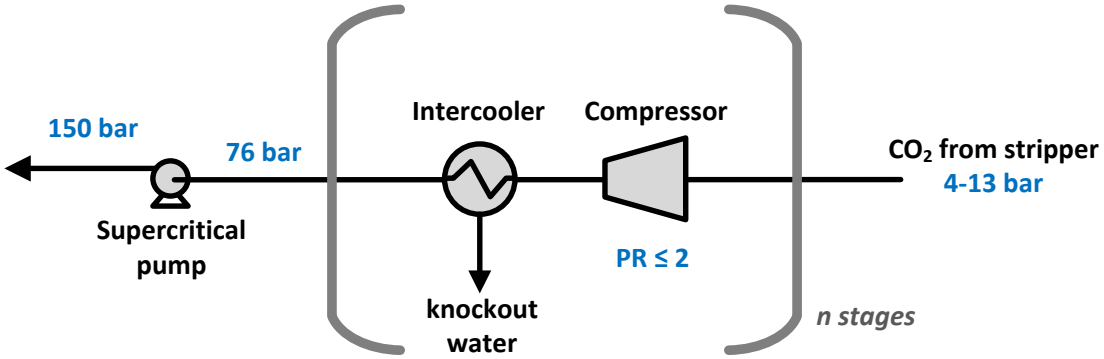

Figure 2.5: Multi-stage compressor with supercritical pump

Table 2.1: Multi-stage compressor specifications

Maximum pressure ratio/stage	2
Compressor polytropic efficiency (%)	86
Intercooling temperature (°C)	40
Intercoolers pressure drop (bar)	0
Aftercooling temperature (°C)	30
Supercritical pump efficiency (%)	65
Multi-stage compressor outlet P (bar)	76
Final target P (bar)	150

Figure 2.6 compares the estimated compression work from the correlation developed by Van Wagener (2011) and the updated compressor configuration with inlet

pressure 1–20 bar. The minimum compression work is calculated from the difference of Gibbs free energy between inlet pressure and 150 bar at 40 °C. The updated compression work is about 1 kJ/mol CO_2 lower, mostly due to the higher compressor efficiency, 86% rather than 72%. This demonstrates the potential energy savings from operating at high stripper pressure. The stripper pressure using PZ at 150 °C can be up to 10 bar, which reduces the compression work by almost 50% compared to conventional stripper less than 2 bar.

Figure 2.7 shows the thermodynamic efficiency of CO_2 compression ($\eta_{th,comp}$), which is defined as the ratio of the minimum work to the actual work. The thermodynamic efficiency for the updated compressor is around 72–74% while it was less than 60% in previous work.

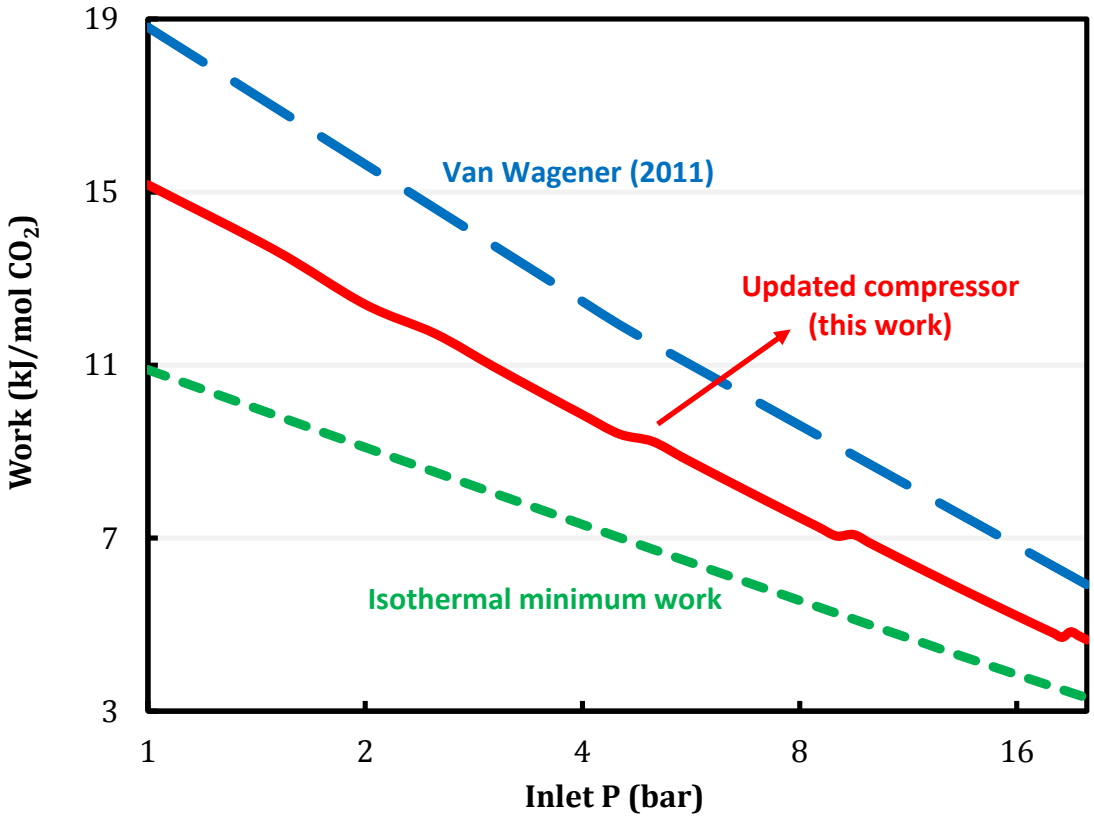

Figure 2.6: Compression work with updated configuration and efficiency.

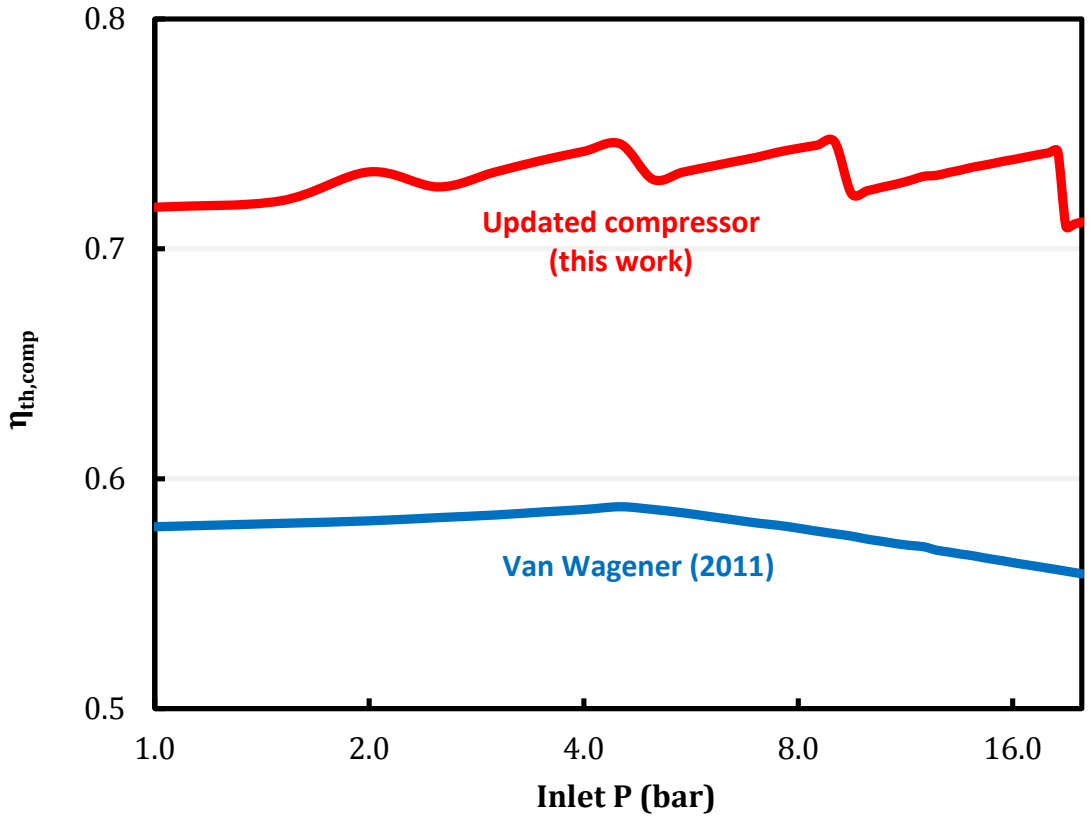

Figure 2.7: Thermodynamic efficiency of CO_2 compression.

2.5.3 Compression work correlation

A correlation (Equation 2.8) that can be used to estimate the compression work from 1 to 149 bar of inlet pressure is developed by regressing the simulation results shown in Figure 2.8. The same compressor configuration and specifications described above were used. The R-squared of regression is 99.9%.

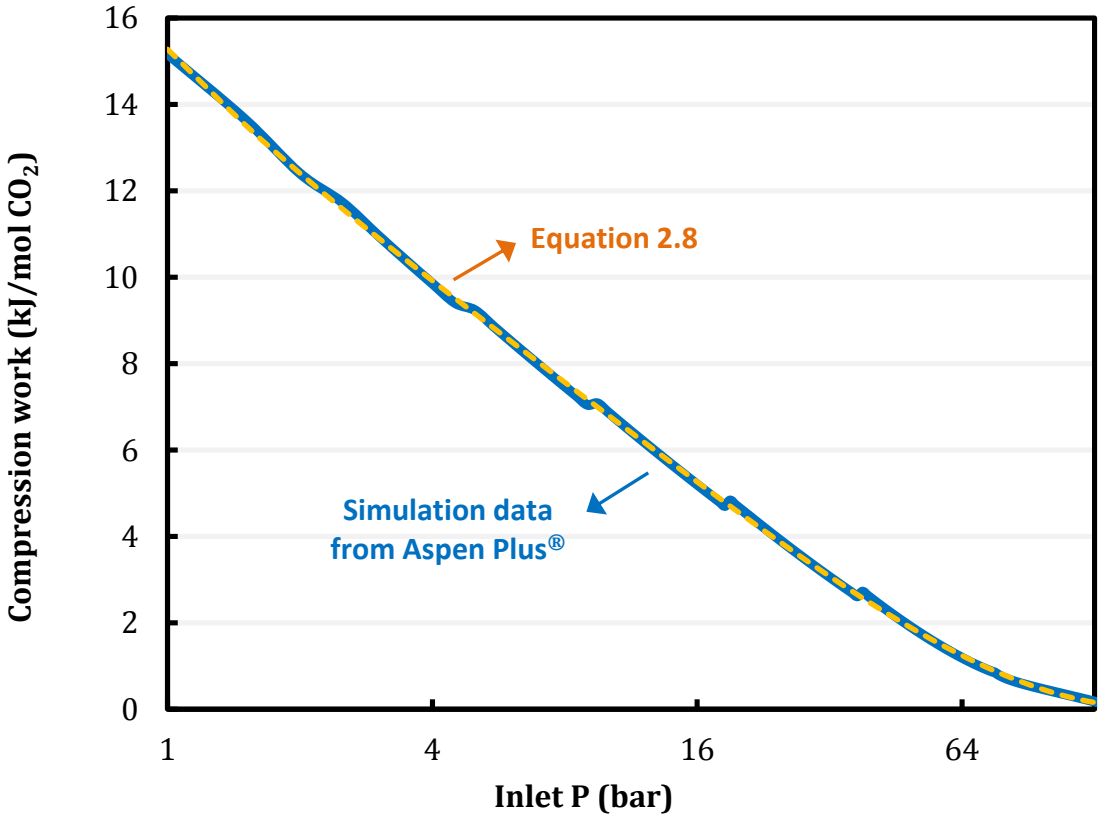

Figure 2.8: CO_2 compression work with inlet pressure from 1–149 bar; final pressure 150 bar.

$$W_{comp}\left(\frac{kJ}{mol\ CO_2}\right) = 15.3 - 4.6lnP_{in} + 0.81(lnP_{in})^2 - 0.24(lnP_{in})^3 + 0.03(lnP_{in})^4$$

$$1\ bar \leq P_{in} \leq 149\ bar \qquad (2.8)$$

Chapter 3: Process Irreversibility Analysis

3.1 INTRODUCTION

Alternative stripper design is a promising means of reducing energy use. In a conventional distillation column, alternative heat integration such as vapor recompression and the heat-integrated distillation column have been widely investigated (Luyben, 1983; Nakaiwa et al., 2003; Shenvi et al., 2011). The heat of condensation in the rectifying section can be used to vaporize the liquid in the stripping section after the vapor is compressed to high pressure. The internal heat integration strategies can significantly reduce the reboiler duty by 20–50% (Iwakabe et al., 2006; Y. H. Kim, 2012; Luyben, 1983).

This design concept has been applied to alternative stripper design for CO_2 capture. Rochelle et al. proposed the multi-pressure stripper to recover the condensation heat of water vapor (Jassim et al., 2006; Oyenekan et al., 2007; Van Wagener et al., 2011). The lean vapor compression stripper recovers the waste heat after recompressing a portion of CO_2 and steam that is produced from a low pressure flashing tank (Benson et al., 1979; Cousins et al., 2011; Fernandez et al., 2012). It has been studied and widely applied in pilot-scale CO_2 capture (Singh et al., 2014; Thimsen et al., 2014). Other stripper design strategies such as interheated stripper, double matrix, and cold rich bypass have also been investigated (Madan, 2013; Van Wagener et al., 2014).

Most previous work addressed the problem by comparing the energy performance of each configuration that has been proposed. The approach does not indicate if the best performance has been achieved and is not time-efficient since in theory infinite alternatives could be applied. If the system is already approaching maximum thermodynamic efficiency further process modifications will not be necessary. A systematic examination that diagnoses the inefficiencies of the process is necessary to provide a better design that

maximizes energy efficiency and give the insights of maximum attainable energy efficiency.

Instead of examining each possible configuration, exergy analysis will be used as a tool to identify the inefficiency of the stripping process. Exergy analysis has been used to quantify the irreversibility of the amine scrubbing process (Amrollahi et al., 2011; Geuzebroek et al., 2004; Hanak et al., 2014; McGlashan et al., 2007; Rochedo et al., 2013). However, these analyses did not indicate how to reduce process irreversibility and improve energy efficiency. Also, previous work only studied a single nominal case. The irreversibility can vary significantly with process design and operating parameters. Exergy analysis with various process parameters is necessary to explore optimum design.

Design strategies and a new stripper configuration will be proposed to reduce the inefficiencies based on the analysis. The conventional simple stripper will be the base case. Lean vapor compression will be used to demonstrate why the energy improvement using conventional approaches is limited. Important process parameters such as CO_2 lean loading, temperature approach of exchangers, and packing height will be varied to show how they affect energy efficiency. To minimize the overall cost, economic analysis is required but is not in the scope of this chapter. 8 m PZ will be used as solvent.

Another objective is to investigate the thermodynamic efficiency of the regeneration process. The thermodynamic efficiency (η_{th}) of the separation process is defined as the ratio of minimum work to actual work as shown in Equation 3.1. The actual work is the sum of the minimum work and the lost work (exergy loss, irreversibility). If a process removes all the lost work, the thermodynamic efficiency will approach 100%. The thermodynamic efficiency of typical distillation is about 20% (Fitzmorris et al., 1980; Y. H. Kim, 2012; Yoo et al., 1988). The thermodynamic efficiency of the stripping

process will be estimated to determine the efficiency of the advanced flash stripper and show how much room is still left for improvement.

$$\eta_{th} = \frac{W_{min}}{W_{act}} = \frac{W_{min}}{W_{act}+W_{lost}} \quad (3.1)$$

3.2 METHODS

Simulation results were obtained from Aspen Plus® version 7.3 using "Independence" for PZ with e-NRTL property method to describe the CO_2-amine-H_2O chemistry (Frailie, 2014). The Rigorous rate-based model is used to model heat and mass transfer with equilibrium reactions in the boundary layer. The stripper used 5 meter of the structured packing Mellapak 250X. The Bravo Correlation was used to calculate the mass transfer coefficient and interfacial area of the packing in the stripper (Bravo et al., 1985). No correction of interfacial area will be applied in this chapter. Table 3.1 shows the summary of modeling methods.

Table 3.1: Summary of modeling methods.

Solvent	8 m PZ
Process modeling tool	Aspen Plus® v7.3
Thermodynamic model	Independence
Stripper packing	5 m Mellapak 250X
Correction factor for packing interfacial area	1

3.2.1 Process specifications

Process specifications used in the simulations are summarized in Table 3.2. This work simulates the whole amine scrubbing process except the absorber. Plaza has shown that with an intercooled absorber using 8 m PZ over the range of lean loading from 0.2 to 0.34 mol CO_2/alkalinity, 90% CO_2 removal can be always be attained with a finite packing

area (Plaza, 2011). The rich solvent is typically at 46 ºC with 0.4 CO_2 rich loading over the CO_2 lean loading range. The temperature and the CO_2 loading of the rich solvent were constants.

Operating the stripper at higher temperature is usually more energy efficient. However, the elevated temperature can result in significant thermal degradation of the amine in the reboiler. A reasonable compromise of 150 ºC for PZ was used (Freeman, 2011). The condensing temperature of the heating steam is assumed 155 ºC, 5 K higher than the reboiler temperature. The LMTD of the cross exchanger was specified as 5 K.

Table 3.2: Summary of process specifications.

Reboiler T (ºC)	150
Steam condensing T (ºC)	155
CO_2 rich loading (mol CO_2/mol alkalinity)	0.40
Rich solvent T (ºC)	46
Cross exchanger ΔT_{LM} (K)	5
Cold rich exchanger ΔT_{LM} (K)	20

3.2.2 Theoretical minimum work and lost work

The minimum work (theoretical work, reversible work) of the whole process can be calculated by the difference of Gibbs free energy between inlet and outlet streams (Equation 3.2). The enthalpy (H) and entropy (S) of CO_2 were obtained from the NIST Web Book. CO_2 concentration in the flue gas is assumed to be 12 mol %. Minimum work is defined for this work, separation ($W_{min,sep}$), compression ($W_{min,comp}$), and regeneration ($W_{min,rgn}$).

$$W_{min} = \Delta G = \sum_{out}(H - T_o S) - \sum_{in}(H - T_o S) \quad (3.2)$$

The boundary conditions that define each minimum work are shown in Table 3.3. The minimum work of separation accounts for the amine scrubbing process. The minimum work of compression represents the multi-stage compressors. For example, the isothermal minimum work at 40 ºC for separating 12% CO_2 at 1 bar to pure CO_2 at 150 bar is 18.2 kJ/mol CO_2. This includes 7.3 kJ/mol CO_2 separation work (12% CO_2 to pure CO_2 at 1 bar) and 10.9 kJ/mol compression work (pure CO_2 from 1 bar to 150 bar). Since the reboiler temperature is fixed, the stripper pressure will vary with lean loading.

The minimum work of regeneration ($W_{min,rgn}$) accounts for the stripping process only. It is used to separate CO_2 from the CO_2 rich solvent to pure CO_2 at given stripper pressure. As Equation 3.3 shows, the minimum work of regeneration will be the minimum work of separation ($W_{min,sep}$) plus the lost work of the absorber ($W_{lost,abs}$).

$$W_{min,rgn} = W_{min,sep} + W_{lost,abs} \tag{3.3}$$

Table 3.3: Boundary conditions of minimum work calculations.

Minimum work	**Inlet**	**Outlet**
Separation ($W_{min,sep}$)	12% CO_2 (40 ºC, 1 bar)	Pure CO_2 (40 ºC, stripper P)
Compression ($W_{min,comp}$)	Pure CO_2 (40 ºC, stripper P)	Pure CO_2 (40 ºC, 150 bar)
Regeneration ($W_{min,rgn}$)	CO_2 rich solvent (46 ºC, 1 bar, 0.40 Ldg)	CO_2 lean solvent (40 ºC, 1 bar, varied Ldg) Pure CO_2 (40 ºC, 150 bar)

The lost work is defined as the maximum useful work that would be obtained during the process if the system were brought into equilibrium with the heat sink. The lost work is a result of irreversible operations. The sources can be heat and mass transfer driving forces, mixing, flashing, and mechanical inefficiency. By exergy balance using Equation

3.4, the lost work of the whole process or each unit operation can be calculated. The sink temperature, T_o is set at 313.15 K (40 ºC). T_k is the temperature of the heat source or sink. In this work, the heat source temperature is 155 ºC, 5 K higher than the reboiler temperature. Q and W are the heat duty and work input/output. The enthalpy and the entropy will be obtained from simulations in Aspen Plus®. The minimum work is the thermodynamic limit, which is determined only by inlet and outlet conditions, but the amount of lost work (W_{lost}) depends on how the process is operated. The lost work can be reduced by a better process design that makes the operation more reversible, and leads to less actual work requirement.

$$W_{lost} = \sum \left(1 - \frac{T_o}{T_k}\right) Q + \sum W + \sum_{in}(H - T_o S) - \sum_{out}(H - T_o S) \qquad (3.4)$$

3.3 PROCESS DESCRIPTIONS

3.3.1 Simple stripper

The simple stripper is shown in Figure 3.1. The cold rich solvent is heated by the hot lean solvent in the cross exchanger and then sent to the top of the stripper. The reboiler provides the sensible heat, the heat of CO_2 desorption, and the heat of water vaporization. The hot lean solvent from the reboiler is returned to the absorber after being cooled to 40 ºC by the trim cooler. The hot CO_2 vapor from the top of stripper is cooled to 40 ºC in the overhead condenser with loss of the latent heat of the excess water vapor.

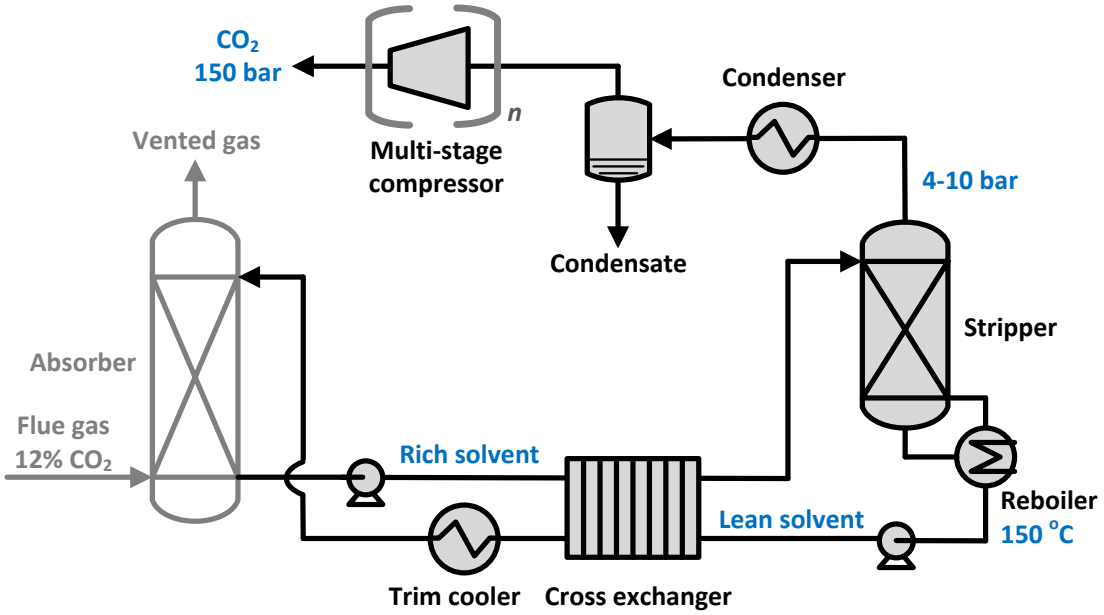

Figure 3.1: Simple stripper.

3.3.2 Lean vapor compression

The lean vapor compression stripper (Figure 3.2) applies the conventional heat integration strategy that has been used in distillation. The simple stripper is modified by adding a flash tank and a single compressor stage. The hot lean solvent coming from the reboiler is flashed, and produces steam and CO_2 in the flash tank at lower pressure. The flashed vapor is pressurized by the lean vapor compressor, and sent to the bottom of the packing section in the stripper. The additional stripping steam provides a heat source for heating the rich solvent in the stripper with packing. Compared to the simple stripper at the same operating lean loading, the stripper pressure with lean vapor compression is higher, and the rich solvent that goes into the top of the stripper is colder. The lean vapor compressor is analogous to the first stage of the multi-stage compressor for CO_2 compression. The stripper serves as a direct contact cooler that recovers the latent heat of steam.

The temperature of the flashed vapor at the lean vapor compressor inlet is around 140 ºC. After compression the hot vapor is over 200 ºC, which might exceed the temperature limit of typical compressor materials. The lean vapor compression work is included in the calculation of the total equivalent work. The pressure ratio of the lean vapor compressor for each lean loading was optimized to minimize the total equivalent work. With a high pressure ratio, less stripping steam heat will be lost in the higher pressure stripper but the lean vapor compression work will increase.

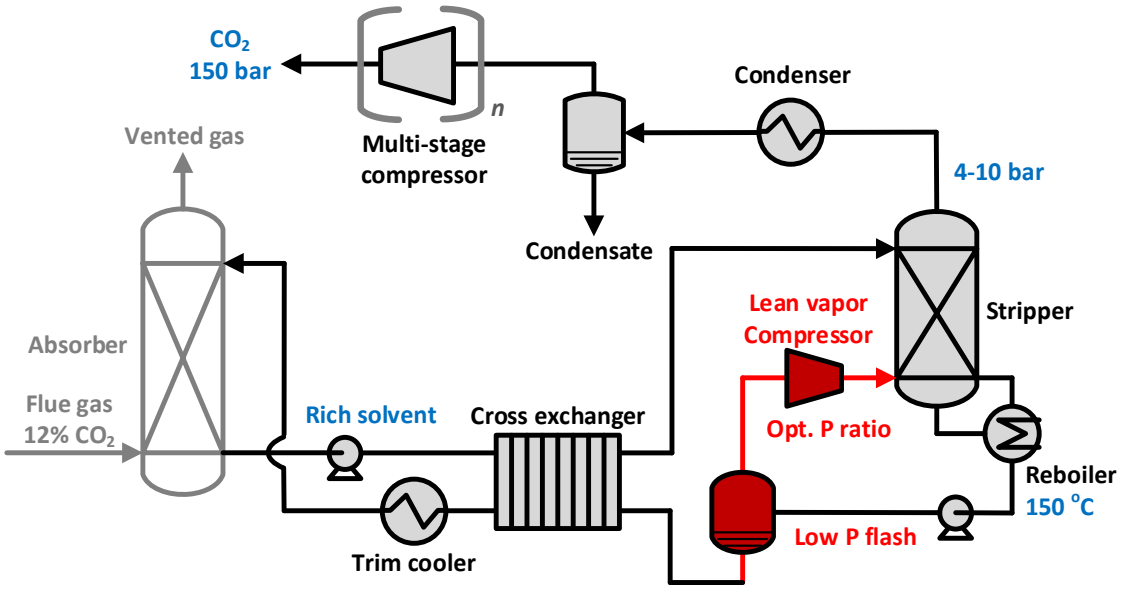

Figure 3.2: Lean vapor compression.

3.4 RESULTS AND DISCUSSIONS

3.4.1 Inefficiency of simple stripper

3.4.1.1 Minimum work and lost work distribution

Figure 3.3 shows the minimum work and lost work of a simple stripper using 8 m PZ. The minimum work of separation purifies the inlet 12% CO_2 at 1 bar to pure CO_2 at

stripper pressure, which depends on the operating lean loading. The minimum work of compression brings the pure CO_2 from stripper pressure to final pressure at 150 bar. Both these values vary with lean loading since the stripper pressure is not constant. The sum of separation and compression minimum work is 18.2 kJ/mol CO_2, which is independent of CO_2 lean and rich loading.

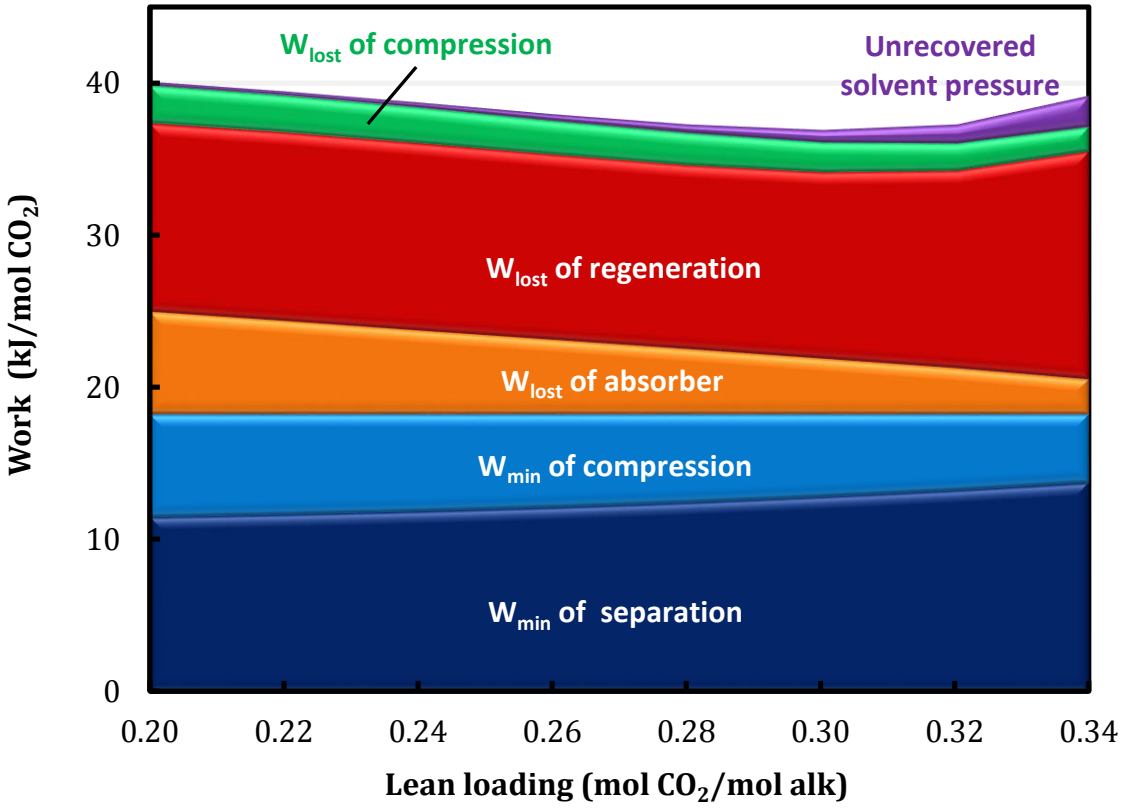

Figure 3.3: Minimum work and lost work of simple stripper using 8 m PZ; rich loading: 0.4; reboiler T: 150 °C; cross exchanger ΔT_{LM}: 5 K; 5 m packing; correction for interfacial area: 1.

The lost work from the absorber, regeneration, compression, and unrecovered solvent pressure are also shown in Figure 3.3. The lost work of the absorber can be regarded as from a typical intercooled absorber with finite packing area. It varies with the CO_2 lean loading since the inlet and outlet conditions of the absorber are fixed except

for the CO_2 lean loading. Because the CO_2 partial pressure decreases with CO_2 lean loading, a large driving force of CO_2 partial pressure causes the lost work of the absorber to increase at a lower lean loading. At higher lean loading, even though the minimum work of regeneration required is lower, the absorber may require more packing area due to insufficient mass transfer driving force.

The lost work of compression is obtained from the difference between the actual work of compression and the isothermal minimum work of compression at 40 ºC. The lost work of compression comes from the inefficiency of the compressors (86% polytropic efficiency is used) and non-isothermal operation. The lost work of unrecovered solvent pressure shows the amount of work that the lean solvent at the stripper pressure can generate if it is brought to 1 bar. Practically, the unrecovered solvent pressure of the lean solvent will be used to overcome the pressure drop through the cross exchangers, the trim cooler, and the static head of the absorber.

The actual work required by the process is the sum of the minimum work values and all of the lost work. The lost work of regeneration accounts for 60–70% of total lost work. It is the major reason that the simple stripper is inefficient.

3.4.1.2 Lost work of regeneration

The lost work of regeneration can be distributed into the unit operations. Figure 3.4 shows this distribution for a simple stripper using 8 m PZ with varied lean loading.

The lost work of the reboiler reflects the amount of heat duty and the temperature approach between the solvent and the heating steam. 5 K temperature approach between the steam and the reboiler temperature was assumed. The lost work of the trim cooler and the pump increases when the lean loading increases due to decreasing solvent capacity (i.e., increasing solvent rate) and increasing stripper pressure.

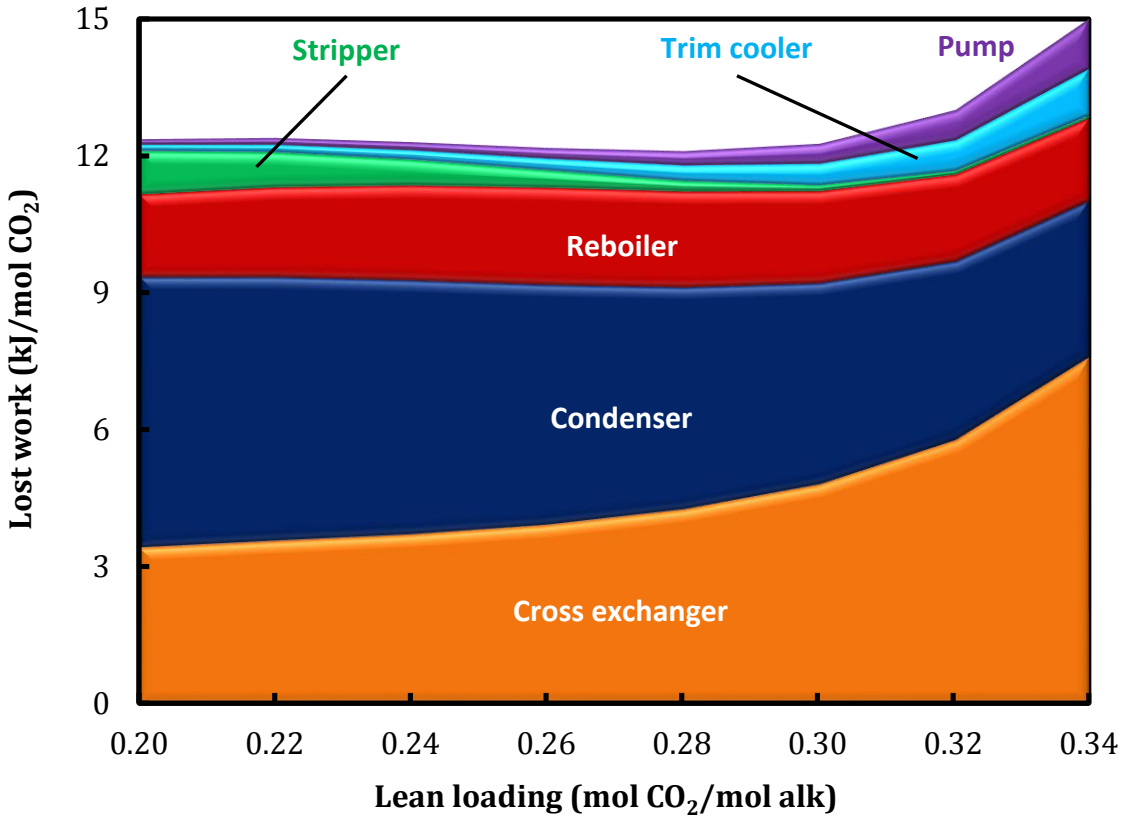

Figure 3.4: Lost work of regeneration of simple stripper using 8 m PZ; rich loading: 0.4; reboiler T: 150 °C; cross exchanger ΔT_{LM}: 5 K; 5 m packing; correction for interfacial area: 1.

The overhead condenser and the cross exchanger are the two major lost work sources. They account for over 70% of the lost work of regeneration. When the CO_2 is stripped out, a large amount of water vapor leaves the stripper and is removed in the overhead condenser. The lost work of the condenser is mainly caused by the loss of latent heat of the stripping steam. From the Gibbs-Helmholtz equation of CO_2 desorption reaction (Equation 3.5), either increasing the regeneration temperature or using solvents that have higher heat of absorption (ΔH_{abs}) will increase the partial pressure of CO_2 (P^*_{CO2}), providing better selectivity of CO_2 over the water vapor. However, elevated regeneration

temperature will cause more solvent degradation and a higher pressure heating steam requirement.

$$\frac{d\left(lnP^{*}_{CO_2}\right)}{dT} = \frac{\Delta H_{abs}}{RT^2} \tag{3.5}$$

The lost work of the cross exchanger is the temperature difference times the amount of heat exchanged between the cold rich solvent and the hot lean solvent. Even with a small LMTD of 5 K, the lost work of the cross exchanger is significant because of the large exchanger duty, which is 2 to 5 times the reboiler duty. It is sensitive to the lean loading because of the change in solvent cyclic capacity. For example, the solvent circulation rate at 0.28 lean loading is around 50% of that at 0.34 lean loading. The lower solvent flow rate results in a lower heat duty in the cross exchanger, so the lost work of the cross exchanger decreases with decreasing lean loading.

3.4.2 Inefficiency of lean vapor compression

There are two reasons that the lean vapor compression gives better energy performance than the simple stripper. First, additional stripping steam is produced in the low pressure flash tank, providing the opportunity for the rich solvent to capture the extra heat in the stripper. However, the stripping steam has to be pressurized before the heat is recovered, which requires additional compression work. Second, similar to the multi-pressure stripper and double matrix stripper (Jassim et al., 2006; Oyenekan et al., 2007; Van Wagener et al., 2011), the stripper is operated at higher pressure compared to the simple stripper at the same lean loading, which inherently reduces the stripping steam.

Figure 3.5 shows the lost work of regeneration with lean vapor compression. The lost work of the condenser is only reduced by 1/3. This implies that this stripper design is not capable of fully recovering the waste heat from the stripping steam. A portion of the lost work is shifted from the reboiler to the stripper column since the superheated

stripping steam is delivered into the stripper and preheats the rich solvent. The lean vapor compressor and the flash tank also result in lost work.

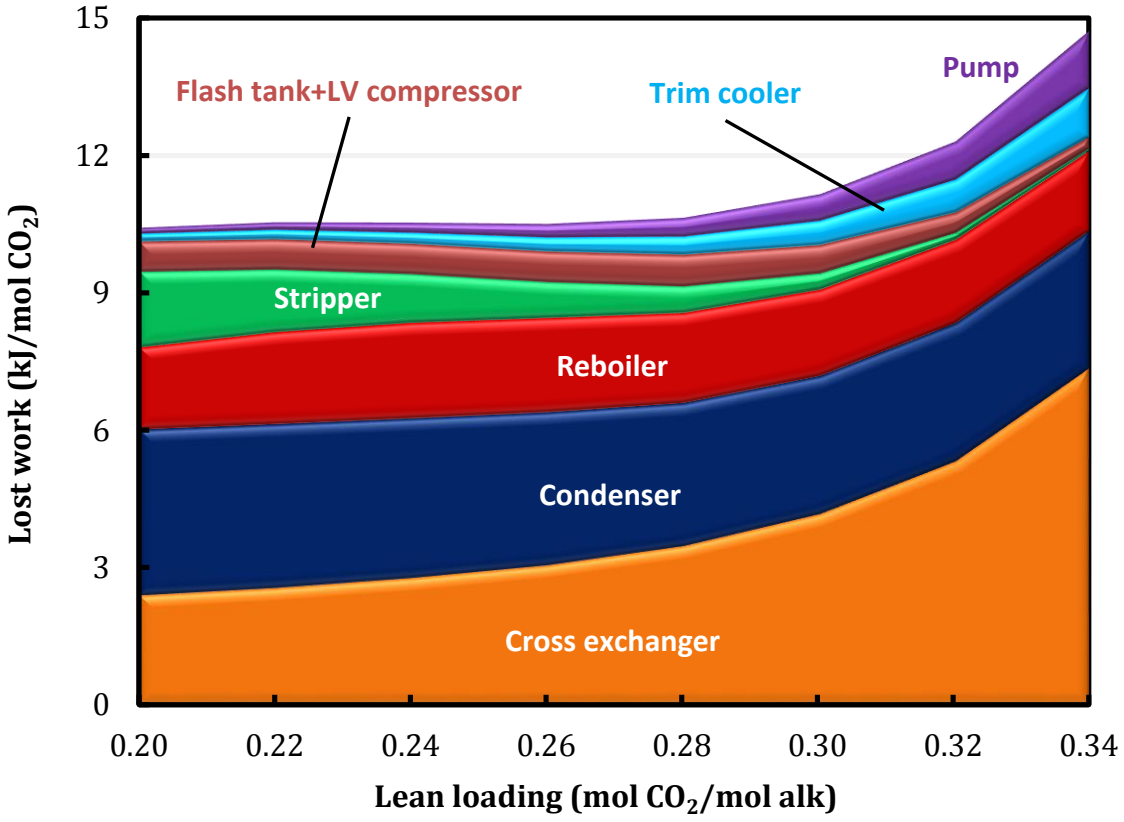

Figure 3.5: Lost work of regeneration of lean vapor compression using 8 m PZ; rich loading: 0.4; reboiler T: 150 °C; cross exchanger ΔT_{LM}: 5 K; 5 m packing; correction for interfacial area: 1; optimum pressure ratio of lean vapor compressor at each lean loading.

3.4.3 Proposed design strategies

The significant lost work from the condenser and the cross exchanger is the primary reason that the simple stripper is not energy efficient. To reduce the irreversibility, analysis of heat and mass transfer in the stripper and the cross exchanger will be explored. Alternative design strategies can be proposed accordingly.

3.4.3.1 Heat and mass transfer in the stripper

The lost work of the stripper column of the simple stripper is relatively low. It can be explained by the temperature profile and the CO_2 concentration profile of the stripper column shown in Figure 3.6. For the simple stripper, the bottom is the reboiler that heats the solvent up to 150 ºC. The temperature of the rich solvent going into the top of the stripper is around 140 ºC, only 10 ºC higher than the bottom reboiler temperature. Since the liquid is hot, it cannot condense any stripping steam from the vapor phase. The temperature profile shows that the pinch at the top of the stripper and most of the packing is wasted.

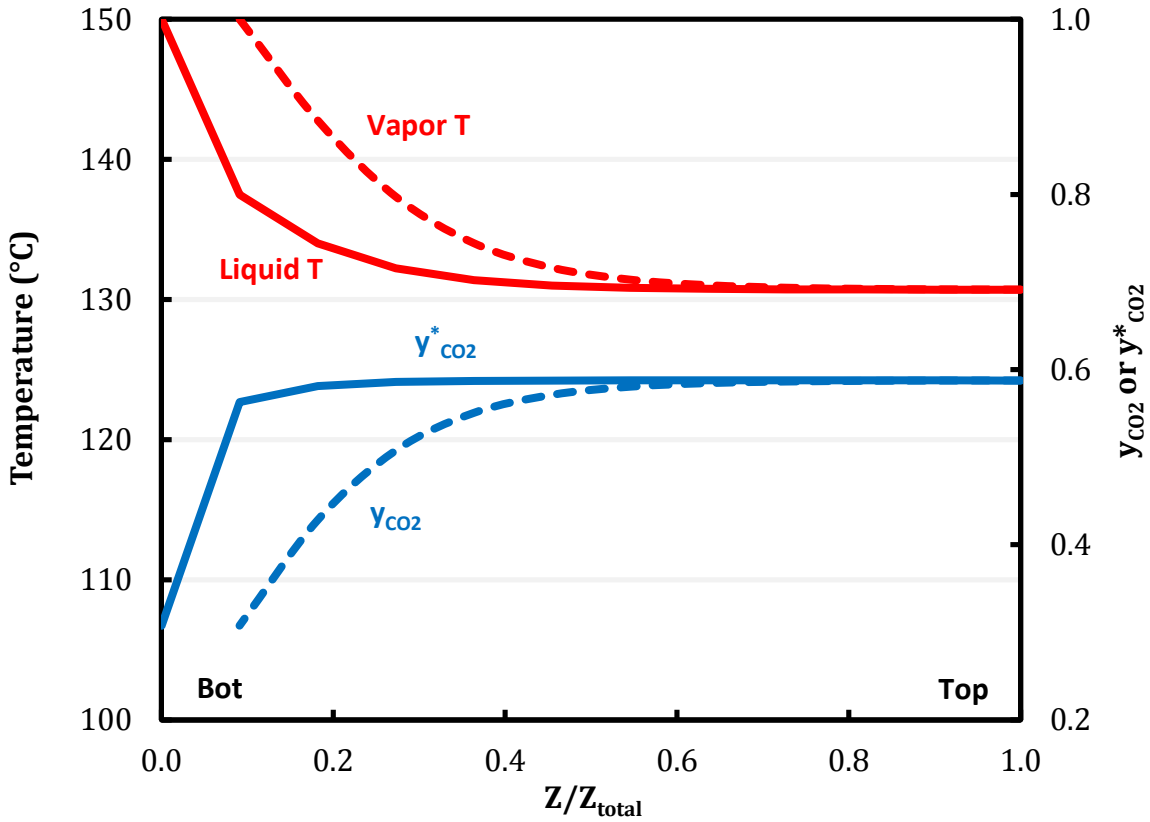

Figure 3.6: Temperature and CO_2 concentration profile of stripper column for simple stripper using 8 m PZ; lean loading: 0.24; rich loading: 0.4; reboiler T: 150 °C; cross exchanger ΔT_{LM}: 5 K; 5 m packing; correction for interfacial area: 1.

The CO_2 concentration profile shows the stripping conditions using the CO_2 mole fraction in the vapor phase (y_{CO2}) and the equilibrium CO_2 mole fraction in the liquid phase (y^*_{CO2}), which is the ratio of equilibrium partial pressure of CO_2 to the stripper pressure. The vapor coming from the reboiler contains 30% CO_2 and 70% H_2O, and it leaves the stripper with 60% CO_2 and 40% H_2O. The equilibrium CO_2 partial pressure of the solvent depends on the CO_2 loading and the solvent temperature. Before the rich solvent goes into the stripper, the hot solvent flashes out a portion of CO_2, so the rich solvent at the top is at 0.34 CO_2 loading instead of 0.4. This lower CO_2 loading causes a low equilibrium mole fraction of CO_2. The CO_2 concentration also pinches at the top. The appearance of pinches for both heat and mass transfer implies that the simple stripper is a poor design that could not effectively condense the stripping steam and strip CO_2. To improve the stripper, both heat and mass transfer performance should be considered. The rich solvent that goes to the stripper should be at or below its bubble point to avoid flashing.

3.4.3.2 Self-contained heat integration using cold rich solvent

The reasons for limited energy reduction of the lean vapor compression are clear from Figure 3.5. First, the lost work of the condenser has not been fully recovered. Over 60% of that is still left. Second, additional recompression work has to be provided before the stripping steam heat is recovered. In fact, the vapor only needs to be compressed for heat integration if its dew point temperature is lower than the bubble point of the heat sink. If a low temperature heat sink is available, the waste heat from the vapor can still be recovered without being "upgraded".

Therefore, it is straightforward to use the cold rich solvent at 46 ºC as the heat sink to recover the rest of the stripping steam heat. However, direct contact should be avoided. When the solvent is cold, the equilibrium partial pressure of CO_2 could be lower than that

in the vapor coming from the stripper. If cold rich solvent and hot CO_2 vapor directly contact in the stripper, the CO_2 will be re-absorbed to the solvent, which will cause even more heat duty for CO_2 stripping.

3.4.3.3 Temperature pinch of the cross exchanger

The cross exchanger is the other major source of lost work. A reversible heat exchanger should avoid severe temperature pinch, i.e., temperature-enthalpy lines of cold and hot streams should be parallel. Figure 3.7 shows the minimum temperature approach (temperature pinch) in the cross exchanger of the simple stripper. Since the LMTD is specified as 5 K, as the minimum temperature approach is closer to 5 K, the temperature approach can be expected to be more consistent throughout the cross exchanger. The minimum temperature approach is 1.5-4 K with various lean loading. The temperature approach is pinched at the cold end and wide open at the hot end. This implies that the cross exchanger can be made more reversible.

The temperature pinch is caused by the unbalanced flow heat capacity ($\dot{m}C_p$) of the hot and cold streams. For the simple stripper, the flow heat capacity of the rich side is always greater than the lean side due to the loss of CO_2 and water from the stripper. The pinch can be relaxed by bypassing a portion of rich solvent to match similar flow heat capacity.

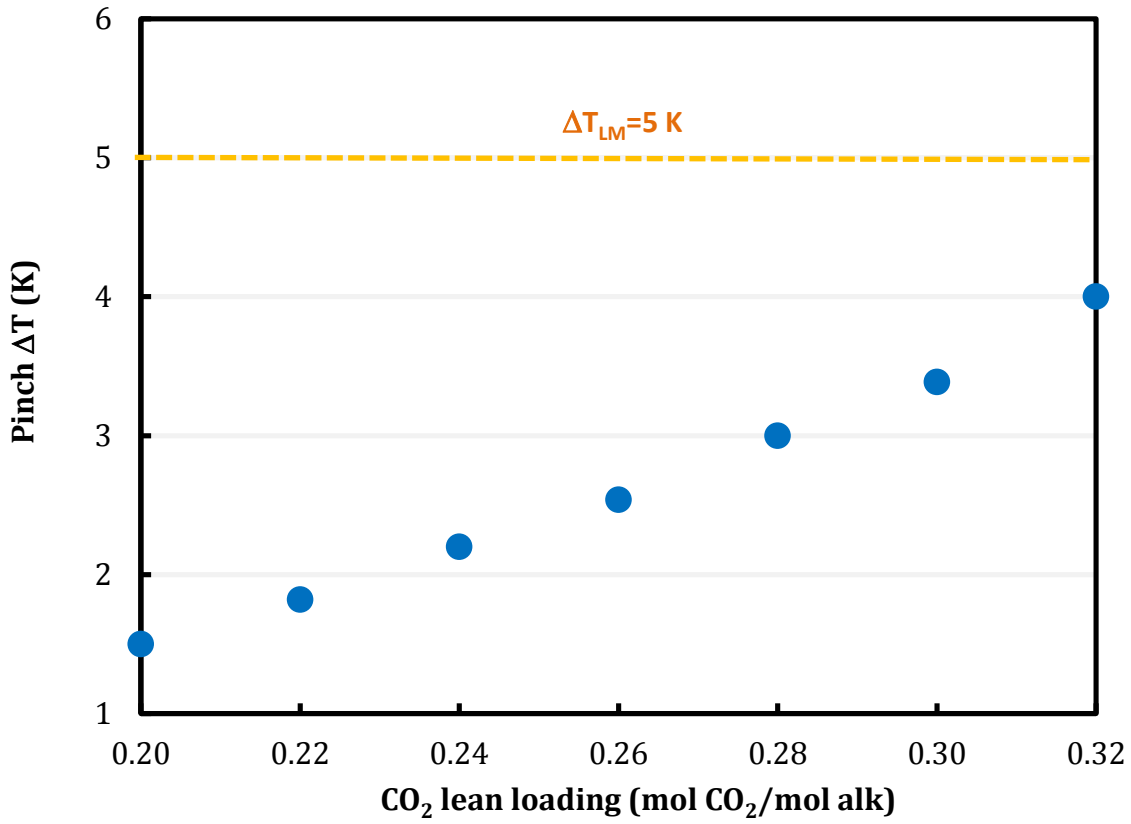

Figure 3.7: Pinch temperature approach of the cross exchanger of the simple stripper using 8 m PZ; rich loading: 0.4; reboiler T: 150 °C; cross exchanger ΔT_{LM}: 5 K.

3.4.4 Advanced flash stripper

3.4.4.1 Proposed stripper configuration

Based on the design strategies, a new stripper configuration, the advanced flash stripper, is proposed and shown in Figure 3.8. The major modifications are the warm rich bypass and the cold rich bypass with the cold rich exchanger.

The cross exchanger is split into two exchangers. The warm rich bypass is extracted and fed to the top of the stripper after mixing with the cold rich bypass. The temperature was selected as the bubble point at the stripper operating pressure. The temperature at bubble point without flashing will maximize the equilibrium partial pressure

of CO_2 for stripping, while still condensing a portion of stripping steam from the vapor phase.

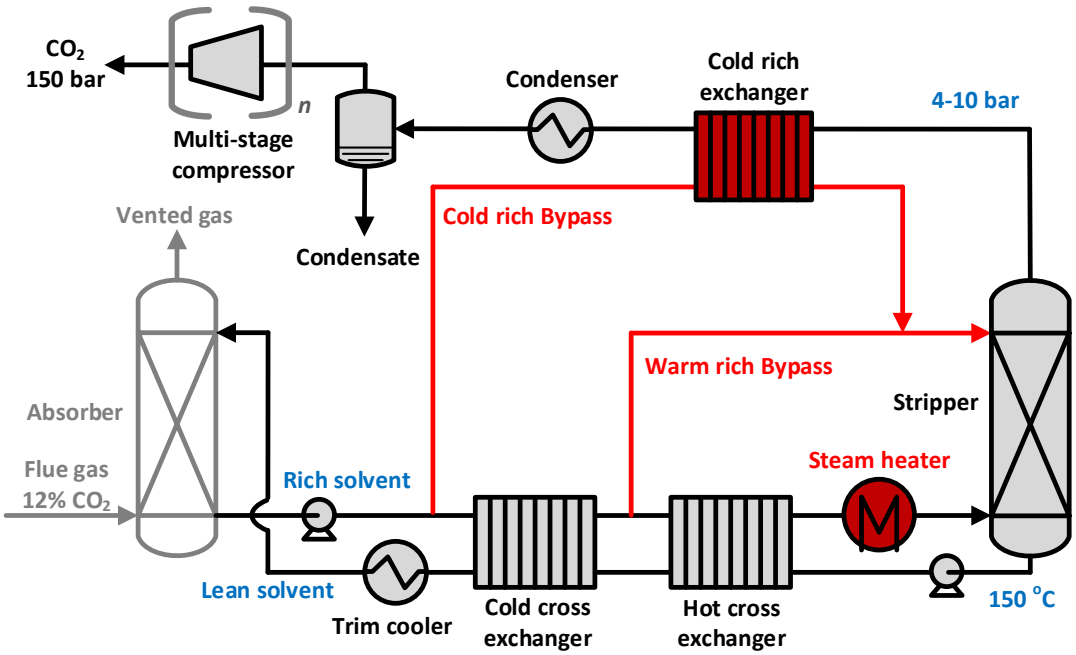

Figure 3.8: Advanced flash stripper

The cold rich solvent serves as a low temperature heat sink to recover the rest of the stripping steam heat. The heat is recovered by the rich exchanger instead of by direct contact in the stripper to avoid re-absorption. The rich exchanger preheats a portion of the cold rich solvent by hot vapor coming out of the stripper. The cold and warm rich bypass also help relax the temperature pinch in the cross exchanger.

The optimized cold and warm rich bypass rate will maximize the potential benefits from the stripping steam heat recovery, the CO_2 stripping performance in the stripper column, and the cross exchanger performance. For each lean loading the bypasses are optimized to minimize the total equivalent work. Higher bypass rates are required at low lean loading as more stripping steam needs to be recovered.

After cold and warm rich solvent bypasses, the rest of the rich solvent is heated by a steam heater and fed into the bottom of the stripper. The regeneration temperature of the stream coming from the flash tank was 150 ºC. The reboiler in a typical stripper is replaced by a steam heater, which has the same function as the reboiler except the solvent is heated convectively. Since the amine tends to thermally degrade at high temperature, the convective steam heater with less solvent hold-up and residence time will minimize thermal degradation.

3.4.4.2 Lost work of regeneration

Figure 3.9 shows the lost work of regeneration of the advanced flash stripper using 8 m PZ. The lost work of the condenser is almost eliminated compared to the simple stripper and the lean vapor compression. The water vapor content from the rich exchanger is only around 5 mol % over the lean loading range. Figure 3.10 shows that the lost work of the condenser with the advanced flash stripper is 50% less than with lean vapor compression. The proposed design strategies significantly reduce the irreversibility of the condenser.

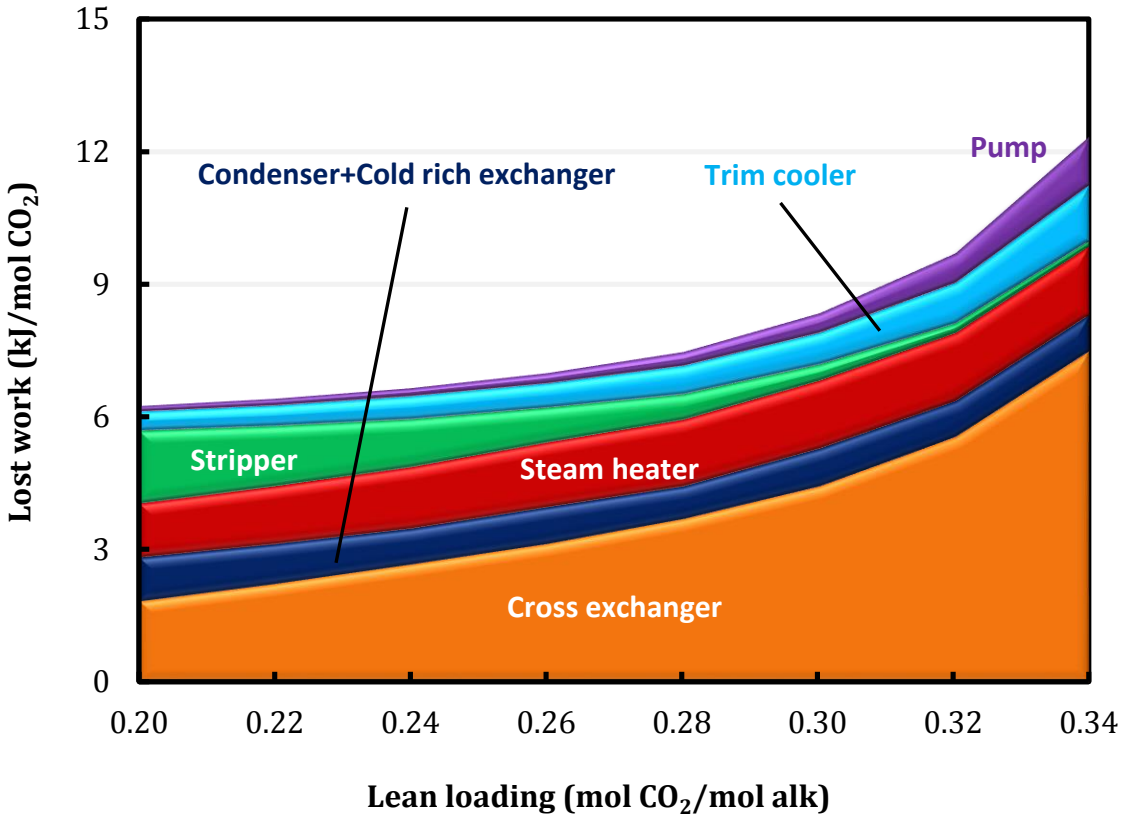

Figure 3.9: Lost work of regeneration of advanced flash stripper using 8 m PZ; rich loading: 0.4; reboiler T: 150 °C; cross exchanger ΔT_{LM}: 5 K; 5 m packing; correction for interfacial area: 1; optimum cold and warm rich bypasses.

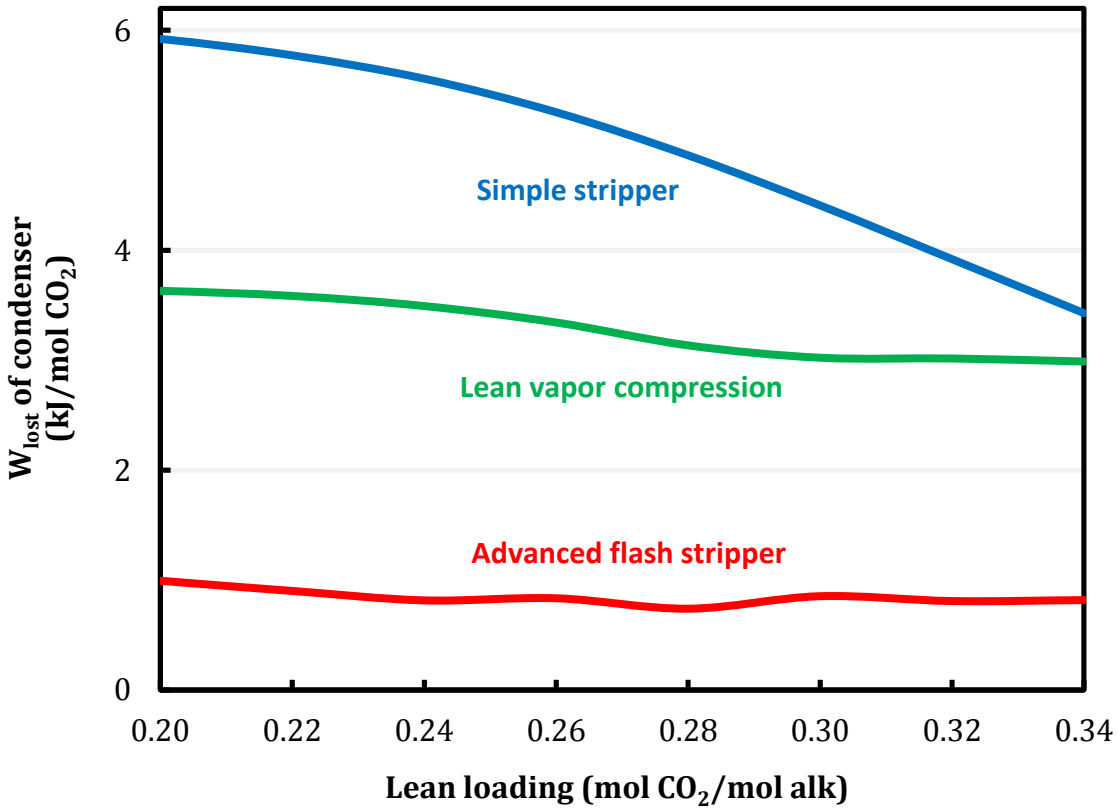

Figure 3.10: Comparison of lost work of the condenser; 8 m PZ; rich loading: 0.4; reboiler T: 150 °C; cross exchanger ΔT_{LM}: 5 K; 5 m packing; correction for interfacial area: 1; optimum pressure ratio for LVC; optimum cold and warm rich bypasses for AFS.

Figure 3.11 compares the heat duty of the reboiler/steam heater. The lean vapor compression reduces the heat duty by 8.4% and the advanced flash stripper reduces it by 16.1% at the optimum lean loading compared to the simple stripper. Figure 3.12 compares the total equivalent work, which includes the compression work, pump work, equivalent work of reboiler duty, and the lean vapor compression work. The advanced flash stripper reduces the total equivalent work by 11.2% at optimum lean loading while the lean vapor compression reduces it by only 3.4%.

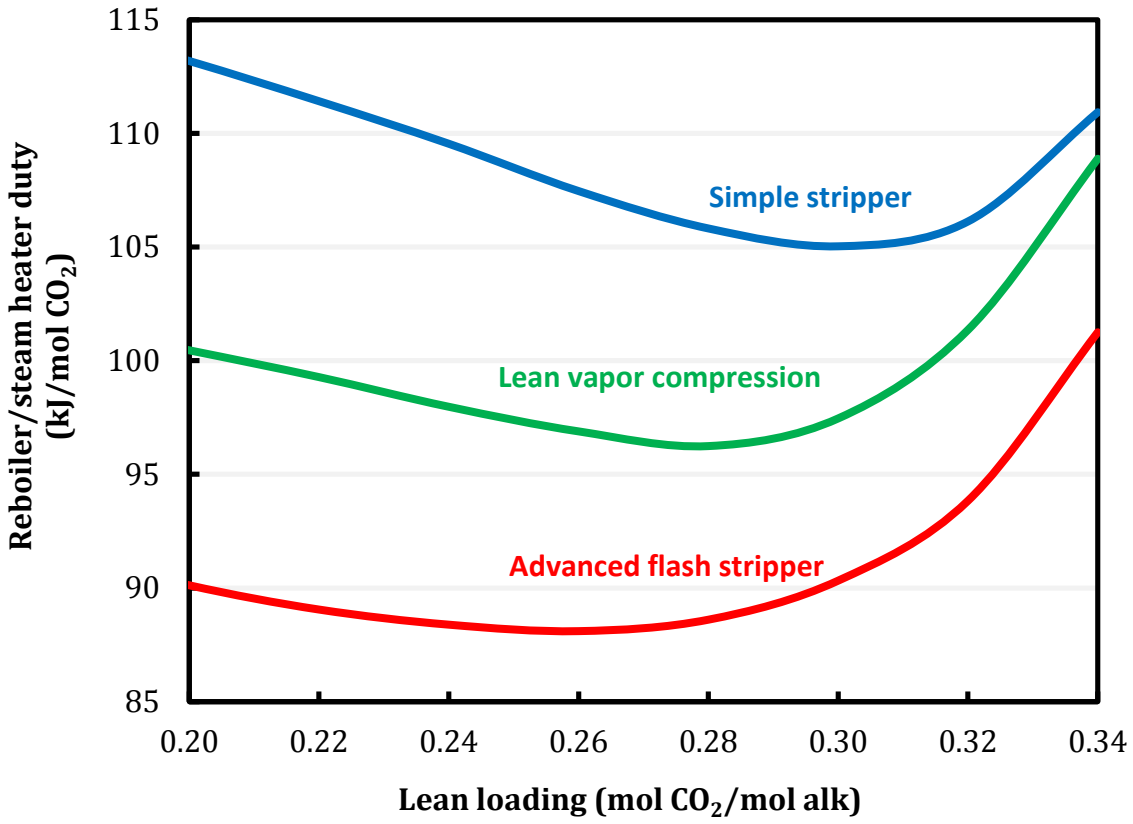

Figure 3.11: Comparison of heat duty of reboiler/steam heater; 8 m PZ; rich loading: 0.4; reboiler T: 150 °C; cross exchanger ΔT_{LM}: 5 K; 5 m packing; correction for interfacial area: 1; optimum pressure ratio for LVC; optimum cold and warm rich bypasses for AFS.

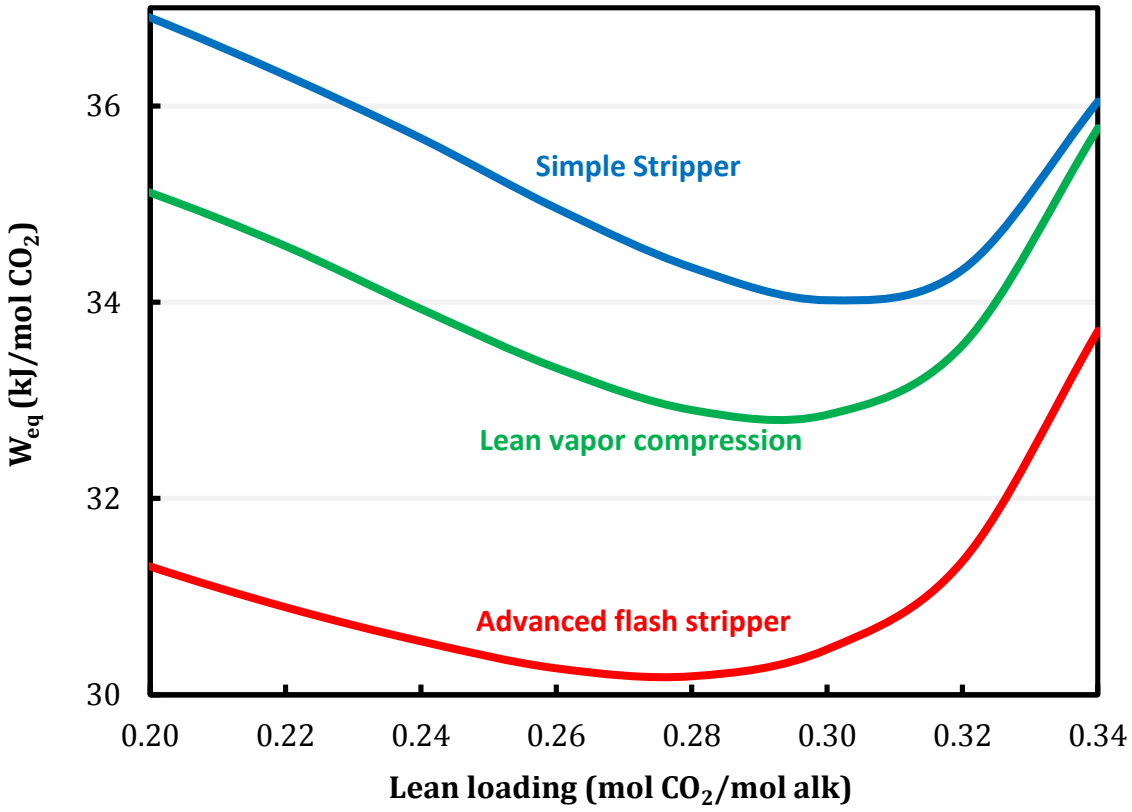

Figure 3.12: Comparison of total equivalent work; 8 m PZ; rich loading: 0.4; reboiler T: 150 °C; cross exchanger ΔT_{LM}: 5 K; 5 m packing; correction for interfacial area: 1; optimum pressure ratio for LVC; optimum cold and warm rich bypasses for AFS.

3.4.4.3 Cold and warm rich bypass

The temperature and the CO_2 concentration profile of the stripper shown in Figure 3.13 explain the energy improvement. The pinch shown in the simple stripper (Figure 3.6) has disappeared. The advanced flash stripper avoids heat and mass transfer pinches and provides more opportunity for the stripper packing to recover the stripping steam heat and strip CO_2 from the rich solvent. The adjustable warm rich bypass rate can change the slope of the operating line (CO_2 concentration and temperature of vapor) to match the equilibrium line. With optimum bypasses that minimize the reboiler duty, the

temperature profiles of the vapor and the liquid are nearly parallel. Both heat and mass transfer show consistent driving force throughout the column, which implies that the packing is utilized more efficiently.

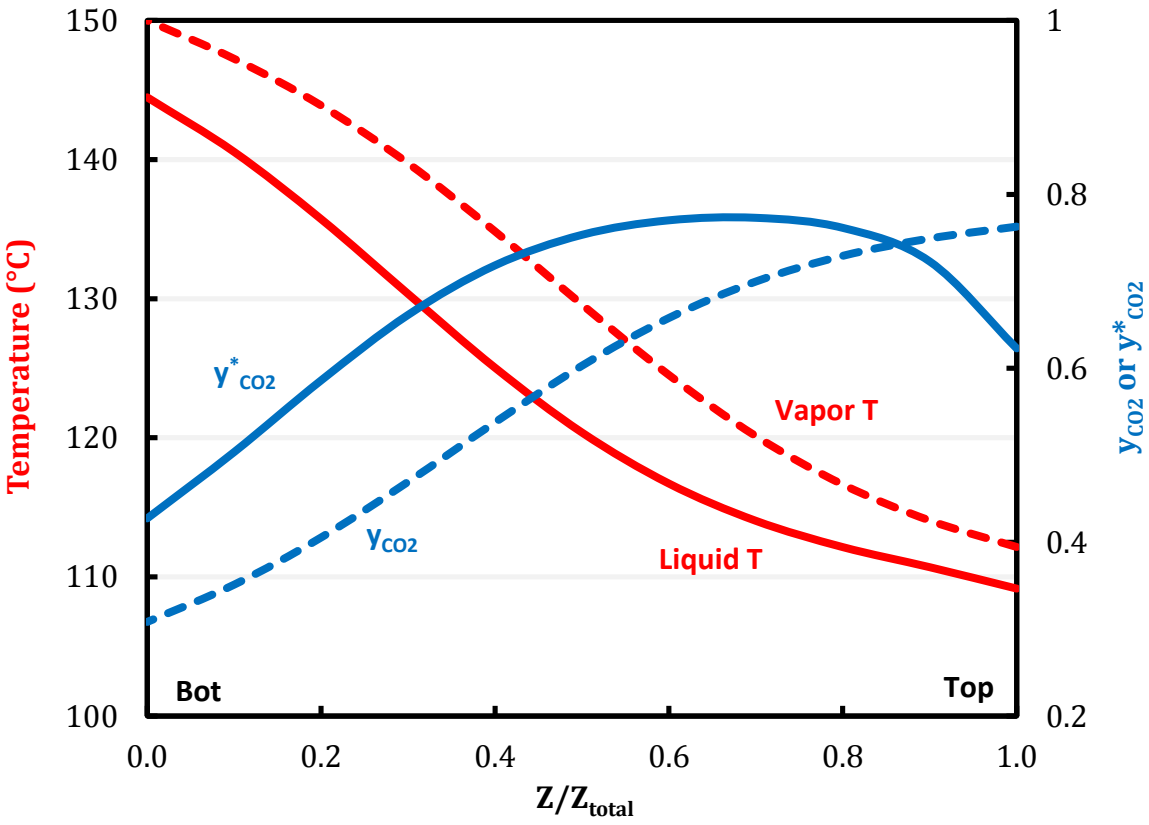

Figure 3.13: Temperature and CO_2 concentration profile of stripper column for the advanced flash stripper; 8 m PZ; lean loading: 0.24; rich loading: 0.4; reboiler T: 150 °C; cross exchanger ΔT_{LM}: 5 K; 5 m packing; correction for interfacial area: 1; optimum cold and warm rich bypasses.

The temperature of the rich solvent that goes to the stripper is determined by both cold rich bypass and warm rich bypass. The adjustable bypass rates give the flexibility to determine the temperature. At low temperature, more stripping steam can be recovered in the stripper but re-absorption may occur as the CO_2 is absorbed from the vapor. In the

CO_2 concentration profile in Figure 3.13, the re-absorption can be seen at the top of the stripper. Even with re-absorption, this case gives the minimum reboiler duty by recovering more stripping steam.

3.4.4.4 Irreversibility of the cross exchanger

The reversibility of the cross exchanger can be understood by following the ratio of the flow heat capacity ($\dot{m}C_p$) of the rich and lean streams. The cross exchanger will be reversible if the flow heat capacity between rich and lean solvent is well-matched. To maximize the performance of the cross exchanger, the ratio of the flow heat capacity should be close to unity.

Figure 3.14 shows the ratio of the flow heat capacity of rich to lean stream in single phase before the rich solvent vaporizes. Since the specific heat capacity is similar over the operating conditions, the flow heat capacity is mainly affected by the solvent flow rate. For the simple stripper, the ratio is greater than unity, around 1.01–1.09. The loss of water vapor and CO_2 from the stripper results in lean solvent flow that is less than the rich solvent. For the advanced flash stripper, the ratio of flow heat capacity is reduced to 0.96–0.99. The cold rich bypass reduces the flow rate of rich solvent that goes to the cross exchanger. At optimized bypass rate, the flow rate of the rich solvent is even lower than the lean solvent, so the ratio of the flow heat capacity is less than unity. The fact that the ratio is not exactly at unity implies that it is worthwhile extracting more solvent to recover the stripping steam heat rather than balancing the temperature approach of the cross exchanger.

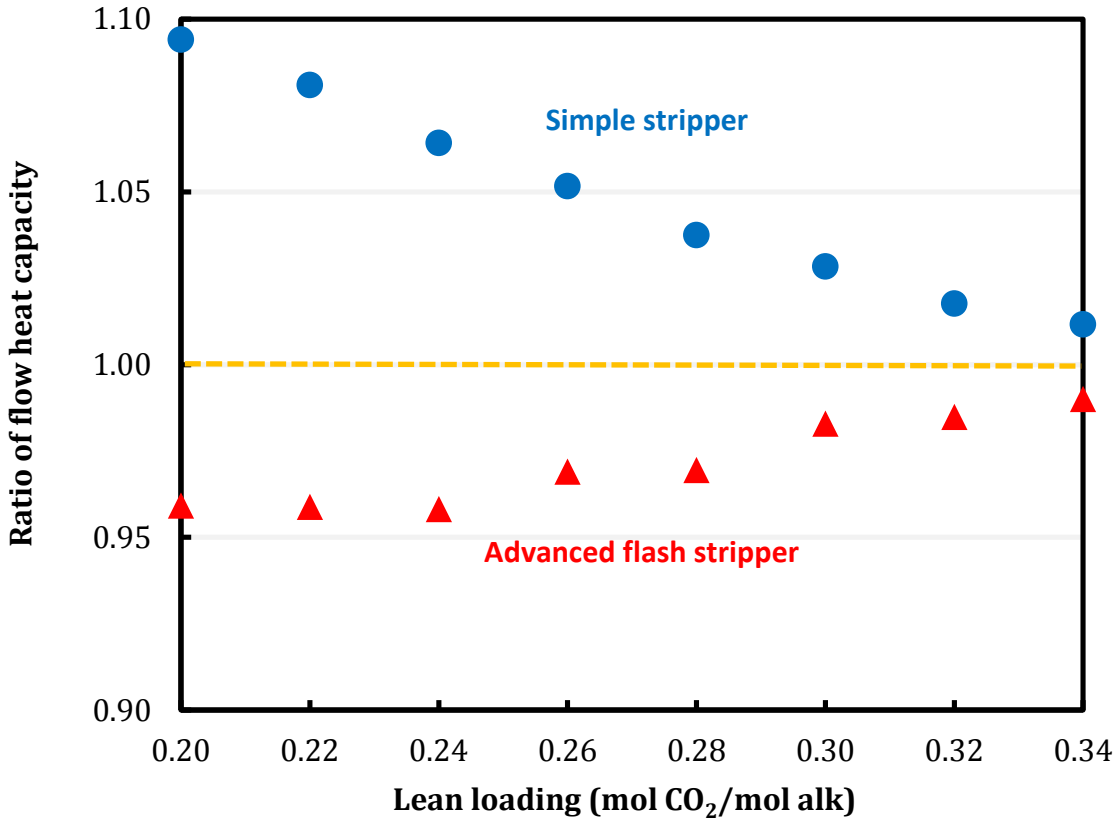

Figure 3.14: Flow heat capacity ratio of rich solvent to lean solvent of the cold cross exchanger (single phase); 8 m PZ; rich loading: 0.4; reboiler T: 150 °C; cross exchanger ΔT_{LM}: 5 K; optimum cold and warm rich bypasses.

When the rich solvent starts vaporizing, the heat of vaporization makes the specific heat capacity at the rich side much higher than the lean side that stays in single phase. Figure 3.15 shows the ratio of the flow heat capacity with vaporization. The ratio of the simple stripper is around 1.4–1.8, far from the desired unity. For the advanced flash stripper, the ratio is reduced to 1.1–1.3. The extraction of cold and warm rich bypass help balance the flow heat capacity with lower rich solvent rate in the cross exchanger. Generally, the advanced flash stripper provides a more reversible cross exchanger than the simple stripper.

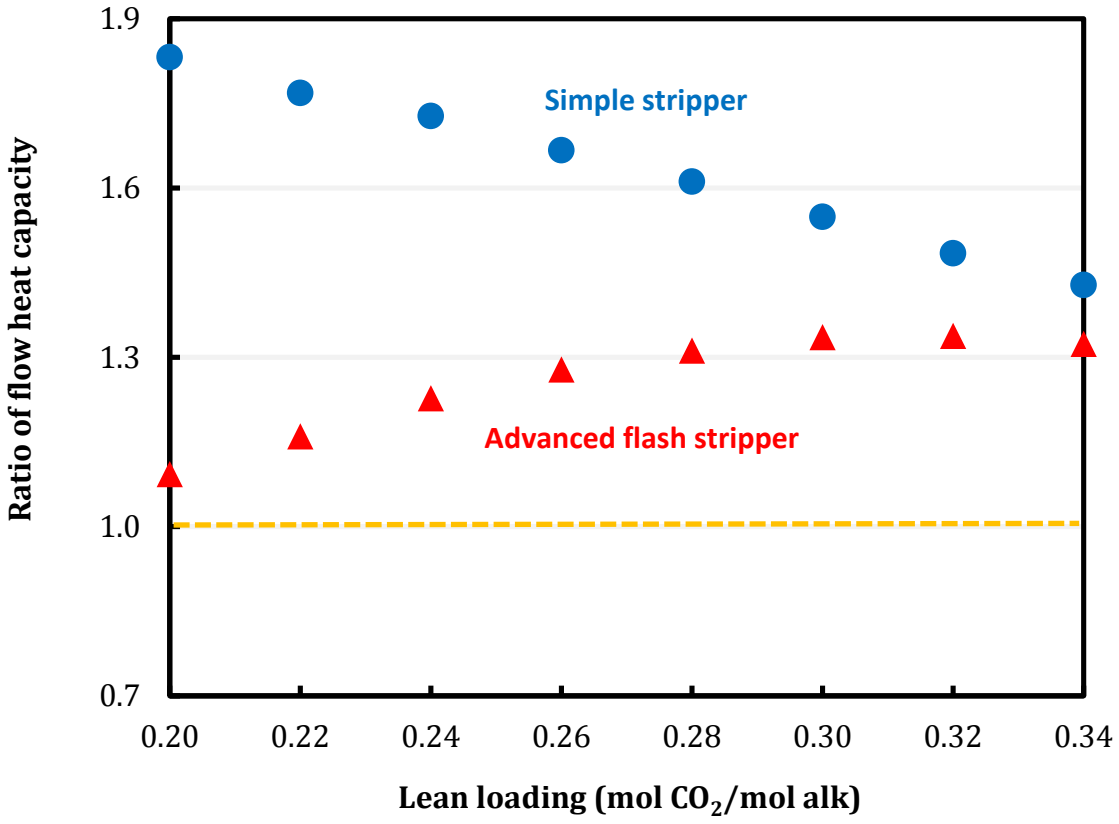

Figure 3.15: Flow heat capacity ratio of rich solvent to lean solvent of the hot cross exchanger (flashing phase); 8 m PZ; rich loading: 0.4; reboiler T: 150 °C; cross exchanger ΔT_{LM}: 5 K; optimum cold and warm rich bypasses.

The lost work of the cross exchanger can be potentially reduced by using a tight temperature approach or increasing the solvent capacity. However, an excessively small temperature difference should be avoided due to the prohibitive cost of the cross exchanger. Operating at lower CO_2 lean loading will increase the cyclic capacity because less solvent will be circulating between the absorber and the stripper. Figure 3.9 showed that significant lost work of the cross exchanger is avoided at low loading. With the simple stripper this strategy will not be effective, as the lost work of the condenser will offset the reduction (Figure 3.4), but for the advanced stripper, the low lean loading region is exactly where the advanced flash stripper reduces the lost work of the condenser the most.

3.4.4.5 Irreversibility of the reboiler/steam heater

The lost work of the reboiler (steam heater for advanced flash stripper) will increase with increasing steam temperature. The relationship can be expressed by the heat duty-equivalent work conversion factor in the total equivalent work calculation. When the steam is extracted from the power plant, steam at higher temperature will cause more electricity loss. For example, using steam at 180 ºC leads to an additional 15% electricity penalty compared to that at 155 ºC with equivalent reboiler duty.

In this work, 5 K temperature difference is used for the reboiler. Ideally, using steam with temperature as low as possible can minimize the lost work of the reboiler. However, an excessively small temperature approach should be avoided.

3.4.5 Thermodynamic efficiency of regeneration

The thermodynamic efficiency can be used to quantify the potential for energy improvement by comparing the actual work to the minimum work, which is defined in Equation 3.1. The thermodynamic efficiency of CO_2 compression is around 73% over the range of inlet pressure from 1 to 20 bar.

Since this work focuses on developing the design strategies for the stripping process, the thermodynamic efficiency of regeneration will more adequately represent the performance of the regeneration process only. Equation 3.6 defines the thermodynamic efficiency of regeneration ($\eta_{th,rgn}$) as the ratio of the minimum work of regeneration to the actual work of regeneration. The minimum work of regeneration is defined in Table 3.2. The actual work of regeneration ($W_{act,rgn}$) includes the heat provided to the reboiler/steam heater and the pump work of the rich solvent pump. This work used feasible design parameters to demonstrate the maximum energy efficiency that can be attained in practice. Unrealistic assumptions such as infinite heat/mass transfer area are avoided.

$$\eta_{th,rgn} = \frac{W_{min,rgn}}{W_{act,rgn}} \tag{3.6}$$

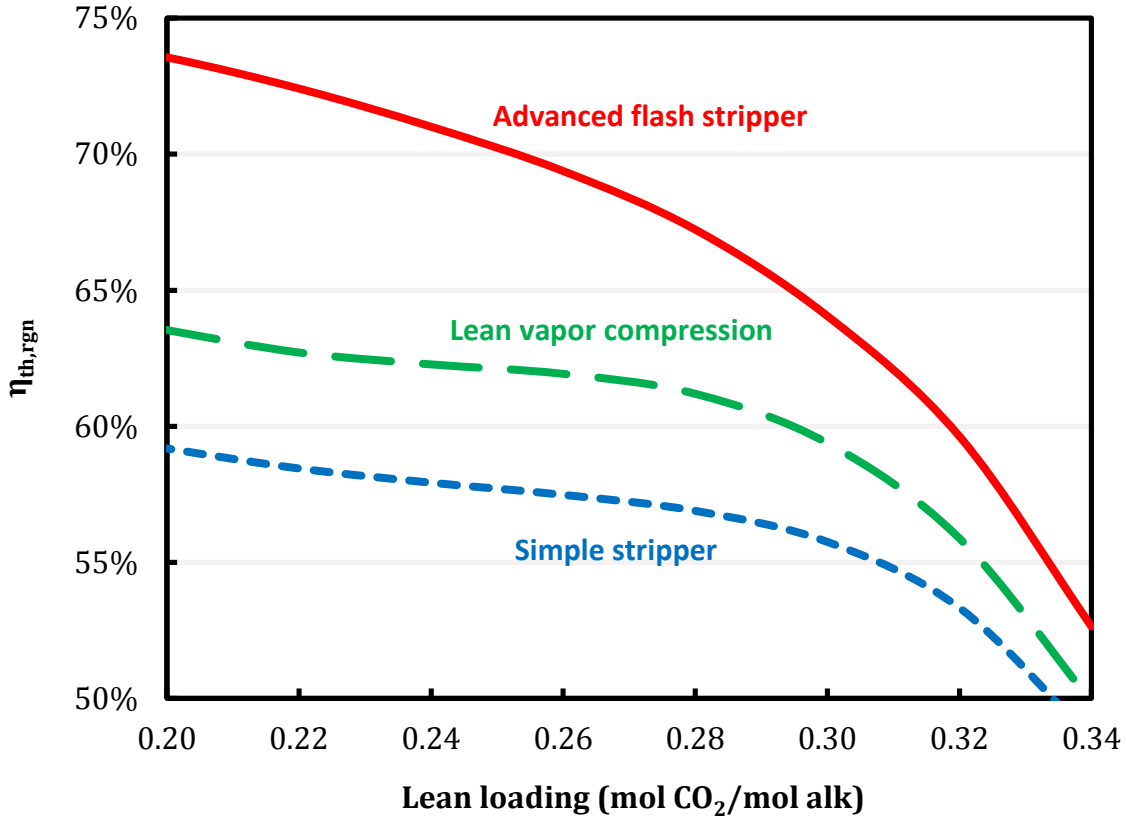

Figure 3.16: Comparison of thermodynamic efficiency of regeneration; 8 m PZ; rich loading: 0.4; reboiler T: 150 °C; cross exchanger ΔT_{LM}: 5 K; 5 m packing; correction for interfacial area: 1; optimum pressure ratio of LVS; optimum cold and warm rich bypasses for AFS.

Figure 3.16 compares the thermodynamic efficiency of regeneration. The efficiency of the simple stripper is 50–60% and the advanced flash stripper is 55–74% in the range of operating lean loading. For the simple stripper, the low efficiency at high lean loading is mainly due to the dominating lost work of the cross exchanger. At lower lean loading where the lost work of the condenser dominates, the efficiency is relatively flat because the minimum work also increases. The advanced flash stripper is nearly

stripping steam free, so the efficiency is mainly driven by the lost work of the cross exchanger for the entire lean loading range. The advanced flash stripper improves the most at lower lean loading where the stripping steam is significant.

The advanced flash stripper gives the maximum thermodynamic efficiency at 74%. It is remarkable compared to typical distillation with heat integration that is only around 20% (Fitzmorris et al., 1980; Y. H. Kim, 2012; Yoo et al., 1988). The remaining lost work from the cross exchanger is difficult to reduce since PZ has already provided a superior solvent capacity compared to other solvents (Li, Voice, et al., 2013). Therefore, the energy efficiency of the regeneration process with the advanced flash stripper using 8 m PZ is approaching the thermodynamic limit from which further improvement is expected to be marginal.

3.5 CONCLUSIONS

- The lost work of the condenser and the cross exchanger were identified as the two major reasons that the simple stripper is not energy efficient. The advanced flash stripper using cold and warm rich bypasses is proposed to reduce the lost work.
- The warm rich bypass reduces the work loss associated with condensing water vapor resulting from the stripping steam.
- The cold rich bypass recovers the rest of the stripping steam heat by providing a low temperature heat sink while avoiding CO_2 re-absorption.
- The advanced flash stripper overcomes the weaknesses of lean vapor compression and almost eliminates the lost work of the condenser. The cold and warm rich bypasses also make the cross exchanger more reversible by balancing the flow heat capacity between the rich and lean streams.

- The advanced flash stripper reduces the reboiler duty by 16.1% and the total equivalent work by 11.2% compared to the simple stripper.
- The advanced flash stripper reaches a remarkable thermodynamic efficiency at 55–74% over a range of operating lean loading.
- The regeneration process is close to a reversible operation compared to common distillation. Further improvement of energy efficiency is expected to be limited.

Chapter 4: Energy Performance of Advanced Stripper Configurations

4.1 INTRODUCTION

The irreversibility of the condenser has been identified as the major reason that makes the amine scrubbing process inefficient and is responsible for over 50% of the lost work in the regeneration process. Several alternative stripper configurations have been proposed to reduce the stripping steam heat loss. The configurations mainly applied two approaches: heat integration and isothermal stripping. Table 4.1 summarizes the alternative stripper configurations proposed by previous work.

The heat integration approach uses the latent heat of the stripping steam to preheat the rich solvent, which needs to be heated from the absorber temperature up to the reboiler temperature at 120–150 °C. Representative configurations include rich solvent bypass, interheated stripper, and vapor recompression. The rich solvent bypass extracts a portion of rich solvent to be contacted with the hot CO_2 vapor in the stripper, where the stripping steam is condensed with releasing the latent heat. The interheated stripper integrates the lean/rich cross exchanger into the stripper column and results in a colder stripper feed than the conventional simple stripper. Vapor recompression applies the heat integration strategy that has been used for conventional distillation. The hot CO_2 vapor with steam from the stripper is compressed by a multi-stage compressor to elevate the condensing temperature of the stripping steam. A part of reboiler duty can be provided by the heat integration with the compressor intercoolers. Most of the waste heat is obtained from the latent heat of water vapor so the energy improvement will be limited if the stripping steam has been already recovered by other approaches before entering the compressor train.

Isothermal stripping aims at regenerating CO_2 at the highest temperature possible throughout the stripping process. The maximum stripping temperature is usually limited by the thermal degradation of the amine. When the CO_2 is stripped from rich loading to

lean loading, operating the stripper isothermally will lead to the highest partial pressure of CO_2, which can improve the selectivity of CO_2 over stripping steam and reduce the mechanical compression work. The overall performance will depend on the efficiencies of thermal compression and mechanical compression. The multi-pressure stripper integrates the CO_2 compressor with the stripper column and operates at different pressure levels. Additional compression work is required to compress the stripping steam. The matrix stripper and the multi-stage flash attain high stripper pressure by providing reboiler duty at each stage instead compressing the CO_2 vapor. Theoretically, an isothermal stripper can be achieved if infinite stages are used.

Table 4.1: Alternative stripper configurations proposed to reduce stripping steam heat

Type	Configuration	Sources
Heat integration	Rich solvent bypass	(Eisenberg et al., 1979) (Soave et al., 2002) (Van Wagener et al., 2014) (Madan, 2013)
	Interheated stripper	(Leites et al., 1993) (Oyenekan et al., 2007) (Van Wagener et al., 2011)
	Vapor recompression	(Jassim et al., 2006)
Isothermal stripping	Multi-pressure stripper	(Jassim et al., 2006) (Oyenekan et al., 2007)
	Lean vapor compression	(Ebnson et al., 1979) (Reddy et al., 2009)
	Matrix stripper	(Oyenekan et al., 2007)
	Multi-stage flash	(Van Wagener et al., 2011)

This work propose new configurations that apply rich exchanger bypass. The energy performance will be compared to other alternatives previously proposed using the

same metric. In order to show the improvement with different solvent properties, the stripper configurations will be modeled using two common solvents, PZ and MEA in Aspen Plus®. The overall energy performance will be indicated by the total equivalent work in a wide range of operating lean loading.

4.2 SIMULATION METHODS

8 m PZ and 9 m MEA were chosen as solvents. The thermodynamic models used for MEA and PZ in this work were "Phoenix" and "Independence", respectively. Modeling details can be found in Frailie (2014) and Plaza (2011). These models have been regressed in Aspen Plus® with experimental data including amine volatility, heat capacity, CO_2 solubility, and amine pK_a over a range of amine concentration and CO_2 loading.

4.2.1 Modeling stripper with updated MEA model

Van Wagener (2011) predicted the stripper performance for 9 m MEA using the thermodynamic model developed by Hilliard (Hilliard, 2008). The Hilliard model tends to overestimate the partial pressure of CO_2 (P^*_{CO2}) as amine concentration and temperature increase. The error can have significant effect on predicting the stripper pressure and the overall energy performance. "Phoenix" is an updated model that has fixed the problem and was regressed by including more high temperature data. It showed an adequate fit that matches experimental data and can predict the partial pressure of CO_2 over the temperature range from 40 to 160 °C (Plaza, 2011). Figure 4.1 compares the partial pressure of CO_2 predicted by the two models. The predicted P^*_{CO2} by the Hilliard model is almost twice that predicted by the Phoenix model at 120 °C where the stripper is typically operated for MEA. The stripper pressure at 120 °C can be over-predicted by 1 to 4 bar in the lean loading range as shown in Figure 4.2. The over-prediction of P^*_{CO2} not only

underestimated the compression work and the stripping steam heat but also misjudged the optimum lean loading. This work will demonstrate the energy performance of alternative strippers with an updated model for MEA.

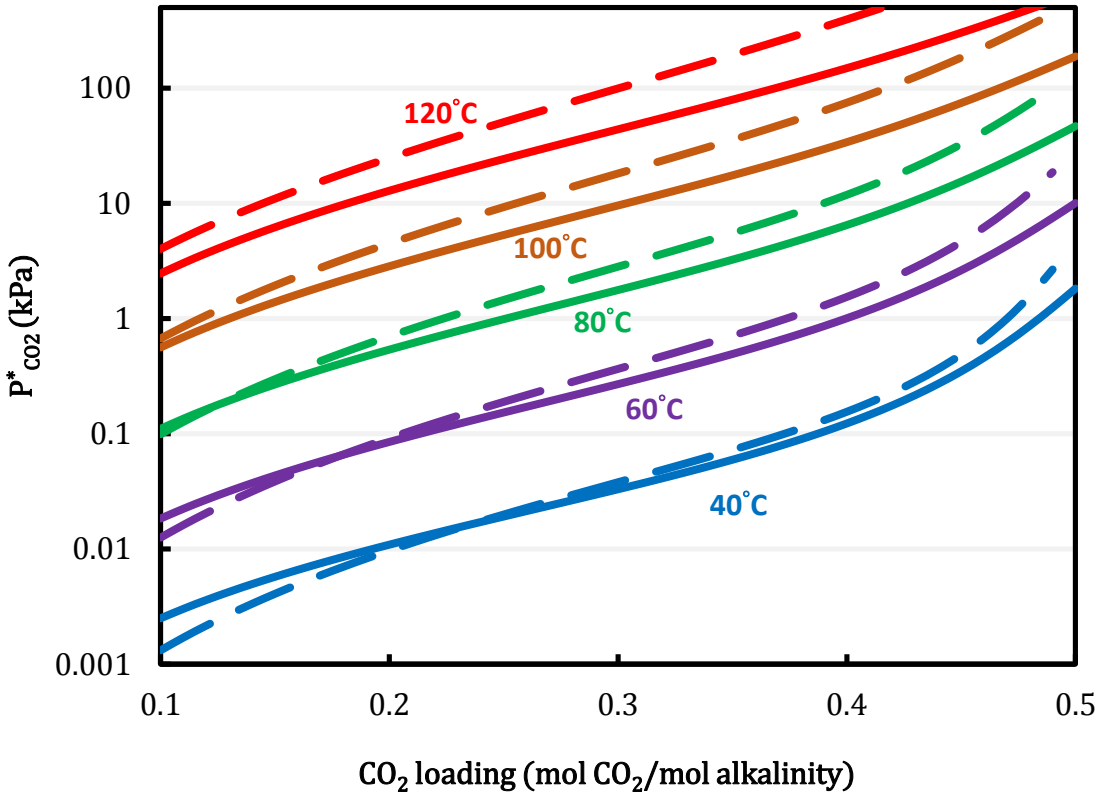

Figure 4.1: CO_2 partial pressure predicted by Hilliard model (dashed line) and Phoenix model (solid line).

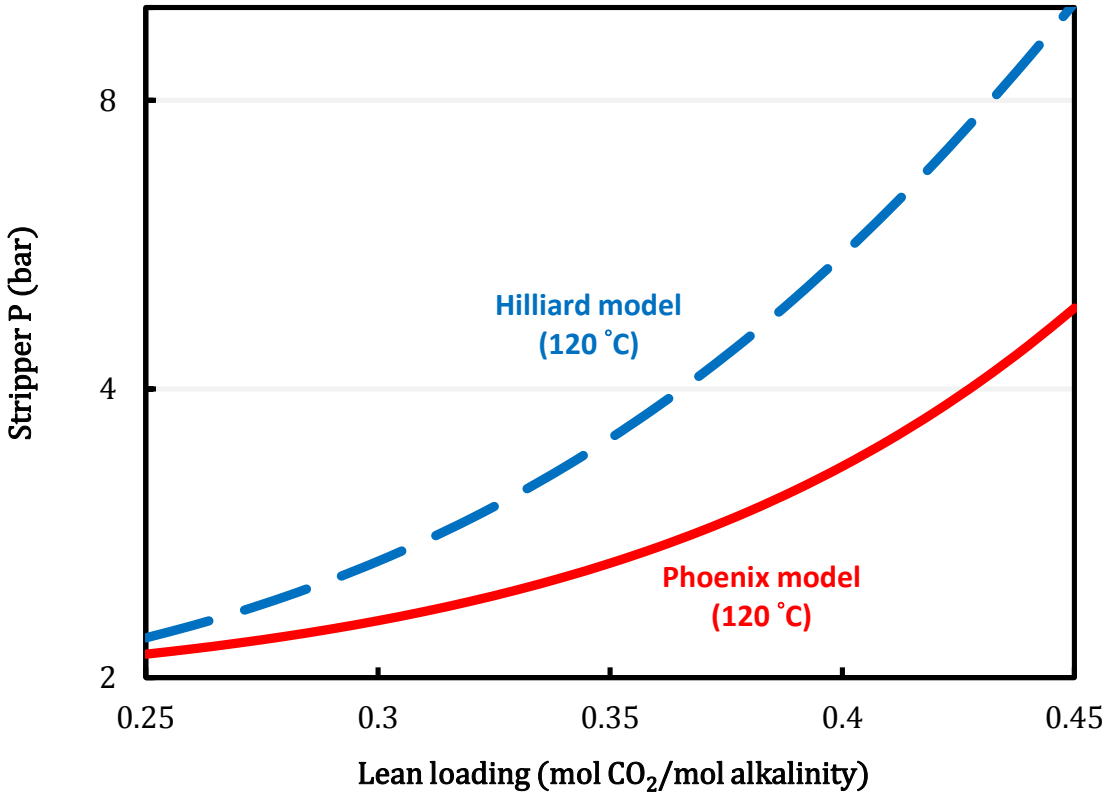

Figure 4.2: Over-predicted stripper pressure by Hilliard model at 120 °C.

4.2.2 Stripping steam for PZ and MEA

The amount of stripping steam generated will be determined by the vapor-liquid equilibrium between CO_2, water, and amine at high temperature. Figure 4.1 shows the mole fraction of CO_2 in the vapor phase at stripper temperature predicted by Aspen models®. The vapor phase consists of CO_2 and steam since amine is relatively less volatile and its mole fraction is lower than 1%. The CO_2 product coming up from the reboiler will contain 20–80% stripping steam before being counter-currently contacted with solvent in the stripper.

As indicated by Equation 1.4, the selectivity of CO_2 and steam can be improved by higher heat of absorption and operating temperature. Even though MEA can only be

operated at 120 °C, it still provides a relatively higher CO_2 mole fraction than PZ at 150 °C since it has a higher heat of absorption. Operating at a higher lean loading will significantly reduce the stripping steam but the lean loading also has impact on other contributors to energy use. Exploring optimum lean loading that minimizes the total equivalent work will compromise between these energy tradeoffs.

$$\frac{P_{CO_2}{}^*(T)}{P_{H_2O}{}^*(T)} = \frac{P_{H_2O}{}^*(T_{ref})}{P_{CO_2}{}^*(T_{ref})} exp\left[\left(\frac{\Delta H_{abs}-\Delta H_{vap}}{R}\right)\left(\frac{1}{T_{ref}}-\frac{1}{T}\right)\right] \quad (1.4)$$

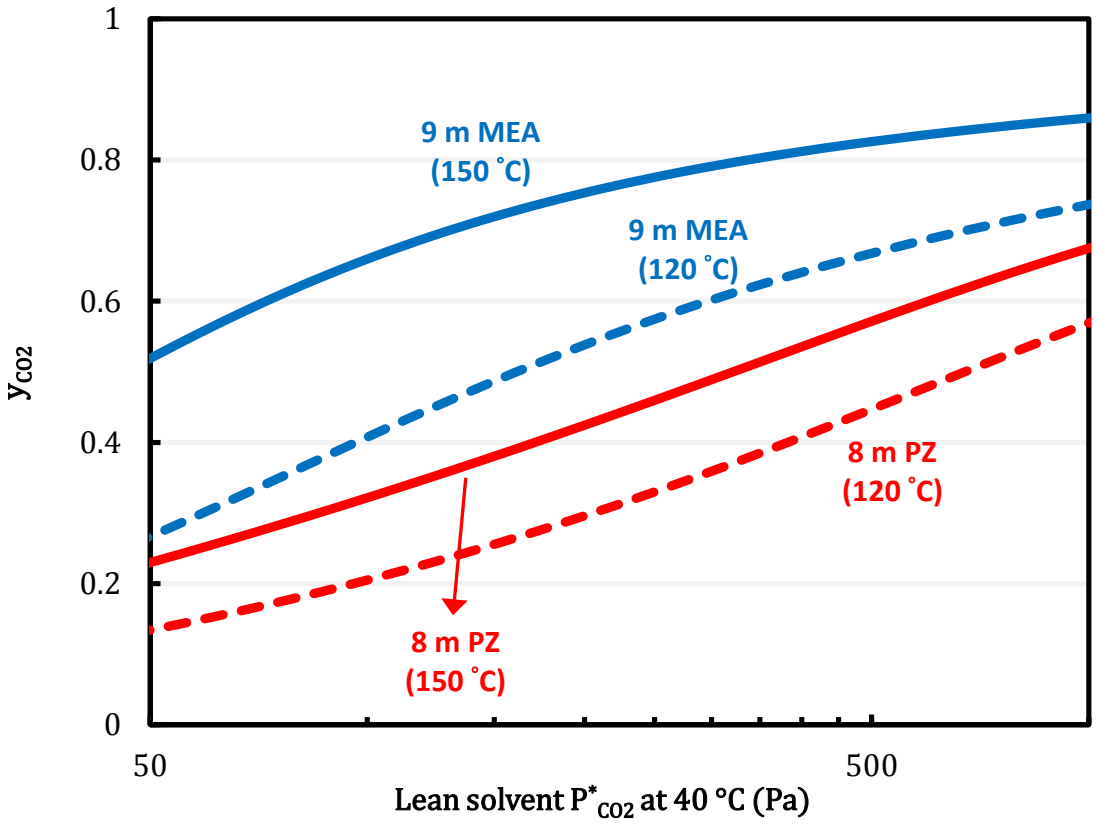

Figure 4.3: CO_2 mole fraction in the vapor phase with varied lean loading predicted by Independence for PZ and Phoenix for MEA.

4.2.3 Process specifications

Process specifications used in the simulations are shown in Table 4.2. Because the absorber was not simulated, typical rich solvent conditions including rich loading and

temperature were fixed as constants. The total packing height in the stripper is fixed at 2 m except for the configurations with two packing sections where 1 m is used for each section. The Bravo Correlation was used to calculate the mass transfer coefficient and interfacial area of the packing in the stripper (Bravo et al., 1985). Rich solvent was set at 46 °C with CO_2 loading (mol CO_2/mol alkalinity) of 0.5 for MEA and 0.4 for PZ according to typical results with an intercooled absorber (Plaza, 2011).

Reboiler temperature involves the tradeoff between energy efficiency and degradation rate. A reasonable compromise of 150 °C for PZ and 120 °C for MEA was used (Davis, 2009; Freeman, 2011). The steam temperatures used to calculate the equivalent work were 155 °C and 125 °C for PZ and MEA, respectively assuming a 5 K temperature approach.

The LMTD of the heat exchanger was calculated rigorously as described in Chapter 2. For the cross exchanger and the interheated exchanger, the LMTD was specified as 5 K. For the cold rich exchanger, which has poorer heat transfer between vapor and liquid, the LMTD was set at 20 K.

Table 4.2: Process simulation specifications.

Solvent	8 m PZ	9 m MEA
Process modeling tool	Aspen Plus® v7.3	
Thermodynamic model	Independence	Phoenix
Rich loading (mol CO_2/mol alkalinity)	0.40	0.50
Reboiler T (°C)	150	120
Steam T (°C)	155	125
Stripper packing	2 m Mellapak 250X	
Correction factor for packing interfacial area	1	
Rich solvent T (°C)	46	
Cross exchanger LMTD (K)	5	
Cold rich exchanger LMTD (K)	20	
Interheated exchanger LMTD (K)	5	

4.3 PROCESS DESCRIPTIONS

4.3.1 Simple stripper

The simple stripper shown in Figure 4.4 is the base case. The rich solvent is preheated in the cross exchanger and then sent to the top of stripper. The hot lean solvent from the reboiler is returned to the absorber through the cross exchanger. The hot CO_2 rich vapor from the top of stripper is cooled to 40 °C in the overhead condenser with loss of the latent heat of the excess water vapor.

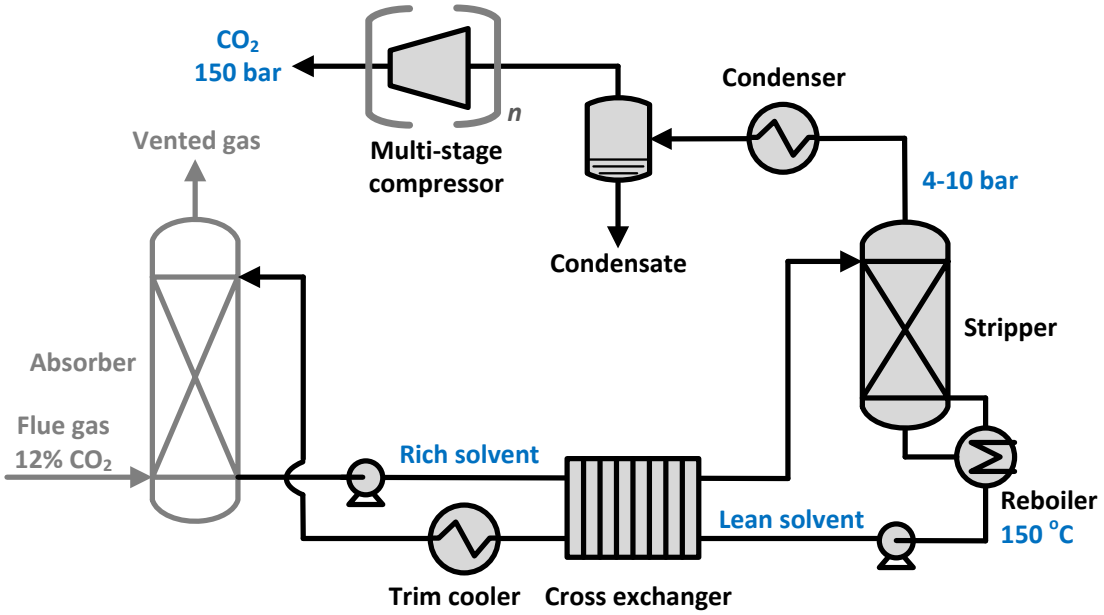

Figure 4.4: Simple stripper.

4.3.2 Conventional alternatives

4.3.2.1 Lean vapor compression (LVC)

The lean vapor compression (Figure 4.5) can reduce the stripping steam heat by operating the stripper at a higher pressure at a given lean loading compared to the simple stripper. The hot lean solvent is flashed in a flash tank at lower pressure. The flashed vapor is then pressurized by the lean vapor compressor, and sent to the bottom of the packing section in the stripper. The stripper serves as a direct contact cooler that recovers the latent heat of steam by a cooler stripper feed. The lean vapor compression was demonstrated in pilot plant tests and showed the savings of reboiler duty can be up to 20% (Knudsen et al., 2011).

In this work the pressure ratio of the lean vapor compressor for each lean loading will be optimized to minimize the total equivalent work. With a high pressure ratio, less stripping steam heat will be lost in the higher pressure stripper but the lean vapor

compression work will increase. The additional lean vapor compression work will be included in the total equivalent work.

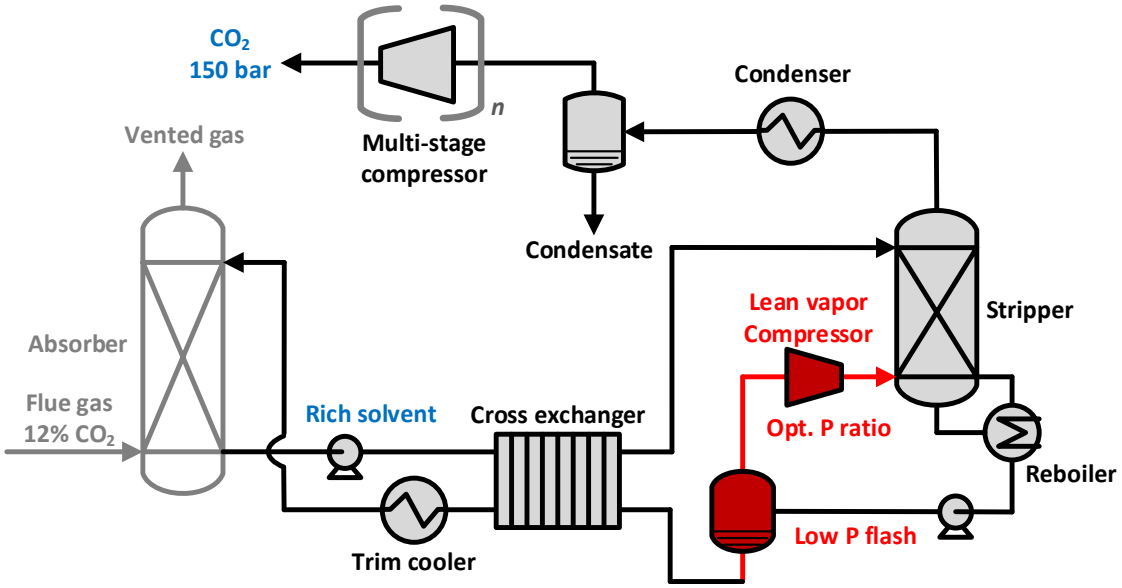

Figure 4.5: Lean vapor compression.

4.3.2.2 Interheated stripper

The interheated stripper was proposed by Leites (1993) and has been studied by Rochelle et al. (Oyenekan et al., 2007; Van Wagener et al., 2011). All the solvent is extracted from the middle of stripper, heated by the hot lean solvent in the interheated exchanger, and sent back to next section of the stripper. Van Wagener showed that the interheated stripper offers the best energy savings among several alternatives including two-stage flash, double matrix, and multi-pressure using MEA and PZ.

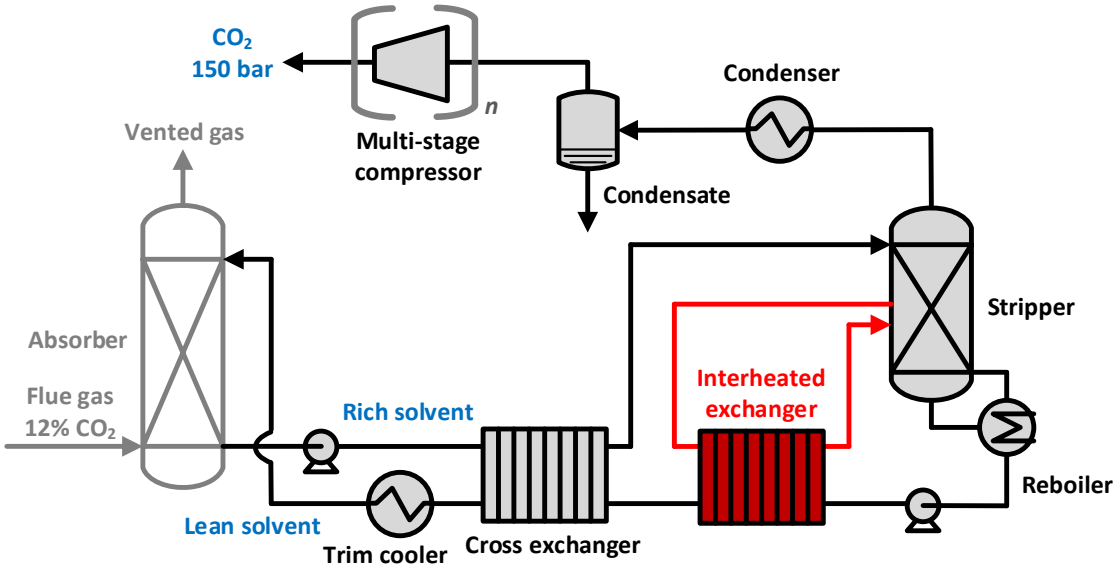

Figure 4.6: Interheated stripper.

4.3.2.3 Cold rich bypass

Figure 4.7 shows the simple stripper with cold rich bypass. A portion of the cold rich solvent is bypassed and sent to the top of the stripper without being heated by the cross exchanger. The bypassed solvent will be preheated in the stripper by condensing the stripping steam out of the CO_2 vapor. A pilot plant test in UT Austin applied the cold rich bypass to a two-stage flash stripper and showed over 20% of heat duty reduction (Madan et al., 2013). The concept can be extended by extracting the rich solvent at different temperature levels and feeding into appropriate locations in the stripper to match the heat and mass transfer driving force. In theory the stripper column can approach reversible operation if infinite feeds of rich solvent are applied. However, a diminishing return of energy savings was observed with an increasing number of bypasses and more stripper packing is required to fully realize the benefits (Madan, 2013).

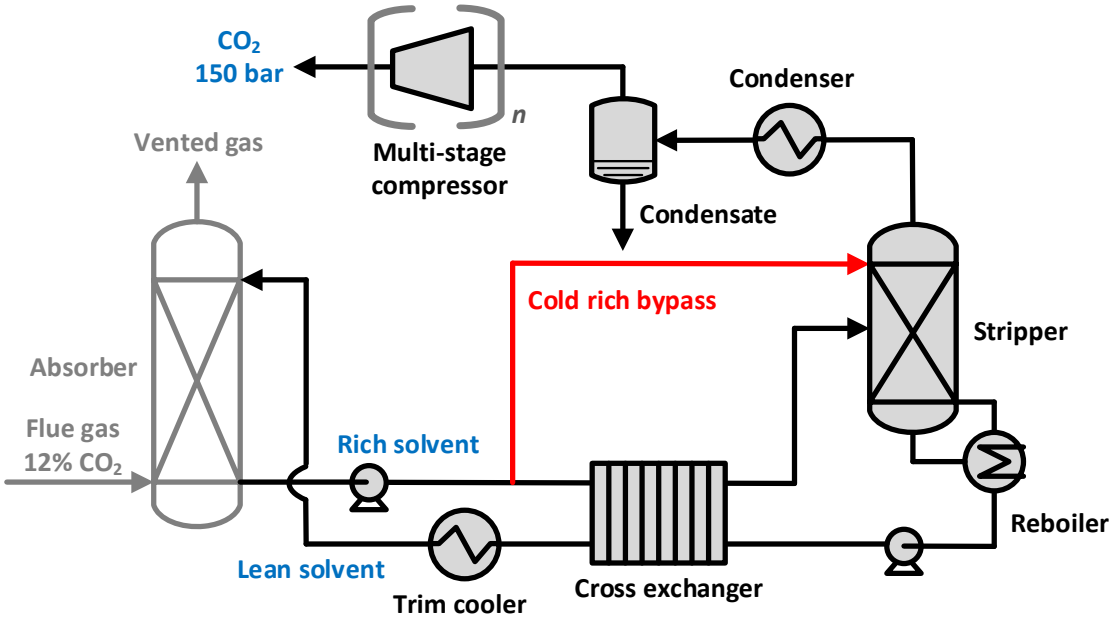

Figure 4.7: Simple stripper with cold rich bypass.

4.3.3 Rich exchanger bypass strategy

4.3.3.1 Simple stripper with rich exchanger bypass

The rich exchanger bypass strategy is proposed in this work to improve the cold rich bypass configuration by avoiding CO_2 re-absorption in the stripper. Figure 4.8 shows the simple stripper with rich exchanger bypass. An exchanger is used to recover the stripping steam heat instead direct contacting with the CO_2 vapor in the stripper. After being heated, the bypass rich solvent is mixed with the hot rich solvent and fed to the top of the stripper. The cold rich bypass rate will be optimized with a minimum total equivalent work.

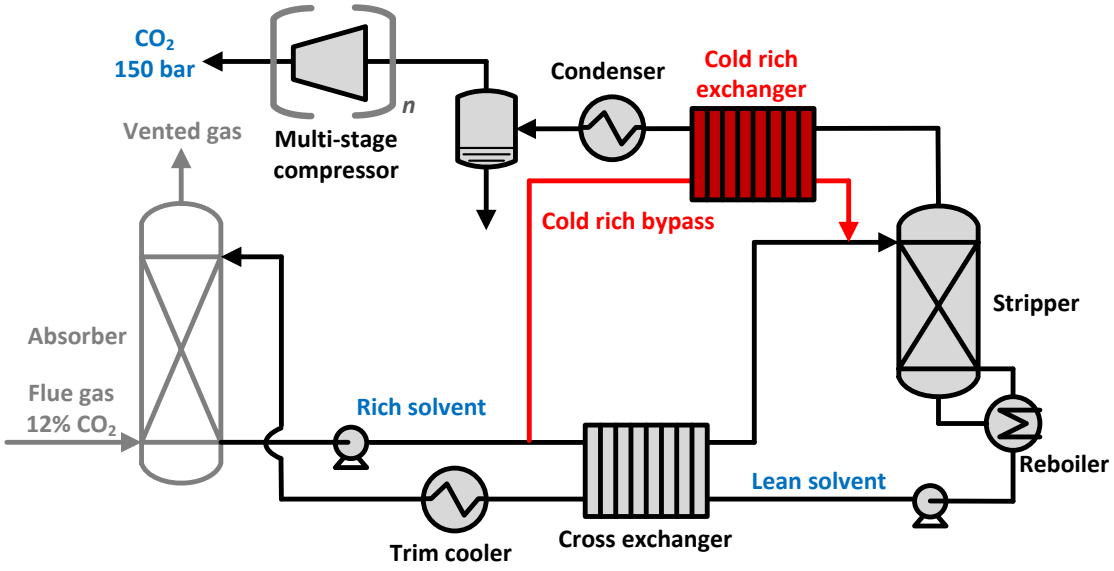

Figure 4.8: Simple stripper with cold rich exchanger bypass.

4.3.3.2 Advanced reboiled stripper (ARS)

Figure 4.7 shows the advanced reboiled stripper proposed in this work. A combination of the rich exchanger bypass and the warm rich bypass is applied. The warm rich bypass is drawn from the cross heat exchanger and fed to the top of stripper. The temperature was selected as the bubble point temperature, which will maximize the equilibrium partial pressure of CO_2 and increase the mass transfer driving force for CO_2 and water transfer. The cold rich solvent serves as a low temperature heat sink to recover the rest of the stripping steam heat while avoiding CO_2 re-absorption. As discussed in Chapter 3, the cold and warm rich bypass also help relax the temperature pinch in the cross exchanger.

The combination of cold and warm rich bypass is expected to work more efficiently. The optimized cold and warm rich bypass rate will maximize the potential benefits from the stripping steam heat recovery, the CO_2 stripping performance in the stripper column, and the cross exchanger performance.

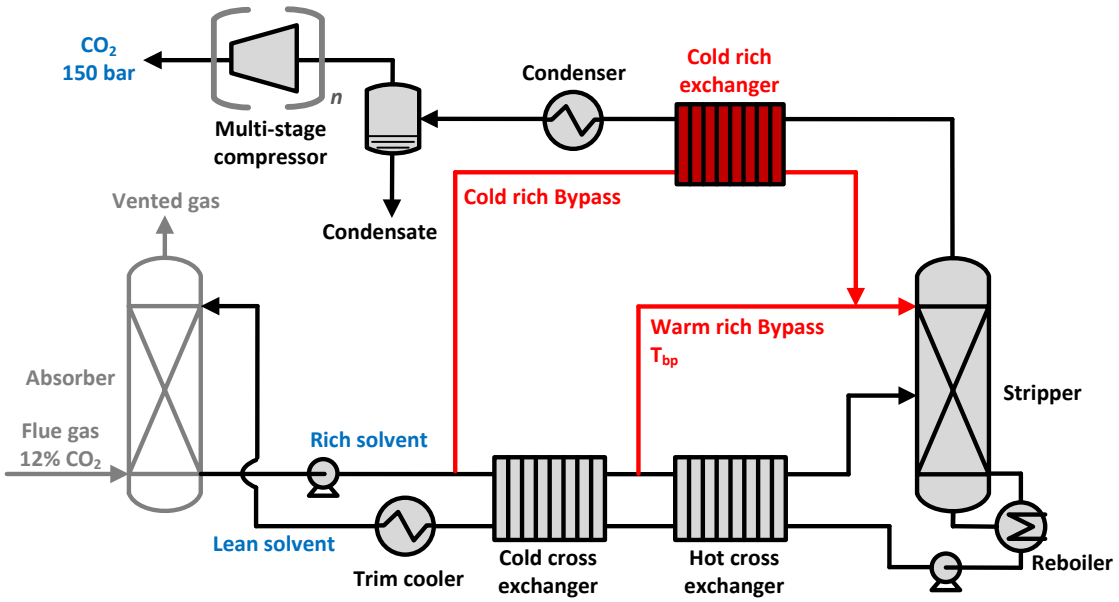

Figure 4.9: Advanced reboiled stripper (ARS).

4.3.3.3 Advanced flash stripper (AFS)

In the advanced flash stripper (Figure 4.10), the reboiler is replaced by a convective steam heater in order to minimize the residence time at higher temperature, where the amine tends to thermally degrade the most. The rich solvent will be heated by the steam heater and the vapor and liquid will be separated in the stripper sump. The separated vapor will go up along the stripper and counter-currently contacted with the warm rich bypass while condensing stripping steam.

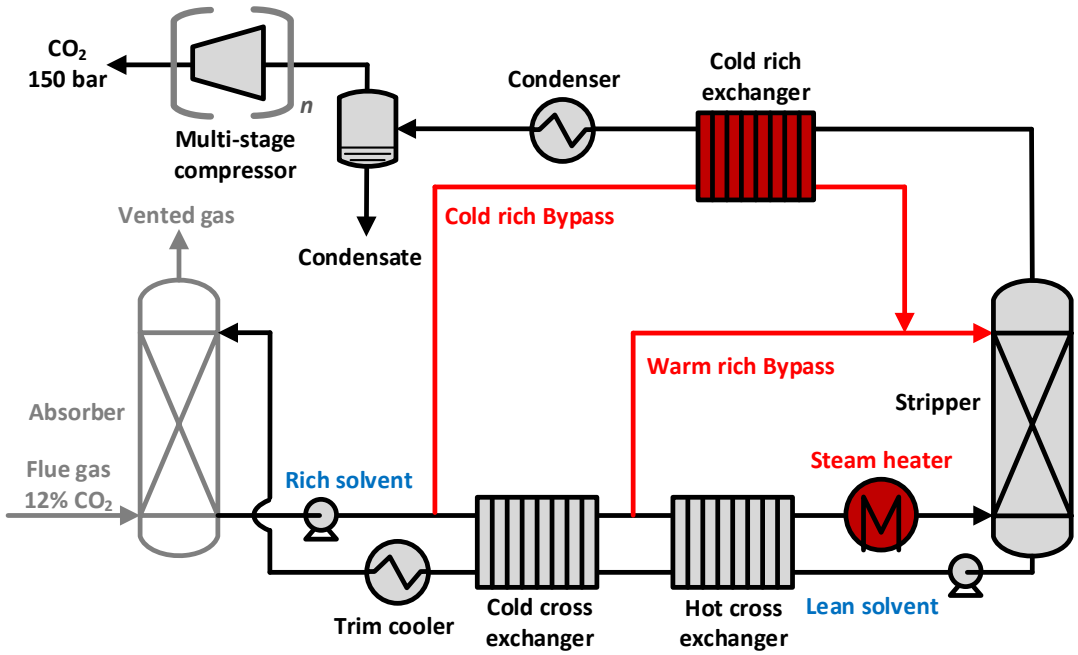

Figure 4.10: Advanced flash stripper (AFS).

4.4 Results and Discussions

4.4.1 Tradeoffs of optimum lean loading

Figures 4.11 and 4.12 compare the total equivalent work of alternative strippers at varied lean loading using 8 m PZ and 9 m MEA, respectively. The optimum lean loading is around 0.28–0.30 for PZ and 0.36–0.38 for MEA. Results at optimum lean loading are summarized in Tables 4.3 and 4.4.

The lean loading is one of the most important operating parameters that affect the energy performance. As lean loading varies, energy tradeoffs involve the stripping steam heat, sensible heat, compression work, and pump work. Since the rich loading is constant in the simulations, the difference between the lean and the rich loading determines the cyclic capacity and the solvent circulation rate. Higher lean loading can reduce the stripping steam heat and the compression work by enhancing the partial pressure of CO_2, but the sensible heat increases due to reduced solvent capacity.

4.4.2 Energy performance of conventional alternatives

The conventional alternatives including the lean vapor compression, the cold rich bypass, and the interheated stripper provide 4–7% energy savings compared to the simple stripper. The improvement is limited at higher loading because the stripping steam is suppressed by higher partial pressure of CO_2. The interheated stripper has the best performance among the conventional alternatives previously proposed. Since a portion of the sensible heat from the hot lean solvent is already recovered in the interheated exchanger, the stripper feed becomes colder and results in a similar effect of warm rich bypass, which reduces the flashing at the top of the stripper.

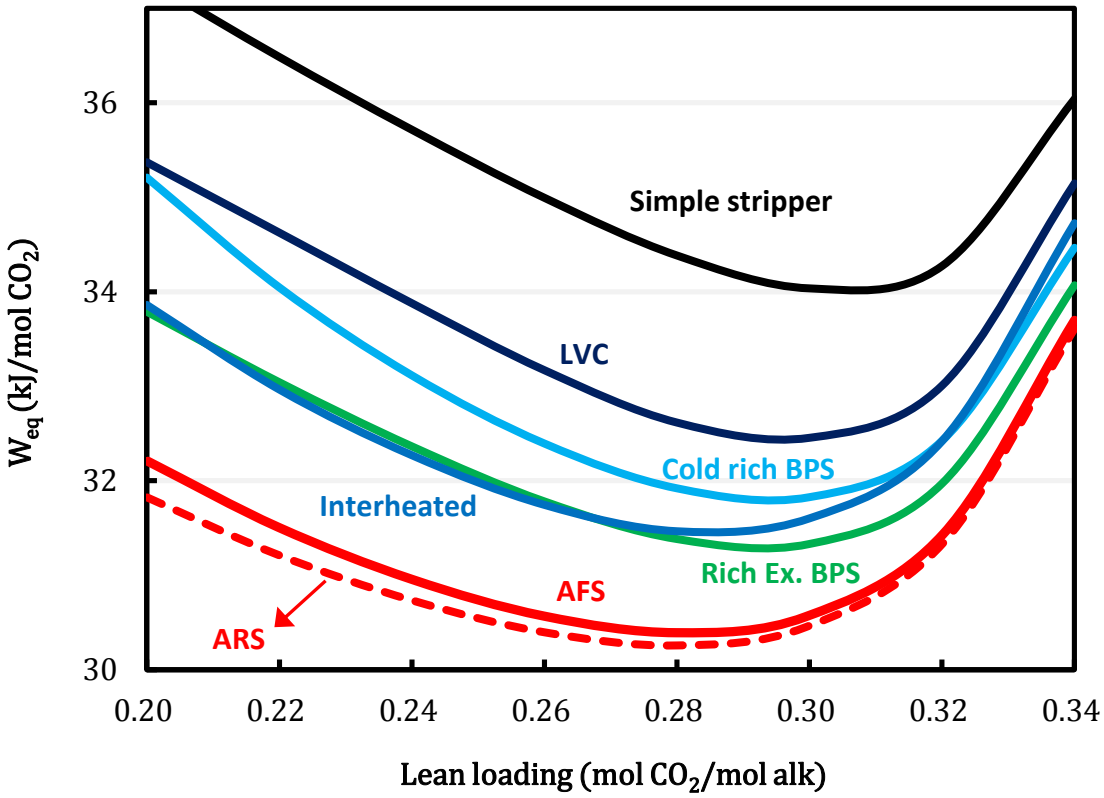

Figure 4.11: Comparison of total equivalent work of alternative strippers using 8 m PZ; rich loading: 0.4; cross exchanger ΔT_{LM}: 5 K; 2 m packing; correction for interfacial area: 1; reboiler T: 150 °C; optimum pressure ratio for LVC; optimum bypass rates.

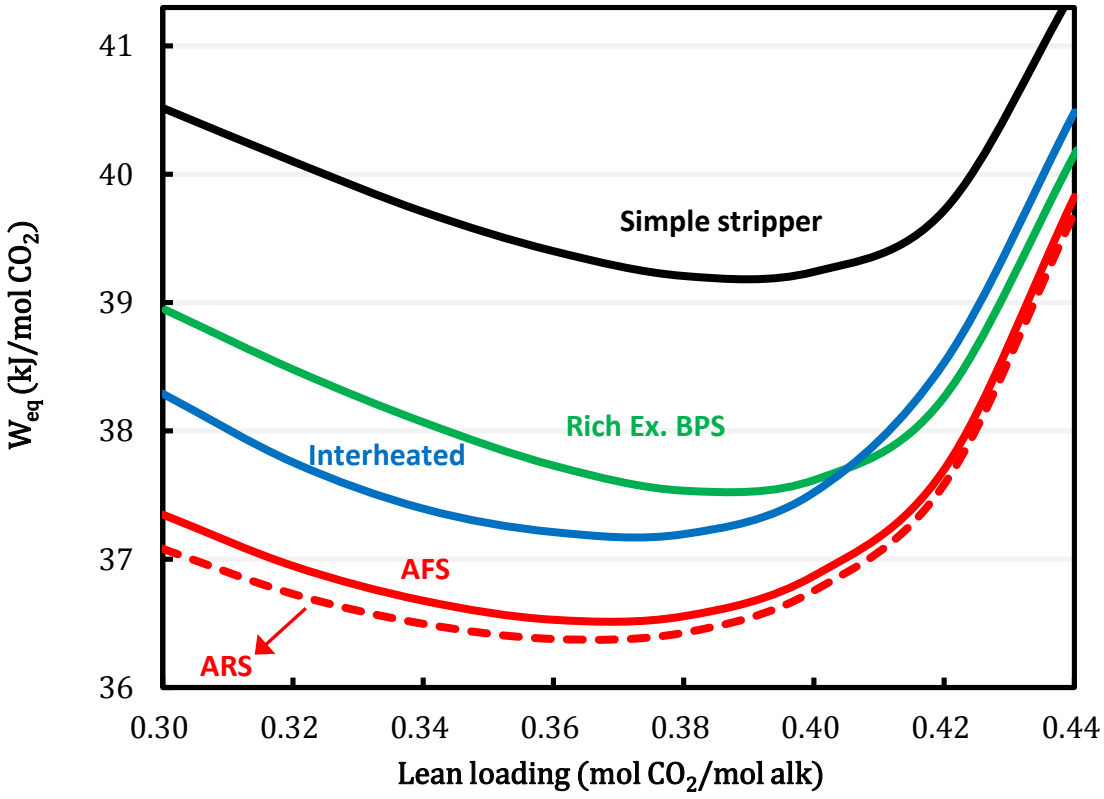

Figure 4.12: Comparison of total equivalent work of alternative strippers using 9 m MEA; rich loading: 0.5; cross exchanger ΔT_{LM}: 5 K; 2 m packing; correction for interfacial area: 1; reboiler T: 120 °C; optimum bypass rates.

Table 4.3: Optimum results for 8 m PZ; rich loading: 0.4; cross exchanger ΔT_{LM}: 5 K; 2 m packing; correction for interfacial area: 1; reboiler T: 150 °C; optimum pressure ratio for LVC; optimum bypass rates.

	Opt. ldg (mol/mol)	P_{strp} (bar)	CBPS (%)	WBPS (%)	Energy (kJ/mol CO_2)			
					Q_{reb}	W_{heat}	W_{comp}	W_{eq}
Simple stripper	0.30	8.6	-	-	105	25.4	7.4	34.0
LVC	0.30	8.6	-	-	98	23.6	7.7	32.5
Cold rich BPS	0.30	8.6	5	-	96	23.2	7.4	31.8
Interheated stripper	0.28	7.4	-	-	94	22.7	7.9	31.5
Rich Ex. BPS	0.30	8.6	7	-	94	22.7	7.4	31.3
ARS	0.28	7.4	6	15	89	21.5	7.9	30.2
AFS	0.28	7.4	6	20	89	21.6	7.9	30.3

Table 4.4: Optimum results for 9 m MEA; rich loading: 0.5; cross exchanger ΔT_{LM}: 5 K; 2 m packing; correction for interfacial area: 1; reboiler T: 120 °C; optimum bypass rates.

	Opt. ldg (mol/mol)	P_{strp} (bar)	CBPS (%)	WBPS (%)	Energy (kJ/mol CO_2)			
					Q_{reb}	W_{heat}	W_{comp}	W_{eq}
Simple stripper	0.38	3.0	-	-	144	27.7	11.0	39.2
Interheated stripper	0.38	3.0	-	-	134	25.7	11.0	37.2
Rich Ex. BPS	0.38	3.0	10	-	136	26.0	11.0	37.5
ARS	0.36	2.8	8	24	129	24.7	11.3	36.4
AFS	0.36	2.8	7	24	129	24.9	11.3	36.5

4.4.3 Rich exchanger bypass

The drawback of the cold rich bypass is that the CO_2 has potential to be re-absorbed back to the solvent since the partial pressure of CO_2 at the cold rich temperature is low. Figure 4.13 shows the McCabe-Thiele plot of the stripper using the cold rich bypass. The

CO_2 loading increases from the rich loading at 0.4 to 0.44 at the top by absorbing CO_2 from the vapor. The highlighted area indicates the re-absorption region where the CO_2 transfer is from vapor to solvent. Then the CO_2 loading gradually reduces to the specified lean loading 0.28 at the bottom. Additional heat duty is required to regenerate the CO_2 that was unnecessarily re-absorbed. The rich exchanger bypass addresses the problem while still providing an adequate heat sink for heat recovery.

Herrin proposed to use a heat exchanger to preheat the hot rich solvent by the overhead vapor (Herrin, 1989). However, rich solvent at high temperature does not have the issue of CO_2 re-absorption. Feeding the hot rich solvent into the stripper should give a better energy performance since the CO_2 can be stripped at the same time while the stripping steam is condensed. The cold rich solvent is a better candidate to recover the stripping steam heat using a heat exchanger.

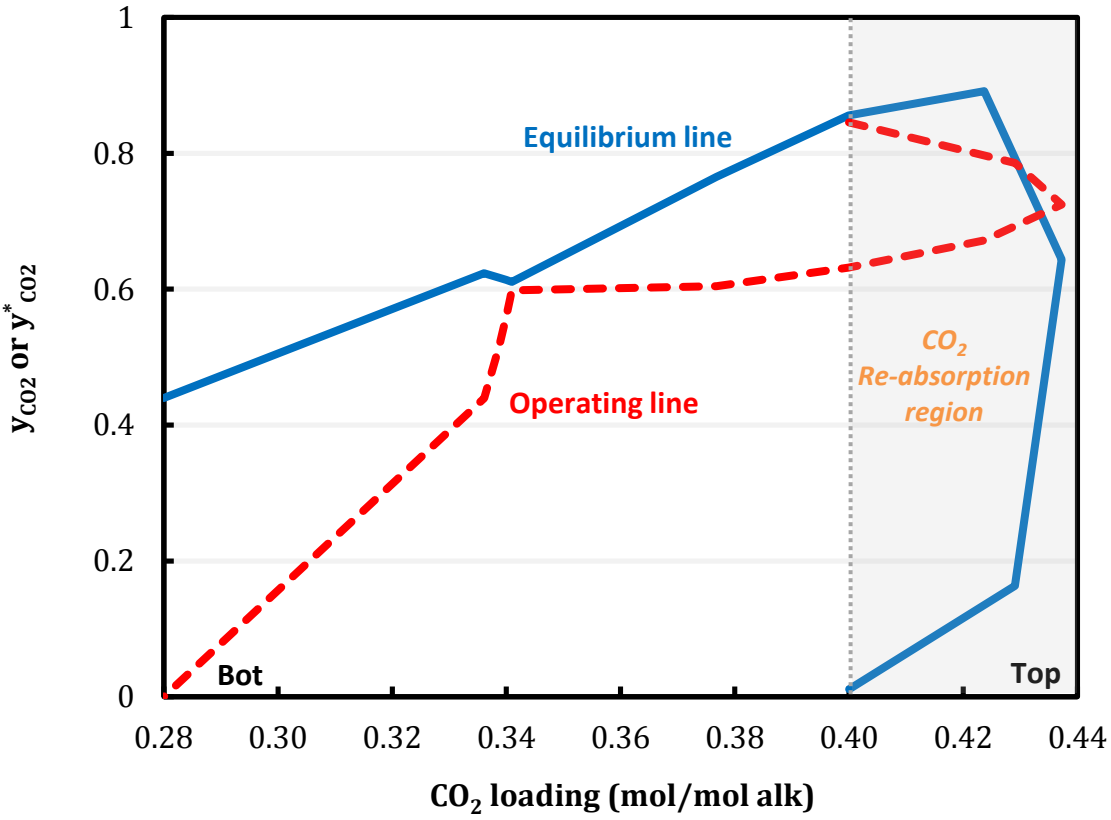

Figure 4.13: McCabe-Thiele plot of cold rich bypass configuration using 8 m PZ; rich loading: 0.5; lean loading; 0.28; cross exchanger ΔT_{LM}: 5 K; 2 m packing; correction for interfacial area: 1; reboiler T: 150 °C; optimum bypass rates.

The cold rich exchanger bypass shows 2–4% less total equivalent work compared the cold rich bypass using PZ. It should be noted that the performance of the heat recovery depends on the specified cold rich exchanger LMTD and stripper packing height. The reboiler duty can be reduced with a smaller temperature approach or more packing by increasing heat transfer area. An optimum design should be determined by economic analysis that considers the capital cost and energy cost together.

4.4.4 Advanced reboiled/flash stripper

The proposed advanced reboiled/flash stripper gives the best energy performance among all the alternatives. The heat duty/total equivalent work is reduced by 15%/11% and 10%/7%, respectively for PZ and MEA at optimum lean loading. The ARS is slightly better than the AFS since it contains an extra stripper feed, which makes the stripper operate more counter-currently. The difference of the total equivalent work is around 1%.

The steam temperature was assumed as 155 °C for PZ in the equivalent work calculation for the AFS. However, the actual steam temperature will depend on the actual solvent temperature in the steam heater. Since 150 °C was specified at the stripper sump, where the hot rich solvent and solvent bypass mix, the solvent temperature at the steam heater outlet must exceed 150 °C. Adjusted steam temperature that takes account of the actual operating temperature of the steam heater is calculated.

Table 4.5 shows the adjusted steam temperature needed to satisfy a 5 K LMTD and compares the total equivalent work that calculated by assumed steam temperature (155 °C) and by adjusted steam temperature. When the bypass rate becomes higher as lean loading decreases, the main rich solvent stream needs to be heated to a higher temperature by the steam heater to achieve 150 °C at the stripper sump. The adjusted steam temperature is 153–157 °C in the lean loading range and results in less than 1% difference of total equivalent work.

Table 4.5: Adjusted steam temperature and total equivalent work for AFS using 8 m PZ; rich loading: 0.4; cross exchanger ΔT_{LM}: 5 K; 2 m packing; correction for interfacial area: 1; reboiler T: 150 °C; optimum bypass rates.

Lean loading	**0.20**	**0.24**	**0.28**	**0.32**
Total bypass rate (%)	61	44	26	14
Solvent T in (°C)	145	142	141	141
Solvent T out (°C)	155	154	153	151
Adjusted steam T (°C)	157	155	154	153
W_{eq} at T_{stm}=155 °C (kJ/mol CO_2)	32.2	31.0	30.4	31.4
W_{eq} at adjusted T_{stm} (kJ/mol CO_2)	32.5	31.0	30.3	31.1

4.4.5 Effect of packing height

The sensitivity of stripper packing height is tested for the simple stripper and the AFS in Figure 4.14. The AFS can obtain more energy savings by increasing packing height than the simple stripper. Increasing the stripper packing height enhances the stripper performance and leads to less cold rich bypass. Little energy reduction is obtained as the packing height increases from 5 to 10 m, which implies the driving force in the stripper is almost pinched. The advanced reboiled/flash stripper with two adjustable bypasses is a flexible system that can maximize energy performance at various design specifications and operating conditions.

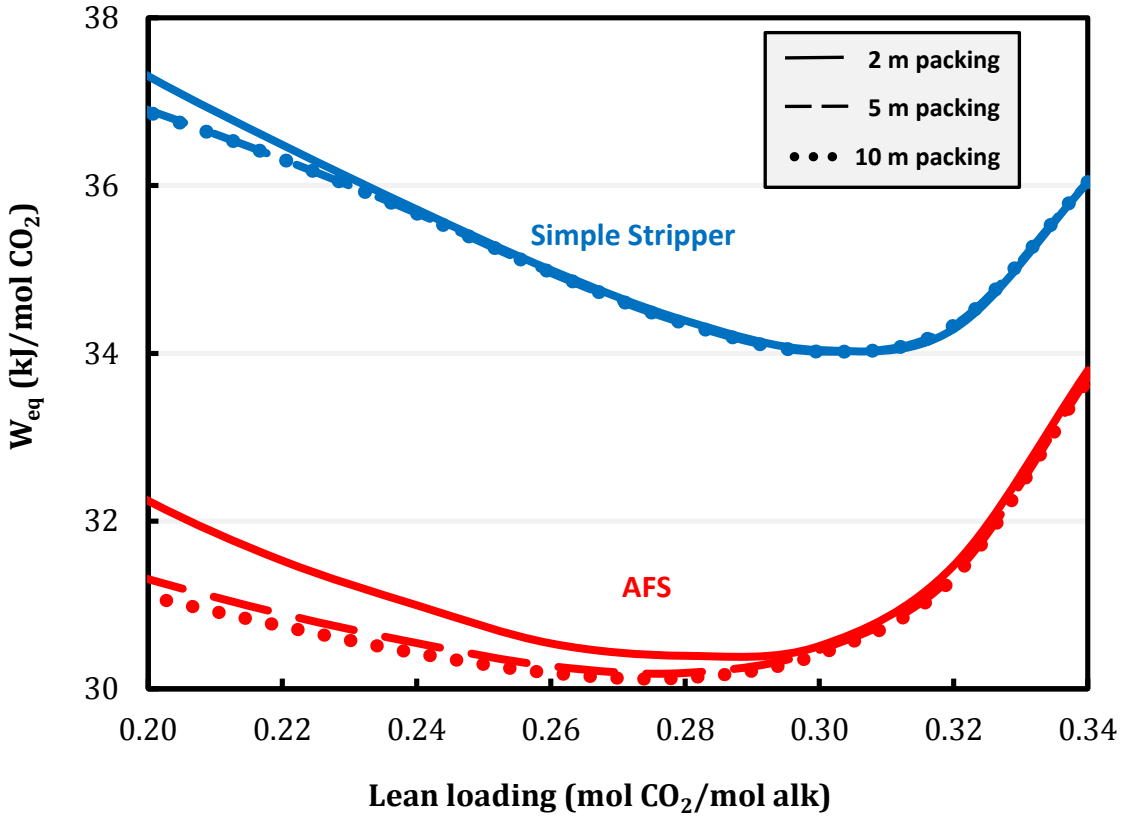

Figure 4.14: Total equivalent work with varied stripping packing height using 8 m PZ; rich loading: 0.4; cross exchanger ΔT_{LM}: 5 K; correction for interfacial area: 1; reboiler T: 150 °C; optimum bypass rates.

4.4.6 Effect of warm rich bypass temperature

A sensitivity analysis of the warm rich bypass temperature is tested in Figure 4.15. The base case is at bubble point and two other testing cases were specified at 5 K and 10 K subcooling. The bypass rates were optimized for each case. In real operations, the temperature will be determined by the cross exchanger performance. A colder stripper feed might result in CO_2 re-absorption. However, since the warm rich bypass is mixed with the cold rich bypass before entering the stripper, the AFS has the degree of freedom to self-adjust the actual feed temperature by the mixing ratio and reduces the impact of re-

absorption. The total equivalent work at bubble point outperforms the subcooling cases at lower lean loading but the difference is less than 3%.

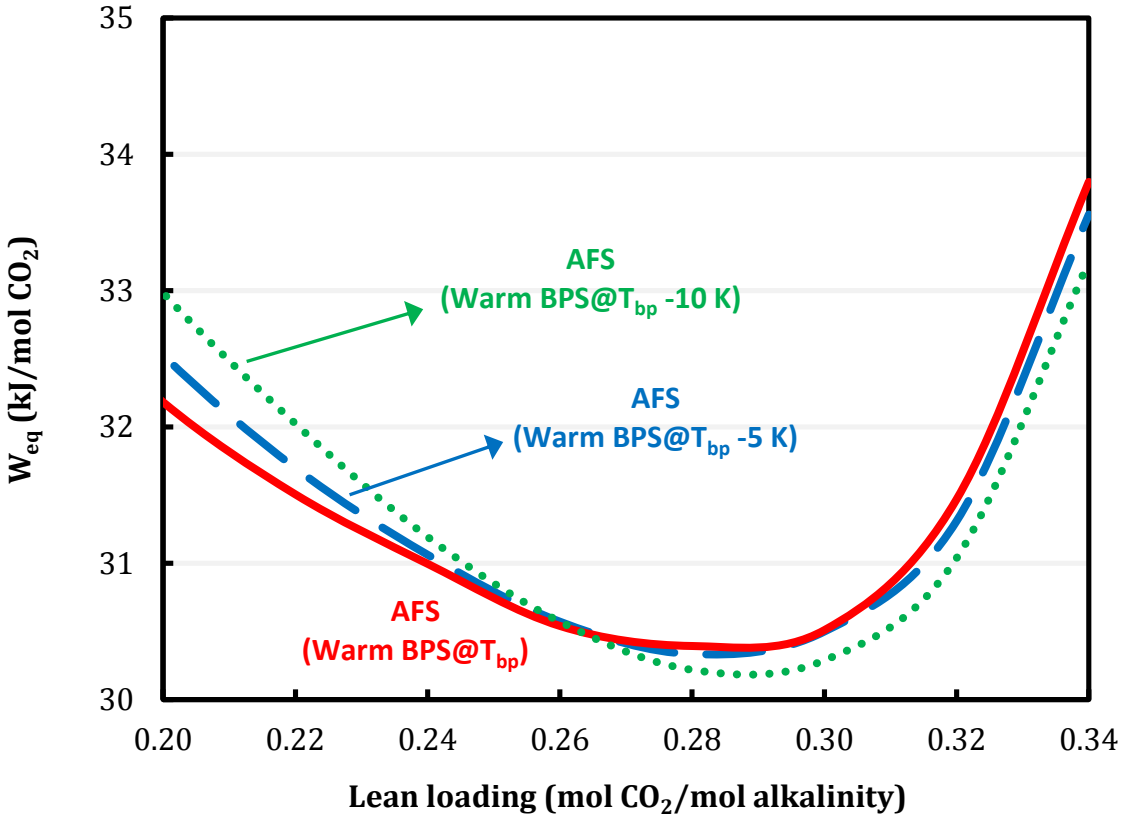

Figure 4.15: Total equivalent work with varied warm rich bypass temperature using 8 m PZ; rich loading: 0.4; cross exchanger ΔT_{LM}: 5 K; 2 m packing; correction for interfacial area: 1; reboiler T: 150 °C; optimum bypass rates.

4.5 Overall comparisons

Figure 4.16 compares the the total equivalent work of simple stripper, conventaionl stripper alternatives and the AFS, and the ARS proposed in this work. Most the configurations target at reducing stripping steam heat but using different ways. A major reduction can be seen between the simple stripper and any alternatives. The AFS and the ARS provide another break through. The ARS that has an additional stripper feed can give additional improvement but is marginal. The diminishing returns suggests that

further improvement by process modifications will be limited. Overall, the AFS reduces the total equivalent work by 13% using 8 m PZ.

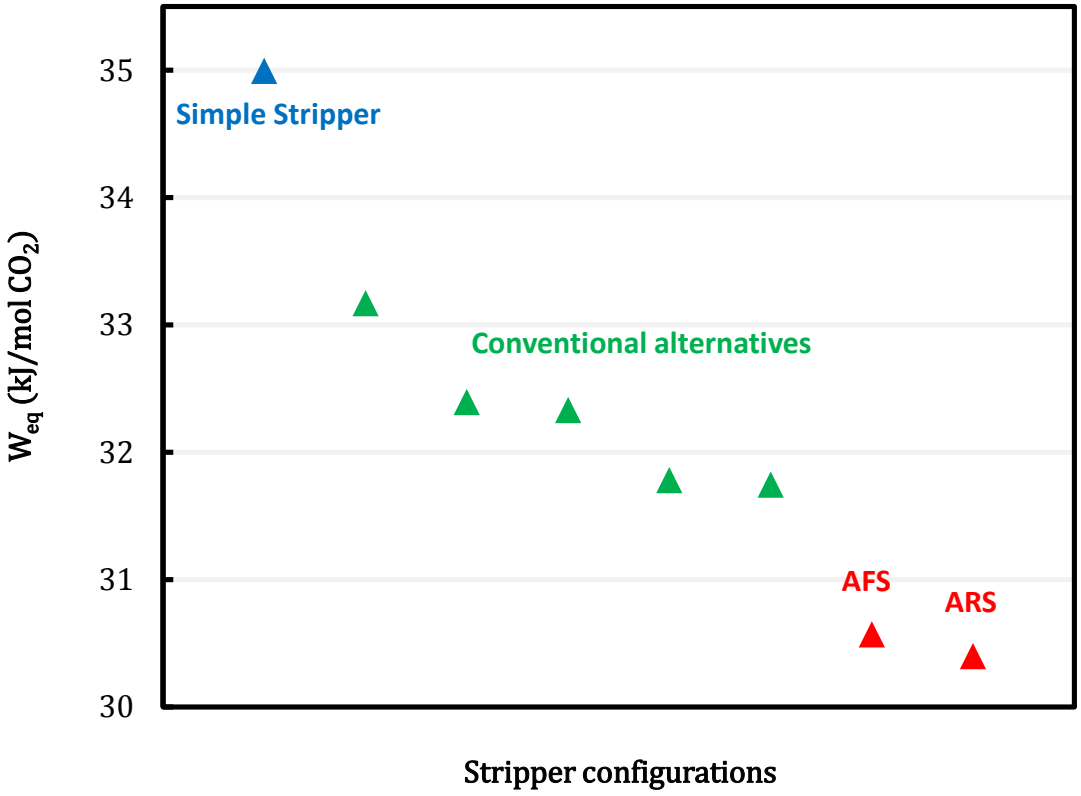

Figure 4.16: Total equivalent work of alternative stripper configurations; 8 m PZ; lean loading: 0.26; rich loading: 0.4; cross exchanger ΔT_{LM}: 5 K; 2 m packing; correction for interfacial area: 1; reboiler T: 150 °C; optimum bypass rates.

4.6 CONCLUSIONS

- The cold rich bypass configuration was improved by the rich exchanger bypass to avoid CO_2 re-absorption using a heat exchanger.
- Compared to other alternative strippers that have been proposed to reduce the stripping steam heat, the advanced reboiled/flash stripper provides the best energy

performance. It uses 11% less total equivalent work with 8 m PZ and 7% less with 9 m MEA compared to the simple stripper.

- The optimum lean loading that minimizes the total equivalent work is 0.28–0.30 for 8 m PZ and 0.36–0.38 for 9 m MEA at constant rich loading. The energy improvement is more significant at lower lean loading where the stripping steam is excessive.
- The AFS needs to use a relatively higher steam temperature than the ARS when the bypass rate is high but the impact on the total equivalent work is less than 1% in a typical lean loading range.

Chapter 5: Pilot Plant Test of the AFS

5.1 INTRODUCTION

Pilot plant tests for advanced solvents and configurations are crucial as steppingstones to commercial-scale plants. Several studies have tested new solvents in pilot-scale experiments and show over 10% energy reduction compared to the standard solvent, 30 wt % MEA (Bumb et al., 2014; Knudsen et al., 2009; Mangalapally et al., 2012; Nakamura et al., 2014; Ohashi et al., 2011). Aqueous PZ has been considered a new standard solvent with twice the absorption rate and greater CO_2 capacity than MEA (Rochelle et al., 2011). PZ has the potential to minimize the energy requirement and environmental impact of CO_2 capture. 8 m PZ has been tested at the Separations Research Program (SRP) of The University of Texas at Austin (UT Austin) (E. Chen et al., 2013; Plaza et al., 2013; Van Wagener et al., 2013) and the Tarong CO_2 capture pilot plant in Australia (Cousins et al., 2015). The lowest reboiler duty in the Tarong test was 2.9 GJ/tonne CO_2, 15% lower than 30 wt % MEA using the same facility. The EVN power plant in Austria using 7 m PZ found 14% heat duty savings (Rabensteiner et al., 2015). 5 m PZ (30 wt %) has sparked interest since it has a wider solid solubility window, lower viscosity, and greater rate of CO_2 absorption than 8 m PZ (E. Chen et al., 2014). 5 m PZ has potential to be used at an over-stripping lean loading that gives greater CO_2 absorption rate, mass transfer driving force, and cyclic CO_2 capacity.

Previous work on alternative stripper configurations focused on process development evaluated by computational simulations but such configurations have rarely been demonstrated in pilot-scale experiments. The lean vapor compression and the interheated stripper have been applied in pilot plants using 30 wt % MEA with heat duty of 2.9–3.5 GJ/tonne CO_2 (Knudsen et al., 2011; Stec et al., 2015). UT Austin

demonstrated the two-stage flash with cold rich solvent bypass in 2011 and the heat duty was 2.7 GJ/tonne CO_2 using 8 m PZ (Madan et al., 2013).

Chapter 3 has shown that the advanced flash stripper (AFS) can effectively recover most of the stripping steam heat loss. A lower rich solvent flow rate in the cross exchanger will also help balance the flow heat capacity between the lean and the rich solvent, and relieve the temperature pinch. The improvement of energy performance comes from reducing the irreversibility in the overhead condenser, the stripper, and the cross exchanger.

The first pilot plant test of the AFS was carried out at UT Austin in March 2015, and lasted 3 weeks. The objectives of this campaign were to demonstrate reliable operation and energy performance using PZ. This work will present and interpret the pilot plant results. The "Independence" model for PZ developed by Frailie (Frailie, 2014) will be validated using pilot plant data and used to explore the optimum design and operating conditions.

5.2 OVERVIEW OF SRP PILOT PLANT

The CO_2 capture pilot plant is located at the Pickle Research Campus in north Austin, Texas. The integrated absorption and stripping process treats synthetic flue gas equivalent to a 0.1–0.2 MW coal-fired power plant, capturing around 3 tonne CO_2/day. A simplified flowsheet is shown in Figure 5.1.

The flue gas was synthesized by mixing air with the CO_2 recycled from the stripper overhead. The CO_2 inlet concentration is controlled by adjusting a CO_2 makeup flow rate. The absorber is packed with 6 meters of Raschig Super-Pak (RSP-250) structured packing divided into two beds. The solvent is intercooled between the two beds with the flexibility to turn the cooling on and off. The CO_2-rich solvent from the absorber is

pressurized by the rich solvent pump, preheated in the cross exchangers, and further heated in two steam heaters in series. The vapor and liquid are then separated in the flash tank. The CO_2 lean solvent is sent back to the absorber after being cooled in the cross exchangers and the trim cooler.

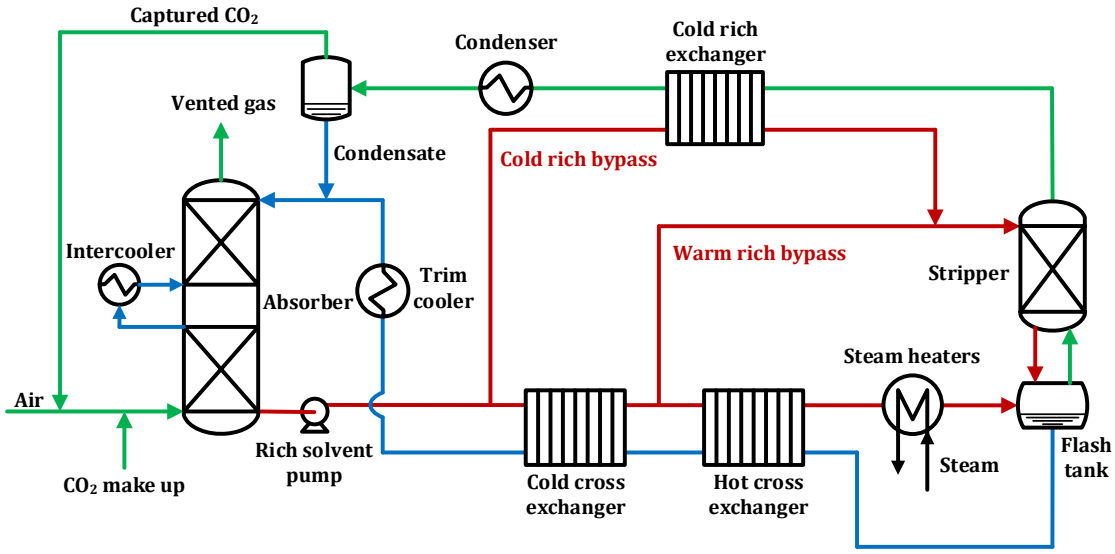

Figure 5.1: SRP CO_2 capture pilot plant with advanced flash stripper.

Two bypasses are extracted from the rich solvent, the cold rich bypass and the warm rich bypass. The cold rich bypass is preheated in the cold rich exchanger by the hot vapor from the stripper. The warm rich solvent is extracted between the warm and hot cross exchangers, mixed with the heated cold rich bypass, and sent to the top of the stripper. The warm rich solvent is counter-currently contacted with the vapor in the stripper, which is packed with 2 m of Raschig Super-Ring No. 0.3 (RSR no. 0.3) random packing. The rich solvent will condense a portion of water vapor from the CO_2 in the stripper and recover the latent heat since the inlet solvent temperature at the top is lower than a conventional simple stripper. Table 5.1 summarizes the column design and the operating conditions.

Table 5.1: Summary of column design and operating conditions.

Column design	
Absorber diameter (m)	0.43
Absorber packing type/height (m)	RSP-250/6.1
Stripper diameter (m)	0.15
Stripper packing type/height (m)	RSR no. 0.3/2
Operating conditions	
CO_2 in flue gas (%)	6 and 12
PZ (molality)	5 and 8
Flue gas rate (kg/hr)	1700–3500
Solvent rate (kg/hr)	700–1100
L/G (kg/kg)	2.3–4.9
Capture rate (%)	68–97
Stripper T (ºC)	135–149
Stripper P (bara)	4.2–7.0
Rich loading (mol CO_2/mol alkalinity)	0.20–0.27
Lean loading (mol CO_2/mol alkalinity)	0.35–0.41

The 3-week 2015 campaign included 17 runs with 5 m PZ and 4 runs with 8 m PZ. The test matrix is shown in Table 5.2, which included variations of flue gas rate, solvent flow rate, stripper temperature, stripper pressure, bypass rate, and intercooling on/off. The CO_2 concentration of the synthetic flue gas was controlled at 12% by manipulating the CO_2 make up flow, except in Run 19 which was at 6%. The flue gas to solvent ratio is 2.9–4.3 (kg/kg) and the CO_2 capture rate is 68–97%. The CO_2 lean loading was varied by manipulating the stripper pressure while the flash tank temperature was automatically controlled by adjusting the steam rate. The absorber performance determined the CO_2 rich loading, which directly affected the energy performance.

Table 5.2: 2015 SRP Pilot plant operating conditions using the AFS and PZ.

Run	PZ (m)	Flue gas rate (kg/hr)	Solvent rate (kg/hr)	Capture rate (%)	Cold BPS ratio (%)	Warm BPS ratio (%)	P_{strp} (bar)	T_{strp} (°C)
1	4.7	749	2265	85	8	38	4.2	140
2	4.9	744	2489	97	7	30	4.2	140
3	4.9	728	2491	94	10	37	5.9	149
4	4.9	753	2490	94	10	32	5.9	149
5	5.0	752	2491	94	10	32	5.9	149
6	5.0	730	2957	89	7	23	5.9	145
7	5.3	726	3442	80	6	19	5.9	145
8	5.1	736	3443	96	8	19	5.9	145
9	5.1	1042	3442	80	8	19	5.9	145
10	5.0	1059	3168	87	11	19	5.9	149
11	5.0	732	2262	89	10	31	5.9	149
12	4.9	730	3441	94	7	18	5.9	145
13	7.4	1039	3507	68	7	18	5.9	145
14	8.0	1041	3539	75	8	17	5.9	145
15	7.8	719	3534	93	8	17	5.9	145
16	8.0	740	2574	91	8	21	6.5	149
17	5.0	716	2482	93	11	28	6.0	149
18	5.0	717	2485	96	0	29	6.0	148
19	5.0	733	1721	92	6	41	4.2	135
20	4.9	737	2080	84	13	33	5.7	149
21	4.9	759	2507	75	5	23	7.0	149

The steady-state value of each operating condition was determined as the average over a 30-minute period. Lean and rich solvent samples were taken in each run. PZ was determined by manual acid titration of the lean solvent. Total CO_2 in the solvent was determined by manual titration in methanol and by estimation from on-line density measurements using the correlation developed by Freeman (Freeman et al., 2011). The second method shows more consistent lean loading at the same stripper temperature and pressure throughout the campaign and also gives better CO_2 mass balance closure (see Section 5.3.1). The density-predicted CO_2 loading is considered more reliable and will be used in this analysis as the measured CO_2 loading.

5.3 PILOT PLANT RESULTS

5.3.1 Material balance

The CO_2 mass balance around the stripper can be quantified by comparing the CO_2 regenerated on the gas side and the liquid side. The CO_2 regenerated on the gas side was measured from the stripper overhead. The CO_2 regenerated on the liquid side ($\dot{m}_{CO_2,L}$) was calculated using Equation 5.1, which depends on the mass flow rate ($\dot{m}_{rich}$, $\dot{m}_{lean}$) and the CO_2 mass fraction ($x_{CO_2,rich}$, $x_{CO_2,lean}$) of the lean and the rich solvent. Figure 5.2 shows a good CO_2 balance closure throughout the campaign with a 2.2% average error.

$$\dot{m}_{CO_2,L} = \dot{m}_{rich} x_{CO_2,rich} - \dot{m}_{lean} x_{CO_2,lean} \quad (5.1)$$

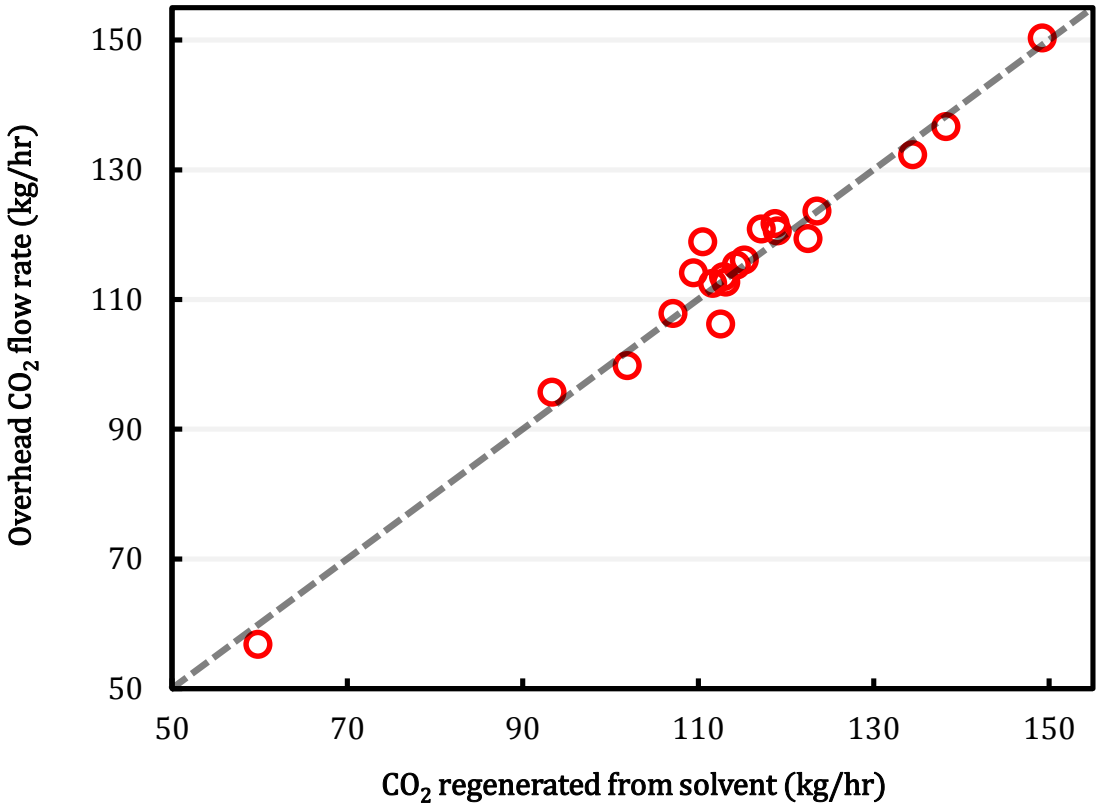

Figure 5.2: CO_2 mass balance around the stripping process; average error: 2.2%.

5.3.2 Enthalpy balance and heat loss

The enthalpy balance can be calculated around the stripping process including two cross exchangers, the steam heater, the stripper, the flash tank, the cold rich exchanger, the condenser, and the condensate separator. The material streams across the boundary include the rich solvent entering the cold cross exchanger, the lean solvent leaving the cold cross exchanger, the CO_2 vapor, and the condensate leaving the condensate separator. The enthalpy of the material streams were obtained from the Independence model for PZ, which provides the predictions of heat capacity and heat of CO_2 absorption at measured temperature, pressure, and composition. Heat input and output include the steam heater duty, the condenser cooling duty and the system heat loss. The steam heater duty was

calculated using the heating steam flow rate and the evaporated enthalpy at measured steam temperature and pressure. The condenser cooling duty was calculated from the cooling water flow rate and the temperature at the inlet and outlet of the condenser. The heat loss can be calculated by enthalpy balance using Equation 5.2 for each run.

$$\dot{Q}_{loss} = \left(\dot{H}_{rich} - \dot{H}_{lean} - \dot{H}_{CO_2} - \dot{H}_{H_2O}\right) + \dot{Q}_{stm} - \dot{Q}_{cond} \quad (5.2)$$

where:

$\dot{H}_{rich}$: enthalpy of the rich solvent entering the cold cross exchanger

$\dot{H}_{lean}$: enthalpy of the lean solvent leaving the cold cross exchanger

$\dot{H}_{CO_2}$: enthalpy of the CO_2 leaving the condensate separator

$\dot{H}_{H_2O}$: enthalpy of the condensate leaving the separator

$\dot{Q}_{stm}$: measured steam heater duty

$\dot{Q}_{cond}$: measured condenser cooling duty

The calculated heat loss can be correlated with the temperature gradient between the flash tank temperature (T_h) and the ambient temperature (T_{amb}) using Equation 5.3. The heat loss constant, C_{hloss}, represents the product of the exposed area and the overall heat transfer coefficient of heat loss. The average C_{hloss} of 21 runs is 102.7 W/K with 7.5% standard deviation. The heat loss was also calculated in the pre-start up test with water before the campaign. The average C_{hloss} during the water test is 100.8 W/K. The consistent heat loss constant of the amine and the water system assures the validity of the calculated heat loss.

$$\dot{Q}_{loss} = C_{hloss}(T_h - T_{amb}) \quad (5.3)$$

5.3.3 Energy performance

The process heat duty is obtained by subtracting the heat loss from the measured steam heater duty. Figure 5.3 shows the heat loss and the process heat duty. The process

heat duty of the AFS is 2.1–3.0 GJ/tonne CO_2 including 17 runs below 2.5 GJ/tonne CO_2. Figure 5.4 compares the process heat duty of the 2015 campaign with previous SRP campaigns in 2011 using a two-stage flash and 8 m PZ (Madan et al., 2013; Van Wagener et al., 2013). The AFS reduces the heat duty by over 25%.

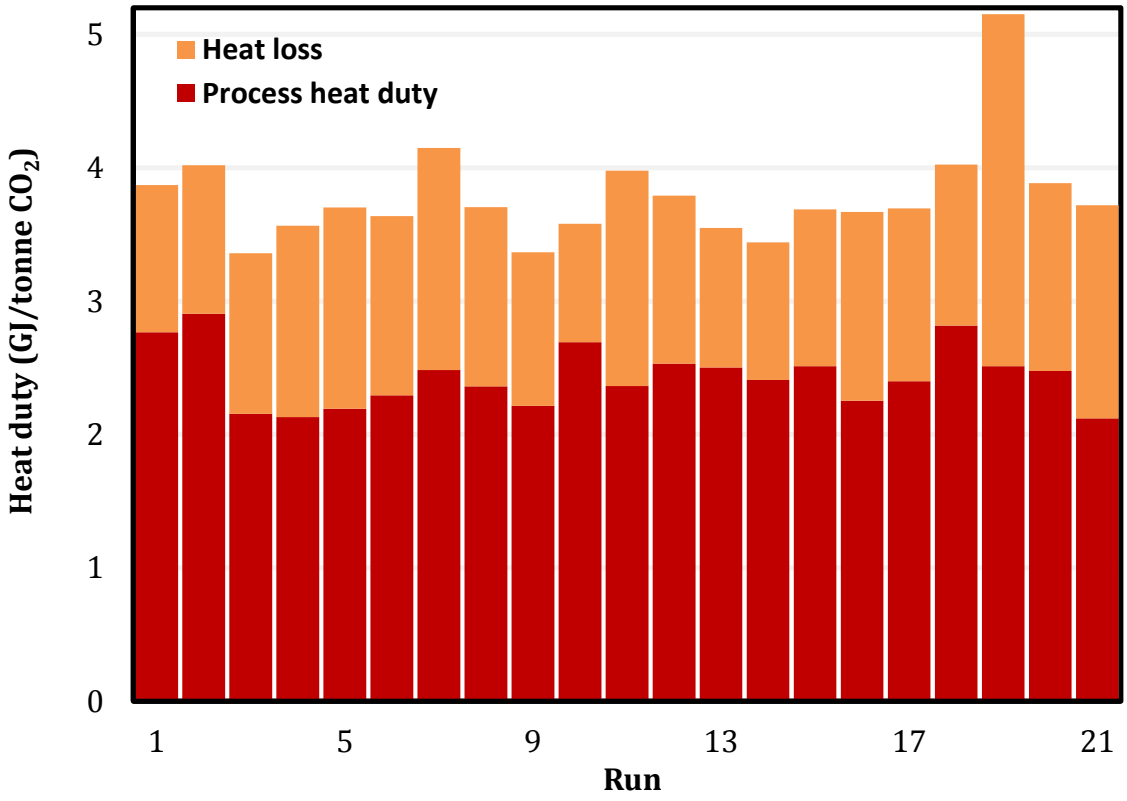

Figure 5.3: Heat loss and process heat duty of the AFS.

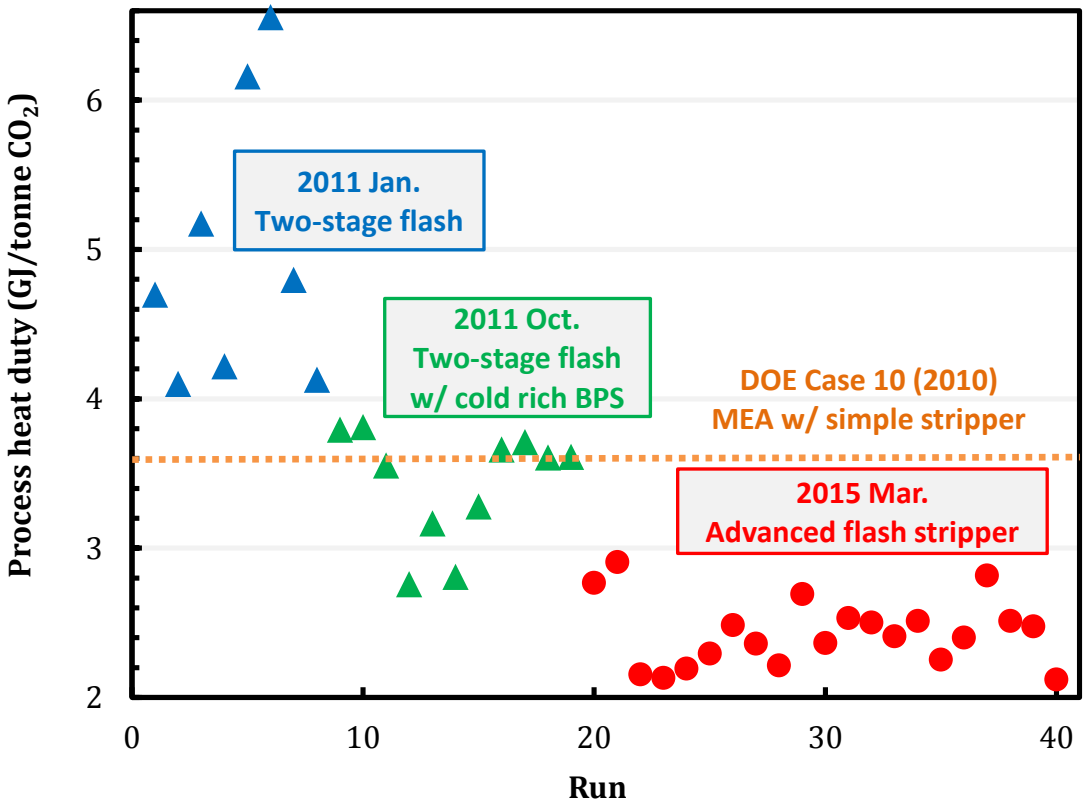

Figure 5.4: Process heat duty of SRP pilot plant campaigns since 2011.

The total equivalent work (W_{eq}) described in Chapter 2 (Equation 2.5–2.7) is used to indicate the overall energy performance for CO_2 capture and compression, which includes pump work, compression work and heat duty work.

$$W_{eq} = W_{heat} + W_{pump} + W_{comp} \tag{2.5}$$

Heat duty work (Equation 2.6) converts the heat duty to electricity by multiplying the turbine efficiency, 90%, and the Carnot cycle efficiency. T_{stm} is the heating steam condensing temperature, which is around 10 K higher than the flash tank temperature in this campaign. The Q_p is the process heat duty. The pump work is calculated using Equation 2.7. $\dot{V}_{rich}$ is the rich solvent volume flow rate and the P_{rp} is the rich solvent pump outlet pressure. The head provided by the rich pump was used to overcome the

pressure drop of the cross exchangers and the steam heaters, and reach stripper pressure. The total pressure drop of the heat exchangers is around 2 bar. The pump efficiency, η_p, is assumed as 65%. The compression work to 150 bar is estimated using the correlation (Equation 2.8) as a function of stripper pressure.

$$W_{Heat} = 90\% \left(\frac{T_{stm}-313K}{T_{stm}}\right) Q_p \tag{2.6}$$

$$W_{pump} = \frac{\dot{V}_{rich}(P_{rp}-1\ bar)}{\eta_p} \tag{2.7}$$

$$W_{comp}\left(\frac{kJ}{mol\ CO_2}\right) = 15.3 - 4.6lnP_{in} + 0.81(lnP_{in})^2 - 0.24(lnP_{in})^3 + 0.03(lnP_{in})^4$$

$$1\ bar \leq P_{in} \leq 149\ bar \tag{2.8}$$

The breakdown of total equivalent work is shown in Figure 5.5. Since the stripper pressure only varied from 4 to 7 bar, the compression work and the pump work are nearly constant. The total work requirement is dominated by the heat duty work. The lowest total equivalent work achieved was 32.0 kJ/mol CO_2.

The U.S. Department of Energy (DOE) reviewed amine scrubbing for CO_2 capture and developed base cases (NETL, 2010). The Case 10 uses MEA with a simple stripper at 1.6 bar to capture CO_2 from coal-fired power plants. The reported heat duty is around 3.6 GJ/tonne CO_2. The total equivalent work calculated is 45 kJ/mol CO_2, including 31.8 kJ/mol heat duty work and 13.2 kJ/mol projected compression work. Compared to DOE Case 10, the AFS with PZ reduces the total equivalent work by over 20%. Reduction of compression work is around 5 kJ/mol CO_2 because PZ is more thermally stable, so the stripper can be operated at higher temperature and pressure without significant thermal degradation.

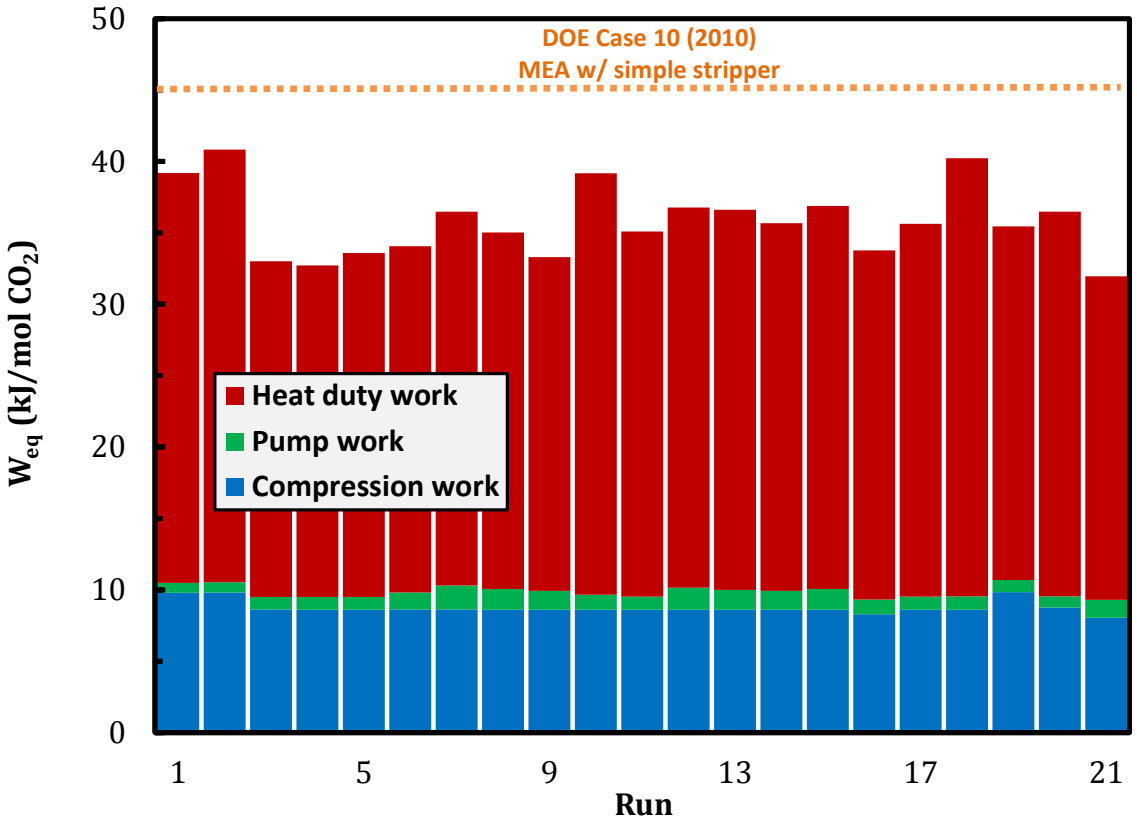

Figure 5.5: Total equivalent work of SRP pilot plant with the AFS.

5.3.4 Rich solvent bypass performance

The heat recovery performance was maintained by manually adjusting the cold and warm rich bypass rates for each run. The cold and warm rich bypasses are used to recover the stripping steam heat from the CO_2 vapor. The vapor temperatures indicate the amount of stripping steam that has been condensed. The analysis in Chapter 3 concluded that the optimum bypass rates usually give a consistent temperature approach between vapor and liquid throughout the stripper column.

The temperature difference between the liquid that enters the stripper and the vapor at the top was maintained at around 7 K in this campaign. The cold rich bypass rate was adjusted to ensure the cold rich exchanger performance by keeping the cold rich exchanger

vapor outlet temperature at 50–70 °C. Figure 5.6 shows the results of rich solvent bypass control. The total bypass ratio includes the cold and the warm rich bypass. The water content from the flash tank is estimated using the Independence model at a given temperature and pressure. Lower lean loading and lower flash tank temperature that reduce partial pressure of CO_2 will result in higher water vapor content in the stripped vapor. The results show that higher water content requires more bypass to maintain the vapor outlet temperature. Four runs highlighted in Figure 5.6 used relatively low bypass rates at given water content and therefore resulted in higher vapor outlet temperature.

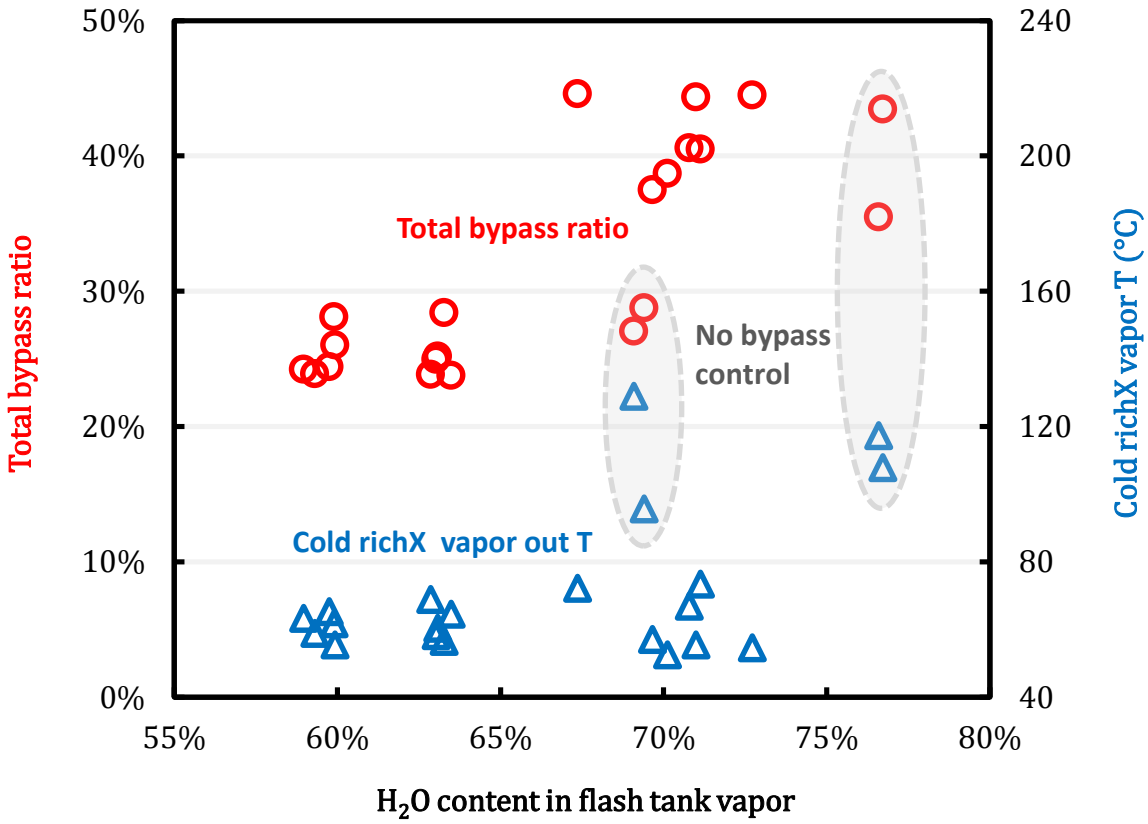

Figure 5.6: Performance of rich solvent bypass; 4 runs highlighted were without bypass control.

Figure 5.7 further demonstrates the effect of bypass on the energy performance. There are 4 runs at identical operating conditions except the bypass ratio. The water content in the vapor phase should be similar at the same flash tank temperature and lean loading. The two runs on the left side of the plot that did not deliver enough bypass to condense the stripping steam led to a 15% increase of heat duty.

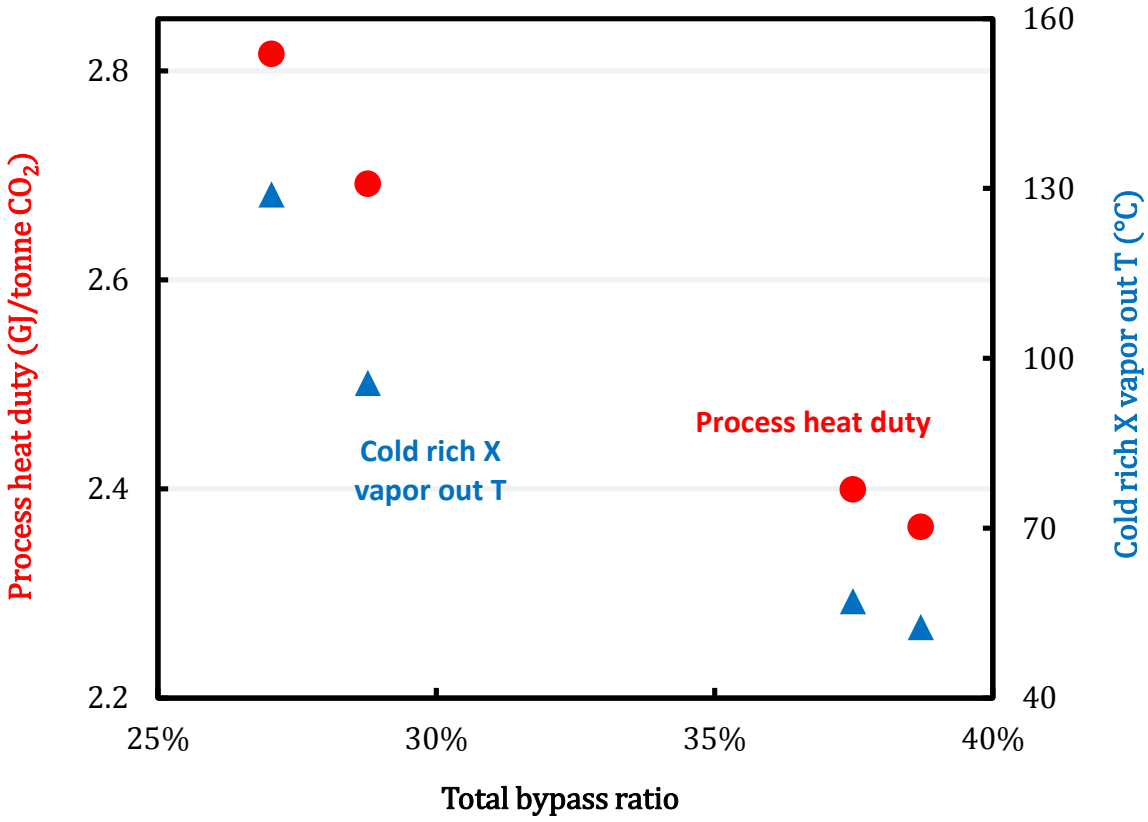

Figure 5.7: Effect of rich solvent bypass; run 10, 11, 17, and 18; 5 m PZ; flash tank T: 149 ºC; rich loading: 0.36; lean loading: 0.20.

5.3.5 Lean loading effect

The lean loading is one of the most important operating parameters that determine minimum heat duty. Chapter 4 has shown a quadratic relationship between lean loading

and heat duty at constant rich loading. Optimum lean loading was found to minimize the energy requirement. Figure 5.8 shows 7 runs at identical operating conditions except the CO_2 lean loading. Since the rich loading is approximately constant, lower lean loading provides better cyclic capacity (i.e., the difference between rich and lean loading, ΔLdg) and less sensible heat requirement. However, lower lean loading will cause more stripping steam to be generated and thus lower the ratio of CO_2 to H_2O in the stripping vapor. Heat duty trade-offs between the sensible heat and the stripping steam heat are expected when the lean loading varies. Diminishing returns of heat duty can be seen at lean loading between 0.23 and 0.25. Based on this, it is inferred that the heat duty is approaching the minimum at the operating lean loadings.

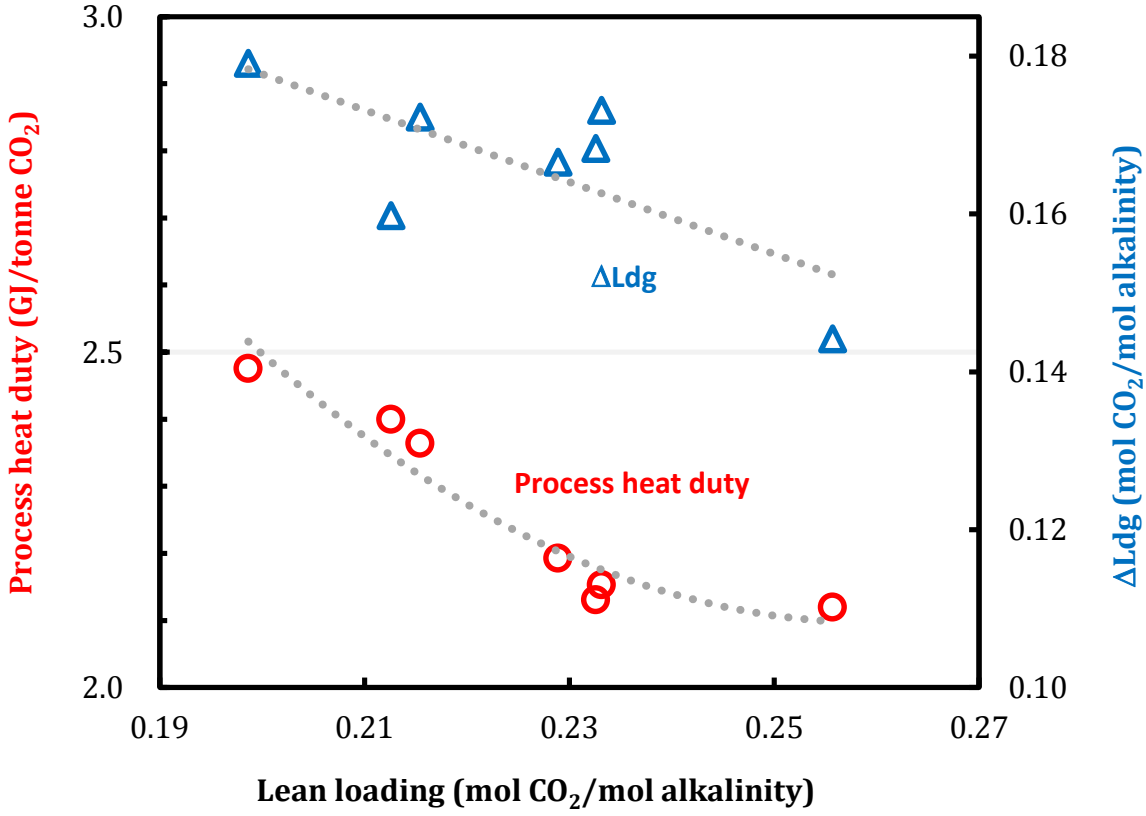

Figure 5.8: Effect of lean loading; run 3, 4, 5, 11, 17, 20, and 21; 5 m PZ; flash tank T: 149 °C; rich loading: 0.39±0.01.

5.3.6 5 m PZ vs. 8 m PZ

It has been demonstrated that 5 m PZ provides better solid solubility and lower viscosity than 8 m PZ. Solvents with lower viscosity can provide better mass and heat transfer performance. This campaign consisted of 4 runs using 8 m PZ, so direct comparisons can be made. Table 5.3 shows that two comparisons are made at the same flash tank temperature and lean loading. Each comparison has similar solvent capacity and bypass ratio. Even though 5 m PZ has a lower equilibrium capacity (mol alkalinity/kg solution) than 8 m, higher liquid side mass transfer rate results in higher rich loading and greater cyclic capacity (ΔLdg). These runs end up with approximately the same ratio of solvent rate to the CO_2 capture rate. The sensible heat requirement and the heat recovery performance are expected to be similar in each comparison. The only reason that 5 m PZ outperformed 8 m PZ with a lower heat duty is the cross exchanger performance. The temperature approach of the cold cross exchanger at the cold end indicates the amount of sensible heat recovered from the lean solvent. A lower temperature approach implies higher heat transfer coefficient. The cross exchanger performance can be quantified by the number of heat transfer units (NTU). The NTU of the cold cross exchanger using 5 m PZ is 20% greater than 8 m PZ because of lower viscosity.

Table 5.3: Comparisons of pilot plant results of 5 m and 8 m PZ.

	Comparison 1 (145 °C 0.24 lean Ldg)		**Comparison 2 (145 °C 0.24 lean Ldg)**	
Run	8	15	9	14
PZ (m)	5	8	5	8
Viscosity at 40 °C (cP)	3.3	9.5	3.3	9.5
Equilibrium capacity (mol alkalinity/kg solution)	7.0	9.5	7.0	9.5
Rich loading (mol CO_2/mol alkalinity)	0.37	0.34	0.39	0.36
Total bypass ratio (%)	25	24	26	24
Cold end ΔT of cold cross X (°C)	6.5	8.4	6.4	8.7
NTU of cold cross X	19.2	15.9	18.9	15.8
Heat duty (GJ/tonne CO_2)	2.36	2.51	2.21	2.41

5.3.7 Heat exchanger performance

The heat transfer coefficient of heat exchangers in the stripping process is evaluated. The log mean temperature difference (LMTD) is calculated from measured inlet/outlet temperatures even for the flashing exchangers with non-linear temperature profiles. The heat transfer coefficient could be under-estimated by under-predicting the LMTD. The heat duty of the cross exchangers is calculated from the lean solvent side with the heat capacity predicted by Aspen Plus®. The steam heater heat duty is dependent on where the heat loss occurs and how much latent heat of steam is actually transferred to the solvent. This analysis will report a conservative heat transfer coefficient by using the process heat duty as steam heater duty. Table 5.4 summarizes the heat exchanger specifications and the operating temperature approaches.

Table 5.4: Heat exchanger specifications of SRP pilot plant.

Heat exchanger	Type	Service (hot/cold)	Area (m^2)	LMTD (K)
Cold cross exchanger	Plate-and-frame	solvent/solvent	40.0	3–6
Hot cross exchanger	Plate-and-frame	solvent/solvent	20.4	2–5
Low T steam heater	Shell-and-tube	steam/solvent	1.3	12–17
High T steam heater	Shell-and-tube	steam/solvent	1.0	8–13
Cold rich exchanger	Plate-and-frame	CO_2 vapor/solvent	3.2	21–34

5.3.7.1 Cross exchangers

Figures 5.9 and 5.10 show the overall heat transfer coefficient of the cold cross exchanger, which is expected to have single phase on both sides. The heat transfer coefficient increases with the solvent rate with a power of 1.15, which is higher than the empirical value 0.6–0.75 for plate-and-frame exchangers (Ayub, 2003). This demonstrates that the heat transfer coefficient can be enhanced by a higher fluid velocity. However, the turbulence also creates higher pressure drop as shown in Figure 5.10. A cross exchanger optimization that determines the optimum fluid velocity by considering the pumping cost and the heat exchanger cost will be performed in Chapter 8.

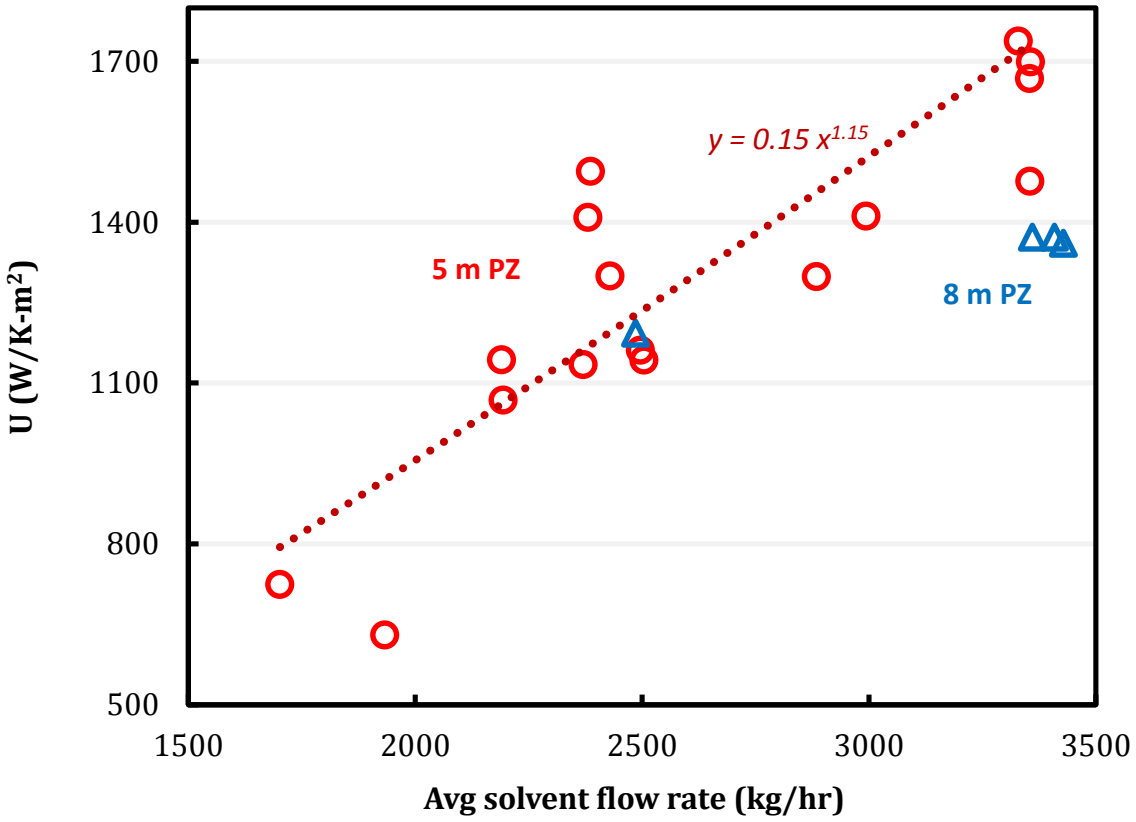

Figure 5.9: Overall heat transfer coefficient of the cold cross exchanger.

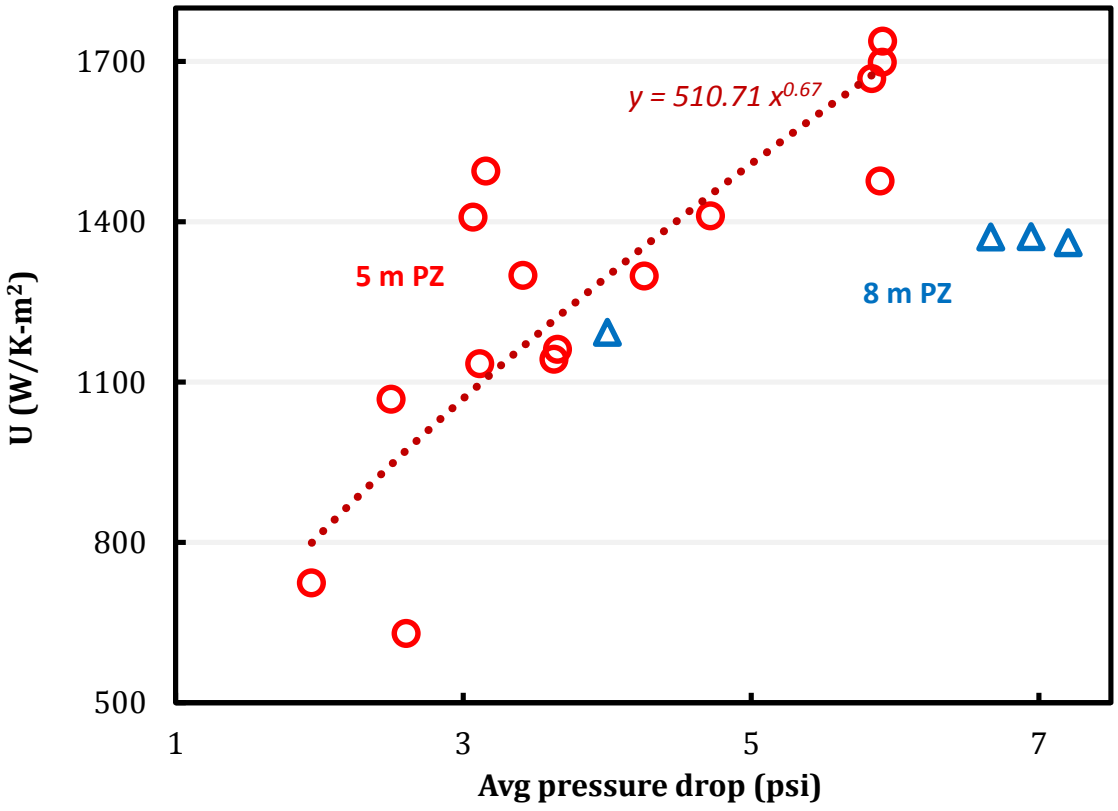

Figure 5.10: Pressure drops of the cold cross exchanger.

The rich solvent is likely to flash in the hot cross exchanger when it exceeds the bubble point. In this case, both convection and nucleate boiling will contribute to the heat transfer at the rich side. Figure 5.11 shows that the heat transfer coefficient is not as sensitive as the cold cross exchanger to the solvent flow rate since the effectiveness of the nucleate boiling is mainly determined by the temperature approach while the single phase all relies on convective heat transfer.

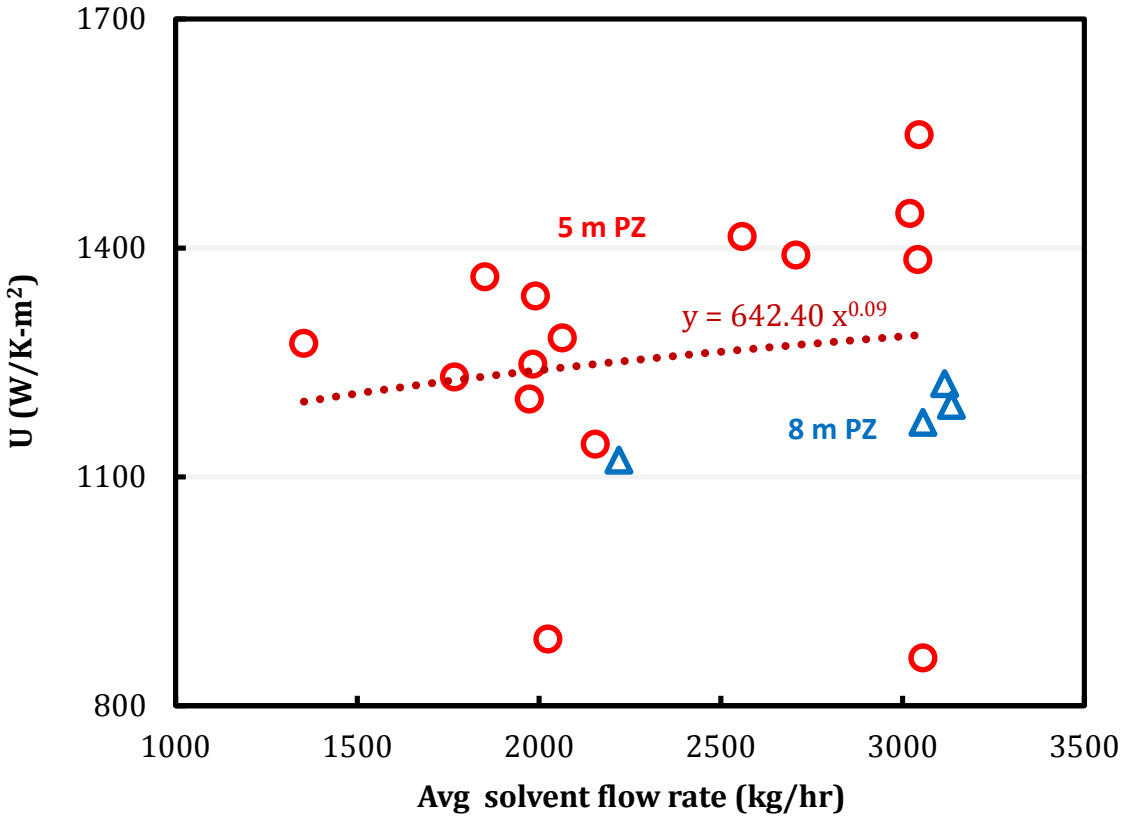

Figure 5.11: Overall heat transfer coefficient of the hot cross exchanger

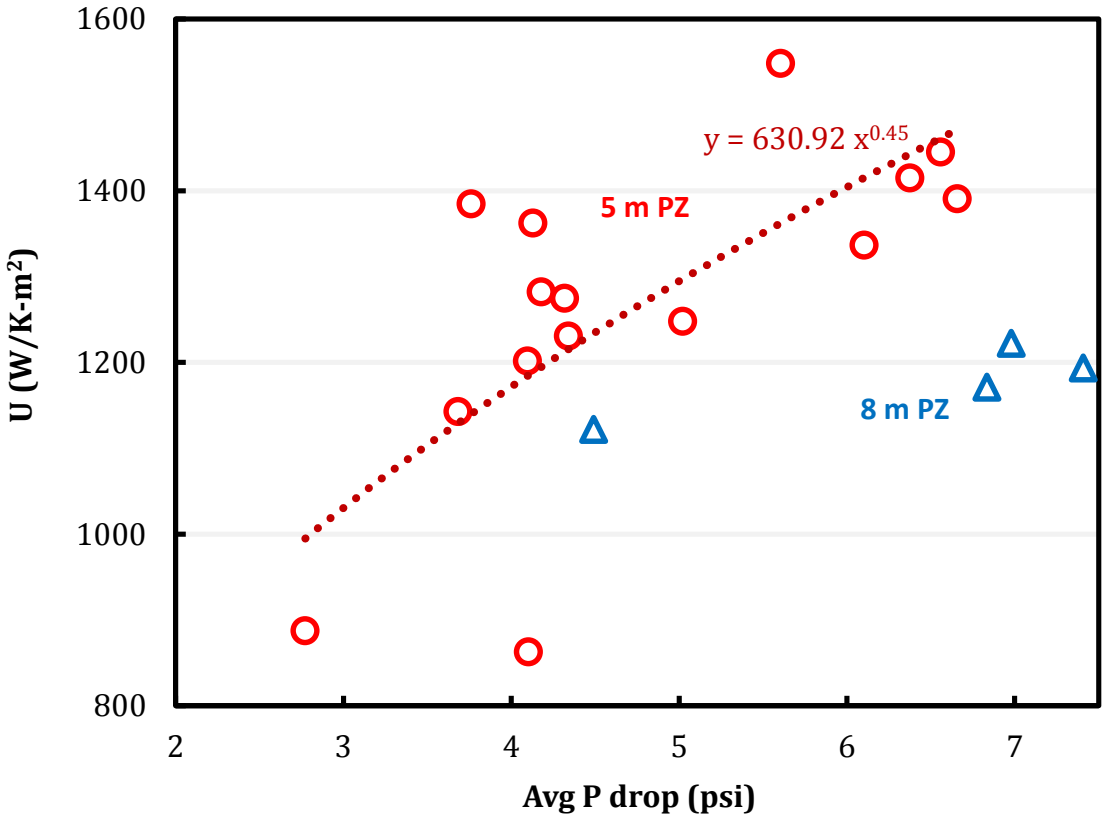

Figure 5.12: Pressure drop of the hot cross exchanger.

5.3.7.2 Steam heaters

Figure 5.13 shows the heat transfer coefficient of the steam heaters, which has no strong correlation with the solvent rate. This implies that nucleate boiling is the dominant heat transfer mechanism. In the nucleate boiling regime, higher heat transfer coefficient can be achieved as the temperature difference between the heating surface and saturation temperature increases. Even though the high temperature steam heater has a relatively lower temperature approach (8–13 K) than the low temperature steam heater (12–17 K), the effective temperature difference between the steam temperature and the bubble point temperature can be actually greater due to the pressure drop. More bubbles generated at

lower pressure creates more turbulence and leads to a higher heat transfer coefficient for the high temperature steam heater.

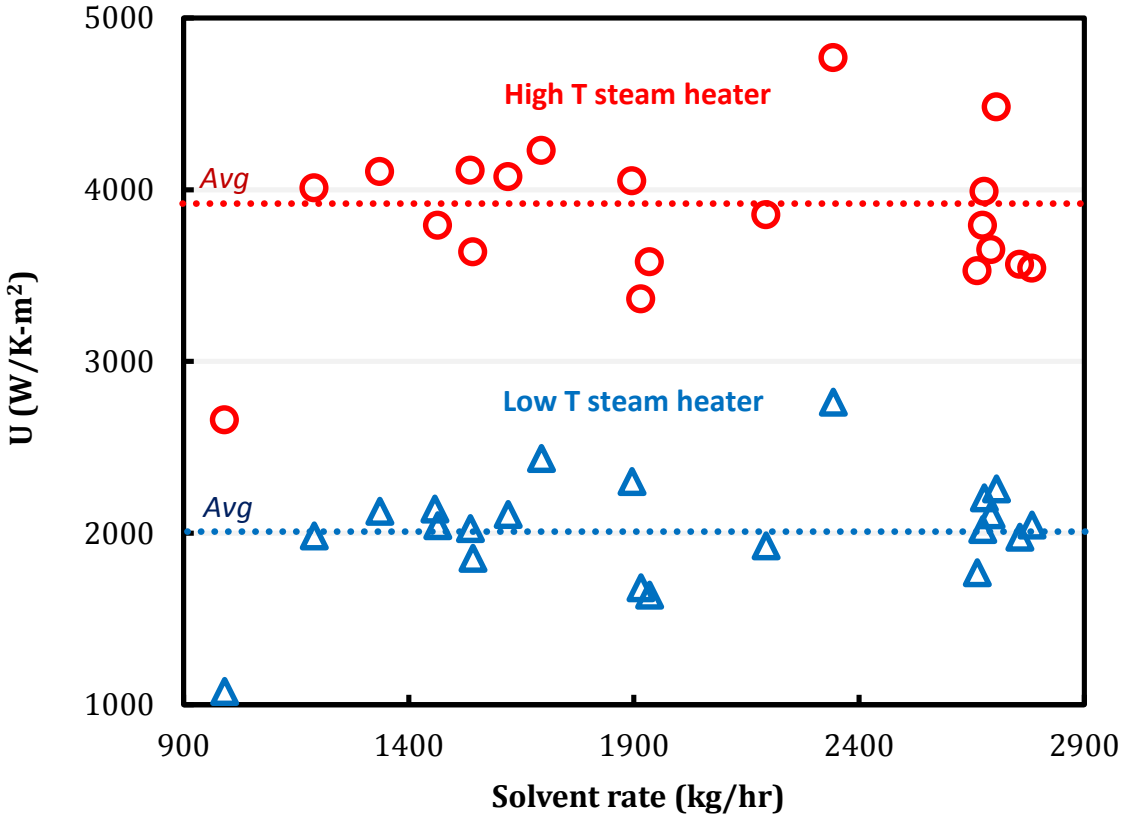

Figure 5.13: Overall heat transfer coefficient of the steam heaters.

5.3.7.3 Cold rich exchanger

The cold rich exchanger has the condensing steam and CO_2 vapor at the hot side and the rich solvent in single phase at the cold side. The heat transfer coefficient is around 250 W/K-m^2 because of the poor heat transfer performance of vapor as shown in Figure 5.14. Condensing steam can make heat transfer more effective than the vapor itself. Generally, CO_2 vapor at higher temperature contains more steam that can be condensed in the cold rich exchanger so results in a higher heat transfer coefficient.

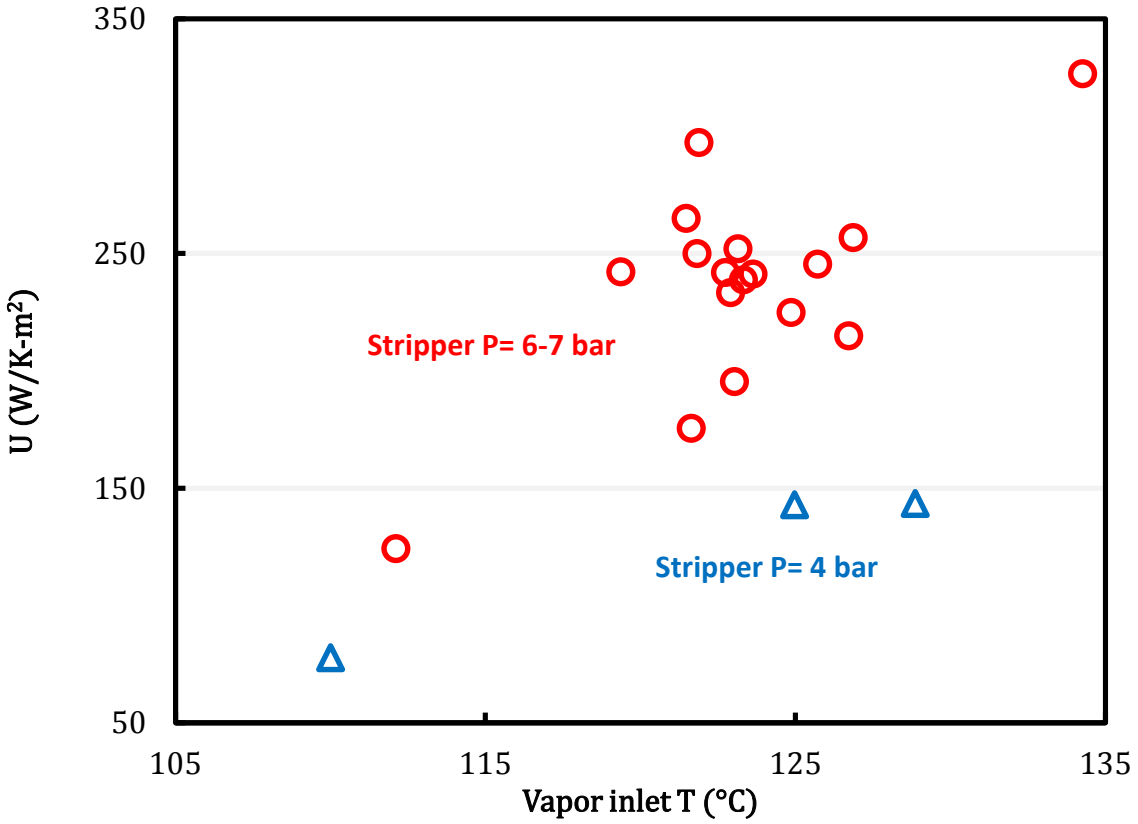

Figure 5.14: Overall heat transfer coefficient of cold rich exchanger.

5.4 MODELING RESULTS

5.4.1 Simulation model and data reconciliation

The Independence model was rigorously regressed in Aspen Plus® with experimental data including amine volatility, heat capacity, CO_2 solubility, and amine pK_a over a range of amine concentration and CO_2 loading (Frailie, 2014). The electrolyte Non-Random Two-Liquid (e-NRTL) property method is used to describe the CO_2-amine-H_2O chemistry accounting for the non-ideality in the aqueous electrolyte system. Aspen Plus® RateSep™ provides a rigorous, rate-based model for heat and mass transfer with equilibrium reactions in the boundary layer. Mass transfer and area models used in the

stripper were developed specifically for RSR no. 0.3 packing by regression of experimental data collected using a pilot-scale column (Wang, 2015).

The data reconciliation was implemented in Aspen Plus® using the Data-Fit tool. Data-Fit minimizes the error of result variables between measured and modeled values by adjusting model-input variables. The objective function in data reconciliation is shown in Equation 5.4. The resulting variables of interest are the process heat duty and the CO_2 production rate, which indicate the energy performance and CO_2 mass balance, respectively.

The model-input variables from pilot plant measurements include the temperature and pressure of the rich solvent, PZ concentration, the lean side outlet temperature of the cold and hot cross exchanger, the temperature and pressure of the flash tank, the liquid side outlet temperature of the cold rich exchanger, and the condenser temperature. The temperature and pressure measurement inputs are considered consistent and reliable, and so will not be adjusted. Two adjustable parameters in the data reconciliation are the CO_2 concentration in the rich solvent (rich loading) and the correction of packing interfacial area for the stripper. The rich loading was adjusted for each run and the packing interfacial area factor is a global parameter that uniformly applies to the whole campaign. Generally, the adjustment of the CO_2 rich loading is responsible for CO_2 mass balance closure, and the packing area factor will be adjusted to match the process heat duty.

$$Min \sum_{i=1}^{n} \left(\frac{Measured_i - Modeled_i}{\sigma_i} \right)^2 \tag{5.4}$$

where:

$Measured_i$: pilot plant measurement of variable i

$Modeled_i$: model prediction of variable i

σ_i: standard deviations of pilot plant measurement of variable i

n: number of result variables

5.4.2 Model validation

Figures 5.15 and 5.16 compare the modeled and density-predicted CO_2 loading. The modeled lean loading was determined by the vapor-liquid equilibrium at given temperature and pressure of the flash tank. The modeled lean and rich loadings are 5.4% and 3.6% higher, respectively.

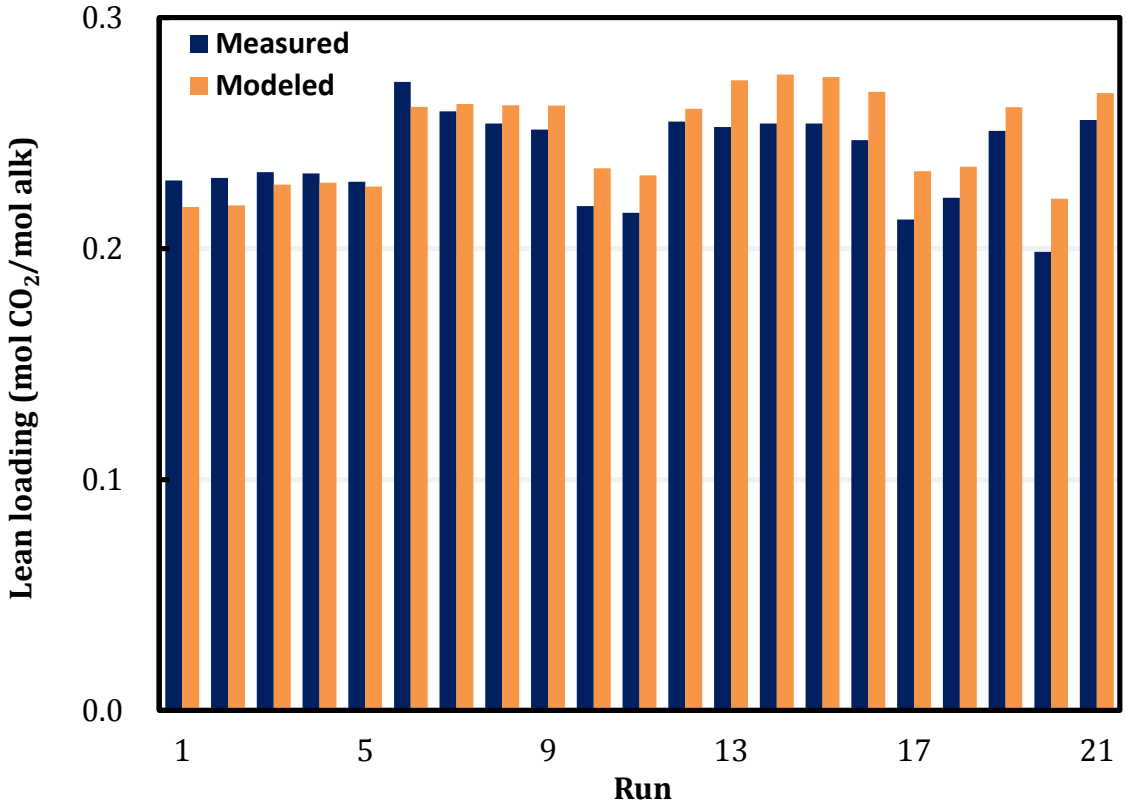

Figure 5.15: Measured and modeled lean loading; average error: 5.4%.

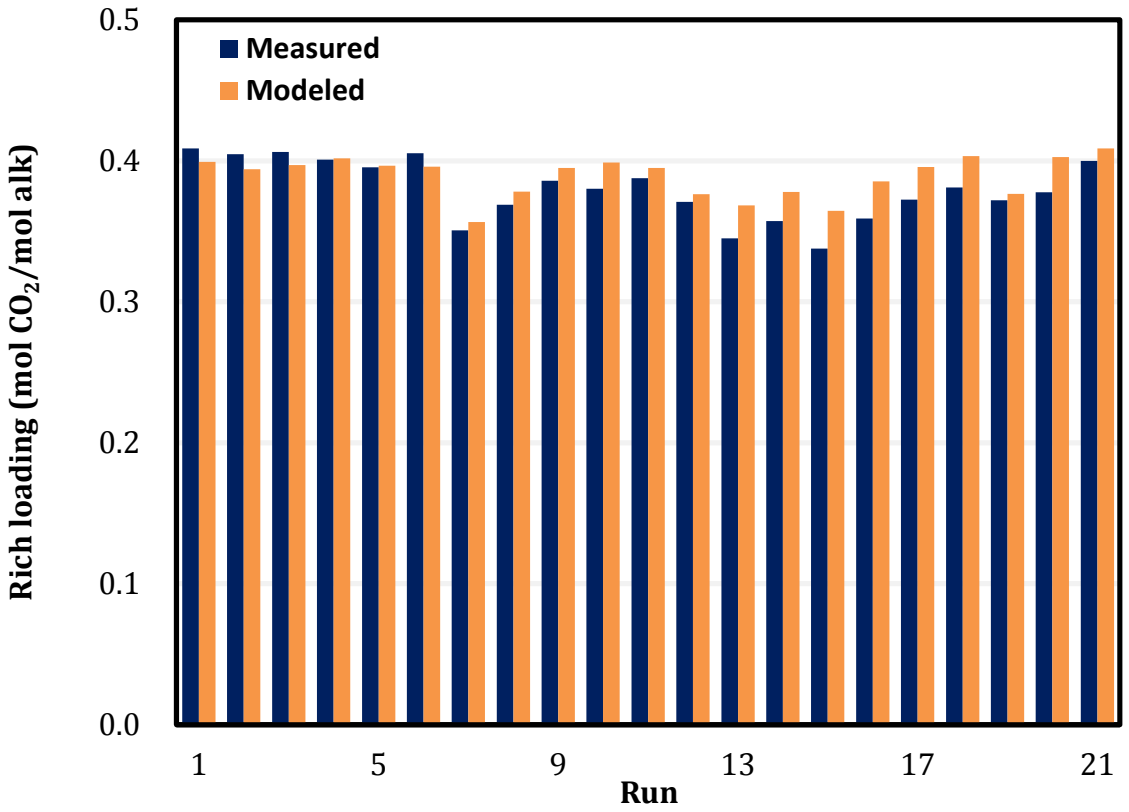

Figure 5.16: Measured and modeled rich loading; average error: 3.6%.

The regressed correction factor for the packing interfacial area is 15.2%±0.17% within 95% confidence interval. The correction accounts for the actual column performance and potential model errors. The actual effective area could be less than the model prediction due to liquid maldistribution that causes un-wetted packing. Model errors could also result from over-predicting the mass transfer coefficient of the liquid and gas side. All the potential errors were reflected on a single correction factor.

The 6-in ID (150 mm) stripper was packed with the random packing RSR no. 0.3 that has the packing size of 15 mm. The diameter-to-packing size ratio of the SRP stripper is 10 while the packing performance data were measured using a column with a ratio of 30.(Wang, 2015) The wall effect is more significant for a small column and will reduce

the effective packing area. It is expect that a large scale plant will reduce the wall effect and increase the packing wetted area.

The diffusion coefficient of amine and reaction product predicted by the model is the most uncertain parameter used in the mass transfer coefficient model. Figure 5.17 compares the diffusivity of amine in amine solution predicted by the Independence model and by the Stokes-Einstein relation, which applies an analogy of viscosity as shown in Equation 5.5 (Snijder et al., 1993; Versteeg et al., 1988). The diffusivity data of amine in water is needed ($D_{am\text{-}water}$). The Independence model uses the same analogy to estimate the diffusivity of CO_2 in amine solution with a power of 0.8. The diffusion coefficient of amine is expected to be about half of CO_2 at the stripper temperature using the modified Stokes-Einstein relation. However, the predicted diffusion coefficient of amine in the model is 4 times greater than expected. The over-prediction of the diffusion coefficient is compensated for by a small correction factor applied to the interfacial area.

$$\frac{D_{am-am}}{D_{am-H_2O}} = \left(\frac{\mu_{water}}{\mu_{am}}\right)^{0.6} \tag{5.5}$$

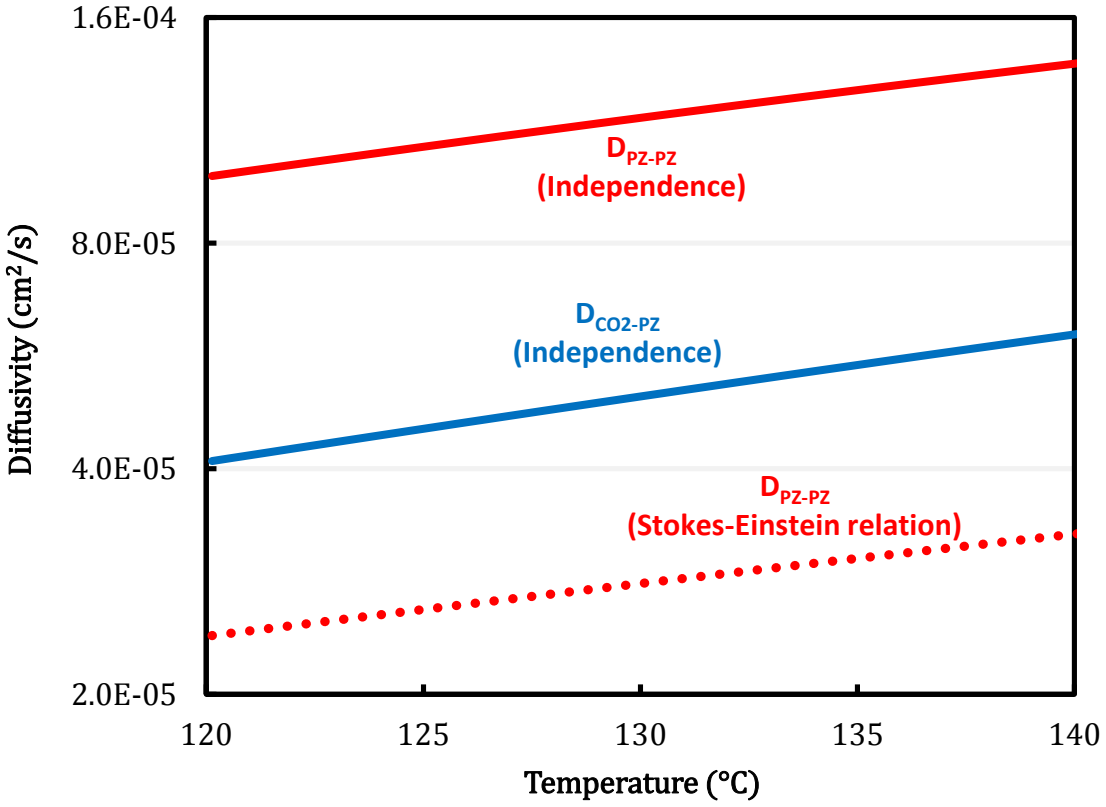

Figure 5.17: Diffusivity of amine and CO_2 in 5 m PZ solution predicted by Independence model and modified Stokes-Einstein relation at stripper conditions.

Figure 5.18 shows that the model predicts well the process heat duty for the whole campaign with a 3.0% average error. Two typical temperature profiles of this campaign are shown in Figures 5.19 and 5.20, representing with and without bypass control, respectively. The open points were measured inside the stripper and the filled points were measured from the liquid or vapor that go into the stripper. Solid lines are model-predicted temperatures. The two measurements at the stripper bottom consistently reflect the liquid temperature but other were more inclined to vapor temperature.

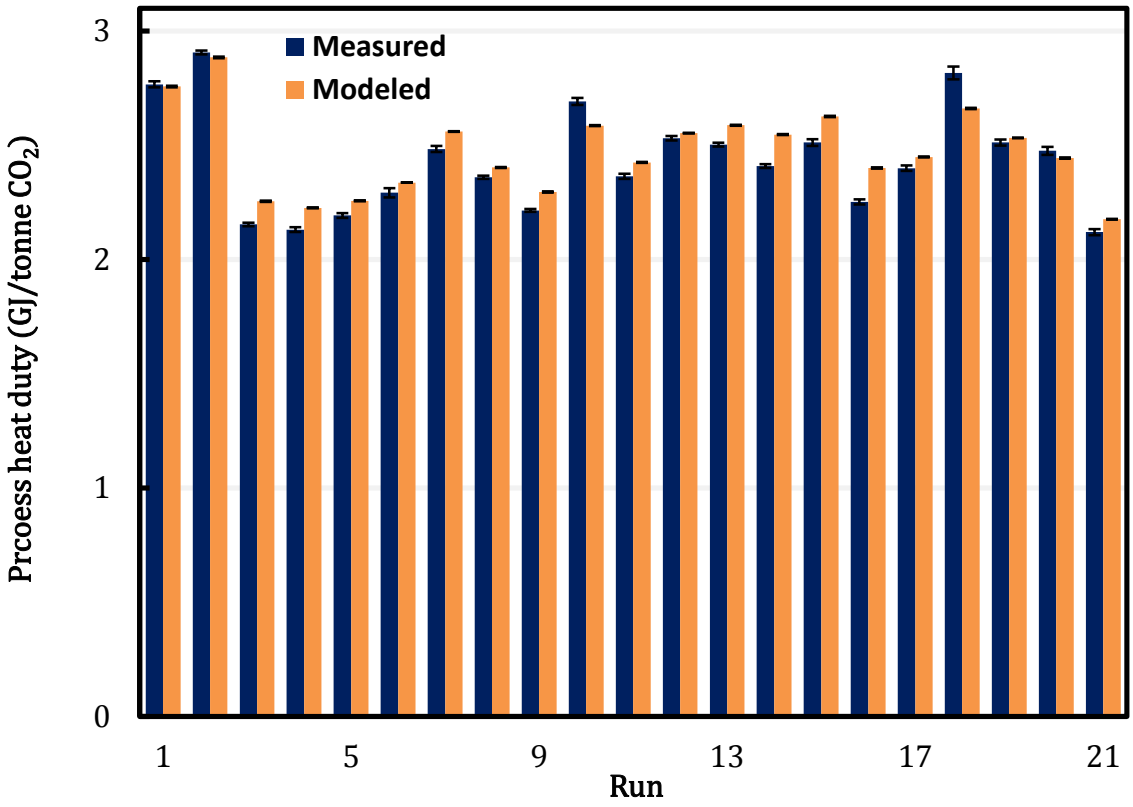

Figure 5.18: Measured and modeled process heat duty; average error: 3.0%.

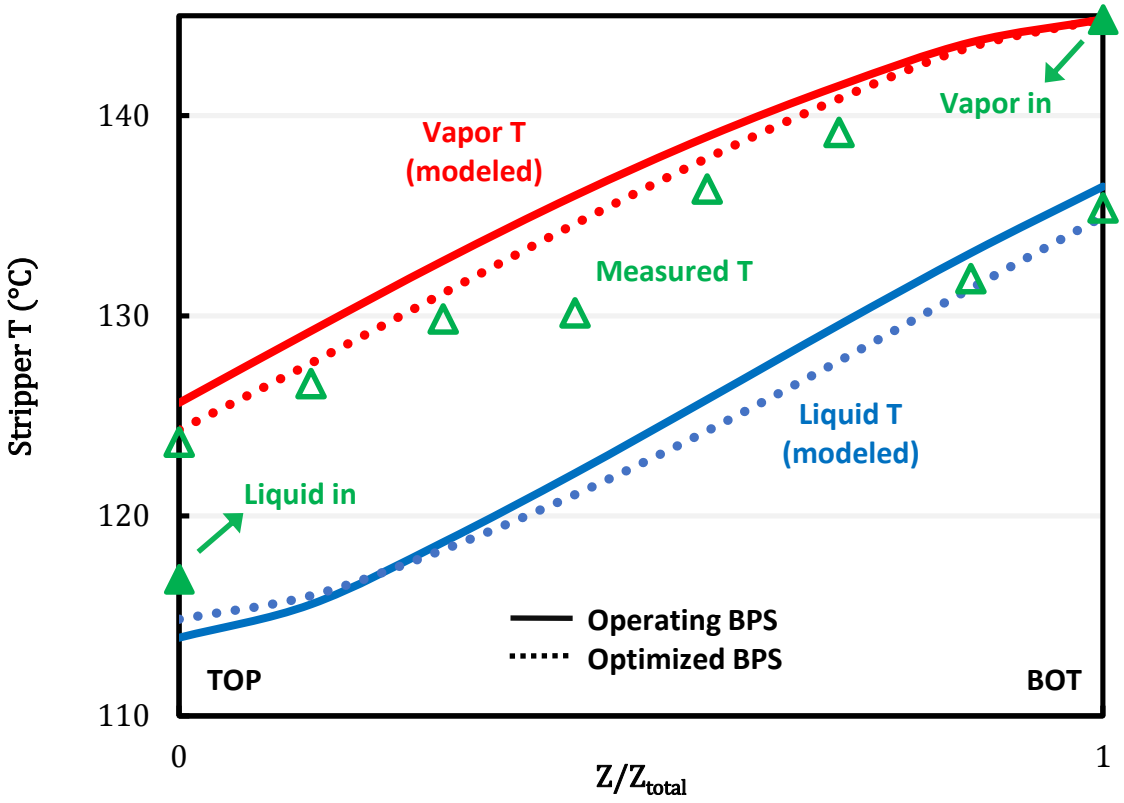

Figure 5.19: Stripper temperature profile; run 6; open points: measured T inside the stripper; filled points: measured T outside the stripper; solid lines: modeled T at operating bypass rates; dotted lines: modeled T at optimized bypass rates.

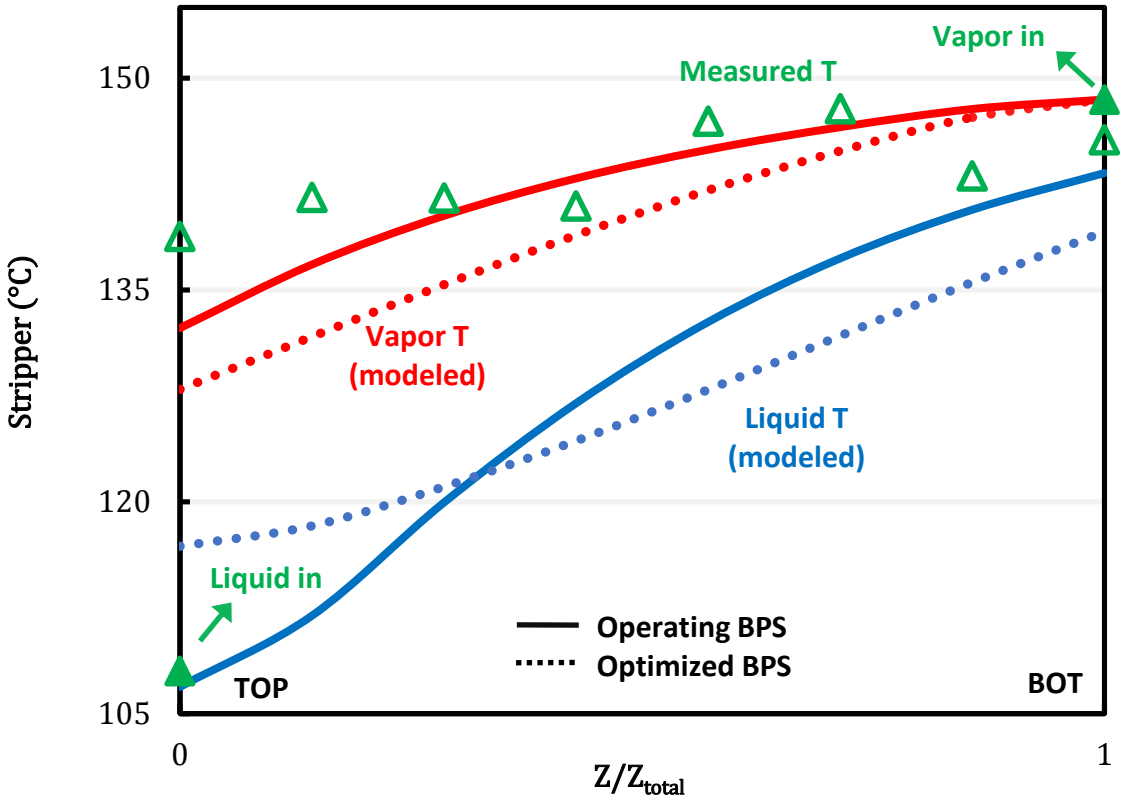

Figure 5.20: Stripper temperature profile; run 18; open points: measured T inside the stripper; filled points: measured T outside the stripper; solid lines: modeled T at operating bypass rates; dotted lines: modeled T at optimized bypass rates.

5.4.3 Rich solvent bypass optimization

The temperature approaches at the top and the bottom of the stripper (the difference between the open and the filled points in Figures 5.19 and 5.20) were controlled to be approximately equal to each other by adjusting the rich solvent bypass during the test. The cold and the warm rich bypass were re-optimized using the validated model to assure the performance of the bypass control strategy. First, the product of the overall heat transfer coefficient and the exchanger area (UA) of the cross exchangers and the cold rich

exchanger was found for each run at operating conditions. Second, bypass rates were varied to minimize the heat duty while UA was kept constant.

Figure 5.21 shows the improvement of the heat duty and the absolute change of the total bypass ratio after optimizing the rich solvent bypass. The changes of heat duty and bypass ratio will approach zero as the operating rich solvent bypass is at optimum. The heat duty was kept within 2% of the minimum when the bypass rates were adequately controlled. The change of total bypass ratio is less than 10%. Four other runs without bypass control needed the bypass ratio to be increased by around 20% to minimize the heat duty. Figure 5.21 also suggests that energy performance can be easily guaranteed as long as the bypass ratio is in the optimum range. This demonstrates the operability and flexibility of a complex system by implementing a simple control strategy.

To further justify the control strategy, temperature profiles before and after bypass optimization are compared in Figures 5.19 and 5.20. The dotted lines are the modeled temperature profiles at optimum bypass ratio. The operating bypass ratio of Run 6 (Figure 5.19) was already close to optimum so the temperature profile shows little change. Run 18 (Figure 5.20) did not deliver enough bypass to the stripper so the temperature approach was different between the top (30 K) and the bottom (5 K). The temperature profile becomes nearly parallel after re-optimizing the bypasses.

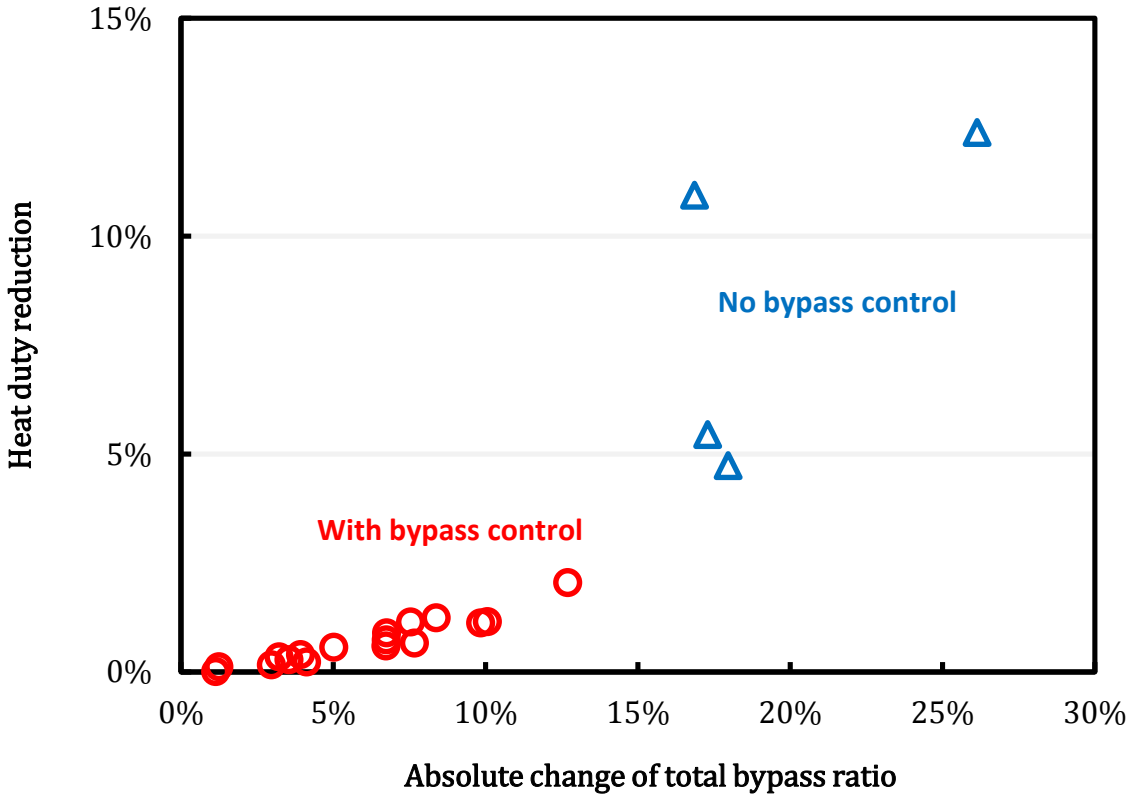

Figure 5.21: Process heat duty improvement after bypass re-optimization; circle: with bypass control; triangle: without bypass control.

5.4.4 Effect of rich and lean loading

A base case with the minimum total equivalent work of the campaign was selected for further studies that extended the operating conditions. Run 21 using 5 m PZ achieved an equivalent work of 32.6 kJ/mol CO_2 with 0.27 lean loading, 0.41 rich loading (modeled value), and 149 °C flash tank temperature. The UA of the cross exchangers and the cold rich exchanger were fixed in the following simulations. The rich solvent bypasses were optimized in all of the cases.

Figure 5.22 shows the total equivalent work with various rich and lean loading. The rich loading reflects the absorber performance and is affected by the liquid to gas ratio

(L/G), the intercooling, and the operating lean loading. The rich loading in this campaign was 0.37−0.41 mol CO_2/mol alkalinity. Higher rich loading is always beneficial because greater cyclic capacity requires a lower solvent rate for CO_2 regeneration.

The optimum lean loading to minimize total equivalent work can be found at each rich loading. The stripping steam heat and sensible heat are dominant at low and high lean loading, respectively. The optimum lean loading shifts with rich loading but the optimum ΔLdg is approximately constant at 0.11 mol CO_2/mol alkalinity. The difference of total equivalent work between the base case and the minimum is less than 1%, which confirms the inference in Section 5.3.3 that the best energy performance has been reached using the existing facility.

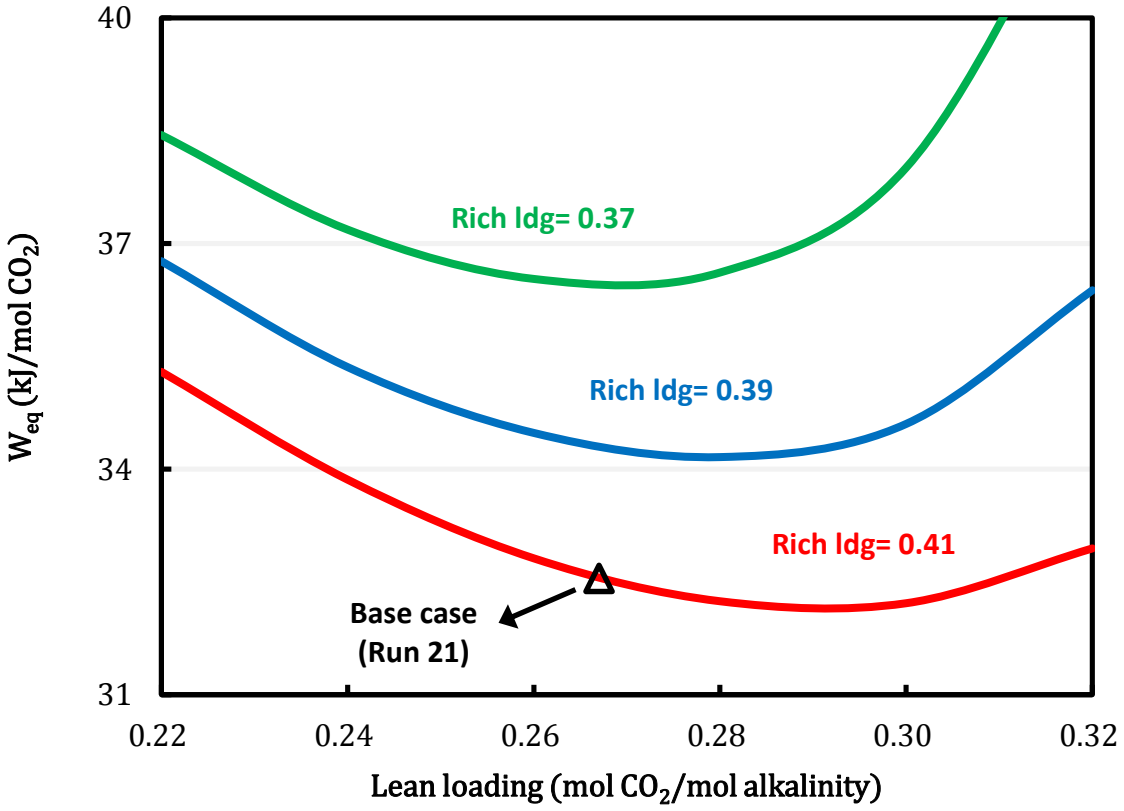

Figure 5.22: Total equivalent work with various lean and rich loading; stripper T: 149 °C; packing: 2 m RSR no. 0.3; correction for interfacial area: 0.15; constant UA; optimized bypass rates.

5.4.5 Effect of striper packing height

The packing height determines the heat recovery performance in the stripper. Figure 5.23 shows the total equivalent work with varied packing height from 1 to 5 m. A correction of interfacial area, 15%, is applied in Aspen Plus® to match the pilot plant data, so that the model had to use 0.8 m of packing to represent 5 m of real packing. Adding packing has more effect at low lean loading where excessive stripping steam needs to be recovered. The reduction of the total equivalent work by increasing packing from 2 m to 5 m is 7% at 0.22 lean loading but 2% at 0.28 lean loading.

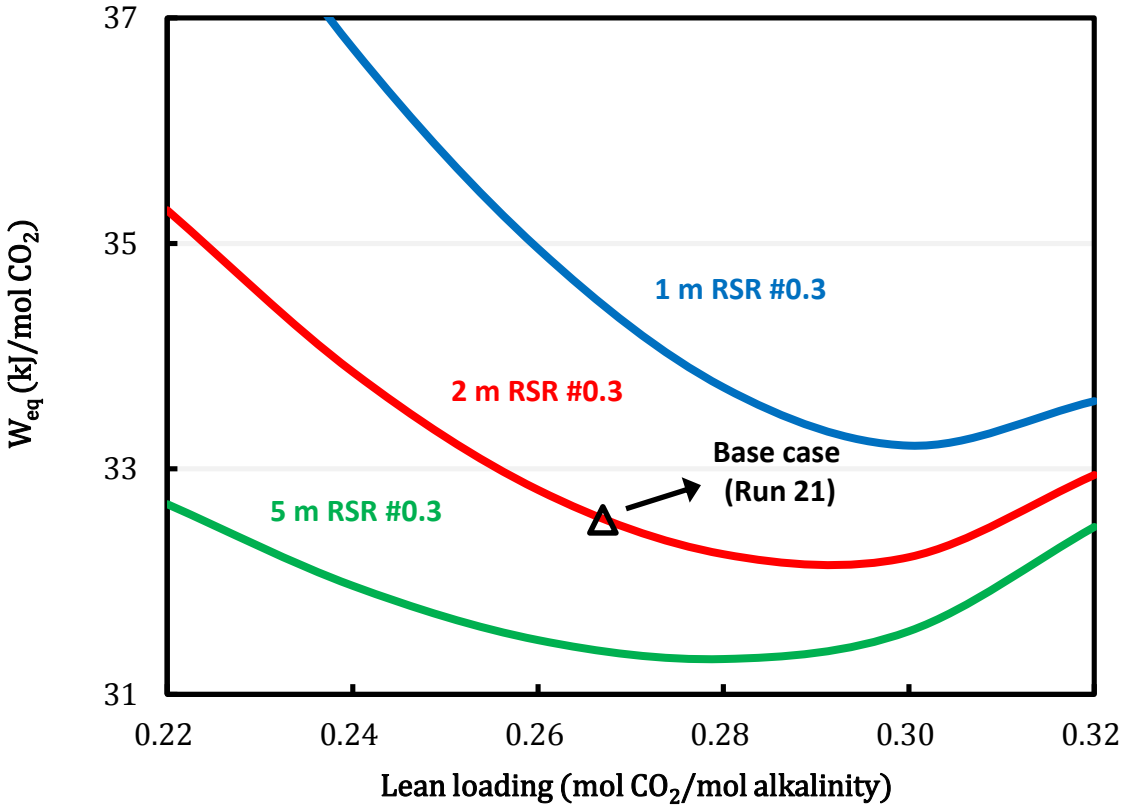

Figure 5.23: Total equivalent work with various packing height and lean loading; packing: RSR no. 0.3; correction for interfacial area: 0.15; rich loading: 0.41; stripper T: 149 °C; constant UA; optimized bypass rates.

Efficiency of packing utilization can be quantified using Equation 5.6. The maximum ($W_{eq,max}$) and the minimum ($W_{eq,min}$) total equivalent work are defined as using 1 m packing and infinite packing, respectively. 1 m is assumed to be the least packing height needed for a packed stripper. The difference between $W_{eq,max}$ and $W_{eq,min}$ is the maximum amount of energy that can theoretically be reduced by adding packing. When the packing utilization efficiency is approaching 100%, little energy improvement will be obtained from increasing packing height.

$$Packing\ utilization\ efficiency = \frac{W_{eq,max} - W_{eq}}{W_{eq,max} - W_{eq,min}} \quad (5.6)$$

Figure 5.24 shows the total equivalent work and the packing efficiency with increasing packing height at 0.22 and 0.28 lean loading. The greatest reduction of total equivalent work is between 1 m and 5 m. After 5 m, adding packing improves the energy performance by less than 2%. The packing utilization efficiency reaches 88% with 5 m packing and then approaches 99% after 10 m. The packing efficiency varies with packing height but not with lean loading.

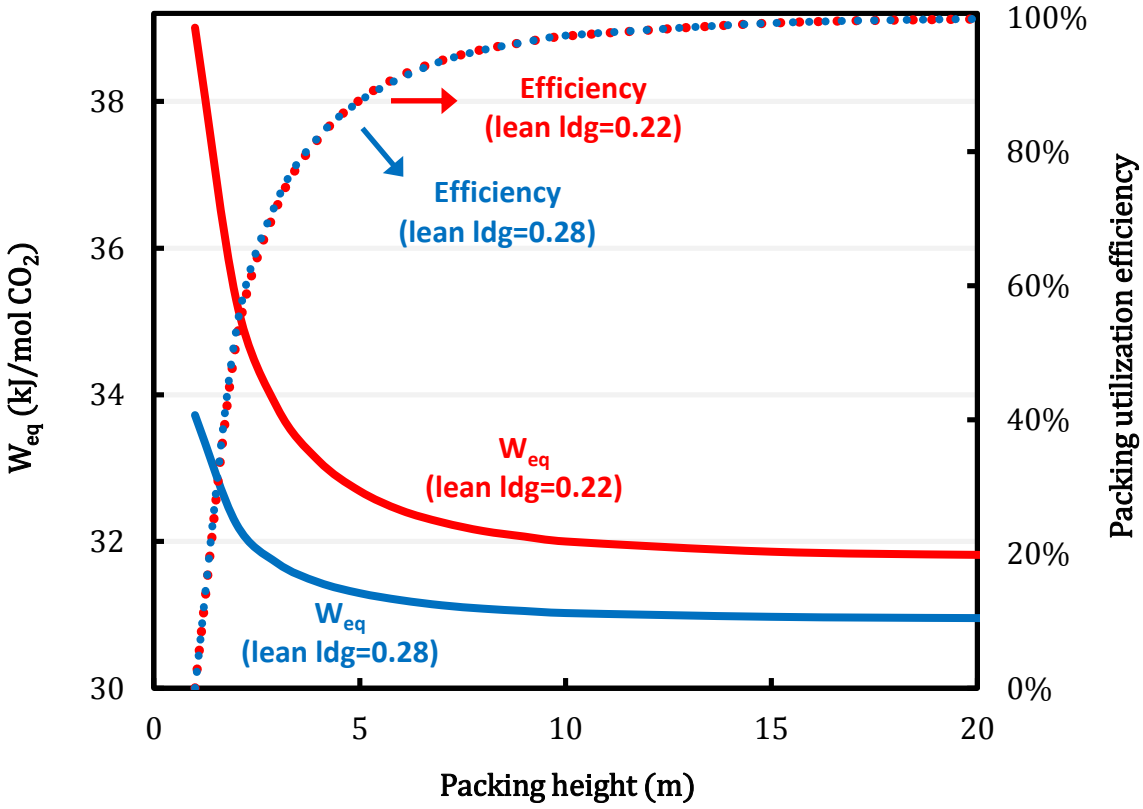

Figure 5.24: Packing utilization efficiency; packing: RSR no. 0.3; correction for interfacial area: 0.15; rich loading: 0.41; stripper T: 149 °C; constant UA; optimized bypass rates.

5.4.6 Effect of cross exchange area

The sensible heat recovered from the hot lean solvent in the cross exchanger is typically 3–5 times the reboiler/steam heater duty. Increasing the cross exchanger area

can effectively reduce the heat duty requirement. The size and performance of the specific heat exchanger in the pilot plant directly affects the measured energy performance.

Figure 5.25 shows the total equivalent work as the cross exchanger area is varied from 50% to 125% of the UA relative to the pilot plant. The reduction of the total equivalent work by increasing the cross exchanger area is more pronounced at higher lean loading where the cyclic capacity is deteriorating. An additional 25% cross exchanger area added to the base case reduces the total equivalent work by 4% at 0.28 lean loading. The cross exchanger in the SRP pilot plant is large, resulting in the minimum temperature approach as 2 K. Increasing cross exchanger area will not significantly reduce the heat duty since the exchanger has been practically pinched.

The average LMTD (ΔT_{LM}) is also indicated in Figure 5.25. The LMTD of the base case is 4.3 K. Lin and Rochelle suggest that the economic optimum cross exchanger LMTD is between 5 and 10 K using 8 m PZ (Lin & Rochelle, 2014). The large exchanger in the existing pilot plant may result in excessive capital cost.

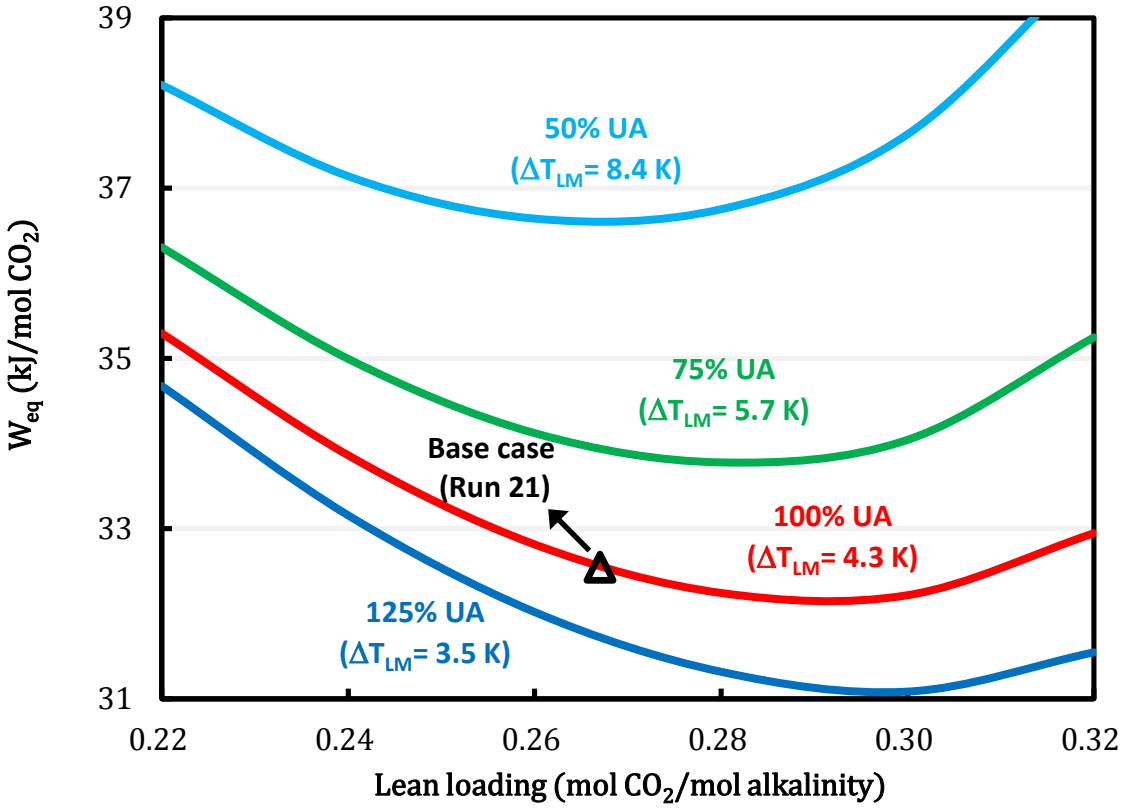

Figure 5.25: Total equivalent work with various cross exchanger UA; packing: 2 m RSR no. 0.3; correction for interfacial area: 0.15; rich loading: 0.41; stripper T: 149 °C; optimized bypass rates.

5.5 IRREVERSIBILITY ANALYSIS

Irreversibility analysis has been used to quantify process inefficiency and potential energy improvement for amine scrubbing processes in Chapter 3. By exergy balance using Equation 3.4, the minimum work and the lost work of each unit operation can be calculated. The sink temperature, T_o, is set at 313.15 K (40 ºC). T_k is the steam temperature. Q and W are the heat duty and work input/output. The enthalpy, H and the entropy, S were obtained from the validated Aspen Plus® model.

$$W_{lost} = \sum \left(1 - \frac{T_o}{T_k}\right) Q + \sum W + \sum_{in}(H - T_o S) - \sum_{out}(H - T_o S) \qquad (3.4)$$

Figure 5.26 shows the minimum work and the lost work averaged by the runs that achieved at least 90% capture rate and implemented bypass control. The minimum work of separation ($W_{min,sep}$) and the minimum work of compression ($W_{min,comp}$) are the theoretical work required to separate CO_2 from flue gas to pure CO_2 at stripper pressure and to compress pure CO_2 isothermally at 40 °C from stripper pressure to 150 bar, respectively.

The lost work of each unit operation indicates irreversible operations. The lost work of the absorber reflects the mass transfer driving force between the flue gas and the CO_2-loaded solvent. The lost work of the heat exchanger is proportional to the exchanger duty and the temperature approach. The cross exchanger and the steam heater are responsible for most of the lost work from heat exchangers. The exchanger duty of the steam heater is about 25% of the cross exchanger, however the temperature approach is greater. The compressor with intercooling is at 72% overall thermodynamic efficiency. Other contributions include the rich pump, the stripper column, the cold rich exchanger, the condenser, the trim cooler, and the un-recovered lean solvent pressure.

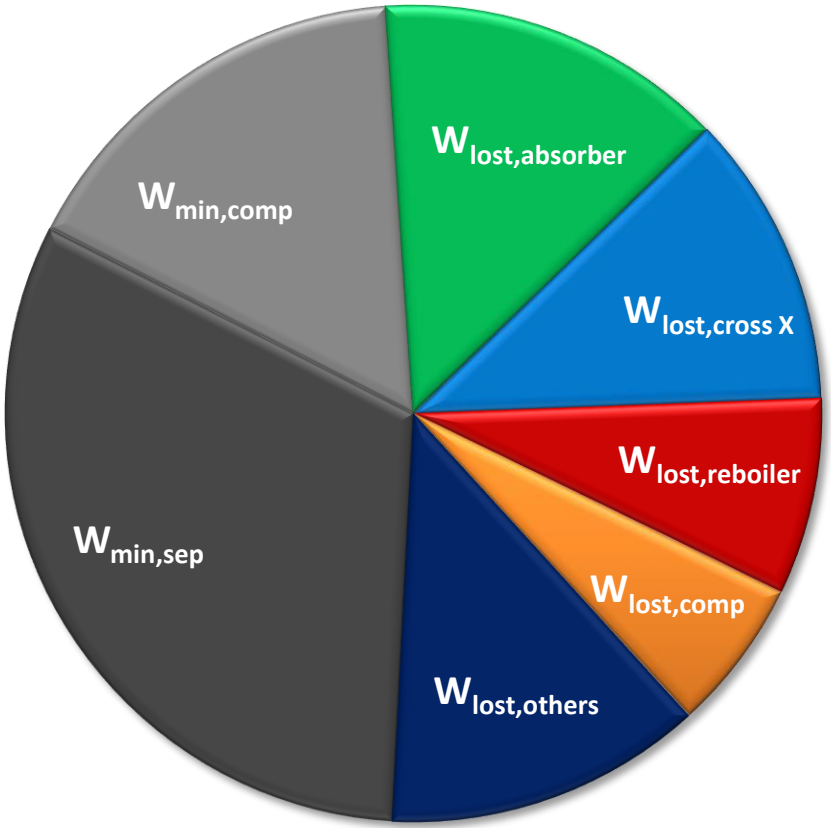

Figure 5.26: Minimum work and lost work distributions of SRP pilot plant with the AFS; average values from the runs that achieved at least 90% capture rate and implemented bypass control.

The overall thermodynamic efficiency including CO_2 separation and compression is about 50%, which is remarkable compared to 20% for conventional separation processes such as distillation (Fitzmorris et al., 1980; Y. H. Kim, 2012; Yoo et al., 1988). The remaining lost work is simply due to the mass and heat transfer driving force, which is inevitable if finite capital is used. Further energy reduction by process modifications will be marginal.

Solvents that provide greater absorption rate and capacity will be the key to better performance. The lost work of the cross exchanger can only be reduced by increasing solvent capacity (i.e., reducing solvent circulation rate and exchanger duty) because the

existing cross exchanger has already achieved a small temperature approach as indicated in Section 5.4.6. A higher absorption rate can effectively reduce the driving force in the absorber with finite packing height.

5.6 CONCLUSIONS

Findings of pilot plant test:

- The CO_2 mass balance was closed with 2.2% average error. Process heat duty and heat loss were identified using enthalpy balance around the stripping process.
- 17 runs have process heat duty 2.1–2.5 GJ/tonne CO_2 and 4 runs without enough rich solvent bypass are 2.5–2.9 GJ/tonne CO_2. The lowest W_{eq} is 32.0 kJ/mol CO_2.
- The AFS shows over 25% heat duty reduction compared to previous SRP campaigns, and over 30% compared to the DOE base case.
- Cold and warm rich solvent bypass were manually controlled to recover the stripping steam heat by maintaining the stripper vapor outlet temperature and the cold rich exchanger vapor outlet temperature. Four runs that did not achieve the temperature target increased the process heat duty by 15%.
- 5 m PZ provides 20% greater number of heat transfer units than 8 m PZ on the cold cross exchanger and results in a lower process heat duty because of lower viscosity.

Findings of simulations:

- The "Independence" model was validated using the pilot plant data and accurately represents the performance of the pilot plant. The modeled lean loading and rich loading show 5.4% and 3.6% average error compared to the density-predicted loading. The modeled and the measured process heat duty has 3% average error.
- The validated model was used to re-optimize the bypass rates. It confirmed that the bypass control strategy used during the test successfully minimized the heat duty.

- Increasing the stripper packing height has a more significant effect at low lean loading. The packing utilization efficiency can reach 88% using 5 m of RSR no. 0.3.
- The existing cross exchanger performed well on recovering the sensible heat from the lean solvent, giving around 2 K pinch temperature approach and 4.3 K ΔT_{LM}. Energy improvement by using more exchanger area will not be significant for the existing pilot plant.
- The irreversibility analysis showed that the thermodynamic efficiency of the SRP pilot plant using the AFS is about 50%. The absorber and the cross exchanger are the two major sources of lost work and can only be addressed by greater absorption rate and solvent capacity, respectively.

ACKNOWLEDGEMENT

The pilot plant data presented in this work was contributed by all of the hard work by the staff in SRP and graduate students from Rochelle's group including Dr. Rochelle and Dr. Eric Chen who planned the campaign and manufactured the AFS, and Dr. Frank Seibert, Micah Perry, Steve Briggs, Robert Montgomery, Di Song, Steven Fulk, Matt Walters, Yue Zhang, Matt Beaudry, Kent Fischer, Paul Nielsen, Darshan Sachde, and Nathan Fine.

Chapter 6: Approximate Stripper Models (ASM)

6.1 INTRODUCTION

Solvent selection is one of important ways to reduce the energy requirement and capital cost for CO_2 capture. Solvent screening has been used to identify important solvent properties such as absorption rate, CO_2 solubility, and thermal stability (Li, 2015). These measured data can be used to quantify individual energy contributions and capital requirement such as cyclic capacity, maximum stripper temperature, absorber packing requirement, and the size of cross exchanger. Process models incorporated with solvent characteristics are necessary in order to evaluate the overall energy performance that reflects the process specifications, operating conditions, and the integration effect of various solvent properties. Rigorous Aspen Plus® models have been developed by regressing thermodynamic and kinetic data over a range of amine concentration and CO_2 loading, and used to simulate advanced processes and scale up (Frailie, 2014; Plaza, 2011; Sherman, 2016) . However, rigorous models require extensive experimental data and are time-consuming to create.

For the purpose of estimating energy performance for promising amines, shortcut models that can reasonably predict energy performance should be adequate. Notz proposed a shortcut method that applies Kremser's equilibrium stage approach, but the model was less accurate at higher lean loading due to the assumption of an isothermal stripper (Notz et al., 2011). Kim developed an enthalpy balance around a simple stripper to approximate the regeneration heat duty assuming that the partial pressure of CO_2 and water is equilibrium with the hot rich solvent that enters the top of the stripper (H. Kim et al., 2015). The assumption does not apply to the low lean loading region since the stripper pinch is no longer at the top. This previous work were all based on the conventional simple stripper.

The goal of this work is to develop an approximate stripper model (ASM) that captures the characteristics of the advanced flash stripper (AFS), which has shown remarkable energy performance and can be regarded as a representative of a highly reversible regeneration process. The model will be developed in MATLAB® with limited input data required. It will be validated with existing models that were developed rigorously in Aspen Plus®.

As shown in Figure 6.1, the ASM will be used to predict the overall energy performance for existing solvent candidates with inputs of by measured solvent properties and process specifications. The prediction can provide a quantitative indicator for solvent selections. The model can also be treated as a generic solvent model. Desired solvent properties and process operating conditions that minimize the energy requirement can be identified. A guidance for future solvent screening can be provided.

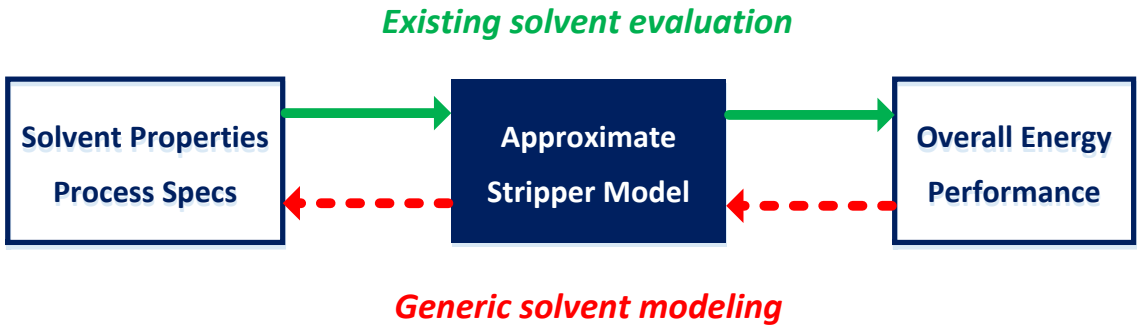

Figure 6.1: Approximate stripper model

6.2 Model Development

The ASMs were developed for the simple stripper and the AFS. The simple stripper serves as the base case so the interactions between solvent properties and stripper configurations can be investigated. The absorber is not in the scope of this paper and will

not be included in the model. Typical rich solvent conditions will be used as input to the model. The ASM is algebraic-equation-based and is solved in MATLAB®. The model calculates material balance, enthalpy balance, and vapor liquid equilibrium but does not include the rigorous mass and heat transfer calculations of the rate-based model in Aspen Plus®. Instead, the ASM specifies the mass and heat transfer driving force between vapor and liquid at both the top and the bottom of the stripper. The major inputs are the CO_2 solubility relationship (i.e., vapor liquid equilibrium of CO_2 in loaded amine) and the heat capacity. The system includes three components: CO_2, amine, and water. It assumes that the amine is non-volatile and CO_2 is not condensable. The CO_2 equilibrium is described by a relation between partial pressure of CO_2 and CO_2 loading in solution, which can be obtained from experimental measurements. The flash calculation of water applies Raoult's law assuming ideal solution and ideal gas. The saturation pressure and the heat of vaporization of water are obtained from the DIPPR database.

6.2.1 Modeling specifications

The simple stripper and the AFS are shown in Figures 6.2 and 6.3, respectively. Since the absorber is not included, the rich loading and temperature are specified for typical intercooled absorber. The partial pressure of CO_2 of the lean solvent (lean P^*_{CO2}) was varied from 0.05 to 1 kPa. Detailed equations are shown in Appendix C. General modeling specifications are described in this section.

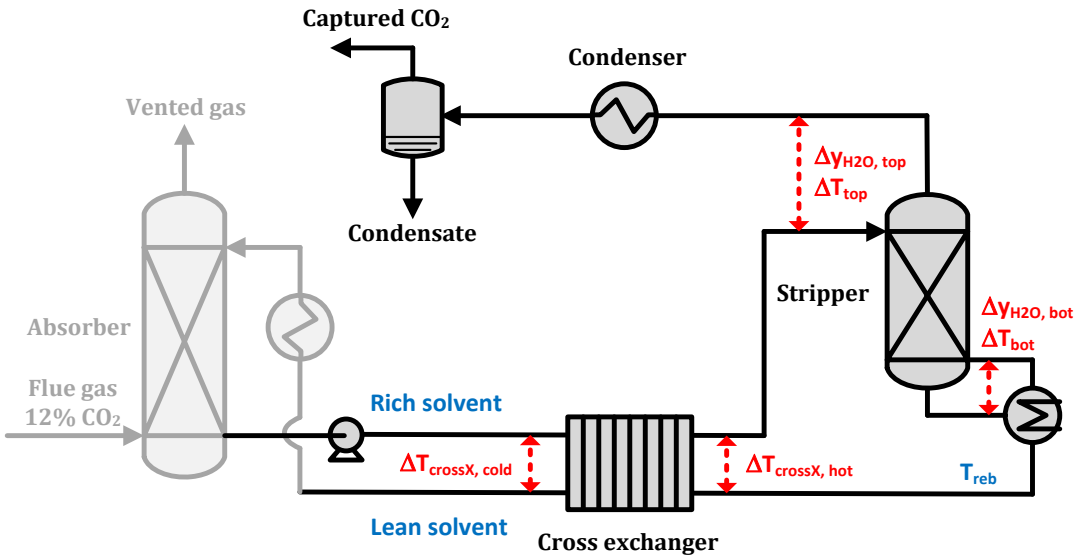

Figure 6.2: Simple stripper.

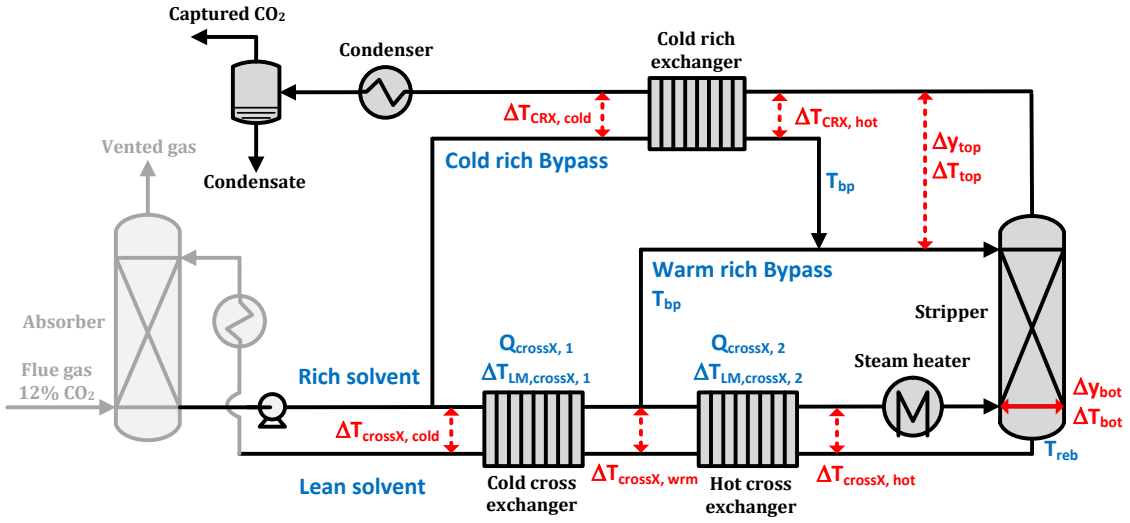

Figure 6.3: Advanced flash stripper.

6.2.1.1 Heat exchangers

The heat exchangers are specified by the log mean temperature difference (LMTD, ΔT_{LM}), which is a log mean average of temperature approaches at the cold end and the hot end assuming a linear temperature-enthalpy profile.

The rich solvent usually flashes and becomes two phases in the cross exchanger when it reaches the bubble point. To minimize the error caused by the nonlinear temperature-enthalpy profile due to flashing, the LMTD calculation of the cross exchanger is split into two regions: the liquid phase region and the flashing region. The heat duty and the LMTD of each region are calculated. The average LMTD ($\Delta T_{LM,crossX,avg}$) is then obtained using Equation 6.1, which weights the LMTD of each region by its exchanger duties. For the advanced flash stripper, the temperature of the warm rich bypass is specified as bubble point temperature, which makes the LMTD calculation approach identical to the simple stripper.

$$\Delta T_{LM,crossX,avg} = \frac{Q_{crossX,1}+Q_{crossX,2}}{\frac{Q_{crossX,1}}{\Delta T_{LM,crossX,1}}+\frac{Q_{crossX,2}}{\Delta T_{LM,CrossX,2}}} \tag{6.1}$$

6.2.1.2 Viscosity correction for cross exchanger

The heat transfer performance of the cross exchanger can be affected by the solvent viscosity. The optimum cross exchanger LMTD is a function of viscosity with a power of 0.175 for plate-and-frame exchanger (Li, 2015). Viscous solvent should be designed with a greater LMTD to avoid the excessive capital cost of cross exchanger due to the degraded heat transfer coefficient. Details of cross exchanger optimization can be found in Chapter 8. To differentiate the viscosity effect on the cross exchanger performance, the specified cross exchanger LMTD can be adjusted based on the solvent viscosity at 40 °C as Equation 6.2 shows. The viscosity of 30 wt% MEA will be used as the reference (μ_{ref}) and 5 K will be the reference LMTD of the cross exchanger ($\Delta T_{LM,ref}$).

$$\Delta T_{LM,crossX,avg} = \Delta T_{LM,ref}\left(\frac{\mu}{\mu_{ref}}\right)^{0.175} \tag{6.2}$$

6.2.1.3 Stripper column

The model approximates the mass and heat transfer of the stripper by specifying the concentration and temperature driving force between the vapor and the liquid. The log mean temperature difference ($\Delta T_{LM,strp}$) and the log mean concentration difference ($\Delta y_{LM,strp}$) are calculated using Equations 6.3 and 6.4, respectively. Since the amine is assumed to be non-volatile, the $\Delta y_{LM,strp}$ of CO_2 will be the same as H_2O.

$$\Delta T_{LM,strp} = \frac{\Delta T_{top} - \Delta T_{bot}}{ln\left(\frac{\Delta T_{top}}{\Delta T_{bot}}\right)} \tag{6.3}$$

$$\Delta y_{LM,strp} = \frac{\Delta y_{top} - \Delta y_{bot}}{ln\left(\frac{\Delta y_{top}}{\Delta y_{bot}}\right)} \tag{6.4}$$

The temperature and concentration difference indicate the heat recovery performance of the stripper and both are affected by the stripper packing height. Table 6.1 shows average temperature (ΔT_{strp}) and concentration (Δy_{strp}) driving force in the AFS obtained from a rigorous Aspen Plus® model that has been validated by the pilot plant data in Chapter 5. A 15% correction factor was applied to the interfacial area of the stripper packing in order to match the plant performance. More packing used will reduce the driving forces and attain better energy performance. 5 meter of Raschig Super-Ring (RSR) no. 0.3 packing in the stripper will result in 5−10% $\Delta y_{LM,strp}$ and 5−7 K $\Delta T_{LM,strp}$ using 5 m PZ.

The stripper pressure was determined at the specified reboiler temperature and lean loading, and then the bubble point temperature of the rich solvent can be calculated. The cold rich bypass temperature at the cold rich exchanger outlet and the warm rich bypass were specified at bubble point temperature. The cold rich bypass ratio was determined by the enthalpy balance around the cold rich exchanger at a given LMTD. The warm rich

bypass ratio was optimized to minimize the total heat duty. Greater bypass rates will be required at low lean loading because more stripping steam needs to be recovered.

Table 6.1: Temperature and concentration driving force from Aspen Plus® simulations using the AFS and 5 m PZ; 15% correction for interfacial area; reboiler T: 150 °C; optimized bypass rates; rich loading: 0.4.

Lean loading (mol CO_2/mol alk)	**0.22**	**0.24**	**0.26**	**0.28**	**0.30**	**0.32**
2 m RSR no. 0.3 stripper packing						
Avg ΔT_{strp} (K)	11.5	12.1	11.6	10.9	9.9	8.7
Avg Δy_{strp} (%)	16.2	15.2	13.4	11.5	9.6	7.7
5 m RSR no. 0.3 stripper packing						
Avg ΔT_{strp} (K)	7.0	6.8	6.5	6.1	5.6	5.0
Avg Δy_{strp} (%)	9.5	8.7	7.8	6.8	5.9	5.0
10 m RSR no. 0.3 stripper packing						
Avg ΔT_{strp} (K)	4.3	4.2	4.0	3.8	3.5	3.2
Avg Δy_{strp} (%)	6.3	5.8	5.3	4.8	4.2	3.7

6.2.2 Solvent characterization

The cyclic capacity and the heat of absorption are the most important solvent properties that determine energy performance. The heat of absorption can be measured directly by calorimetric experiments or obtained from the temperature derivative of the CO_2 solubility measurement (I. Kim et al., 2007, 2011). This model determines the differential heat of absorption (ΔH_{abs}) in Equation 6.5 from Lewis and Randall (Equation XVIII.9) (Lewis et al., 1923). The fugacity of CO_2 (f_{CO2}) is approximated by its partial pressure (P^*_{CO2}). Equation 6.5 has been validated in predicting the calorimetric data for CO_2 absorption in aqueous MEA at typical operating conditions (Mathias et al., 2012). In this work it will be applied to a higher stripper pressure. The fugacity coefficient of CO_2 at 150 °C is 0.95–0.99 at 1–30 bar and 0.9–0.95 at 30–60 bar (Spycher et al., 1988). The

heat of absorption used in this model is only a function of CO_2 loading but is not temperature dependent. It represents an average heat of absorption across the operating temperature range.

$$\Delta H_{abs} = -R\left[\frac{\partial ln f_{CO_2}}{\partial\left(\frac{1}{T}\right)}\right]_{P,x} \approx -R\left[\frac{\partial ln P^*_{CO_2}}{\partial\left(\frac{1}{T}\right)}\right]_{P,x} \quad (6.5)$$

The slope of the solubility curve, k, will affect the cyclic capacity and is defined in Equation 6.6. A flat solubility curve will increase the loading difference between the lean and the rich solvent at given rich and lean partial pressure of CO_2.

$$k(T,\alpha) = \frac{\partial ln P^*_{CO_2}}{\partial \alpha} \quad (6.6)$$

The partial pressure of CO_2 is characterized by the slope of the solubility curve and the heat of absorption as shown in Equation 6.7. The partial pressure is integrated from a reference temperature (T_r) and CO_2 loading (α_r) to the final state via the CO_2 loading dependence and the temperature dependence. Figure 6.4 shows the integrating path.

$$ln P^*_{CO_2}(T,\alpha) = ln P^*_{CO_2,r}(T_r,\alpha_r) + \int_{\alpha_r}^{\alpha} k(T_r,\alpha)d\alpha + \int_{T_r}^{T} -\frac{\Delta H_{abs}(\alpha)}{R} d\left(\frac{1}{T}\right) \quad (6.7)$$

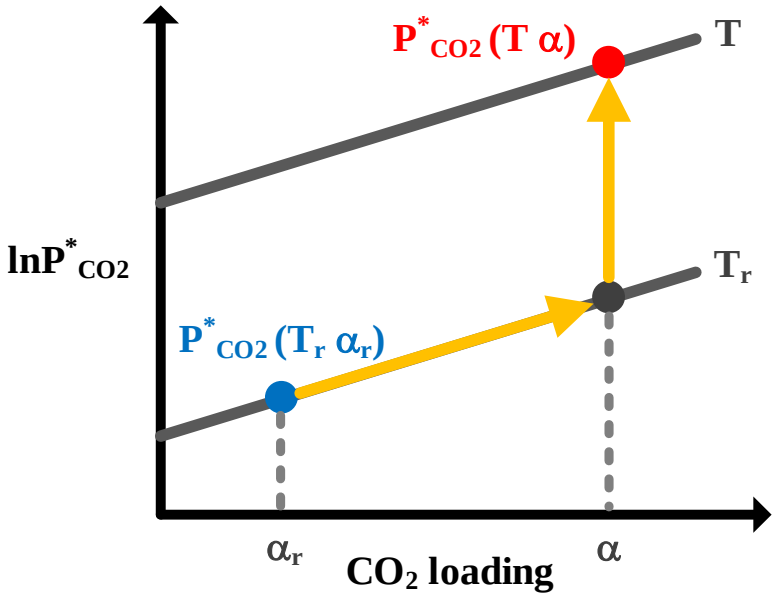

Figure 6.4: Integration path of partial pressure of CO_2 for solvent characterization.

The CO_2 solubility data is usually presented as a semi-empirical equation as a function of temperature and CO_2 loading (Equation 6.8) (Li & Rochelle, 2013). C_1–C_6 are the regressed coefficients. For those solvents with available solubility data, the k and the ΔH_{abs} can be expressed by Equations 6.9 and 6.10, respectively, based on the definitions above. Table 6.2 shows the regressed constants for PZ and MEA using the CO_2 solubility data in a wide range of CO_2 loading and temperature from 40 to 160 °C (Xu, 2011). They will be used to represent the VLE of PZ and MEA in this work and demonstrate the energy performance using the ASM in Section 6.3.

$$lnP^*_{CO_2} = C_1 + \frac{C_2}{T} + C_3\alpha + C_4\alpha^2 + C_5\frac{\alpha}{T} + C_6\frac{\alpha^2}{T} \tag{6.8}$$

$$k = C_3 + 2C_4\alpha + \frac{C_5}{T} + 2C_6\frac{\alpha}{T} \tag{6.9}$$

$$\Delta H_{abs} = -R(C_2 + C_5\alpha + C_6\alpha^2) \tag{6.10}$$

Table 6.2: Regressed constants in Equation 6.8 for MEA and PZ.

Amine	C_1	C_2	C_3	C_4	C_5	C_6	R^2
MEA	38.6	-12379	0	-16	3556	8702	0.994
PZ	35.3	-11054	0	-18.9	4958	10163	0.993

The heat capacity of the CO_2 loaded solution is needed to calculate the enthalpy balance around the heat exchangers, which will affect the sensible heat requirement. The heat capacity of the mixture is estimated by a weight fraction average of pure components shown in Equation 6.11 as a function of temperature. Any enthalpy of mixing is ignored. The heat capacity of aqueous PZ is predicted from a group contribution model (Rayer et al., 2012). The partial heat capacity of CO_2 is assumed to be zero in this model and the sensitivity will be discussed in Section 6.3.

$$C_{p,mix}(T) = C_{p,am}(T)X_{am} + C_{p,H_2O}(T)X_{H_2O} + C_{p,CO_2}(T)X_{CO_2} \qquad (6.11)$$

6.3 MODEL VALIDATION AND INTERPRETATION

6.3.1 Comparison with rigorous Aspen Plus® model

The ASM is compared with the rigorous Aspen Plus® model that has been validated by the pilot plant data from the 2015 campaign at UT Austin using the AFS and 5 m PZ. Figure 6.5 shows the total equivalent work at varied lean loading. The LMTDs of the cross exchanger and the cold rich exchanger are 5 K and 20 K, respectively. The $\Delta T_{LM,strp}$ and the $\Delta y_{LM,strp}$ of the stripper specified in the ASM were obtained from the Aspen Plus® results using 5 meters of RSR no. 0.3 packing.

The results show a 5% systematic bias between the ASM and the Aspen Plus® model, but have the same trend with varied lean loading. The bias is mainly due to the difference in the predicted heat capacity of CO_2 loaded solvent between models. The

approximate model matches the Aspen Plus® model if the partial heat capacity of CO_2 is increased from 0 to 3 kJ/kg-K, which is close to the value predicted by Aspen Plus®.

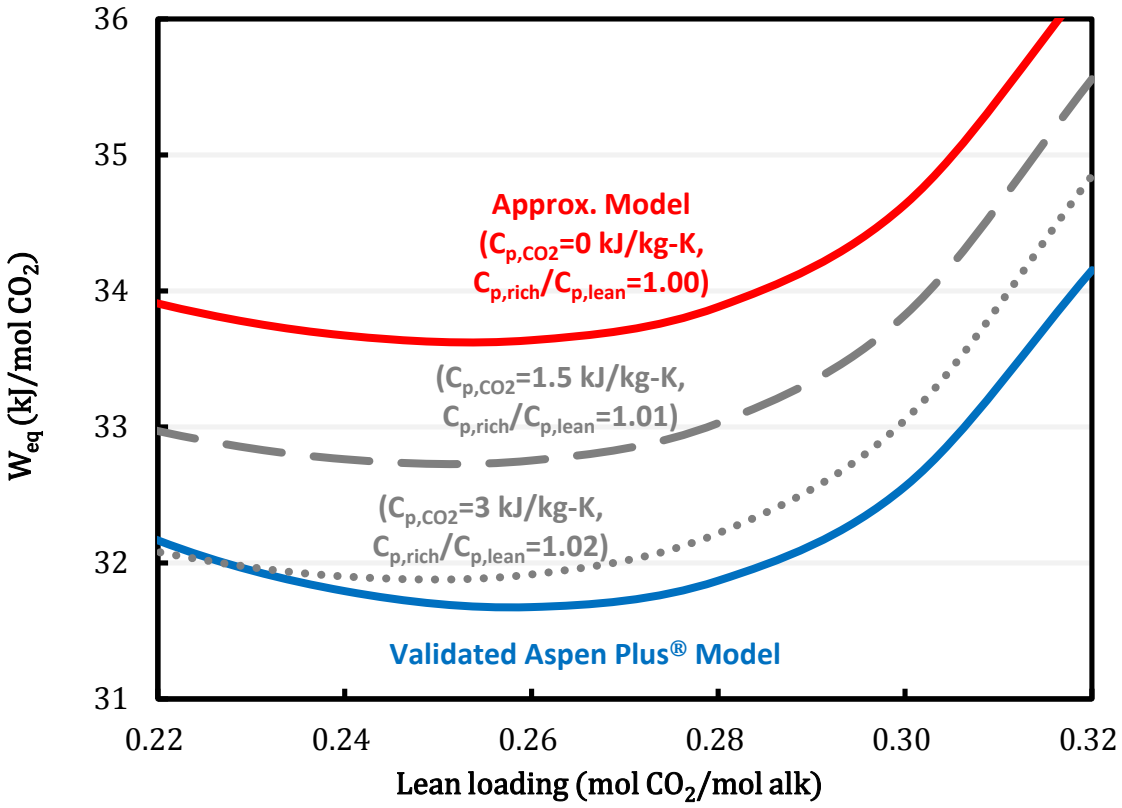

Figure 6.5: Comparison of ASM and the validated Aspen Plus® model using AFS; 5 m PZ; reboiler T: 150 °C; 5 K cross exchanger ΔT_{LM}; 5 m RSR no. 0.3 packing; 0.15 correction factor for interfacial area used in the Aspen Plus® model.

6.3.2 Uncertainties of predicted heat capacity

The sensible heat required depends on the temperature approach of the cross exchanger and is sensitive to the ratio of the heat capacity of the lean and the rich solvent. The temperature change of the lean and the rich solvent in the cross exchanger is around 100 K (approximately from 50 °C to 150 °C). A 1% difference of the heat capacity between the lean or the rich solution will lead to a 1 K difference on the temperature

approach, which is 20% of sensible heat when the LMTD is 5 K. This shows that the consistency of the heat capacity between lean and rich solvent is important to the cross exchanger design and the sensible heat estimate, especially when the cross exchanger has a large number of transfer units (i.e., a large temperature change and a small temperature approach). The heat capacity will mainly affect the sensible heat requirement.

The heat capacity of CO_2-loaded PZ solution were measured using Differential Scanning Calorimeter (DSC) by Hilliard and Nguyen over a range of PZ concentration, CO_2 loading, and temperature (Hilliard, 2008; Nguyen, 2013). The Independence model attempted to predict these data but had limited success (Frailie, 2014).

To compare the predicted partial heat capacity of CO_2, which is the main factor that determines the heat capacity ratio of lean and rich solvent, Equation 6.11 is used as a simple model. Table 6.3 compares the partial heat capacity predicted by experiment data and the Independence model. The reproducibility of the experiments was obtained by running duplicates with DSC using water. Hilliard's data is more consistent than Nguyen's, which potentially has up to 10% of error. The predicted partial heat capacity of PZ are in the same range among the predictions by experiments and the Independence model. But the predicted partial heat capacity of CO_2 by the Independence model is about 10 times the Hilliard's data and 1.5-3 times the Nguyen's data. Improving the consistency of the experiment measurement and the model predictions is recommended for future work in order to accurately predict the sensible heat.

Table 6.3: Partial heat capacity of CO_2 of loaded PZ.

	Hilliard (2008)	**Nguyen (2013)**	**Independence model**
Data reproducibility (%)	±1%	±10%	N/A
PZ (m)	2 and 3.6	8, 10, and 12	5 and 8
CO_2 loading (mol CO_2/mol alk)	0.16–0.4	0.2–0.4	0.2–0.4
Temperature (°C)	40–120	40 150	40–150
Partial C_p of CO_2 (kJ/kg-K)	0.3–0.5	1–2.9	3.6–4
Partial C_p of PZ (kJ/kg-K)	1.8–2.9	2.4–3.1	2.6–3

6.3.3 Model interpretation using MEA and PZ

The ASM is demonstrated using 9 m MEA and 8 m PZ with the simple stripper and the AFS in Figure 6.6. Table 6.4 shows the process specifications. The rich loadings are specified as 0.5 and 0.4 mol CO_2/mol alkalinity for MEA and PZ, respectively, which are typical with an intercooled absorber (Plaza, 2011). The reboiler for MEA is at 120 °C, lower than PZ since it is less thermally stable.

Table 6.4: Process specifications for solvent evaluation.

Amine	**9 m MEA**	**8 m PZ**
Reboiler temperature (°C)	120	150
Rich loading (mol CO_2/mol alkalinity)	0.5	0.4
Rich solvent temperature (˚C)	46	
$\Delta T_{LM,crossX,avg}$ (K)	5	
$\Delta T_{LM,strp}$ (K)	5	
$\Delta y_{LM,strp}$ (%)	5	
Cold rich exchanger ΔT_{LM} (K)	5	

8 m PZ requires 13% less equivalent work than 9 m MEA, mainly a result of the higher capacity of PZ, which is amplified at higher lean loading where a higher circulation rate is required. The AFS further reduces the total equivalent work by over 10% compared to the simple stripper, and the reduction is significant at lower lean loading, where more stripping steam heat is required. The results show the same trends as previous modeling results using rigorous Aspen Plus® models (Lin, Madan, et al., 2014), suggesting that the ASMs are capable of differentiating between solvents and between stripper configurations, and reflecting the effects of lean loading and reboiler temperature.

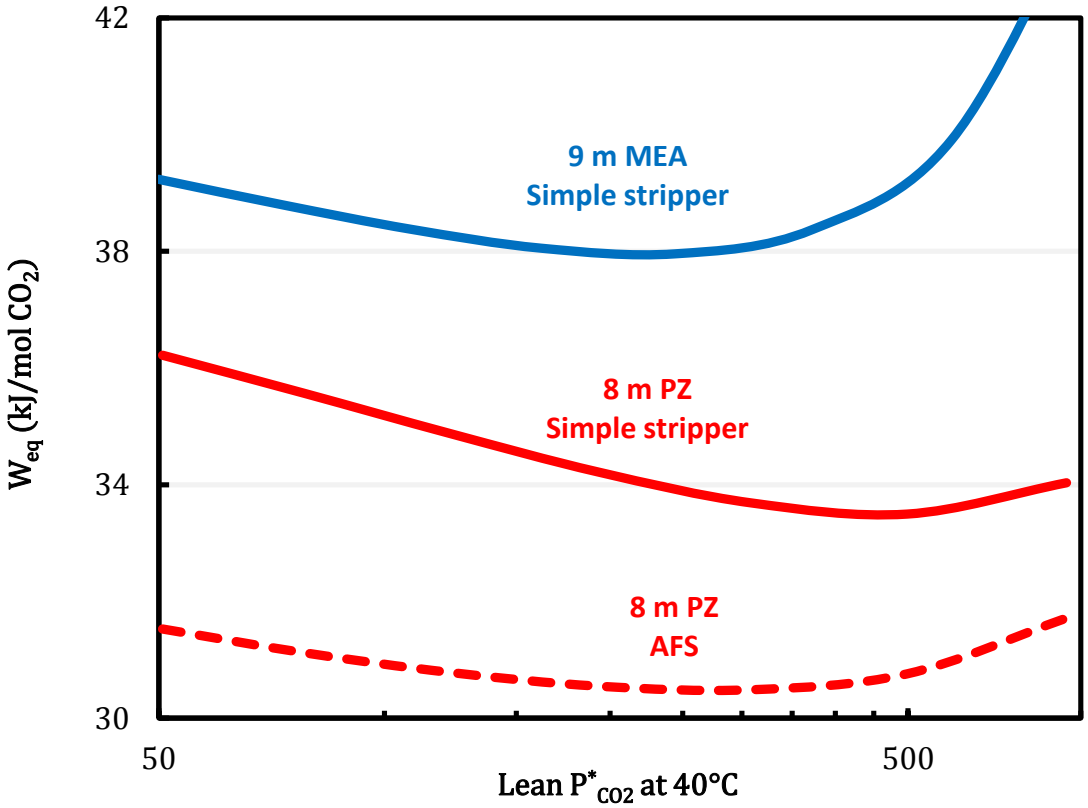

Figure 6.6: Approximate stripper model results of 9 m MEA and 8 m PZ with the simple stripper and the AFS; rich loading: 0.4 for PZ and 0.5 for MEA; cross exchanger ΔT_{LM}: 5 K; reboiler T: 150 °C for PZ and 120 °C for MEA.

6.3.4 Contributions to energy requirement

The ASMs also quantify each contribution to the total equivalent work. The heat duty work can be split into the heat of absorption ($W_{heat,abs}$), the sensible heat ($W_{heat,sen}$), and the stripping steam heat ($W_{heat,stm}$). The average heat of absorption is defined in Equation 6.12, which integrates the differential heat of absorption from lean to rich loading. The stripping steam heat accounts for the latent heat of the remaining steam coming from the stripper (for the simple stripper) or from the cold rich exchanger (for the AFS).

$$\Delta H_{abs,avg} = \frac{\int_{\alpha_{lean}}^{\alpha_{rich}} \Delta H_{abs} d\alpha}{\alpha_{rich} - \alpha_{lean}} \tag{6.12}$$

Figure 6.7 shows the breakdown of the total equivalent work at lean P^*_{CO2} of 0.15 kPa at 40 °C, which is used as a surrogate for lean loading. When comparing PZ and MEA with the simple stripper at the same reboiler temperature, 120 °C, the major energy savings of PZ are from the sensible heat due to the greater capacity of PZ. When the reboiler temperature is elevated to 150 °C, higher stripper pressure reduces the compression work but the work value of the heat duty increases with temperature. The saving of compression work is almost offset by the increase in heat work, and the total equivalent work is about the same. The AFS almost eliminates the stripping steam heat with a slight increase in the sensible heat. When the rich solvent is bypassed to recover the stripping steam heat, less sensible heat can be recovered from the hot lean solvent. These tradeoffs were considered in optimizing the bypass rates that minimize the total equivalent work.

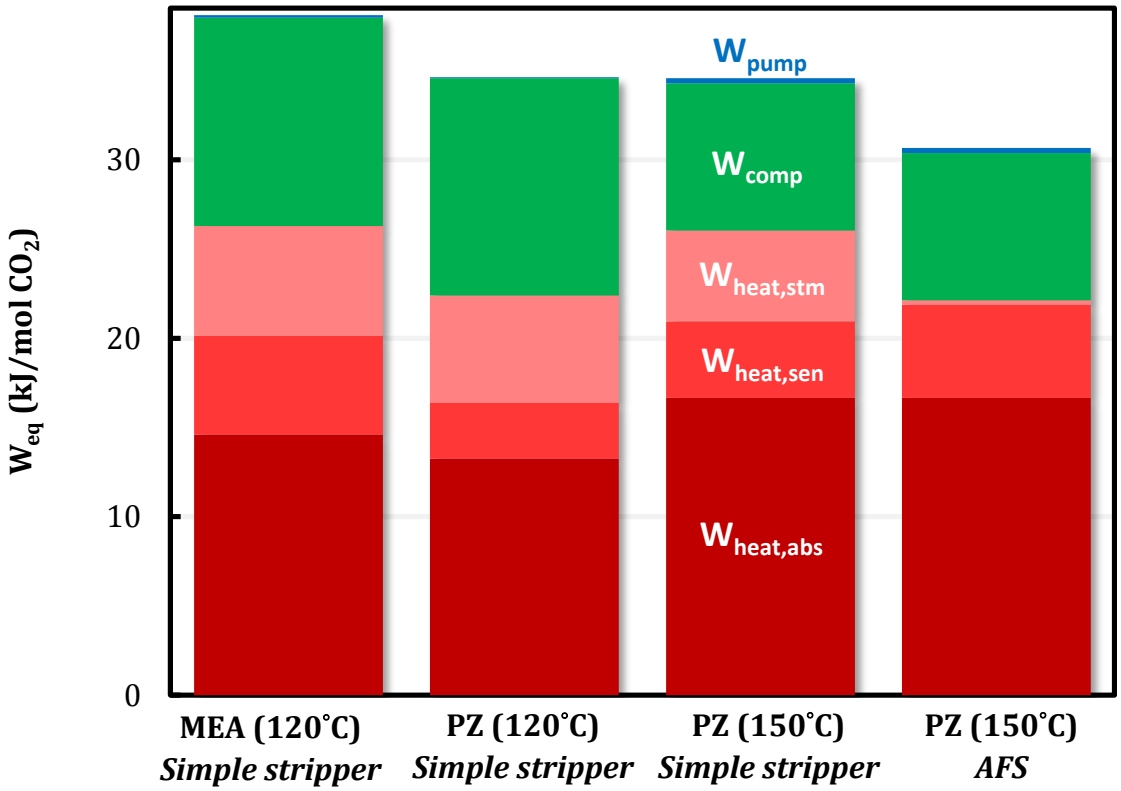

Figure 6.7: Breakdown of energy requirement using approximate stripper models; lean P^*_{CO2}: 0.15 kPa; rich loading: 0.4 for PZ and 0.5 for MEA; cross exchanger ΔT_{LM}: 5 K; reboiler T: 150 °C for PZ and 120 °C for MEA.

6.4 SENSITIVITY ANALYSIS

6.4.1 Effect of rich loading

Since the absorber was not modeled in this work, a sensitivity analysis of the rich P^*_{CO2} was performed. Figure 6.8 shows the total equivalent work and the ΔLdg (i.e., the difference between the rich and the lean loading) using 8 m PZ with a rich P^*_{CO2} of 3 to 7 kPa. The lean loading was optimized at each rich loading to minimize the total equivalent work. The optimum lean loading will track the rich loading so the ΔLdg is almost constant. The AFS has a greater optimum ΔLdg than the simple stripper since it makes use of the additional stripping steam at lower lean loading.

The difference in the total equivalent work between the stripper configurations is nearly constant in this rich loading range, which suggests that the energy savings of the AFS will not be affected by the absorber performance at optimum lean loadings. The rich loading mainly affects the cyclic capacity and the sensible heat requirement.

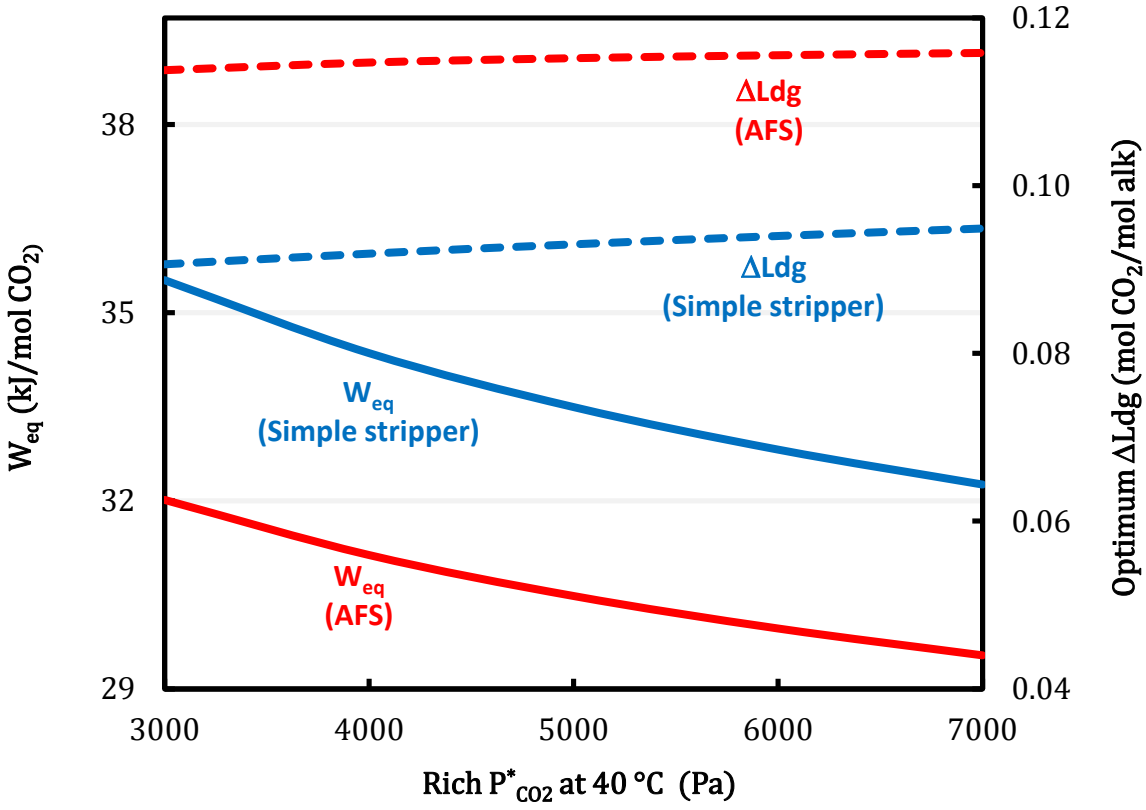

Figure 6.8: Sensitivity to rich loading; 8 m PZ; reboiler T: 150 °C; optimized lean loading.

6.4.2 Effect of VLE slope

The sensitivity to the slope of CO_2 solubility curve is tested by manipulating the k defined in Equations 6.6 and 6.7. Table 6.5 lists the average slope of common amine solvents at 40 °C calculated from the semi-empirical equations regressed by Xu (2011) between P^*_{CO2} from 0.1 to 5 kPa. Typically blending with tertiary and hindered amines

can reduce the VLE slope and improves the solvent capacity (Li, Voice, et al., 2013). More solvent capacity interpreted by VLE data can be found.

Table 6.5: Average slope of CO_2 solubility curve at 40 °C between P^*_{CO2} 0.1 to 5 kPa.

Amine	Average slope, k $\left(\frac{ln(Pa)}{mol\ CO_2/mol\ alk}\right)$
PZ	24.5
MEA	21.9
DGA	23.5
MDEA/PZ (5m/5m)	18.7
MDEA//PZ (7m/2m)	16.6

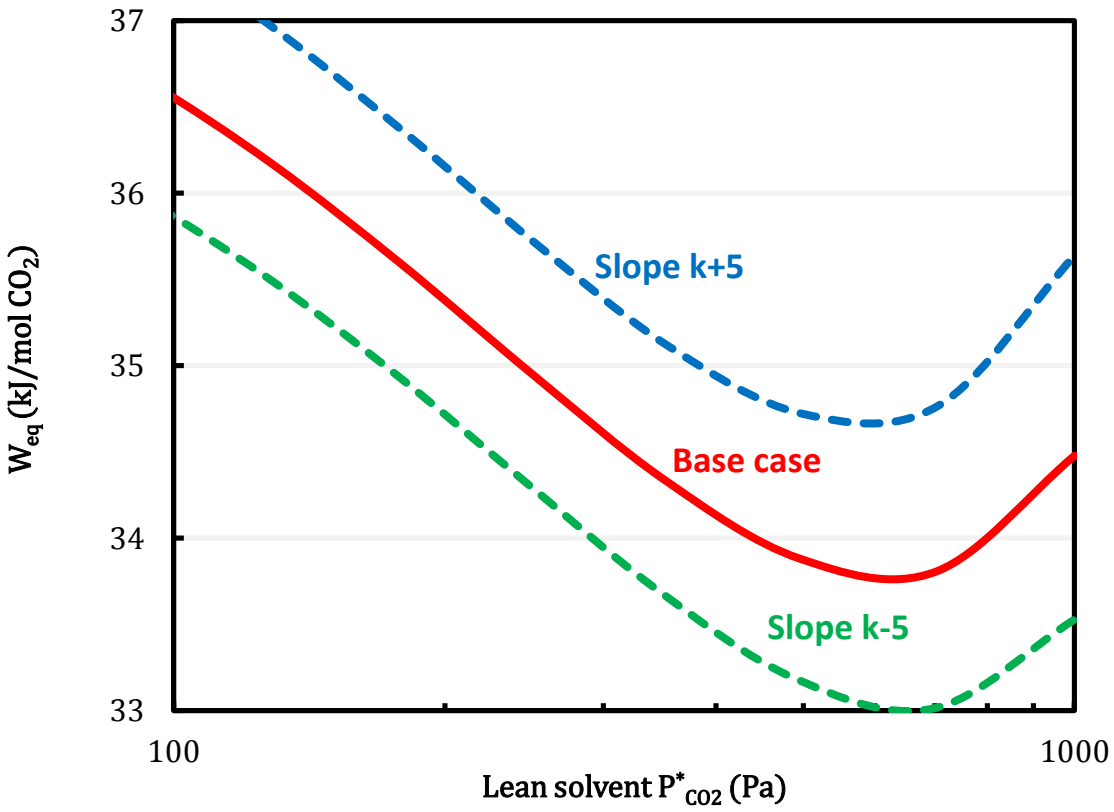

Figure 6.9: Sensitivity to VLE slope, k; simple stripper with 8 m PZ-based solvent; reboiler T: 150 °C; rich solvent P^*_{CO2}: 5 kPa; cross exchanger ΔT_{LM}: 5 K.

Figure 6.9 shows the total equivalent with varied VLE slope (k) by ±5 using the simple stripper. 8 m PZ is used as the base solvent. The rich solvent P^*_{CO2} is fixed at 5 kPa and the lean P^*_{CO2} varies from 0.05 to 1 kPa. The cross exchanger LMTD was specified as 5 K. When the slope changes, both rich and lean loadings will shift with the same direction to satisfy the specified P^*_{CO2}. A steeper slope will result in a tighter window between the rich and lean loadings and increases the solvent circulation rate needed to attain a certain CO_2 removal. The total equivalent work across the lean loading range systematically increases and decreases when the VLE slope changes.

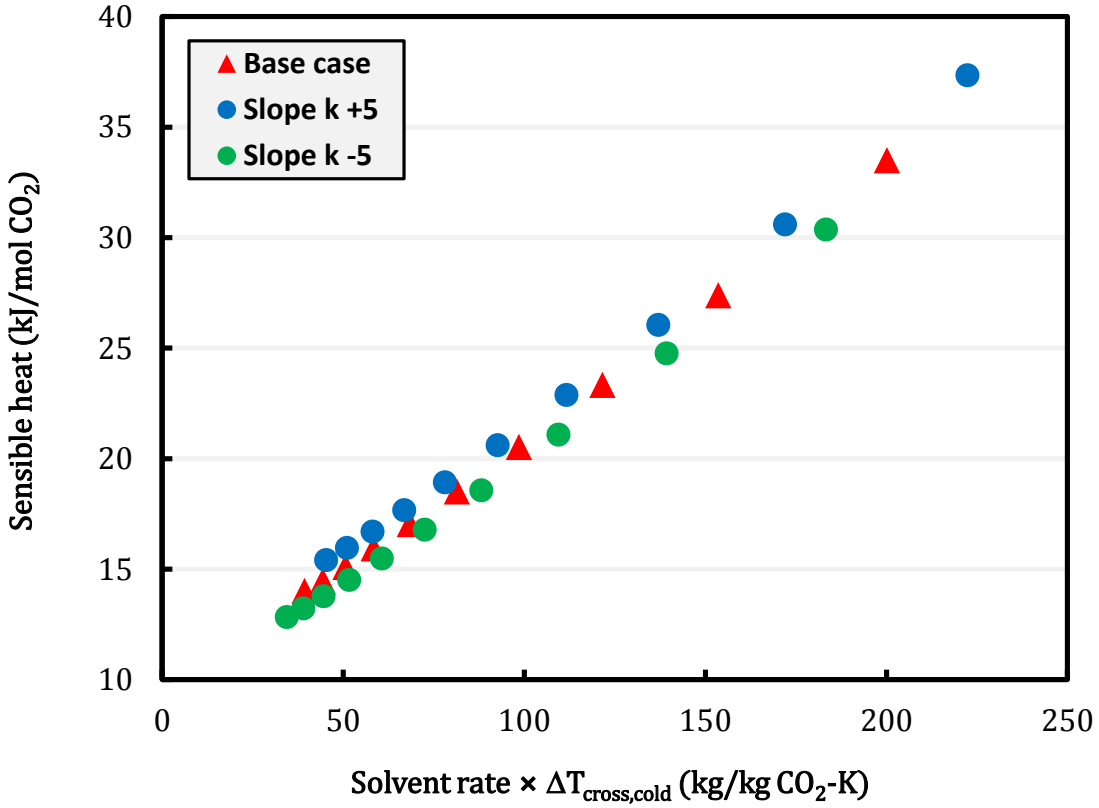

Figure 6.10: Sensible heat requirement with varied VLE slope, k (ln Pa/mol CO_2); simple stripper with 8 m PZ-based solvent; reboiler T: 150 °C; lean P^*_{CO2}: 0.05–1 kPa; rich solvent P^*_{CO2}: 5 kPa; cross exchanger ΔT_{LM}: 5 K.

The sensible heat requirement is mainly determined by the solvent rate and the cold side temperature approach of the cross exchanger, which is caused by the unbalance solvent rate between rich and lean. The VLE slope will ultimately reflect on the solvent circulation rate. Figure 6.10 shows that the sensible heat requirement of different VLE slopes are almost fall on the same line. This suggests that predicting the sensible heat requirement is straightforward and can be simply estimated by the cyclic capacity and the temperature approach of the cross exchanger.

6.5 CONCLUSIONS

- Approximate stripper models (ASM) were developed to predict the energy performance for the simple stripper and the AFS.
- The total equivalent work is sensitive to the predicted heat capacity of solvent especially when the cross exchanger has a large heat transfer unit. Generally the ASM showed a similar trend that was predicted by the rigorous Aspen Plus® model.
- The ASMs are capable of differentiating between solvents and between stripper configurations, and reflecting the effects of lean loading and reboiler temperature.
- As the rich loading varies from 3 to 7 kPa, a constant optimum ΔLdg was found and the energy savings by the AFS is not affected.

Chapter 7: Optimizing Heat of Absorption using the ASM

7.1 INTRODUCTION

Important solvent properties that affect energy performance include absorption rate, cyclic capacity, heat of absorption, and thermal stability. A higher absorption rate can reduce the packing in the absorber and make the solvent CO_2 richer, which increases the mass transfer driving force in the stripper. The cyclic capacity determines the solvent required to achieve a certain removal. The sensible heat needed to heat the solvent to the reboiler temperature will be proportional to the circulation rate. The heat of absorption is used to reverse the chemical reactions and strip the CO_2 from the rich solvent. A thermally stable solvent can be operated at a relatively high reboiler temperature and stripper pressure. High absorption rate, greater cyclic capacity, and good thermal stability are always desirable.

Typically the solvent performance has been represented as the reboiler duty based on experimental measurements at limiting conditions. Low heat of absorption has been considered advantageous in some previous solvent screening (Chowdhury et al., 2013; Goto et al., 2009). However, several researchers have suggested that a lower heat of absorption does not always reduce overall energy use since it can affect other contributions (Oexmann et al., 2010; Rochelle et al., 2011). The solvents with higher heat of absorption will have higher CO_2 partial pressure at stripper temperature, and so will have the potential to reduce the stripping steam heat and the compression work. The stripping steam heat has been identified as one of the major causes of irreversibility of the amine scrubbing process, and accounts for 30–50% of the lost work from the regeneration in Chapter 3. Higher CO_2 partial pressure can improve the selectivity of CO_2 to H_2O and reduce stripping steam heat. The compression work typically accounts for 1/3 of the total energy

requirement. Determining the desirable heat of absorption is not as straightforward as determining other properties.

The objective of this work is to quantify the optimum heat of absorption, and identify favorable operating conditions and stripper configurations that minimize the total energy requirement. Understanding the effect of the heat of absorption will facilitate solvent screening. The effect of the heat of absorption was evaluated using shortcut models of the simple stripper. Oyenekan and Rochelle tested the sensitivity using generic solvent with heat of absorption from 60 to 170 kJ/mol (Oyenekan et al., 2006). Heat equivalent work and compression work were used to indicate energy performance. Bhown noted that the work value of the extracted steam can have a significant impact on the selection of heat of absorption (Heberlea et al., 2014). Kim indicated the optimum heat of absorption is 60−80 kJ/mol by minimizing the reboiler duty at a constant stripper pressure at 1−3 bar (H. Kim et al., 2016). However, using only the reboiler duty as the indicator of energy performance and limiting the stripper pressure might not fully reflect the actual performance. Most previous work focused mainly on the conventional simple stripper but the energy requirement can be highly influenced by alternative configurations.

Approximate stripper models (ASM) developed in Chapter 6 will be used to explore the effect of heat of absorption by estimating the total equivalent work. Concentrated PZ will serve as the base solvent.

7.2 MODELING METHOD

7.2.1 ASMs with generic solvent

The ASMs for the simple stripper and the AFS that have been validated were described in Chapter 6. PZ-based generic solvent will be used in this work. By using Equation 6.7 to calculate the partial pressure of CO_2, the heat of absorption can be

manipulated by varying the ΔH_{abs} while keeping the slope of VLE curve (k) unchanged at given temperature and CO_2 loading so the solvent capacity will not be affected. The ΔH_{abs} and k of base solvent are obtained from Equation 6.9 and 6.10, which are derived from the semi-empirical equation (Equation 6.8). Table 7.1 shows the regressed constants for PZ using the CO_2 solubility data in a wide range of CO_2 loading and temperature from 40 to 160 °C (Xu, 2011).

$$lnP^*_{CO_2}(T,\alpha) = lnP^*_{CO_2,r}(T_r,\alpha_r) + \int_{\alpha_r}^{\alpha} k(T_r,\alpha)d\alpha + \int_{T_r}^{T} -\frac{\Delta H_{abs}(\alpha)}{R} d\left(\frac{1}{T}\right) \quad (6.7)$$

$$lnP^*_{CO_2} = C_1 + \frac{C_2}{T} + C_3\alpha + C_4\alpha^2 + C_5\frac{\alpha}{T} + C_6\frac{\alpha^2}{T} \quad (6.8)$$

$$k = C_3 + 2C_4\alpha + \frac{C_5}{T} + 2C_6\frac{\alpha}{T} \quad (6.9)$$

$$\Delta H_{abs} = -R(C_2 + C_5\alpha + C_6\alpha^2) \quad (6.10)$$

Table 7.1: Regressed constants for semi-empirical Equation 6.8 for PZ.

Amine	**C_1**	**C_2**	**C_3**	**C_4**	**C_5**	**C_6**	**R^2**
PZ	35.3	-11054	0	-18.9	4958	10163	0.993

7.2.2 Process specifications

The simple stripper and the AFS shown in Figures 7.1 and 7.2 are representative of a conventional and a highly reversible regeneration process, respectively. They will be compared in order to investigate the effect of alternative stripper configurations.

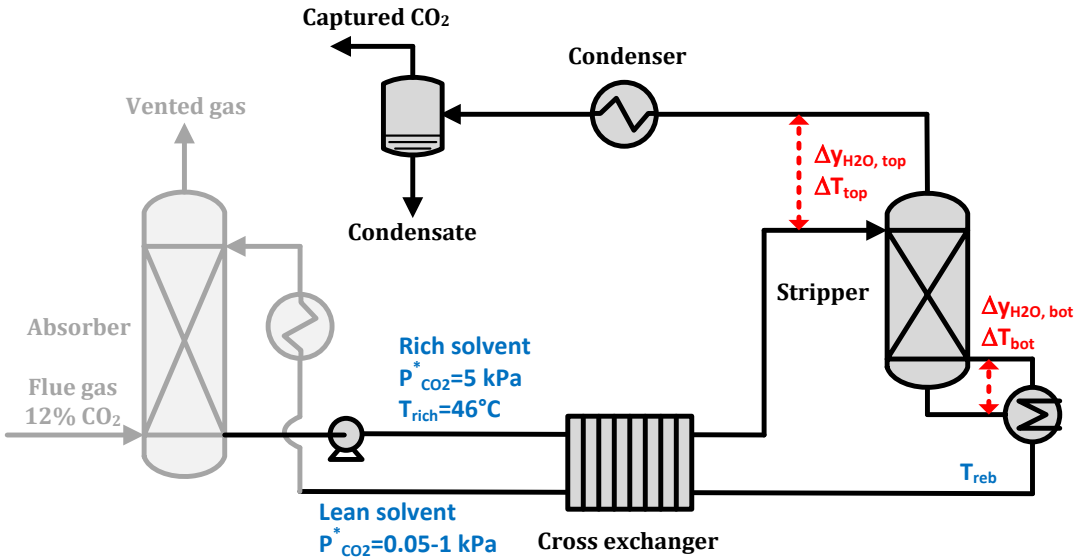

Figure 7.1: Simple stripper

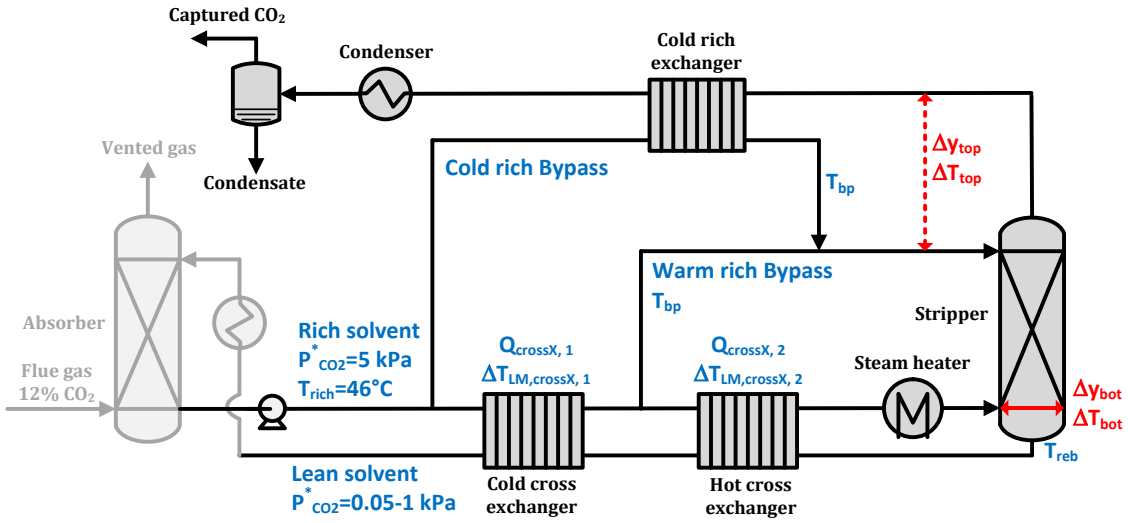

Figure 7.2: Advanced flash stripper

Table 6.2 shows the process specifications. The partial pressure of CO_2 of the rich solvent (rich P^*_{CO2}) is fixed as 5 kPa at 40 °C assuming a reasonable driving force in the absorber that treats the flue gas at 12% from coal-fired power plants. The rich solvent temperature is assumed to be 46 °C, a typical temperature with an intercooled absorber.

The partial pressure of CO_2 of the lean solvent (lean P^*_{CO2}) at 40 °C was varied from 0.05 to 1 kPa. The specification method of the stripper and the heat exchangers were described in Chapter 6. The $\Delta T_{LM,strp}$ and the $\Delta y_{LM,strp}$ of H_2O were specified as 5 K and 5%, respectively. The average cross exchanger LMTD is 5 K.

Table 7.2: Process specifications.

Rich solvent temperature (˚C)	46
Reboiler T (°C)	150
Rich P^*_{CO2} of generic solvents (kPa)	5
Lean P^*_{CO2} of generic solvents (kPa)	0.05-1
$\Delta T_{LM,crossX,avg}$ (K)	5
$\Delta T_{LM,strp}$ (K)	5
$\Delta y_{LM,strp}$ (%)	5
Cold rich exchanger ΔT_{LM} (K)	5

7.2.3 Overall energy performance

The total equivalent work is a more useful metric of energy use than heat duty alone. The total equivalent work consists of pump work (W_{pump}), compression work (W_{comp}), and heat duty work (W_{heat}). It assumes that the pump efficiency (η_{pump}) is 65% and the lean solvent pressure can be recovered by a hydro-turbine with 90% efficiency ($\eta_{hydro\text{-}tb}$). The average heat of absorption is defined in Equation 6.12, which integrates the differential heat of absorption from lean to rich loading. The stripping steam heat accounts for the latent heat of the remaining steam coming from the stripper (for the simple stripper) or from the cold rich exchanger (for the AFS).

$$\Delta H_{abs,avg} = \frac{\int_{\alpha_{lean}}^{\alpha_{rich}} \Delta H_{abs} d\alpha}{\alpha_{rich} - \alpha_{lean}} \quad (6.12)$$

7.3 RESULTS AND DISCUSSIONS

7.3.1 Tradeoffs of heat of absorption

Figure 7.3 shows the effect of the heat of absorption on the total equivalent work using the simple stripper. The lean P^*_{CO2} is 0.15 kPa and reboiler temperature is 150 °C. The original average heat of absorption of PZ is around 70 kJ/mol and was manually increased up to 100 kJ/mol. The sensible heat stays constant since the solvent capacity was kept unchanged. When the heat of absorption increases, the compression work and the stripping steam heat decrease due to the elevated partial pressure of CO_2 and stripper pressure. The strategy depends on whether the savings can compensate for the increase in the heat of absorption. The energy reductions show diminishing returns and the pump work begins to dominate at 100 kJ/mol CO_2 heat of absorption. The compression work decreases linearly with heat of absorption while the pump work increases exponentially. The optimum heat of absorption that minimizes the total equivalent work is around 90 kJ/mol for the simple stripper. If only the heat duty is considered, the optimum is between 70−80 kJ/mol.

Figure 7.4 shows the total equivalent work of the AFS as the heat of absorption varies within the same range from 70 to 100 kJ/mol CO_2. The stripping steam heat is significantly reduced by the rich solvent bypasses and makes the total equivalent work flat at low heat absorption. The optimum heat of absorption is pushed toward a lower value. The slight increase of the sensible heat is due to the unbalanced temperature approach of the cross exchanger when cold rich bypass is extracted.

Tables 7.3 and 7.4 are the tabulated representations of Figure 7.3 and 7.4, respectively including the stripper pressure and reboiler duty.

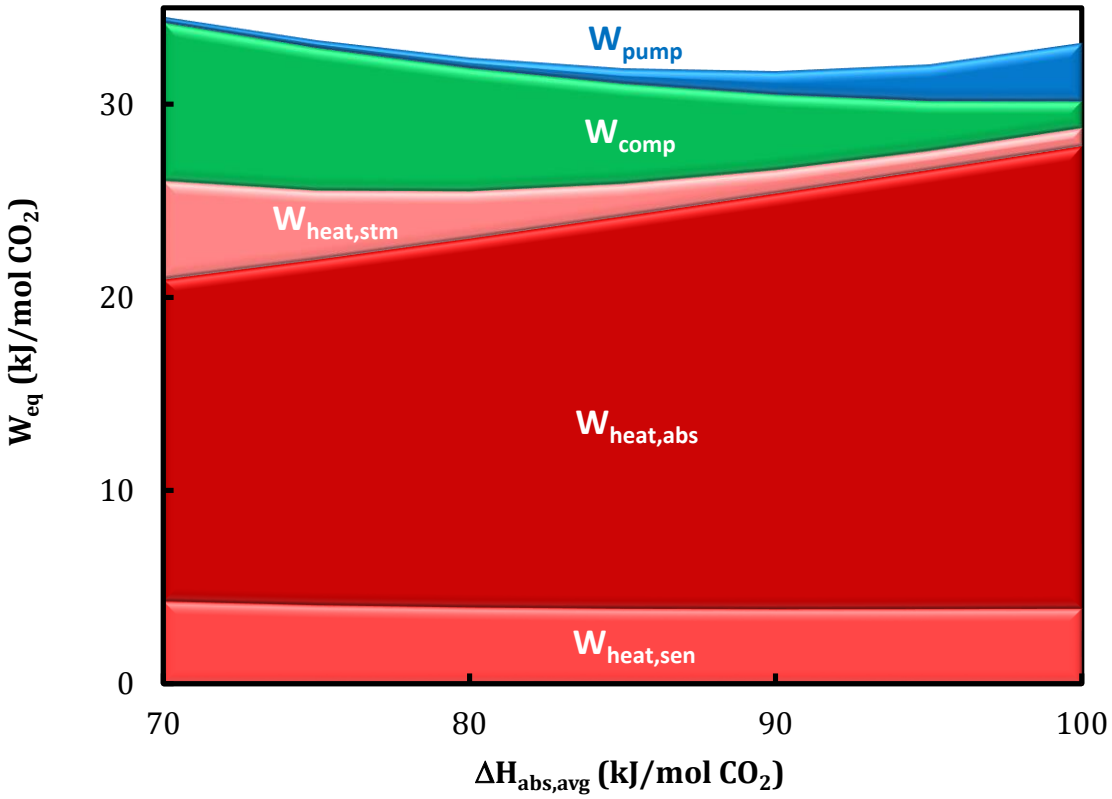

Figure 7.3: Effect of heat of absorption for simple stripper; PZ-based generic solvent; reboiler T: 150 °C; rich solvent P^*_{CO2} at 40 °C: 5 kPa; lean solvent P^*_{CO2} at 40 °C: 0.15 kPa; cross exchanger ΔT_{LM}: 5 K.

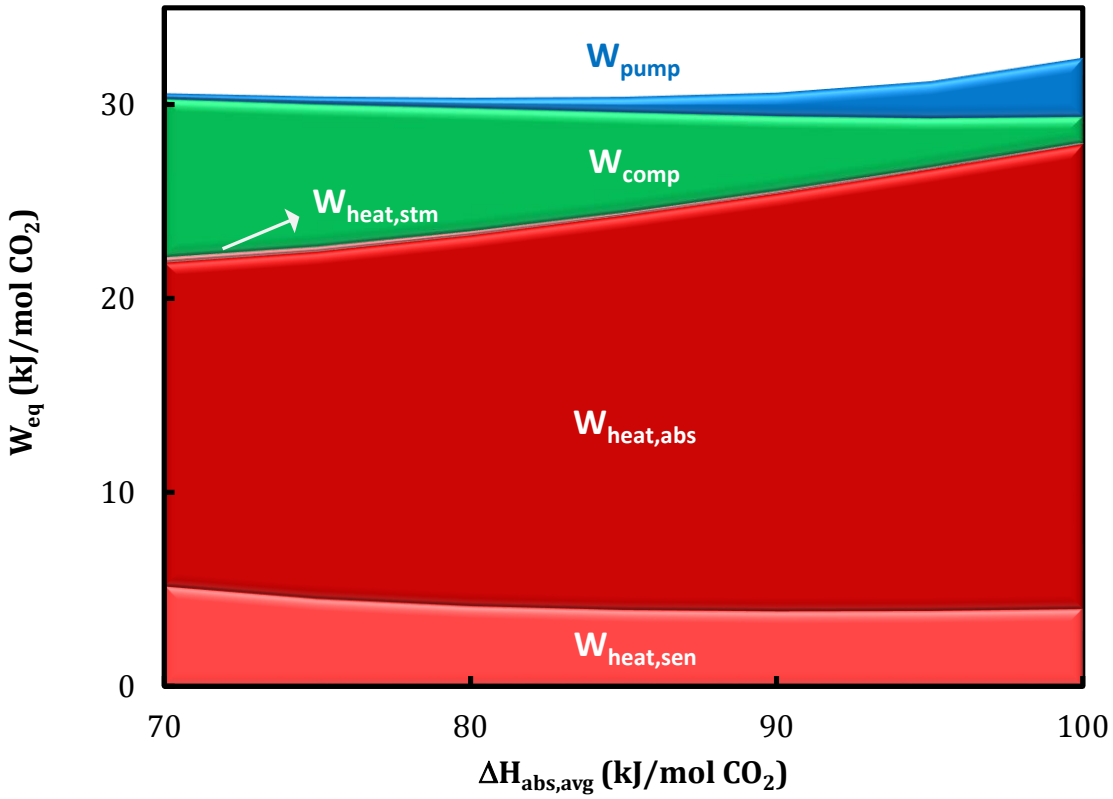

Figure 7.4: Effect of heat of absorption for AFS; PZ-based generic solvent; reboiler T: 150 °C; rich solvent P^*_{CO2} at 40 °C: 5 kPa; lean solvent P^*_{CO2} at 40 °C: 0.15 kPa; cross exchanger ΔT_{LM}: 5 K.

Table 7.3: Energy performance with varied heat of absorption using simple stripper; PZ-based generic solvent; reboiler T: 150 °C; rich solvent P^*_{CO2} at 40 °C: 5 kPa; lean solvent P^*_{CO2} at 40 °C: 0.15 kPa; cross exchanger ΔT_{LM}: 5 K.

Heat of absorption (kJ/mol CO_2)	**70**	**80**	**90**	**100**
Stripper P (bar)	6.8	11.6	24.9	60.7
Equivalent work (kJ/mol CO_2)				
W_{eq}	34.5	32.4	31.7	33.2
W_{heat}	26.0	25.5	26.6	28.8
W_{comp}	8.2	6.4	3.9	1.4
W_{pump}	0.3	0.5	1.2	3.0
Reboiler duty (kJ/mol CO_2)				
Q_{reb}	107.7	105.5	110.1	119.0
Q_{stm}	21.1	10.1	5.1	3.9

Table 7.4: Energy performance with varied heat of absorption using AFS; PZ-based generic solvent; reboiler T: 150 °C; rich solvent P^*_{CO2} at 40 °C: 5 kPa; lean solvent P^*_{CO2} at 40 °C: 0.15 kPa; cross exchanger ΔT_{LM}: 5 K.

Heat of absorption (kJ/mol CO_2)	**70**	**80**	**90**	**100**
Stripper P (bar)	6.8	11.6	24.9	60.7
Equivalent work (kJ/mol CO_2)				
W_{eq}	30.6	30.4	30.6	32.4
W_{heat}	22.1	23.5	25.5	28.0
W_{comp}	8.2	6.4	3.9	1.4
W_{pump}	0.3	0.5	1.2	3.0
Reboiler duty (kJ/mol CO_2)				
Q_{reb}	91.6	97.1	105.6	115.9
Q_{stm}	1.1	0.8	0.5	0.3

7.3.2 Effect of stripper configuration

The stripping steam heat can be avoided by the AFS using rich solvent bypasses or by solvents with higher heat of absorption, which suppress the partial pressure of water. Figure 7.5 compares the optimum heat of absorption of both stripper configurations at 0.15 kPa of lean P^*_{CO2}. The optimum heat of absorption of the AFS is around 80 kJ/mol, around 10 kJ/mol less than the simple stripper. The simple stripper has higher total equivalent work than the AFS especially at 60-80 kJ/mol that most current solvents have. The total equivalent work of the AFS is less sensitive to heat of absorption, implying that it is a flexible system that can be applied to a wide range of heat of absorption while still minimizing the energy use.

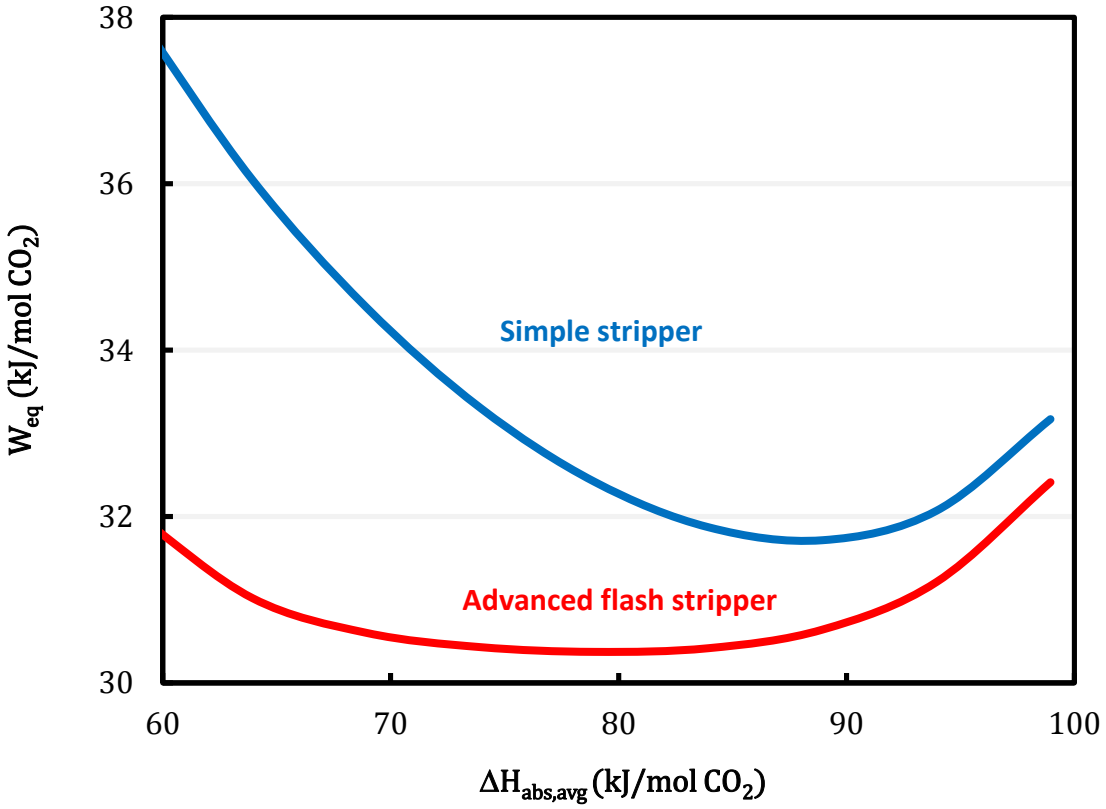

Figure 7.5: Sensitivity of total equivalent work to heat of absorption; PZ-based generic solvent; reboiler T: 150 °C; rich solvent P^*_{CO2} at 40 °C: 5 kPa; lean solvent P^*_{CO2} at 40 °C: 0.15 kPa; cross exchanger ΔT_{LM}: 5 K.

Using the solvent at optmimum heat of absorption can be seen as the best-case scenario that minimize the energy requirement if the "perfect" solvent can be found. Figure 7.6 quantifies the potential energy improvement by comparing the total equivalent work of the base solvent with 70 kJ/mol and the generic solvent with an optimum heat of absorption. The energy reduction by optimizing the heat of the absorption can be up to 10% for the simple stripper but the improvement is limited for the AFS since the stripping steam has been already reduced by the rich solvent bypasses. The AFS does not need a solvent with the optimum heat of absorption to achieve remarkable energy performance.

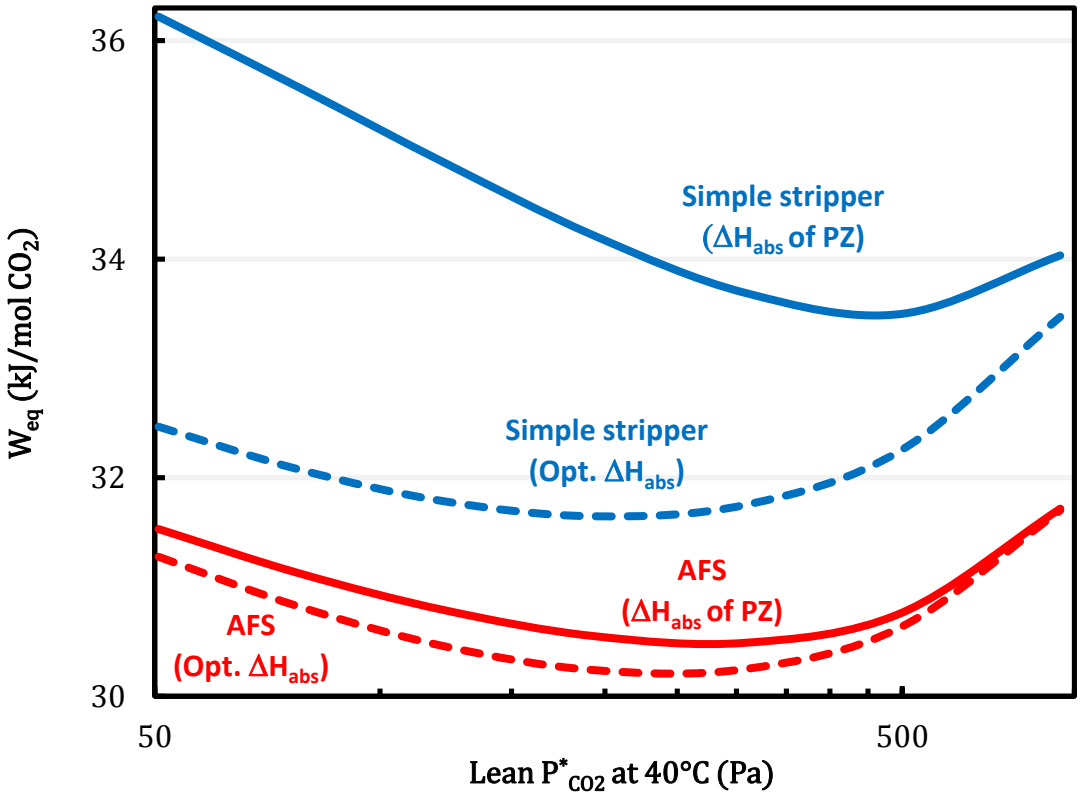

Figure 7.6: Comparison of total equivalent work between original and optimized heat of absorption; PZ-based generic solvent; reboiler T: 150 °C; rich solvent P^*_{CO2} at 40 °C: 5 kPa; cross exchanger ΔT_{LM}: 5 K.

7.3.3 Effect of CO_2 lean loading

Lean loading is the most important operating parameter. The absorber performance is better at lower lean loading because of enhanced absorption rate and mass transfer driving force. To achieve optimal stripper performance, the selected lean loading needs to compromise on the stripping steam heat, the compression work, and the cyclic capacity. In Figure 7.6, the total equivalent work is improved more at lower lean loading where the stripping steam heat and the compression work are the major energy requirement.

Figure 7.7 shows the optimum heat of absorption ranges from 70 to 125 kJ/mol, which varies with the lean loading, reboiler temperature, and stripper configurations. Generally, the desirable heat of absorption is higher than current solvents such as MEA and PZ. The average heat of absorption of the current solvent is typically 60−80 kJ/mol, depending on which type of reaction dominates. Amine can react with CO_2 via carbamate and bicarbonate formation reactions. CO_2 absorption dominated by carbamate formation (primary and secondary amines) usually gives a higher heat of absorption than bicarbonate formation (tertiary amines) (I. Kim et al., 2011).

The simple stripper and the operating conditions at low reboiler temperature and low lean loading will generate significant stripping steam and should have a higher heat of absorption to boost the partial pressure of CO_2.

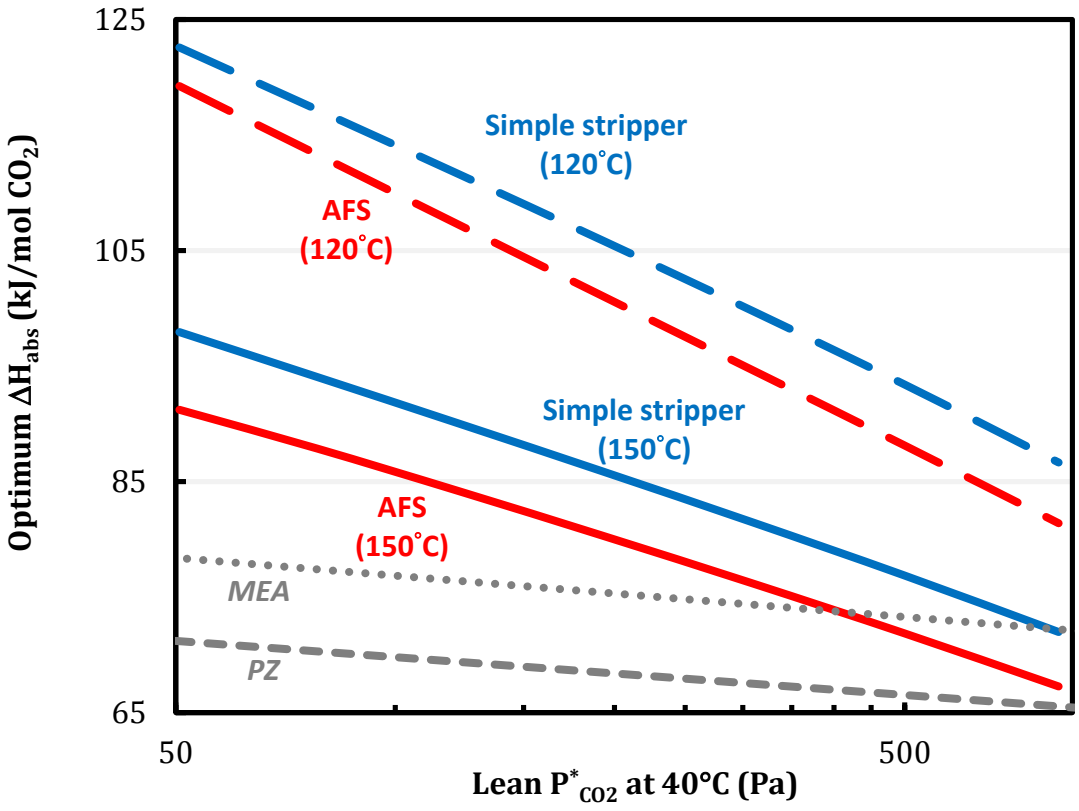

Figure 7.7: Optimum heat of absorption with varied lean loading; PZ-based generic solvent; reboiler T: 120 and 150 °C; rich solvent P^*_{CO2} at 40 °C: 5 kPa; cross exchanger ΔT_{LM}: 5 K.

7.3.4 Effect of reboiler temperature

Elevating the reboiler temperature is an alternative way to maximize the partial pressure of CO_2 and further reduce the stripping steam heat and the compression work. This strategy determines if the weakness of a low heat of absorption can be compensated by elevating the reboiler temperature. The reboiler duty will always decrease with increasing reboiler temperature but the equivalent work is not necessarily reduced because extracting high pressure/temperature steam will incur a greater electricity penalty. The value of equivalent work depends on the Carnot cycle efficiency.

The reboiler temperature is optimized at 120–170 °C with a range of heat of absorption from 65 to 110 kJ/mol in Figure 7.8. Higher reboiler temperature is needed to minimize the total equivalent work for the solvents with lower heat of absorption. The simple stripper also needs a relatively high reboiler temperature compared to the AFS, but they converge to the same temperature as the heat of absorption approaches 100 kJ/mol. The difference of total equivalent work between the simple stripper and the AFS still exists, even at optimum reboiler temperature.

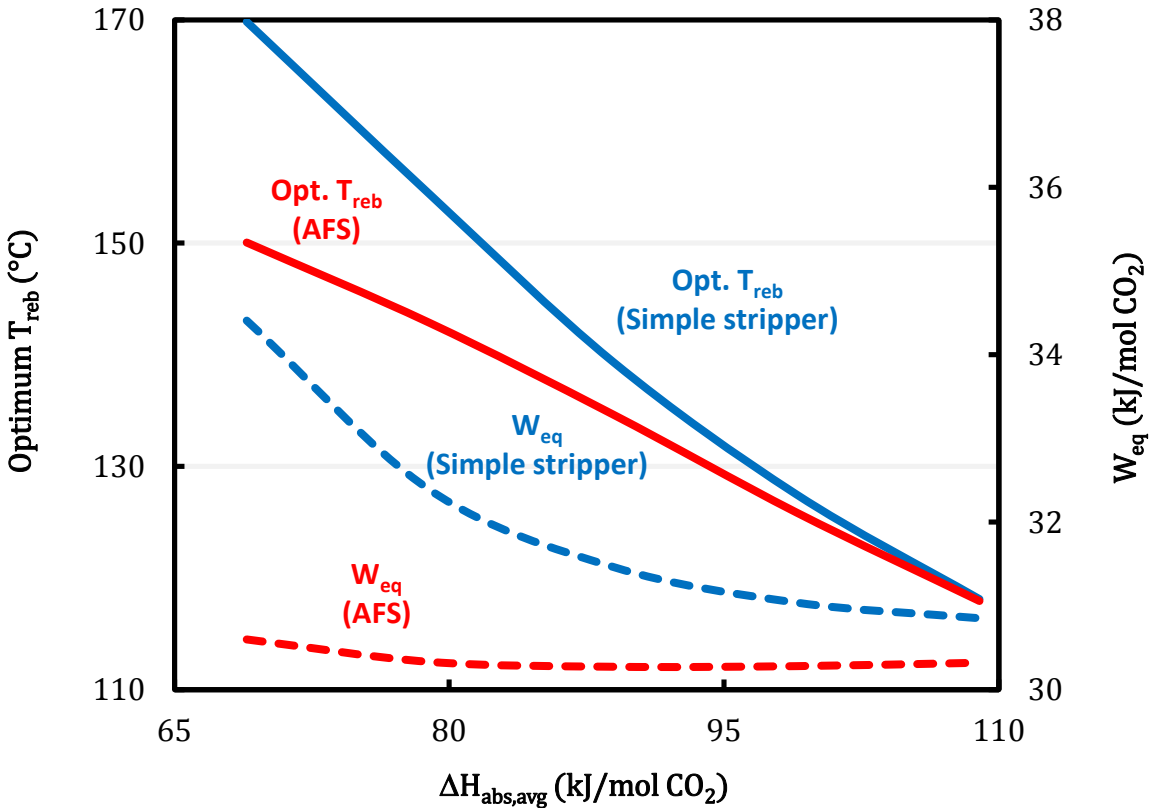

Figure 7.8: Optimum reboiler T and total equivalent work at varied heat of absorption; PZ-based generic solvent; rich solvent P^*_{CO2} at 40 °C: 5 kPa; lean solvent P^*_{CO2} at 40 °C: 0.15 kPa; cross exchanger ΔT_{LM}: 5 K.

However, the energy savings from optimizing the reboiler temperature is insignificant. Figure 7.9 shows the tradeoffs. The reduction of the compression work is almost the same as the increasing heat duty work when the reboiler temperature increases. The difference is less than 1% from 120 to 180 °C, a typical range of steam temperature from the IP/LP crossover pipe of a power plant. Unlike the heat of absorption strategy, elevating the reboiler temperature will make the whole heat duty more expensive as work instead of just the heat of absorption itself. This strategy will not be as effective as utilizing heat of absorption. The capture plant will be flexible enough to use any available IP/LP steam from the existing power plant without degrading the energy performance. The thermal stability of the solvent will be the only limitation. Higher stripper pressure will still be cost-effective because of the reduced size of the compressor train.

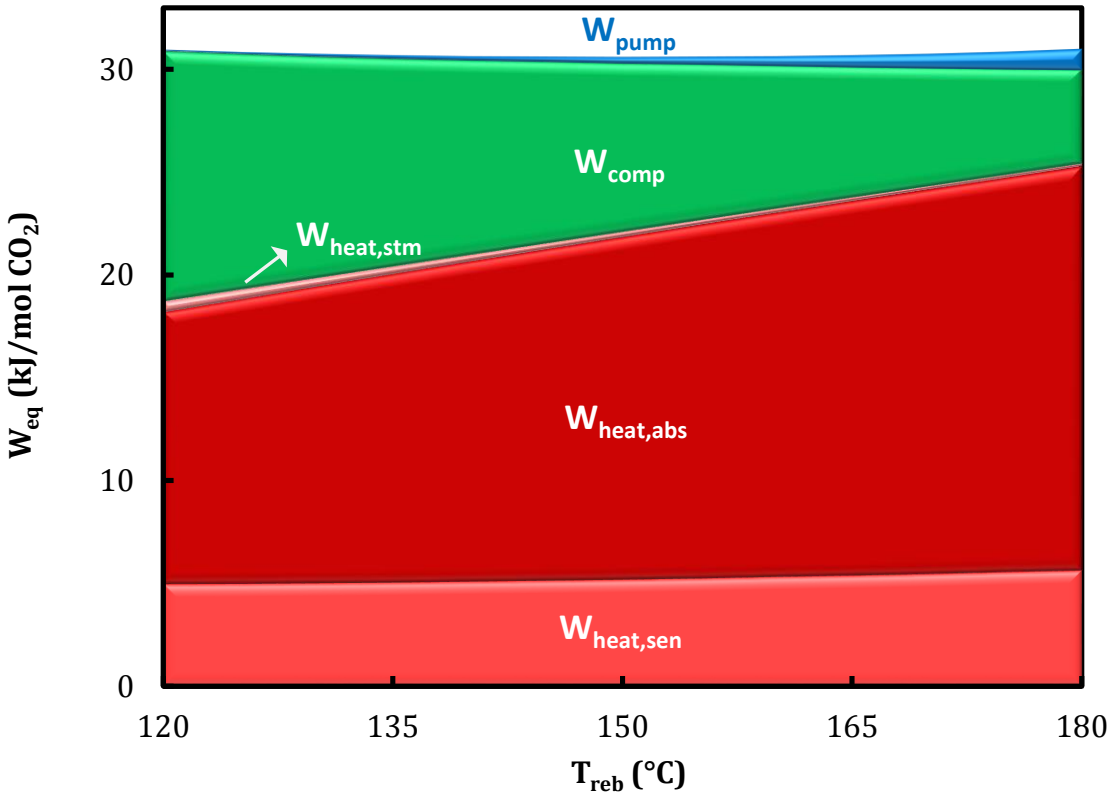

Figure 7.9: Effect of reboiler temperature on total equivalent work using AFS; PZ-based generic solvent; average heat of absorption: 70 kJ/mol; rich solvent P^*_{CO2} at 40 °C: 5 kPa; lean solvent P^*_{CO2} at 40 °C: 0.15 kPa; cross exchanger ΔT_{LM}: 5 K.

7.3.5 Effect of compression efficiency

In this process, the CO_2 can be pressurized thermally or mechanically. The optimum heat of absorption is determined by compromising between thermal compression and mechanical compression. Thermal compression pressurizes and heats up the solvent to attain a high stripper pressure. The efficiency is determined by the heat-to-electricity conversion factor and the pump efficiency. The mechanical compression compresses the CO_2 from the stripper pressure to 150 bar by a multi-stage compressor and the efficiency depends on the polytropic efficiency of the compressor and the intercooling between

stages. Using a solvent with higher heat of absorption or increasing the reboiler temperature will increase the thermal compression and reduce the mechanical compression. Optimizing heat of absorption will maximize the overall compression efficiency.

A sensitivity analysis was performed by accounting for a wide range of thermal and mechanical compression efficiencies. The base case assumes 86% compressor polytropic efficiency ($\eta_{comp,poly}$) and 90% steam turbine isentropic efficiency ($\eta_{stm\text{-}tb}$). The analysis covers the practical range from 72 to 99% for both the compressor and steam turbine. The pump work is considered a part of thermal compression so the same discounting factor of steam turbine efficiency is applied to the pump.

Figure 7.10 shows the optimum heat of absorption as a function of the product of the thermal and the mechanical efficiency. The efficiencies of the base case serve as the reference. Two extreme cases are indicated on the plot. The case at 72% polytropic compressor efficiency and 72% steam turbine efficiency will favor thermal compression because the heat is relatively cheap and mechanical compression is the least efficient. Applying a high heat of absorption is worthwhile to increase the stripper pressure and reduce the mechanical compression. On the other hand when the compressor efficiency and the steam turbine efficiency are both at 99%, it is advantageous to switch to mechanical compression. The electricity penalty caused by the extracted steam becomes more pronounced when the steam turbine is more efficient. The heat of absorption will be too costly to pursue high stripper pressure, so it results in a low optimum heat of absorption.

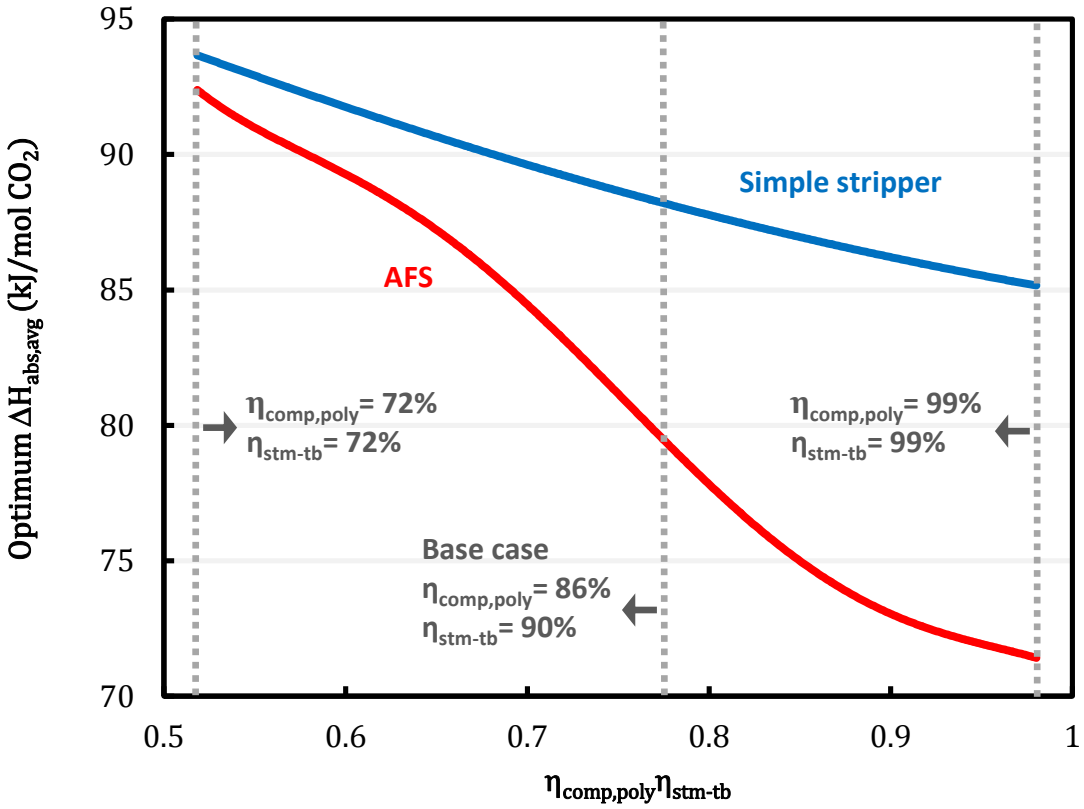

Figure 7.10: Sensitivity of thermal and mechanical compression efficiency; PZ-based generic solvent; reboiler T: 150 °C; rich solvent P^*_{CO2} at 40 °C: 5 kPa; lean solvent P^*_{CO2} at 40 °C: 0.15 kPa; cross exchanger ΔT_{LM}: 5 K.

The AFS always has a lower optimum heat of absorption than the simple stripper since less benefit can be obtained from increasing the heat of absorption. At high steam turbine efficiency, the AFS does not need high heat of absorption but can still effectively reduce the stripping steam. If the efficiency of the turbine and the compressor are improved, the heat of absorption of existing solvents can be closer to the optimum, especially for the AFS.

7.4 CONCLUSIONS

- Using solvents with high heat of absorption can increase the partial pressure of CO_2 and effectively reduce the stripping steam heat and the compression work. Optimum heat of absorption can be found when the energy reductions show diminishing returns and the increase in the pump work is dominant.
- The optimum heat of absorption varies from 70 to 125 kJ/mol. The simple stripper and the operating conditions at low reboiler temperature and low lean loading will need a higher optimum heat of absorption to boost the partial pressure of CO_2.
- By increasing the heat of absorption, the total equivalent work can be reduced by 10% for the simple stripper and less than 1% for the AFS.
- The AFS always has a lower optimum heat of absorption than the simple stripper since the stripping steam heat is already eliminated by the rich solvent bypasses.
- The AFS is a flexible system that can be applied to a wide range of heat of absorption while still minimizing the energy requirement. Further reduction by increased heat of absorption is marginal.
- Increasing the partial pressure of CO_2 by reboiler temperature will not effectively reduce the total equivalent work. The savings of compression work is almost offset by the increase in the heat duty work.
- Improving the efficiency of the steam turbine and compressor will favor mechanical compression rather than thermal compression, and results in an optimum heat of absorption as low as 70−85 kJ/mol, which is close to that of available solvents.

Chapter 8: Optimum Design of Lean/Rich Amine Cross Exchanger

8.1 INTRODUCTION

In the amine scrubbing process, the lean/rich amine cross exchanger is used to recover the sensible heat from the hot lean solvent. The exchanger heat duty is 3 to 5 times the actual reboiler duty input. Since a large amount of heat is transferred, the capital cost of the cross exchanger is one of the cost centers, accounting for 20–30% of capital cost (Lin & Rochelle, 2014).

To reduce the cross exchanger cost, the most important design parameter, the LMTD should be optimized. Furthermore, the heat transfer performance can be enhanced by increasing the pressure drop and using a less viscous solvent. This chapter aims at investigating the pressure drop and viscosity effect on the cross exchanger performance and reducing the capital cost by providing an optimum design. The plate-and-frame exchanger will be considered to be the type used for the cross exchanger. Mechanical and structure design will not be in the scope of this work.

8.1.1 Plate-and-frame exchanger (PHE)

The plate-and-frame type exchanger (PHE) has become a commonly used heat exchanger because of the advantages over the conventional shell-and-tube exchanger: the compactness, high thermal efficiency, and easy maintenance and reconfiguration. A typical PHE is shown in Figure 8.1. The hot and cold fluids flow between thin plates where the heat transfer area is provided. The ports on the corner of plates serve as fluid collectors or distributors. The plates are sealed by gaskets or welding to avoid fluid mixing and leakage. Typical maximum pressure and temperature rating for gasketed PHE is 20–28 bar and 100–200 °C depending on the gasket material. Higher pressure and temperature can be tolerated with a welded PHE.

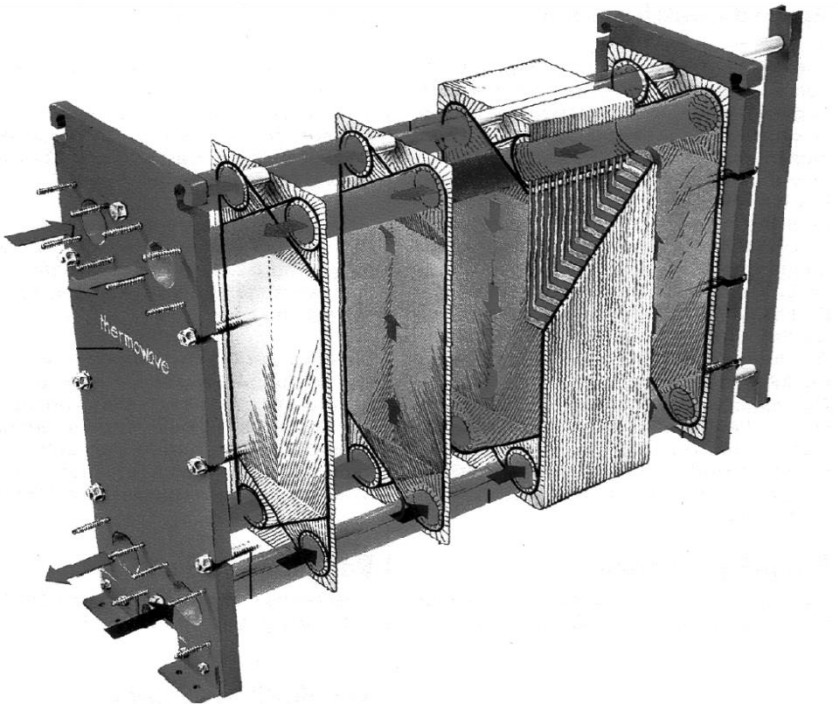

Figure 8.1: Plate-and-frame exchanger (Reppich, 1999).

The heat transfer performance can be enhanced by corrugated plates, which produces additional turbulence. Turbulent flow can be attained even at a low Reynolds number (Re) from 100 to 300 relative to 10^4 for a smooth tube. As shown in Figure 8.2, the corrugation angle, θ, is the primary geometry variable, which can be selected between 0 and 90º. As the corrugation angle increases, better heat transfer coefficient can be obtained but the pressure drop also increases.

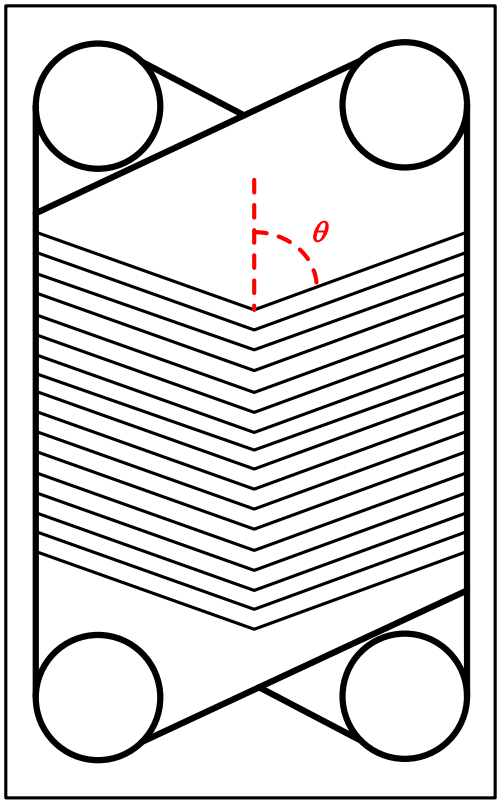

Figure 8.2: Corrugated plate and corrugation angle, θ.

8.2 LITERATURE SURVEY OF HEAT TRANSFER CORRELATION FOR PHE

Empirical correlations developed from experimental data can be used to estimate the heat transfer coefficient and the pressure drop. Table 8.1 summarizes the correlations from literature for the heat transfer coefficient and the pressure drop for PHE. Two dimensionless groups, Nusselt number (Nu) and Fanning friction factor (f) are used to calculate the heat transfer coefficient (h) and the total pressure drop (ΔP), respectively, as shown in Equations 8.1 and 8.2.

$$h = Nu\frac{D_e}{k} \tag{8.1}$$

$$\Delta P = \frac{2fL_T\rho u^2}{D_e} \tag{8.2}$$

Table 8.1: Summary of empirical correlations of heat transfer and pressure drop for PHE.

Author/year	Fluid	Heat transfer	Pressure drop
(Okada et al., 1972)	Water	$Nu = 0.327Re^{0.65}Pr^{0.4}\ (\theta = 60)$ $Nu = 0.157Re^{0.66}Pr^{0.4}\ (\theta = 30)$	
(Rosenblad et al., 1975)	Water	$Nu = 0.289Re^{0.697}Pr^{0.33}$	
(Vaie, 1975)	Water	$Nu = 0.298(\phi)^{1-0.646}Re^{0.646}Pr^{0.316}$	$f = (36\phi Re^{-1} + 0.2)\phi$
(Kumar, 1984)	Water	$Nu = 0.348Re^{0.663}Pr^{0.33}\left(\frac{\mu}{\mu_w}\right)^{0.17}\ (\theta = 60)$ $Nu = 0.108Re^{0.703}Pr^{0.33}\left(\frac{\mu}{\mu_w}\right)^{0.17}\ (\theta = 30)$	$f = 2.99Re^{-0.183}(\theta = 60)$ $f = 0.76Re^{-0.215}(\theta = 30)$
(Heavner et al., 1993)	Water	$Nu = 0.308Re^{0.667}Pr^{0.33}\left(\frac{\mu}{\mu_w}\right)^{0.17}\ (\theta_{avg} = 56.5)$ $Nu = 0.118Re^{0.720}Pr^{0.33}\left(\frac{\mu}{\mu_w}\right)^{0.17}\ (\theta_{avg} = 33.5)$	$f = 1.441Re^{-0.1353}(\theta_{avg} = 56.5)$ $f = 0.545Re^{-0.1555}(\theta_{avg} = 33.5)$
(Roetzel et al., 1994)	Water	$Nu = 0.371Re^{0.703}Pr^{0.33}$	
(Thonon et al., 1995)		$Nu = 0.2946Re^{0.7}Pr^{0.33}\ (\theta = 60)$ $Nu = 0.2267Re^{0.631}Pr^{0.33}\ (\theta = 30)$	$f = 0.37Re^{-0.172}(\theta = 60)$ $f = 0.572Re^{-0.217}(\theta = 30)$
(Talik et al., 1995)	Propylene glycol/water	$Nu = 0.2Re^{0.75}Pr^{0.4}(\theta = 60)$	$f = 48.26Re^{-0.74}(\theta = 60)$
(Manglik et al., 1995)	Water	$Nu = 0.105Re^{0.755}Pr^{0.33}\left(\frac{\mu}{\mu_w}\right)^{0.14}\ (\theta = 45)$	$f = 1.274Re^{-0.15}(\theta = 45)$
(Muley et al., 1999)	Water	$Nu = C_1(\theta)C_2(\phi)Re^{a(\theta)}Pr^{0.33}\left(\frac{\mu}{\mu_w}\right)^{0.14}$	$f = C_3(\theta)C_4(\phi)Re^{-b(\beta\theta)}$
(Warnakulasuriya et al., 2008)	Salt solution	$Nu = 0.292Re^{0.725}Pr^{0.35}\left(\frac{\mu}{\mu_w}\right)^{0.14}\ (\beta = 60)$	$f = 23.8Re^{-0.205}(\theta = 60)$
(Khan et al., 2010)	Water	$Nu = 0.1368Re^{0.7424}Pr^{0.35}\left(\frac{\mu}{\mu_w}\right)^{0.14}\ \beta = 30$ $Nu = 0.1449Re^{0.8414}Pr^{0.35}\left(\frac{\mu}{\mu_w}\right)^{0.14}\ \beta = 60$	

Most literature used water as the working fluid in experiments and reported heat transfer coefficient and pressure drop with varied fluid flow rate. The Nusselt number and the Fanning friction factor are typically regressed by Equations 8.3 and 8.4 as a function of Reynolds number and Prandtl number (Pr). The exponent of the Prandtl number, n, was typically fixed at 0.33 from the boundary layer theory, and the experimental data were regressed to determine the C_{Nu} and m. The friction factor is inversely proportional to the Reynolds number with an exponent, p. The most common corrugation angles tested were 30º and 60º.

$$Nu = C_{Nu} Re^{m} Pr^{n} \tag{8.3}$$

$$f = C_f Re^{-p} \tag{8.4}$$

The empirical correlations are applied to amine solutions to predict the potential performance of the cross exchanger for amine scrubbing. The physical properties of 8 m PZ at typical operating conditions in the cross exchanger are shown in Table 8.2. The physical properties were estimated at 90 ºC, around the average temperature of the cross exchanger from 50 to 140 ºC. Applying the correlations that were regressed by experiment data of water to the amine system assumes the same dependence of heat transfer coefficient on fluid velocity even the amines are more viscous. To understand the viscosity effect on the PHE, measuring the heat transfer coefficient and pressure drop for viscous solvent is necessary in the future. The Prandtl number for 8 m PZ is around 70, which is an order of magnitude higher than water due to the viscosity. The plate spacing (δ) is assumed to be 2 mm so the hydraulic diameter (D_e) is 4 mm.

Table 8.2: Physical properties of 8 m PZ at 90 ºC and CO_2 loading at 0.30.

Viscosity (cP)	3
Thermal conductivity (W/m-K)	0.15
Heat capacity (kJ/kg-K)	3.5

Figure 8.3 shows the Nusselt number predicted by the empirical equations at varied Reynolds number with two common corrugation angles, 30º and 60º. The Dittus-Boelter equation (Dittus et al., 1985) for smooth tube is also plotted. The corrugated plates can enhance the heat transfer coefficient by 2−10 times at the same Reynolds number. The PHE with 60º generally provides a higher heat transfer coefficient, which is almost twice of that with 30º. At the same corrugation angle, the difference of the Nusselt number between correlations can vary more than 50% but the dependence on the Reynolds number is similar.

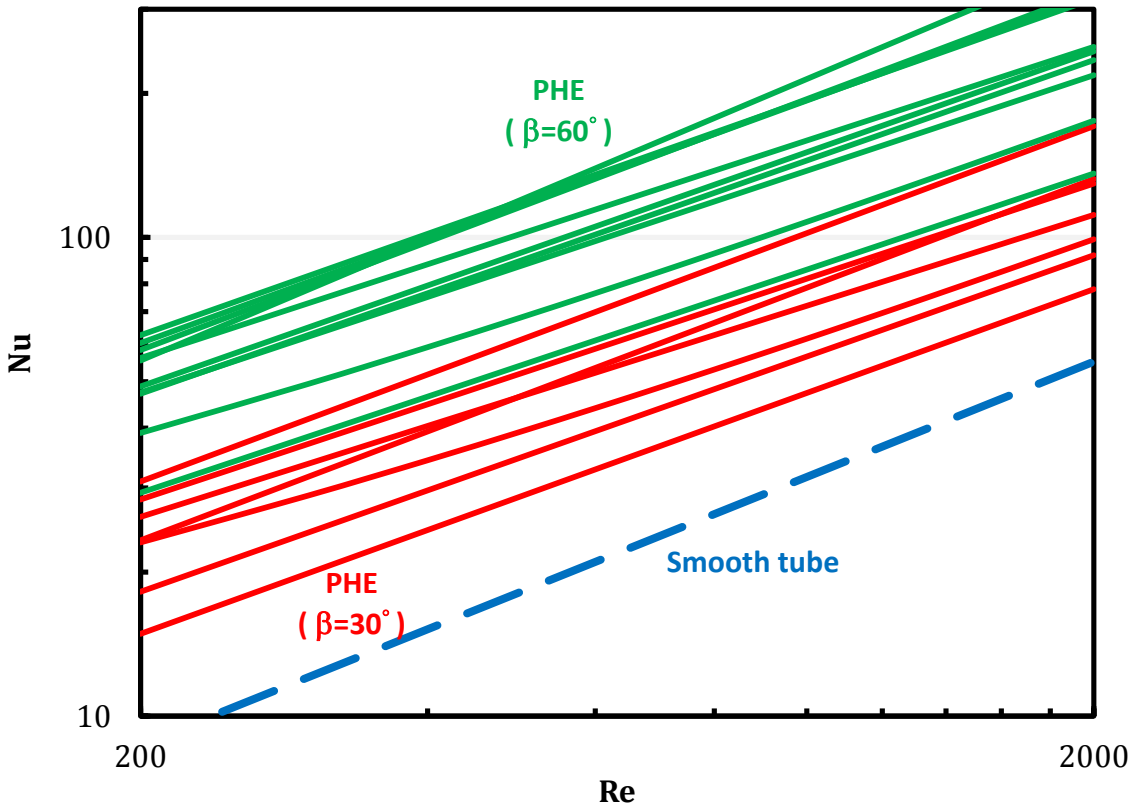

Figure 8.3: Nusselt number predicted by empirical correlations with varied Reynolds number using physical properties of 8 m PZ.

8.3 VISCOSITY EFFECT ON HEAT TRANSFER COEFFICIENT

The heat transfer coefficient can be enhanced by using a less viscous solvent. Based on the form of Equation 8.3, the dependence of heat transfer coefficient on viscosity is m-n. Figure 8.4 shows the dependence predicted by the empirical correlations with varied corrugation angle. Most of the viscosity dependence is between 0.30 and 0.40, which implies that reducing viscosity by 50% can save on cross exchanger cost by 20–25%.

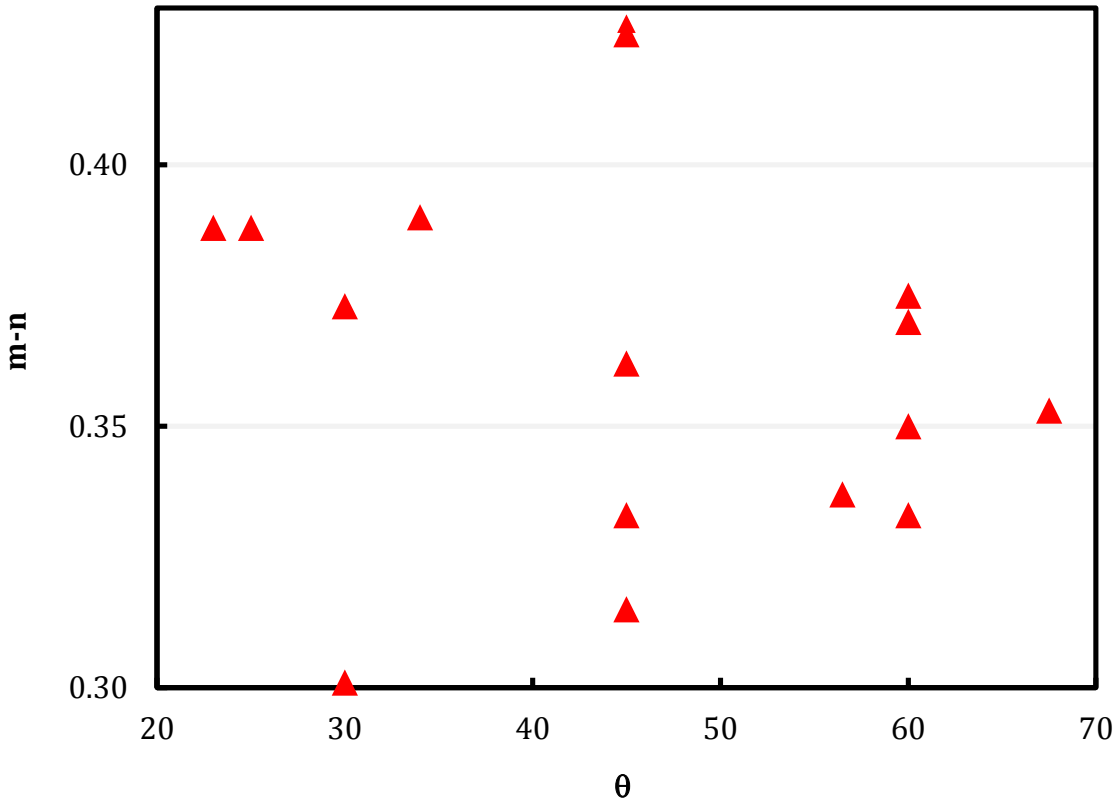

Figure 8.4: The dependence of viscosity on the exchanger cost predicted by empirical correlations with varied corrugation angle.

8.4 Optimizing LMTD by shortcut method

The LMTD of the cross exchanger (ΔT_{LM}) has the most impact on the capital cost. The capital cost of the cross exchanger is sensitive to the LMTD especially for the system that has a large number of heat transfer units (NTU). The temperature change across the cross exchanger is typically around 100 K so the NTU will be 20 if the LMTD is 5 K. The optimum LMTD is tradeoff of energy cost and capital cost. Li adjusted the solvent capacity by taking account of the viscosity effect on the cross changer cost at optimum LMTD (Li, Voice, et al., 2013). A shortcut method that determines the optimum cross exchanger LMTD was derived with the following assumptions:

- The temperature change across the cross exchanger (ΔT_{crX}), heat capacity (C_p), and steam temperature (T_{stm}) are independent of ΔT_{LM}
- Assume the temperature change in the reboiler is the same as ΔT_{LM}

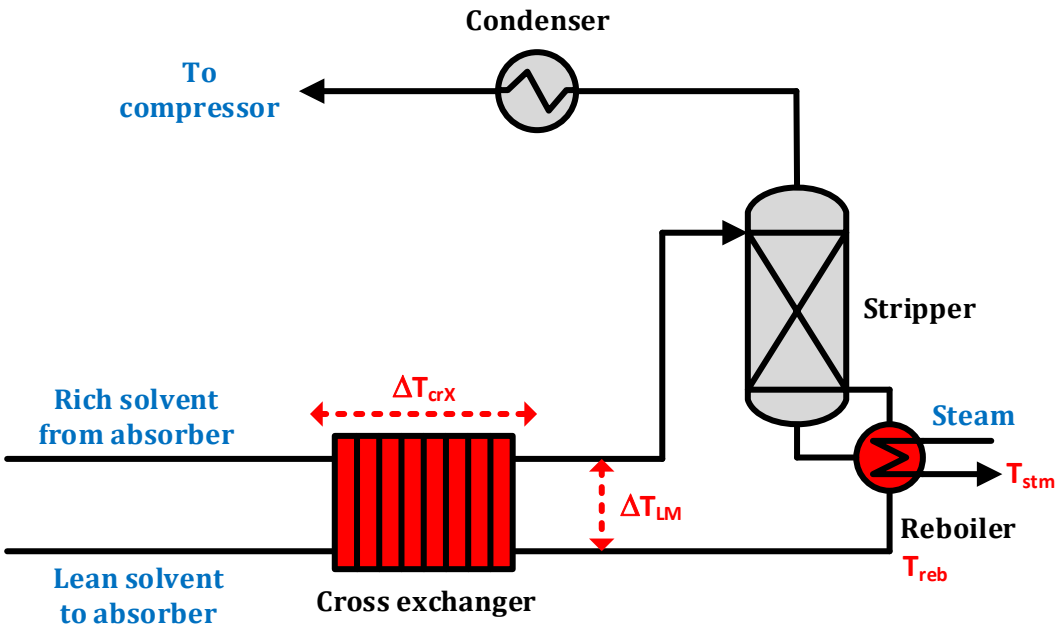

Figure 8.5: Optimization of cross exchanger LMTD.

The optimization includes the CAPEX and OPEX of the cross exchanger and the reboiler as shown in Figure 8.4. The area of the cross exchanger and the reboiler are calculated:

$$A_{crX} = \frac{Q_{crX}}{U_{crX}\Delta T_{LM}} = \frac{\dot{m}C_p\Delta T_{crX}}{U_{crX}\Delta T_{LM}} \tag{8.5}$$

$$A_{reb} = \frac{Q_{reb}}{U_{reb}(T_{stm}-T_{reb})} = \frac{\dot{m}C_p\Delta T_{LM}}{U_{reb}(T_{stm}-T_{reb})} \tag{8.6}$$

The CAPEX and the OPEX are calculated:

$$CAPEX = C_{PEC,crX}A_{crX} + C_{PEC,reb}A_{reb} \tag{8.7}$$

$$OPEX = C_{COE}\eta_{tb}\left(\frac{T_{stm}-T_{sink}}{T_{stm}}\right)Q_{reb} = C_{COE}\eta_{tb}\left(\frac{T_{stm}-T_{sink}}{T_{stm}}\right)\dot{m}C_p\Delta T_{LM} \quad (8.8)$$

$$Total\ cost = C_{PEC,crX}\frac{\dot{m}C_p\Delta T_{crX}}{U_{crX}\Delta T_{LM}} + C_{PEC,reb}\frac{\dot{m}C_p\Delta T_{LM}}{U_{reb}(T_{stm}-T_{reb})} + C_{COE}\eta_{tb}\left(\frac{T_{stm}-T_{sink}}{T_{stm}}\right)\dot{m}C_p\Delta T_{LM} \quad (8.9)$$

$$\frac{\partial(Total\ cost)}{\partial\Delta T_{LM}} = -C_{PEC,crX}\frac{\dot{m}C_p\Delta T_{crX}}{U_{crX}\Delta T_{LM}^{\ 2}} + C_{PEC,reb}\frac{\dot{m}C_p}{U_{reb}(T_{stm}-T_{reb})} + C_{COE}\left(\frac{T_{stm}-T_{sink}}{T_{stm}}\right)\dot{m}C_p \quad (8.10)$$

At optimum LMTD ($\Delta T_{LM,opt}$), the first derivative of total cost is equal to zero:

$$\Delta T_{LM,opt} = \sqrt{\frac{C_{PEC,crX}\Delta T_{crX}}{U_{crX}}}\left[\frac{C_{PEC,reb}}{U_{reb}(T_{stm}-T_{reb})} + C_{COE}\eta_{tb}\left(\frac{T_{stm}-T_{sink}}{T_{stm}}\right)\right]^{-0.5} \quad (8.11)$$

$$\Delta T_{LM,opt} \propto \sqrt{\frac{C_{PEC,crX}\Delta T_{crX}}{U_{crX}}} \quad (8.12)$$

Equation 8.12 shows that the optimum LMTD is a function of heat transfer coefficient, temperature change and the cost of heat exchanger. A greater LMTD should be used to prevent excessive capital cost when the NTU is large and the heat transfer coefficient is small. If the heat transfer performance can be enhanced, a smaller cross exchanger LMTD that increases the thermal efficiency can be applied.

8.5 OPTIMIZING FLUID VELOCITY

When the physical properties of the fluid are given, the only degree of freedom that determines the heat transfer coefficient and the pressure drop is the fluid velocity. The optimum fluid velocity will trade off the enhanced heat transfer performance and the penalty from the pressure drop. An economic optimization can be performed by considering the tradeoffs including the capital cost of the cross exchanger and the cost associated with the pressure drop including the pumping cost and the capital cost of the pump (Martin, 1999). A shortcut method that determines the optimum fluid velocity will be developed for the cross exchanger.

8.5.1 Shortcut method

Figure 8.6 shows the flow pattern and the geometry of a PHE with a single-pass. The fluid velocity is determined by the cross-sectional area that is perpendicular to the flow direction.

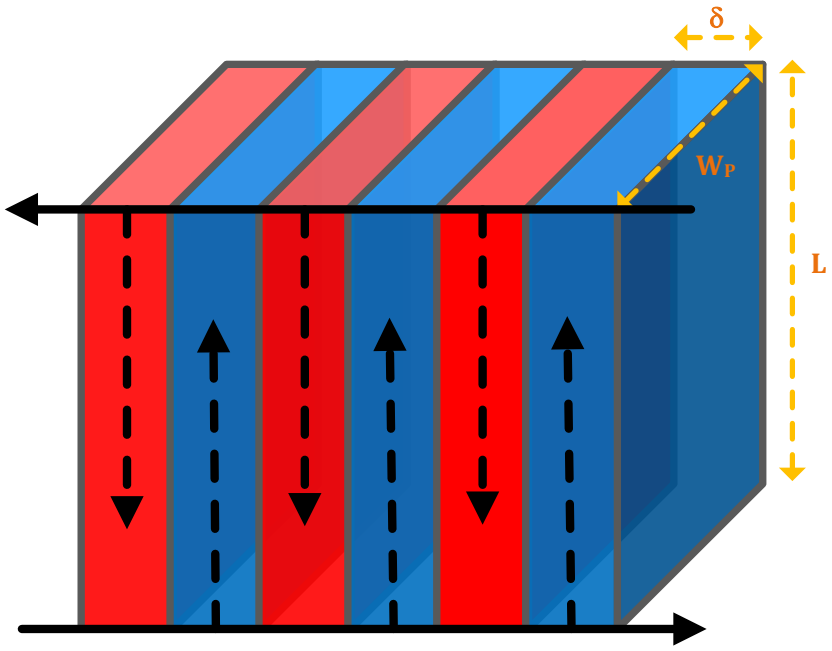

Figure 8.6: Flow pattern and geometry of a single-pass plate-and-frame exchanger.

If the plate spacing (δ) is fixed, the fluid velocity can be varied by adjusting the total plate width (W_T), which is the width of each plate (W_p) multiplied by the total plate number. The mass velocity of each side can be determined by Equation 8.13. The $\dot{m}$ is the mass flow rate of one side.

$$G = \rho u = \frac{\dot{m}}{\delta \times \frac{W_T}{2}} \tag{8.13}$$

Equations 8.3 and 8.4 are used to calculate the heat transfer coefficient and the pressure drop with the empirical parameters: m, n, and p. The pressure drop per unit length (ΔP/L) is proportional to the Reynolds number with exponent 2-p (Equation 8.14).

Substituting the Reynolds number for pressure drop per unit length shows that the dependence of the pressure drop per unit length on Nusselt number is m/(2-p) (Equation 8.15). The dependence will determine the heat transfer enhancement by increasing the pressure drop. The empirical m and p can be obtained from literature that measured heat transfer coefficient and pressure drop with the same experiment set. Figure 8.7 shows the dependence is between 0.35 and 0.40 as predicted by empirical correlations. This implies that increasing the pressure drop per unit length by twice can enhance the heat transfer coefficient by about 30%. The total pressure drop (ΔP) will also depend on the total flow length (L_T).

$$\frac{\Delta P}{L} = \frac{2f\rho u^2}{D_e} \propto Re^{2-p} \tag{8.14}$$

$$h \propto Re^m \propto \left(\frac{\Delta P}{L}\right)^{\frac{m}{2-p}} \tag{8.15}$$

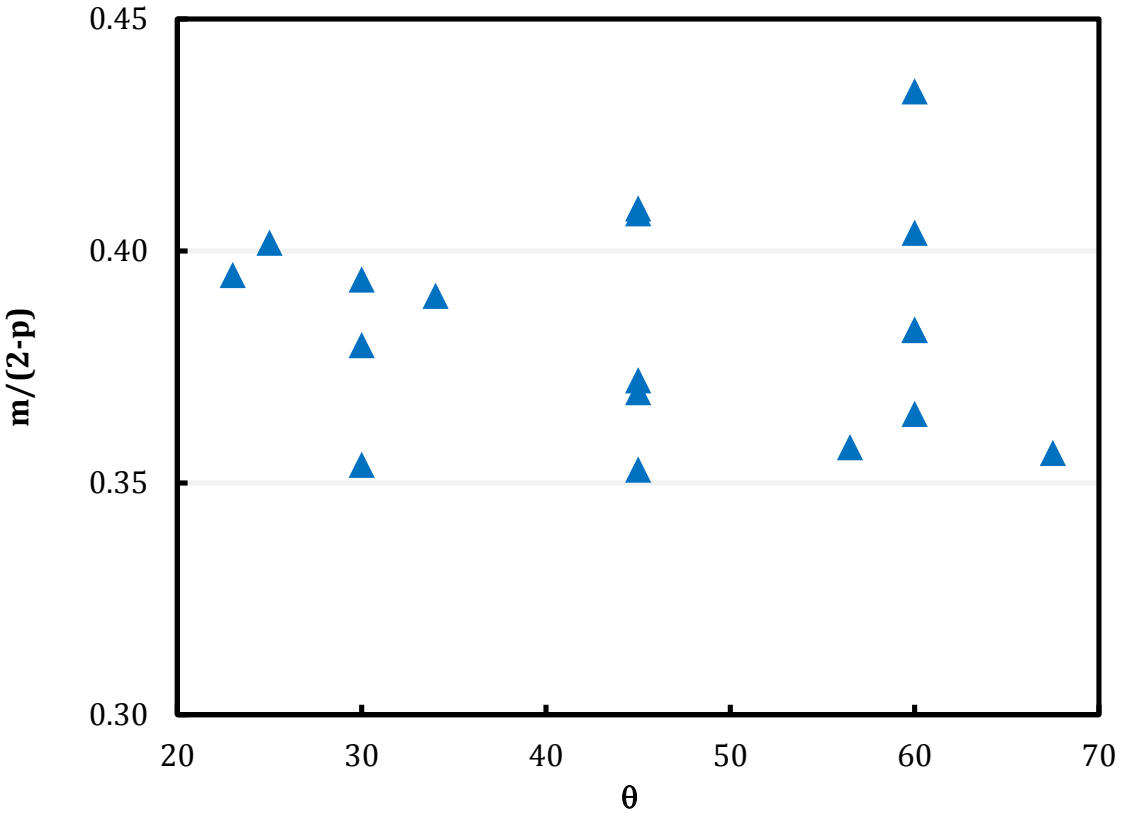

Figure 8.7: The dependence of pressure drop per unit length on Nusselt number predicted by empirical correlations with varied corrugation angle.

To optimize the fluid velocity (u) the total cost associated with the cross exchanger is derived. All the dimensionless groups are taken apart and expressed as a function of the fluid velocity, the physical properties and the constants and exponents from the empirical correlations. Equation 8.16 and 8.17 show the expression of the heat transfer coefficient and the total pressure drop, respectively.

$$h = \frac{k}{D_e} C_{Nu} Re^m Pr^n = C_{Nu} \rho^m {D_e}^{m-1} k^{1-n} {C_p}^n u^m \mu^{n-m} \tag{8.16}$$

$$\Delta P = \frac{2 f_f L \rho u^2}{D_e} = 2 C_f \rho^{1-p} {D_e}^{-p-1} u^{2-p} \mu^p L_T \tag{8.17}$$

If the total width is used to determine the fluid velocity, the total flow length will be determined by the total heat transfer area, A. The total flow length can be related to the heat transfer area and the fluid velocity using Equation 8.18. The equivalent diameter (D_e) is 2 times the plate spacing.

$$L_T = \frac{A}{W_T} = \frac{A}{\frac{\dot{m}}{\rho \delta u}} = \frac{\rho D_e u}{2\dot{m}} A \tag{8.18}$$

The overall heat transfer coefficient, U, is approximated as one half of the heat transfer coefficient on one side assuming negligible thermal resistance of the plate. Equation 8.19 is used to relate the heat transfer area and the overall heat transfer coefficient.

$$A = \frac{Q}{U \Delta T_{LM}} = \frac{\dot{m} C_p \Delta T_{crX}}{U \Delta T_{LM}} \tag{8.19}$$

By rearranging Equations 8.16–19, the heat transfer area and the total pressure drop can be expressed by Equations 8.20 and 8.21. The exchanger area is inversely proportional to the fluid velocity with a power of m, which is around 0.6–0.75 for PHE as literature indicated. The magnitude of m will determine potential heat transfer enhancement by increasing the fluid velocity. The dependence of the fluid velocity on the total pressure drop (ΔP) is 3-m-p. The p affects the friction factor and the m indirectly determines the total flow length. A longer flow length will cause more total pressure drop.

$$A = \dot{m} \frac{\Delta T}{\Delta T_{LM}} \frac{2}{C_{Nu}} \rho^{-m} {D_e}^{1-m} k^{n-1} {C_p}^{1-n} u^{-m} \mu^{m-n} \tag{8.20}$$

$$\Delta P = \frac{\Delta T}{\Delta T_{LM}} \frac{2C_f}{C_{Nu}} \rho^{2-m-p} {D_e}^{1-m-p} k^{n-1} {C_p}^{1-n} u^{3-m-p} \mu^{m-n+p} \tag{8.21}$$

The total cost associated with the cross exchanger optimization includes the energy cost of pump work and the capital cost of the pump and the cross exchanger. The pump work can be calculated using Equation 8.22. After adding the pricing parameters,

Equation 8.24 shows the total cost associated with the cross exchanger, which should be minimized. The optimum velocity is mainly driven by the empirical parameters m and p, the equipment purchased cost of the exchanger and the pump ($C_{PEC,ex}$, $C_{PEC,p}$), the capital scaling and the annualizing factor, α and β, and the cost of electricity, C_{COE} as shown in Equation 8.25.

$$W_{pump} = \frac{\dot{V}\Delta P}{\eta_p} = \frac{\dot{m}\Delta P}{\rho \eta_p} \tag{8.22}$$

$$Cost_{total} = \left(C_{COE} + \alpha\beta C_{PEC,p}\right)\frac{2C_f}{C_{Nu}}\frac{\dot{m}}{\eta_p}\frac{\Delta T}{\Delta T_{LM}}\rho^{1-m-p}{D_e}^{1-m-p}k^{n-1}{C_p}^{1-n}u^{3-m-p}\mu^{m-n+p}$$
$$+\alpha\beta C_{PEC,crX}\dot{m}\frac{\Delta T}{\Delta T_{LM}}\frac{2}{C_{Nu}}\rho^{-m}{D_e}^{1-m}k^{n-1}{C_p}^{1-n}u^{-m}\mu^{m-n} \tag{8.24}$$

At optimum fluid velocity (u_{opt}), $\frac{\partial Cost_{total}}{\partial u} = 0$

$$u_{opt} = \left(\frac{m}{C_f(3-m-p)}\frac{\alpha\beta C_{PEC,crX}}{C_{COE}+\alpha\beta C_{PEC,p}}\eta_p\rho^{p-1}{D_e}^{p}\mu^{-p}\right)^{\frac{1}{3-p}} \tag{8.25}$$

The optimum velocity is independent of the solvent rate, the temperature change of the cross exchanger, and the cross exchanger LMTD. To maintain at optimum fluid velocity, the plate number needs to increase as the solvent rate increases while the plate length will increase as the NTU increases. Viscous solvent will result in a lower optimum velocity since it causes higher pressure drop.

8.5.2 Case study

The optimum velocity in Equation 8.25 is demonstrated using typical design parameters shown in Table 8.3 and plotted with varied m and viscosity in Figures 8.8 and 8.9, respectively. Typical optimum fluid velocity is at 0.32–0.42 m/s. The exponent of the Reynolds number, m determines the heat transfer enhancement with increasing fluid velocity. The greater the m is, it is more efficient to reduce the heat exchanger area by utilizing high the pressure drop so a greater optimum velocity is obtained. The net effect of viscosity on optimum velocity is with a power of –p/(3-p), which is around 0.08 for the base case. Viscous solvent should apply a lower fluid velocity to minimize the total cost.

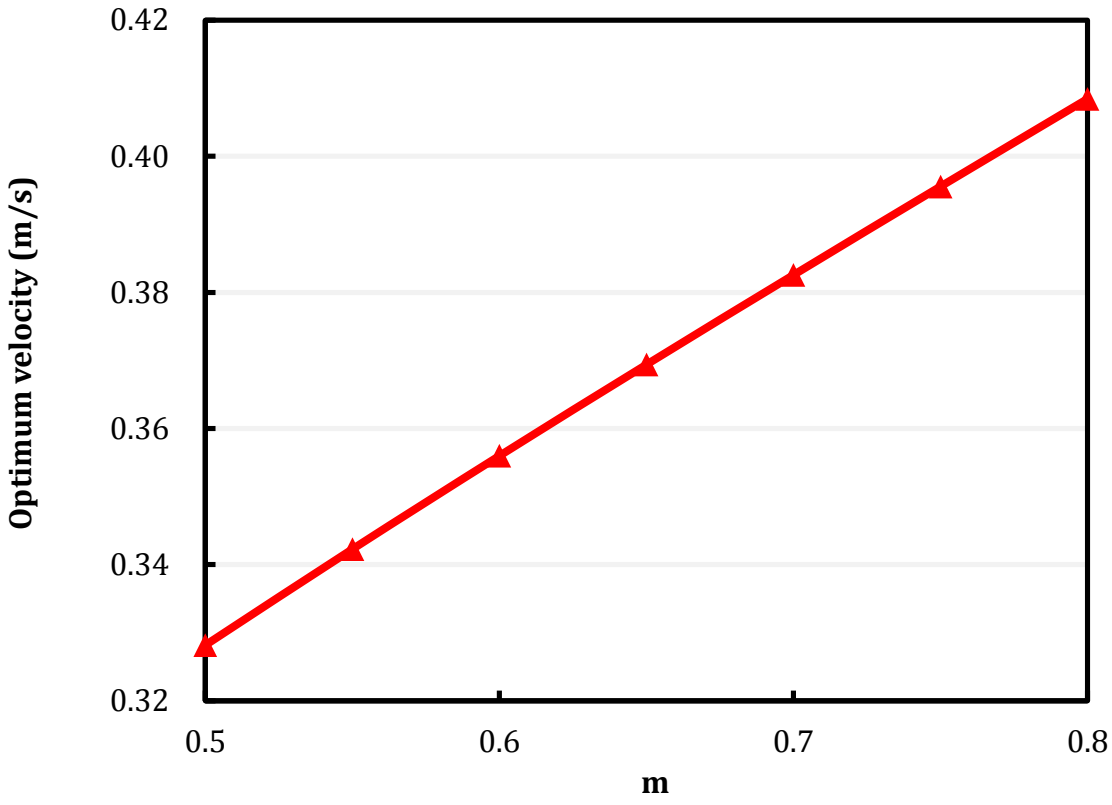

Figure 8.8: Optimum velocity with varied exponent of Reynolds number, m.

Table 8.3: Typical design parameters for PHE.

m	0.66
p	0.21
C_f	1.44
η_p	0.65
ρ (kg/m3)	1000
D_e (m)	0.004
$\frac{\alpha\beta C_{PEC,crX}}{C_{COE} + \alpha\beta C_{PEC,p}}$	100
μ (cP)	3

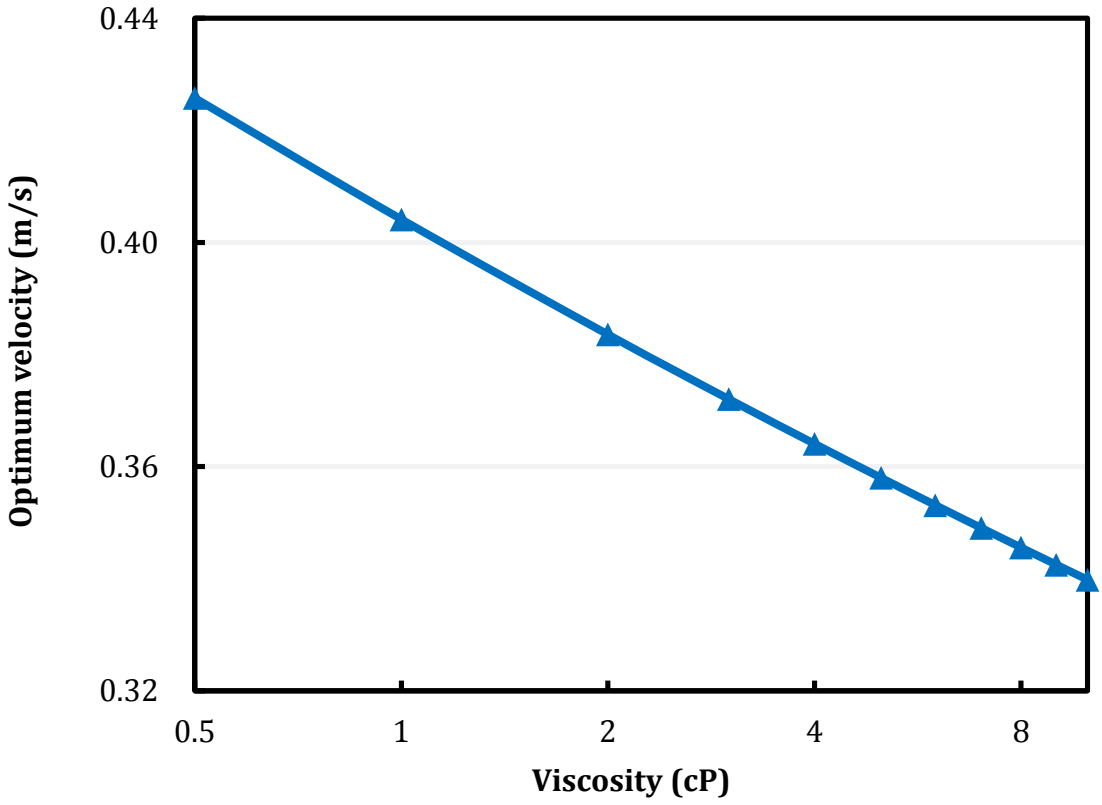

Figure 8.9: Optimum velocity with varied solvent viscosity.

8.6 CONCLUSIONS

To minimize the cross exchanger cost, shortcut methods that determine optimum LMTD and fluid velocity were developed. The optimum fluid velocity is at 0.32–0.42 m/s. Table 8.4 summarizes the dependence between the cross exchanger LMTD, fluid velocity, heat transfer coefficient, and pressure drop. The cross exchanger optimization will be applied to the economic analysis in Chapter 9.

Table 8.4: Summary of dependence between heat transfer coefficient, pressure drop, and viscosity by shortcut method.

Dependence	x	Empirical value
$\Delta T_{LM,opt} \propto h^x$	0.5	-
$h \propto u^x$	m	0.6–0.75
$h \propto \left(\frac{\Delta P}{L}\right)^x$	m/(2-p)	0.35–0.4
$h \propto \Delta P^x$	m/(3-m-p)	0.3–0.35
$u_{opt} \propto \mu^x$	-p/(3-p)	-0.04– -0.08
$h_{opt} \propto \mu^x$	m-n	0.3–0.4
$\Delta P_{opt} \propto \mu^x$	m-n+p	0.3–0.6

NOMENCLATURE

A Heat exchanger area (m^2)
C_{COE} Cost of electricity ($/W-yr)
C_f Constant in pressure drop correlation
C_{Nu} Constant in heat transfer correlation
C_p Heat capacity (kJ/kg-K)
$C_{PEC,crX}$ Purchased equipment cost ($/$m^2$)
$C_{PEC,p}$ Purchased equipment cost ($/W)
D_e Equivalent diameter$(= 2\delta)$
f Fanning friction factor
h Heat transfer coefficient (W/K-m^2)
k Thermal conductivity (W/K-m^2)
L_T Total length of flow path (m)
Nu Nusselt number $(= hD_e/k)$

m Exponent of Re
$\dot{m}$ Solvent mass flow rate
n Exponent of Pr
p Exponent in pressure drop correlation
Q Exchanger heat duty (W)
Re Reynolds number ($= \rho u D_e/\mu$)
T_{stm} Steam temperature (K)
T_{reb} Reboiler temperature (K)
U Overall heat transfer coefficient (W/K-m^2)
$\dot{V}$ Solvent volume flow rate (m^3/s)
u fluid velocity (m/s)
W_p Width of each plate (m)
W_T Total width of plates (m)

Greek

α Scaling factor (-)
θ Corrugation angle
β Annualizing factor (1/yr)
ΔP Total pressure drop (Pa)
$\Delta P/L$ Pressure drop per unit length (Pa/m)
ΔT_{LM} Log mean temperature difference (K)
δ Plate spacing (m)
η_p Pump efficiency
η_{tb} Steam turbine efficiency
μ Solvent viscosity (Pa-s))
ρ Solvent density (kg/m^3)

Subscript

crX Cross exchanger
reb Reboiler
p Pump

Chapter 9: Techno-economic Analysis and Process Optimization

9.1 INTRODUCTION

Energy has been used as the primary performance indicator in previous studies of alternative stripper configurations. However, the overall cost benefit is not guaranteed without considering the capital cost. In order to demonstrate the potential cost benefit that can be brought by the advanced flash stripper (AFS), a techno-economic analysis accounting for both operating cost (OPEX) and capital cost expenses (CAPEX) must be performed.

The major objective of previous economic analyses was to show the competitiveness and economic feasibility of amine scrubbing by comparing the cost of CO_2 avoided (Abu-Zahra et al., 2007; Hammond et al., 2011; Hasan et al., 2012; Huang et al., 2010). Abu-Zahra (2007) studied the effect of lean loading, amine concentration, and removal rate on the overall economics using a non-intercooled absorber and a simple stripper. Most studies were focused on conventional process configurations and solvent (MEA), and there are few direct comparisons to advanced solvents and processes.

Several studies compared the capital cost of alternative strippers (Karimi et al., 2011; Lin & Rochelle, 2014; Schach et al., 2010). Schach (2010) demonstrated the cost savings using absorber intercooling and the matrix stripper but the parametric study of lean loading was at a constant stripper pressure, which limits the possibility to reduce the compressor cost. Karimi (2011) concluded that the lean vapor compression gives the lowest capture cost among five stripper alternatives. However, the effect of lean loading and process optimization regarding capital-energy tradeoffs were not considered. Lin and Rochelle (2014) evaluated the operating and capital cost for the most promising stripper configuration, the advanced flash stripper (AFS) at varied lean loading and stripper pressure. A parametric study was performed to investigate the effect of the cross

exchanger LMTD and the CO_2 lean loading. Little study has been conducted for advanced stripper configurations with a complete process economic optimization.

The objective of this work is to quantify the benefit of AFS by considering OPEX and CAPEX and compare to the conventional simple stripper. A process optimization that minimizes the annualized cost will be explored to guide selection of the optimum equipment design and operating conditions. The simple stripper and the AFS will be modeled in Aspen Plus® using 8 m PZ. The scope of the economics analysis includes the CO_2 regeneration and compression highlighted in Figures 9.1 and 9.2 for the simple stripper and the AFS, respectively. Since the absorber is not included, the rich solvent conditions will be the input to the simulation. The rich loading will reflect the absorber performance.

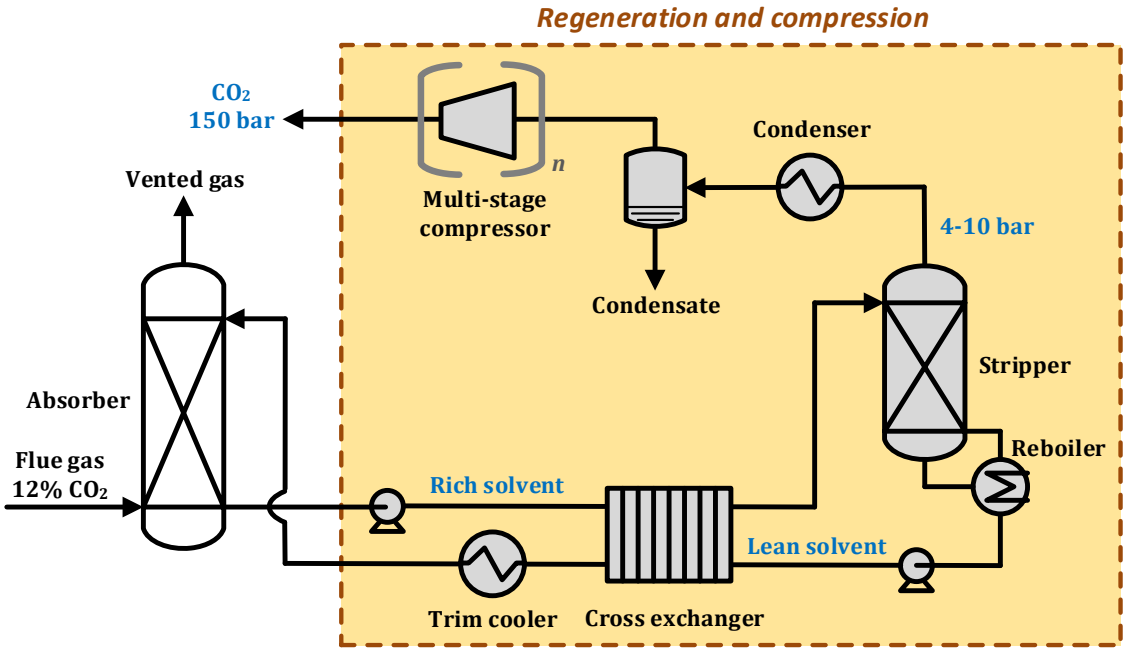

Figure 9.1: Economic analysis scope for the simple stripper.

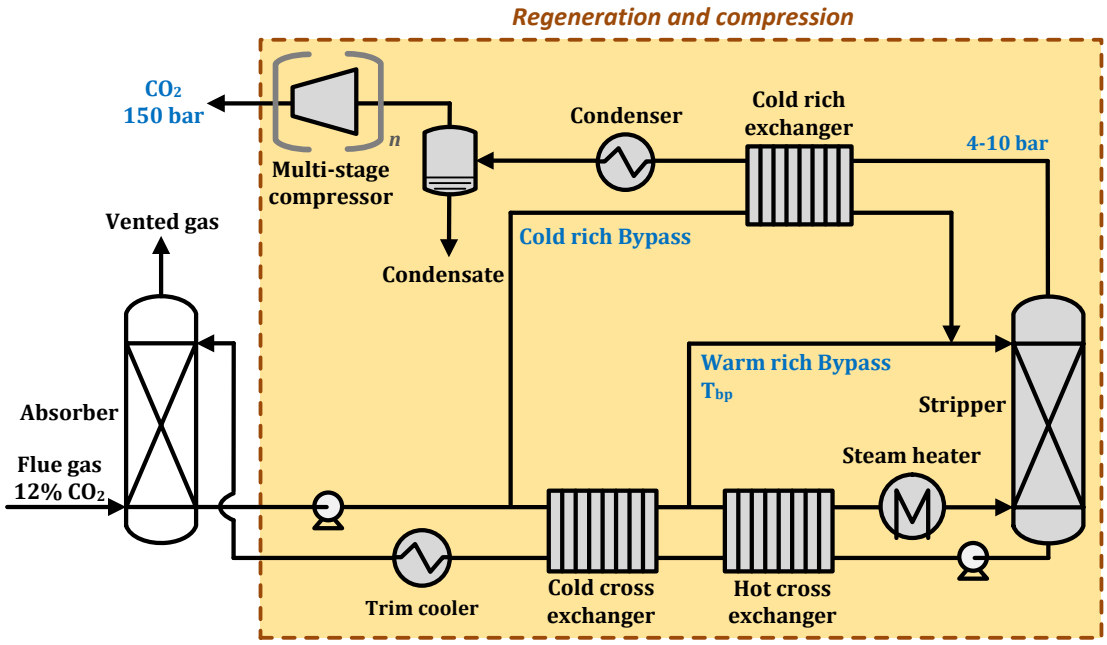

Figure 9.2: Economic analysis scope for the advanced flash stripper.

9.2 Modeling Methods

9.2.1 Process specifications

The capture plant is designed to capture 3.3 million tonnes of CO_2 per year, which corresponds to a 500 MW_e (gross output) coal-fired power plant with 90% removal (Fisher, 2007). The process specifications used in the simulations are shown in Table 9.1. The rich solvent loading and temperature are assumed as 0.4 mol CO_2/mol alkalinity and 46 °C, respectively, which are typical results for an intercooled absorber with 1.1–1.2 L/G and finite packing (Plaza, 2011). The effect of rich loading will be tested in Section 9.3.3

Simulation results were obtained from Aspen Plus® version 7.3 using the Independence model, which was rigorously regressed for PZ (Frailie, 2014). The rigorous rate-based calculation is used in the stripper for heat and mass transfer with equilibrium reactions. The interfacial area is corrected by a factor of 0.15 to agree with

2015 SRP pilot plant data as described in Chapter 5. This is probably a result of an inaccurate value of the amine diffusion coefficient predicted by Independence model.

Table 9.1: Summary of design specifications.

CO_2 capture rate (kg/s)	115.7
Solvent	8 m PZ
Process modeling tool	Aspen Plus® v7.3
Thermodynamic model	Independence
Packing type	RSR no. 0.3
Correction factor of interfacial area	0.15
Regeneration temperature (°C)	150
Rich loading (mol CO_2/mol alk)	0.4
Rich solvent temperature (°C)	46

9.2.2 Costing methods

The annualized cost of CO_2 captured in \$/tonne CO_2 will be used to quantify the capital-energy tradeoffs and justify the cost benefits. The annualized regeneration cost will include the OPEX and the annualized CAPEX of unit operations included in the scope of Figures 9.1 and 9.2.

- CAPEX

The capital cost needs to be converted to \$/tonne CO_2 so it can be compared with energy cost. A simplified estimation method was proposed by Frailie (2014) using Equation 9.1. The scaling factor α converts the purchased equipment cost (PEC) to total capital investment (TCI) and the annualizing factor β annualizes the TCI. The scaling factor includes the direct and indirect installation cost, contingency, contractor's fee, and auxiliary facilities. Typical scaling factor for chemical processes was indicated as 4–6,

which depends on types of process and unit operation (Seider et al., 2003; Turton et al., 2012).

Various estimation methods for CO_2 capture process have been reviewed by Frailie (2014). It was concluded that typical scaling factor is 2–10 and annualizing factor is 0.1–0.3. The annualizing factor takes into account return on investment (10%), taxes (35% of return on investment), depreciation, and maintenance (2–3%). The α and β are recommended as 5 and 0.2, respectively and will be used in this work.

$$Annualized\ CAPEX\left(\frac{\$}{tonne\ CO_2}\right) = \frac{\alpha \times \beta \times PEC}{tonne\ CO_2\ captured\ per\ year} \qquad (9.1)$$

- OPEX

Total equivalent work (W_{eq}) is used to calculate the OPEX by accounting for the electricity penalty due to the steam extraction from the power plant, the CO_2 compression work, and the solvent pumping work. The rich pump work is required to overcome the pressure drops through heat exchangers and move the solvent from the absorber to the pressure of the stripper. The lean solvent is typically at 4–10 bar at 150 °C using PZ. The available pressure will be taken into account when calculating the pump work requirement for the lean solvent.

The operating cost is calculated using Equation 9.2. The cost of electricity (COE) with post-combustion CO_2 capture will increase $41/MWh due to the increased capital and energy consumption for capture process (IEA, 2013). A typical levelized COE, $100/MWh will be used in the analysis. The levelized COE is expected to improve as more commercial capture plants are built due to learning effects. Advanced solvents and processes also have potential to reduce the cost. A sensitivity analysis on $\alpha\beta$ and COE will be performed in Section 9.3.4. Table 9.2 summarizes the costing parameters used in this work.

$$Annualized\ OPEX\left(\frac{\$}{tonne\ CO_2}\right) = \frac{W_{eq} \times \mathrm{COE}}{tonne\ CO_2\ captured\ per\ year} \quad (9.2)$$

Table 9.2: Summary of costing parameters.

Capital scaling factor, α	5
Capital annualizing factor, β	0.2
COE ($/MWh)	100
CEPCI (2015 April)	563
Operational time (days/yr)	329

9.2.3 Calculating purchased equipment cost (PEC)

The unit operations are sized using the simulation data such as pressure, temperature, flow rate, heat duty, and heat exchanger LMTD (ΔT_{LM}) obtained from Aspen Plus®. The PEC of unit operations were acquired either from vendor quotes or empirical correlations, and then scaled to 2015 cost level by the Chemical Engineering Plant Cost Index (CEPCI). Table 9.3 summarizes the equipment sizing and pricing basis.

- Heat exchangers

Sizing heat exchangers requires the exchanger duty, LMTD and the overall heat transfer coefficient (U). The exchanger duty and LMTD are obtained from Aspen Plus® simulations. The U of the cross exchangers will be optimized by considering pressure drop cost and the exchanger cost as described in Chapter 8. The U of the cold rich exchanger and the steam heater are calculated from the 2015 SRP pilot plant results. The condenser and the reboiler are considered to have the same heat transfer mechanism of the cold rich exchanger and the steam heater, respectively so the same values will be used.

- Stripper column

The stripper height consists of one packing section, a sump with 1 min residence time, and 2 meter auxiliary height for distributor and liquid feed. The diameter is determined by 80% flooding approach.

Table 9.3: Summary of equipment sizing and pricing basis.

Class	Name	Type	Material	Sizing basis	Cost source
Column	Stripper	Packed tower	316SS	80% flooding Auxiliary height: 2 m Residence time: 1 min	(Tsai, 2010)
Heat exchanger	Cross exchanger	Plate-and-frame	316SS	Optimized U and ΔT_{LM}	Vendor quote
	Cold rich exchanger	Plate-and-frame	316SS	U: 250 W/K-m^2 Optimized ΔT_{LM}	Vendor quote
	Trim cooler	Plate-and-frame	316SS	U: 1500 W/K-m^2 Cooling water T_{in}/T_{out}: 16/25 °C	Vendor quote
	Condenser	Plate-and-frame	316SS	U: 250 W/K-m^2 Cooling water T_{in}/T_{out}: 16/25 °C	Vendor quote
	Reboiler	Kettle type Shell-and-tube	316SS	U: 2500 W/K-m^2 Optimized steam T	(Seider et al., 2003)
	Steam heater	Fixed-head type Shell-and-tube	Tube: SS Shell: CS	U: 2500 W/K-m^2 Optimized steam T	Vendor quote
Pump	Rich pump	Centrifugal	316SS	Efficiency: 65%	Vendor quote
	Lean pump	Centrifugal	316SS	Efficiency: 65%	Vendor quote
	CO_2 pump	Centrifugal	316SS	Efficiency: 65% Final P: 150 bar	Vendor quote
Compressor	Multi-stage compressor	Centrifugal	316SS	Pressure ratio per stage ≤2 Intercooling to 40 °C Polytropic efficiency: 86% Final P: 76 bar	Aspen Icarus®
Pressure vessel	Condensate tank	Vertical	316SS	Residence time: 5 mins	(Tsai, 2010)

- Pumps

The PEC of pump is mainly determined by the pump work, which is calculated based on the volumetric flow rate of solvent and the head requirement. The rich solvent pumps provide the head to move the solvent from 1 bar to the stripper pressure and the pressure drops across the heat exchangers. A pump for the lean solvent is not necessary when the stripper pressure is sufficient to get the solvent through the cross exchangers, the trim cooler and the absorber. The pressure drops of the steam heater and the trim cooler are assumed as 10 psi (0.7 bar) for each, and the static head of the absorber is assumed as 30 m. The pump efficiency is assumed as 65%.

- Multi-stage compressor

The capital cost of the multi-stage compressor consists of compressors, intercoolers, a motor drive, and a CO_2 supercritical pump as shown in Figure 9.3. The CO_2 is compressed from stripper pressure to above critical pressure using the multi-stage compressor and further pressurized to 150 bar using the CO_2 supercritical pump. The CO_2 is intercooled to 40 °C and aftercooled to 30 °C before entering the pump to reduce the volumetric flow rate. Table 9.4 summarizes the design specifications of the multi-stage compressor. The configuration and specifications are identical to the simulations used to acquire compression work described in Chapter 2.

The sizing uses the simulation results from Aspen Plus® with CO_2 flow rate at 116 kg/s. The PEC of the compressor and motor are obtained from Aspen Icarus® as a function of inlet volume flow rate, pressure rating, and compression work.

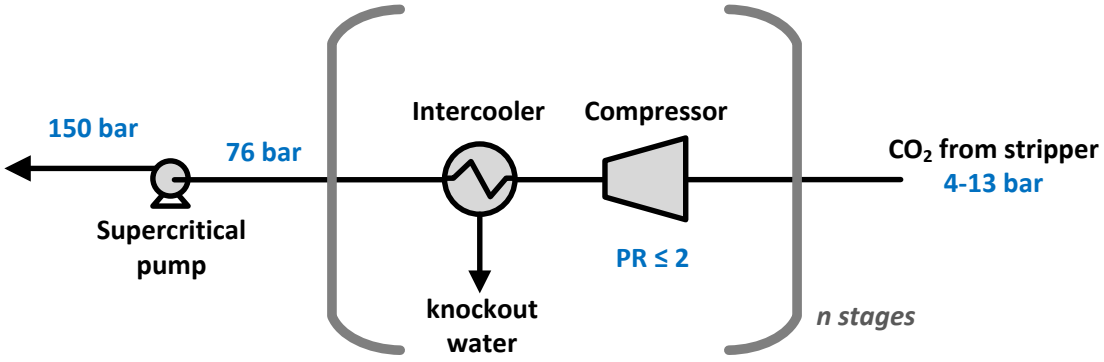

Figure 9.3: Multi-stage compressor with supercritical pump.

Table 9.4: Design specifications of multi-stage compressor.

Maximum pressure ratio/stage	2
Compressor polytropic efficiency (%)	86
Intercooling temperature (°C)	40
Aftercooling temperature (°C)	30
Supercritical pump efficiency (%)	65
Multi-stage compressor outlet P (bar)	76
Final target P (bar)	150

Figure 9.4 shows the PEC of the multi-stage compressor with varied inlet pressure. The capital cost is mainly driven by the cost of the compressor. Step changes can be seen when the number of stages varies, which depends on the specified maximum pressure ratio. The stripper pressure for MEA at 120 °C is typically 1–4 bar and for PZ at 150 °C is 4–10 bar. PZ only requires 3 or 4 stages compared to MEA that that requires 5–7 stages at the typical operating lean loadings. This demonstrates the potential benefit of PZ with higher thermal stability that can be operated at elevated temperature providing higher stripper pressure.

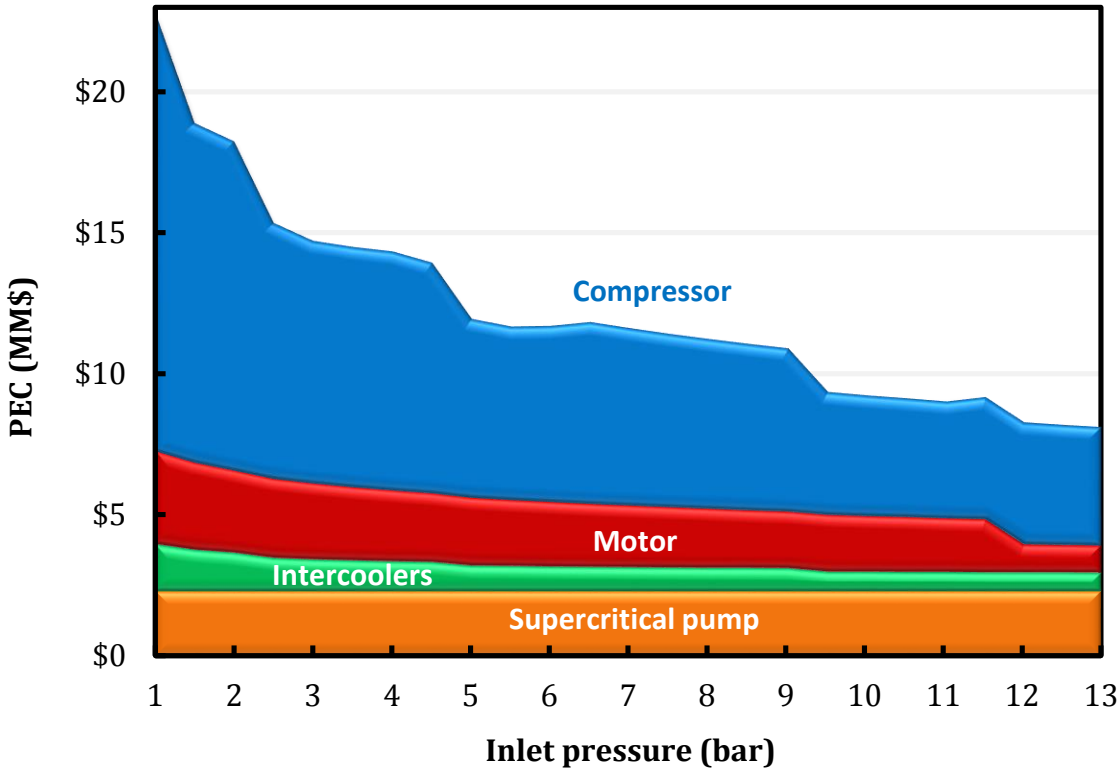

Figure 9.4: Purchased equipment cost of multi-stage compressor with supercritical pump from Aspen Icarus®; CO_2 flow rate: 116 kg/s; 2015 cost level.

The total compressor PEC data is annualized and smoothed by a regressed correlation (Equation 9.3) with 0.98 of R-squared as shown in Figure 9.5. The smooth curve eliminates the discontinuities and reduces the uncertainties from the specified maximum pressure ratio that can vary among manufacturers but still predicts the general trend with varied inlet pressure.

$$Annualized\ Compressor\ CAPEX\left(\frac{\$}{tonne\ CO_2}\right) = -2.05\ ln(P_{in}) + 0.17 ln^2(P_{in}) + 6.76$$

$$1\ bar \leq P_{in} \leq 13\ bar \qquad (9.3)$$

Table 9.5 compares the compressor CAPEX calculated by Equation 9.3 and from other sources including DOE Case 10 (NETL, 2010) and a vendor quote at corresponding

inlet pressures. The cost from DOE case is slightly higher than prediction because it included a dehydration unit. In general Equation 9.3 can adequately predict the compressor CAPEX.

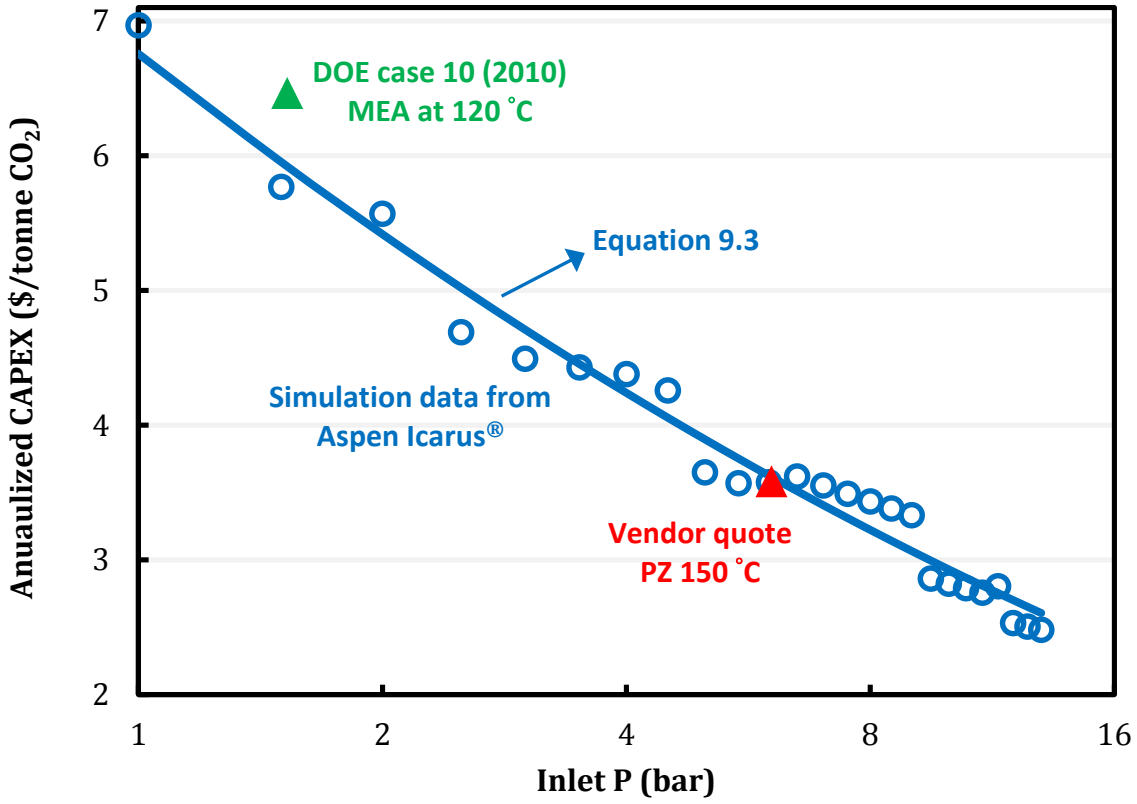

Figure 9.5: Annualized CAPEX of multi-stage compressor; CO_2 flow rate: 116 kg/s; 2015 cost level; αβ=1.

Table 9.5: Comparison of CAPEX of compressor from sources.

	DOE Case 10	**Vendor quote**
Configuration	6 stages centrifugal compressor +intercooling	4 stages centrifugal compressor +intercooling +CO_2 supercritical pump
CO_2 flow rate (kg/s)	152.6	137.6
Inlet P (bar)	1.6	5.9
Final P (bar)	153	150
Annualized CAPEX ($2015/tonne CO_2)	6.4	3.5
Annualized CAPEX by Eq. 9.3 ($2015/tonne CO_2)	6.0	3.6

9.2.4 Process optimization

The CAPEX and OPEX calculations are built in the Aspen Plus® and are calculated simultaneously with simulations. The optimization problem shown in Equations 9.4 and 9.5 are solved for the simple stripper and the AFS, respectively at specified lean loading, rich loading, and reboiler temperature. The decision variables include heat exchanger LMTD (ΔT_{LM}), stripper packing height (H_{pkg}), cold and warm rich bypass rates (F_{cbp}, F_{wbp}), steam saturation temperature (T_{stm}) and pressure drops of the cross exchangers (ΔP_{crx}). The lean loading will optimized by a parametric study.

$$\underset{\Delta T_{LM}, H_{pkg}, T_{stm}, \Delta P_{crx}}{\text{minimize}} \quad annualized\ OPEX + CAPEX \tag{9.4}$$

Subject to: specified *lean loading*, *rich loading*, and T_{reb}

$$\underset{\Delta T_{LM}, H_{pkg}, F_{cbp}, F_{wbp}, T_{stm}, \Delta P_{crx}}{\text{minimize}} \quad annualized\ OPEX + CAPEX \tag{9.5}$$

Subject to: specified *lean loading*, *rich loading*, and T_{reb}

The cross exchanger optimization has been discussed in Chapter 8. The heat transfer coefficient can be enhanced by increasing the fluid velocity. The optimization considers the tradeoffs of the reduction of cross exchanger area and the increase of pumping cost. An optimum heat transfer coefficient can be found. Equations 9.6 and 9.7 were recommended to estimate the heat transfer coefficient and the fanning friction factor for plate-and-frame exchanger (Ayub, 2003). Even though the rich solvent will become a two-phase flow after it reaches the bubble point, the heat transfer calculations will assume single phase. Only liquid properties are used to calculate Reynolds (Re) and Prandtl number (Pr).

$$Nu = 0.3Re^{0.66}Pr^{0.33} \tag{9.6}$$

$$f = 1.44Re^{-0.21} \tag{9.7}$$

9.3. RESULTS AND DISCUSSIONS

9.3.1 Optimum stripper design with minimum regeneration cost

Both the simple stripper and the AFS were simulated and optimized using 8 m PZ. Tables 9.6 and 9.7 summarize the equipment tables for the simple stripper and the AFS at 0.22 lean loading, respectively.

The stripper diameter of the AFS is smaller than the simple stripper since less solvent is fed to the stripper. The warm rich bypass provides a greater driving force for stripping steam recovery and CO_2 stripping so the optimum packing height of AFS is twice that of simple stripper.

The exchanger duty of the cross exchanger is typically 3–5 times the reboiler duty so even a few degrees change of the cross exchanger LMTD can affect the energy performance significantly. To determine the temperature approach of the cross

exchanger, the tradeoffs involve the capital cost and the steam use in the reboiler/steam heater. The AFS has a relatively smaller LMTD of the cross exchanger than the simple stripper, which implies that the sensible heat from the hot lean solvent is recovered in a more efficient way. Previous work showed that the cold and warm rich bypass of AFS can help relax the temperature pinch of the cross exchangers by balancing the mass flow rate between lean and rich solvent and make it more reversible (Lin et al., 2016).

The optimum steam saturation temperatures for the simple stripper and the AFS are 164 °C and 157 °C, respectively. Higher steam saturation temperature can increase the temperature approach between the heating medium and the solvent but will lose more electricity per unit steam usage. The exchanger area of the reboiler/steam heater is directly proportional to the heat duty and the LMTD. The higher heat duty and capital cost of kettle-type reboiler make the simple stripper require a higher steam temperature in order to reduce the reboiler CAPEX.

Table 9.6: Equipment table of simple stripper at 0.22 lean loading.

Class	Name	Design spec	Annualized CAPEX ($/tonne CO_2)
Column	Stripper	Diameter: 10 m Packing H: 3.9 m Column H: 7.2 m	0.4
Heat exchanger	Cross exchanger	U: 1520 W/K-m^2 ΔT_{LM}: 9.8 K ΔP_{lean}: 3.0 bar ΔP_{rich}: 2.1 bar	1.8
	Reboiler	ΔT_{LM}: 13.6 K Steam T: 163.6 °C	1.5
	Condenser	ΔT_{LM}: 69 K	0.2
	Trim cooler	ΔT_{LM}: 26 K	0.1
Pump	Rich pump	Head: 8.2 bar	0.5
	Lean pump	Head: 1.3 bar	0.2
Compressor	Multi-stage compressor	Net output: 23.5 MW	3.6
Pressure vessel	Condensate tank	Diameter: 2.3 m Height: 4.6 m	<0.1
	Annualized CAPEX ($/tonne CO_2)		8.3

Table 9.7: Equipment table of AFS at 0.22 lean loading.

Class	Name	Design spec	Annualized CAPEX ($/tonne CO_2)
Column	Stripper	Diameter: 8.4 m Packing H: 9.8 m Column H: 13.6 m	0.6
Heat exchanger	Cold cross exchanger	U: 1449 W/K-m^2 ΔT_{LM}: 7.9 K ΔP_{lean}: 1.8 bar ΔP_{rich}: 2.7 bar	1.5
	Hot cross exchanger	U: 1831 W/K-m^2 ΔT_{LM}: 6.9 K ΔP_{lean}: 0.7 bar ΔP_{rich}: 1.5 bar	0.6
	Steam heater	ΔT_{LM}: 10.2 K Steam T: 157 °C	0.8
	Cold rich exchanger	ΔT_{LM}: 18 K	0.3
	Condenser	ΔT_{LM}: 35 K	0.1
	Trim cooler	ΔT_{LM}: 27 K	0.1
Pump	Rich pump	Head: 9.4 bar	0.6
	Lean pump	Head: 1.7 bar	0.2
Compressor	Multi-stage compressor	Net output: 23.5 MW	3.6
Pressure vessel	Condensate tank	Diameter: 3.5 m Height: 1.8 m	<0.1
	Annualized CAPEX ($/tonne CO_2)		8.3

The comparison of energy use is shown in Table 9.8. The AFS reduces the heat duty by 20% compared to the simple stripper. Higher steam temperature makes the difference as equivalent work even greater. The pump work and the compression work are approximately the same at the same lean loading, which gives the same stripper pressure.

Table 9.8: Energy use of simple stripper and AFS.

	Simple stripper	**AFS**
Lean loading (mol CO_2/mol alk)	0.22	0.22
Stripper P (bar)	5.5	5.5
T_{steam} (°C)	164	157
Heat duty (kJ/mol CO_2)	120.2	95.7
W_{heat} (kJ/mol CO_2)	30.5	23.1
W_{pump} (kJ/mol CO_2)	0.8	1.0
W_{comp} (kJ/mol CO_2)	8.2	8.2
W_{eq} (kJ/mol CO_2)	39.5	32.3
Energy cost ($/tonne CO_2)	25.4	21.1

Figure 9.6 shows the contributions to the annualized regeneration cost at 0.22 lean loading. The annualized regeneration cost is $33.7 and $29.4/tonne CO_2 for the simple stripper and the AFS, respectively including 70% of OPEX and 30% of CAPEX. The compressor and the cross exchanger are the cost centers of CAPEX. The AFS reduces the annualized regeneration cost by 13% and the major savings come from the reduction of the steam cost. The AFS has the same CAPEX as the simple stripper. Even though the AFS splits the cross exchanger, the total exchanger area does not necessarily increase. Multiple plate-and-frame exchangers are needed for a full-scale plant so the exchanger price per unit area is not affected. The cold rich exchanger can be simply seen as a part of the condenser, which is responsible to condense the stripping steam and cool the CO_2 vapor to 40 °C. The only difference is that the temperature approach using the cold rich

solvent is not as large as using cooling water. The cost savings by the AFS is equivalent to \$12.7 million per year for a 500 MW_e coal-fired power plant.

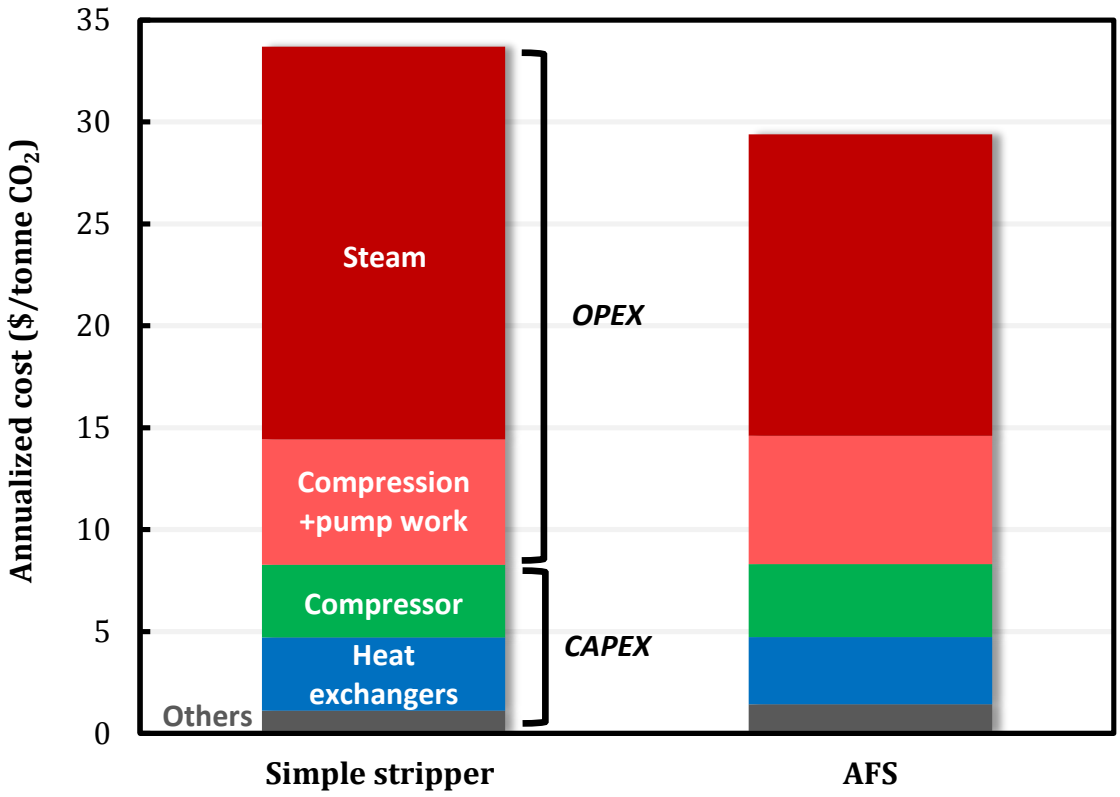

Figure 9.6: Breakdown of annualized regeneration cost at 0.22 lean loading.

9.3.2 Effect of CO_2 lean loading

CO_2 lean loading is the most important operating parameter that should be determined and optimized. At fixed stripper temperature, lean loading can be varied by manipulating the stripper pressure. Figure 9.7 shows the annualized regeneration cost at varied lean loading. The simple stripper (SS) base case specifies 5 K LMTD for the cross exchanger and 2 m stripper packing while optimizing other decision variables as shown in

Equation 9.4. Another two cases with optimum packing height and cross exchanger LMTD are also presented to show each individual effect.

The improvement from optimizing packing height becomes more significant with decreasing lean loading but has little effect at the higher lean loading. Increasing packing height provides heat transfer area for heat recovery from the stripping steam especially at low lean loading region where stripping steam is significant. 2 m of packing is excessive for lean loadings above 0.24 and will saturate the heat and mass transfer at the top of the stripper so little improvement is observed.

The optimum cross exchanger LMTD is primarily affected by solvent capacity (i.e., solvent circulation rate) when the lean loading varies. The annualized regeneration cost is expected to be less sensitive to the cross exchanger LMTD at lower lean loadings because the cross exchanger CAPEX and the sensible heat requirement have less contributions at lower solvent rate. Because excessive stripping steam is still left with the simple stripper, a greater cross exchanger LMTD makes the stripper feed colder and able to condense a portion of stripping steam in the stripper. A similar effect of warm rich bypass can be attained by adjusting the LMTD of the cross exchanger for the simple stripper.

The AFS consistently reduces cost by \$3–4/tonne CO_2 compared to the simple stripper throughout the lean loading range. The optimum lean loading that minimizes the annualized regeneration cost is at 0.22 mol CO_2/mol alkalinity. The cost is flat for both configurations between lean loadings 0.18 and 0.26 with a difference less than \$0.3/tonne CO_2. It should be noted that lower lean loading always gives better absorption performance and reduces the absorber packing requirement. If the absorber CAPEX is included, the optimum lean loading should shift even lower. Other considerations such

as PZ solid solubility, amine volatility, aerosol growth should be taken into account when determining the optimum lean loading.

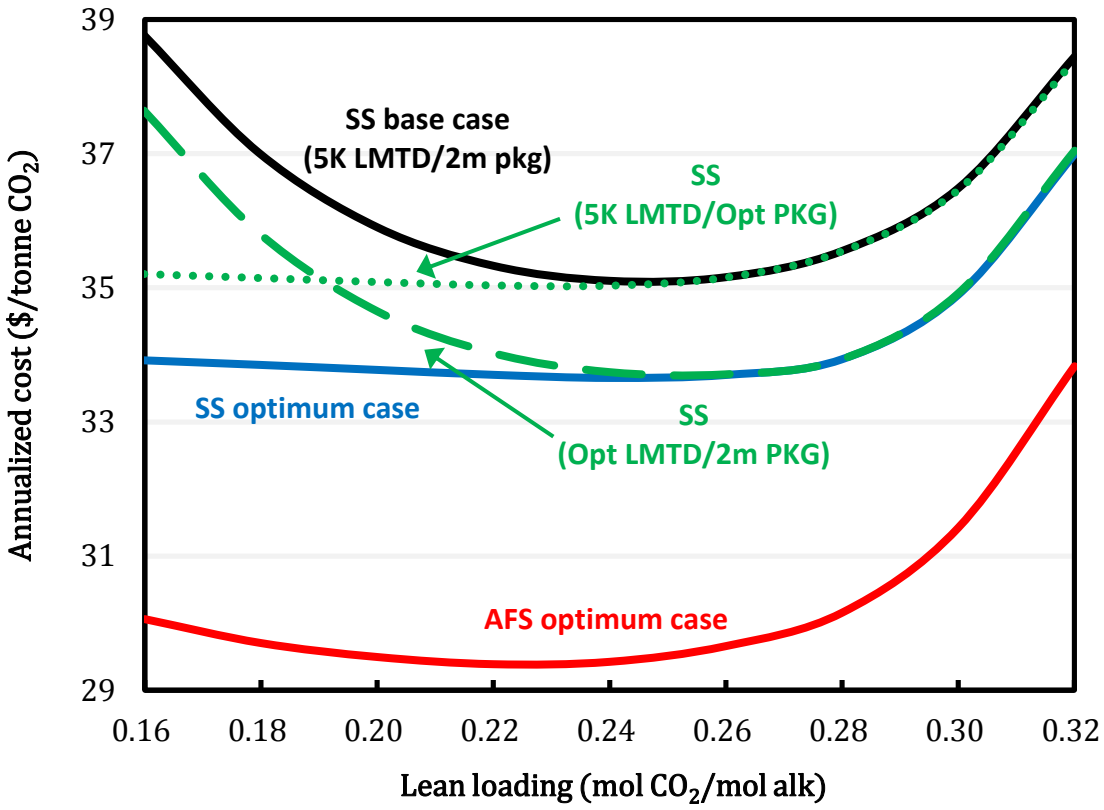

Figure 9.7: Effect of lean loading on annualized regeneration cost; rich loading: 0.4; reboiler T: 150 °C; correction for interfacial area: 0.15.

Figure 9.8 shows the contributions to the annualized regeneration cost with the AFS with varied lean loading. The compression work is driven by the stripper pressure, which varies from 4.6 to 10.2 bar in this lean loading range. The CAPEX and OPEX of the compressor can be reduced by 32% ($3.2/tonne CO_2) as the lean loading increases from 0.16 to 0.32 mol CO_2/mol alkalinity. However, the savings from the compressor CAPEX and OPEX are not enough to compensate the increase of the sensible heat requirement and

the cross exchanger CAPEX. The CAPEX of the cross exchanger increases from \$1.4 to \$5.5/tonne CO_2 and is the cost most sensitive to lean loading.

The optimum lean loading for the AFS is lower than the optimum lean loading considering only the total equivalent work. Even though the OPEX accounts for over 70% of the annualized regeneration cost, the CAPEX is more sensitive to lean loading. The low solvent capacity at high lean loading deteriorates both energy and capital cost, so the optimum is forced to lower lean loading until the compression cost and the heat loss of stripping steam dominate.

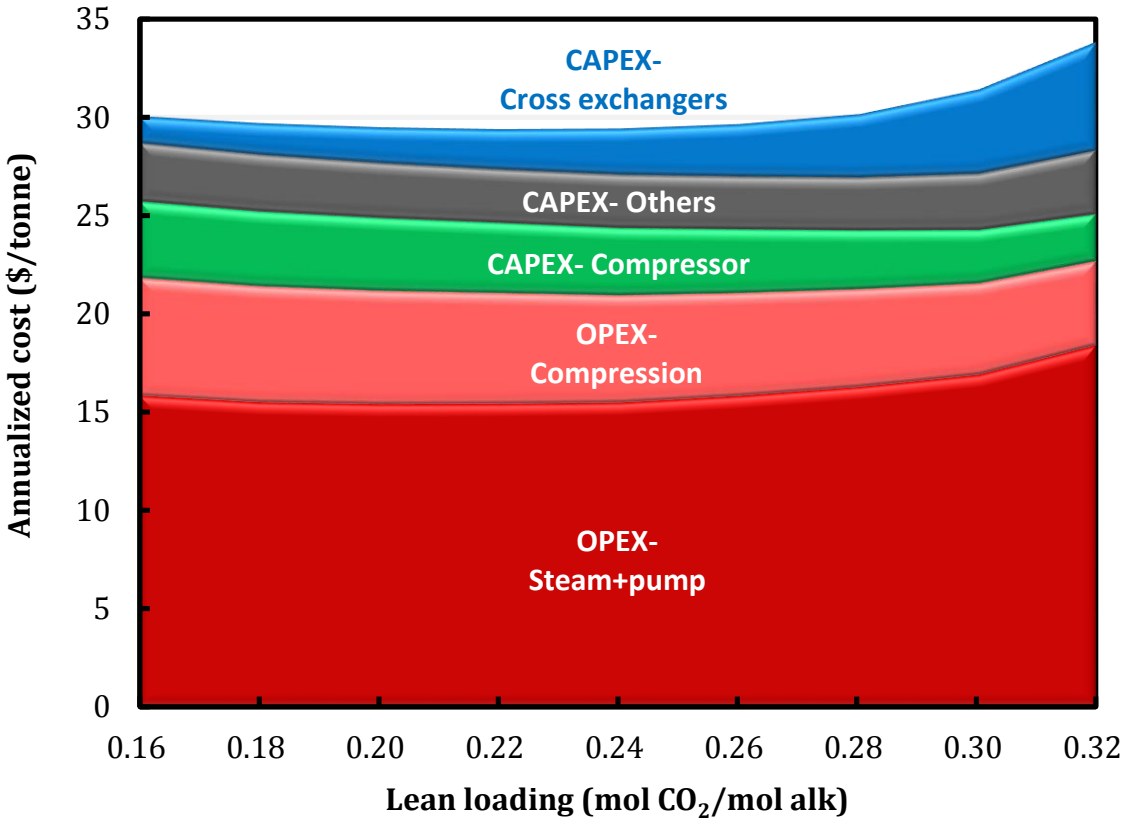

Figure 9.8: Breakdown of the annualized regeneration cost of AFS with varied lean loading.

9.3.3 Effect of rich loading

Since the absorber is not simulated, a sensitivity analysis of rich loading that represents the absorber performance is performed. Figure 9.9 plots the annualized regeneration cost with varied rich loading from 0.36 to 0.40 mol CO_2/mol alkalinity. Increasing the rich loading from 0.38 to 0.40 reduces the annualized regeneration cost by 5–10% depending on the lean loading. The rich loading mainly affects the cyclic capacity and the solvent circulation rate, which is inversely proportional to the difference of rich and lean loading (i.e., ΔLdg). The rich loading makes the most significance at higher lean loading where the sensible heat requirement and the cross exchanger CAPEX dominate.

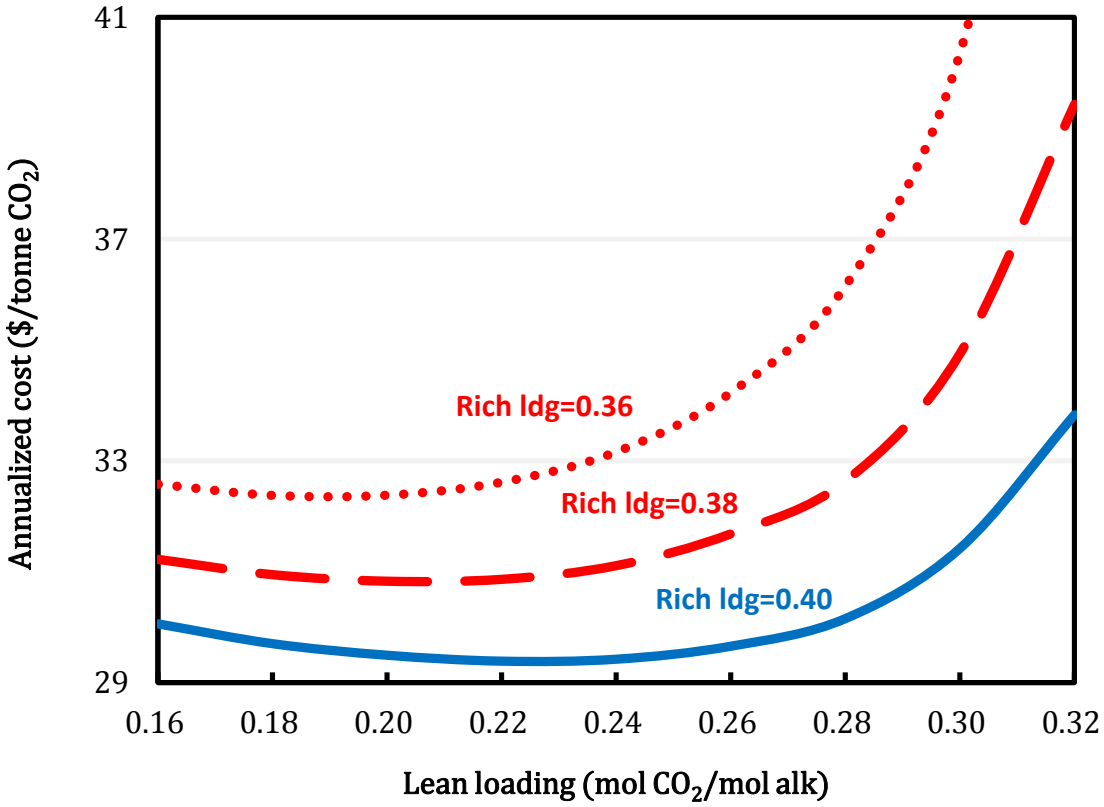

Figure 9.9: Effect of rich loading on annualized regeneration cost with varied lean loading.

The cyclic capacity is isolated by plotting the annualized regeneration cost versus ΔLdg in Figure 9.10. The ΔLdg increases with decreasing lean loading at a constant rich loading. The costs between rich loadings converge at lower ΔLdg (i.e., higher lean loading) but there are still differences at low lean loading region. The secondary effect of the rich loading is on the stripper performance. Richer solvent with a higher partial pressure facilitates CO_2 stripping and water condensation in the stripper by providing a greater driving force between solvent and vapor. Better stripper performance reduces not only the stripper packing height but also the cold rich bypass and prevents a severe pinch in the cross exchanger. The effects of solvent capacity and stripper performance dominate at higher and lower lean loadings, respectively.

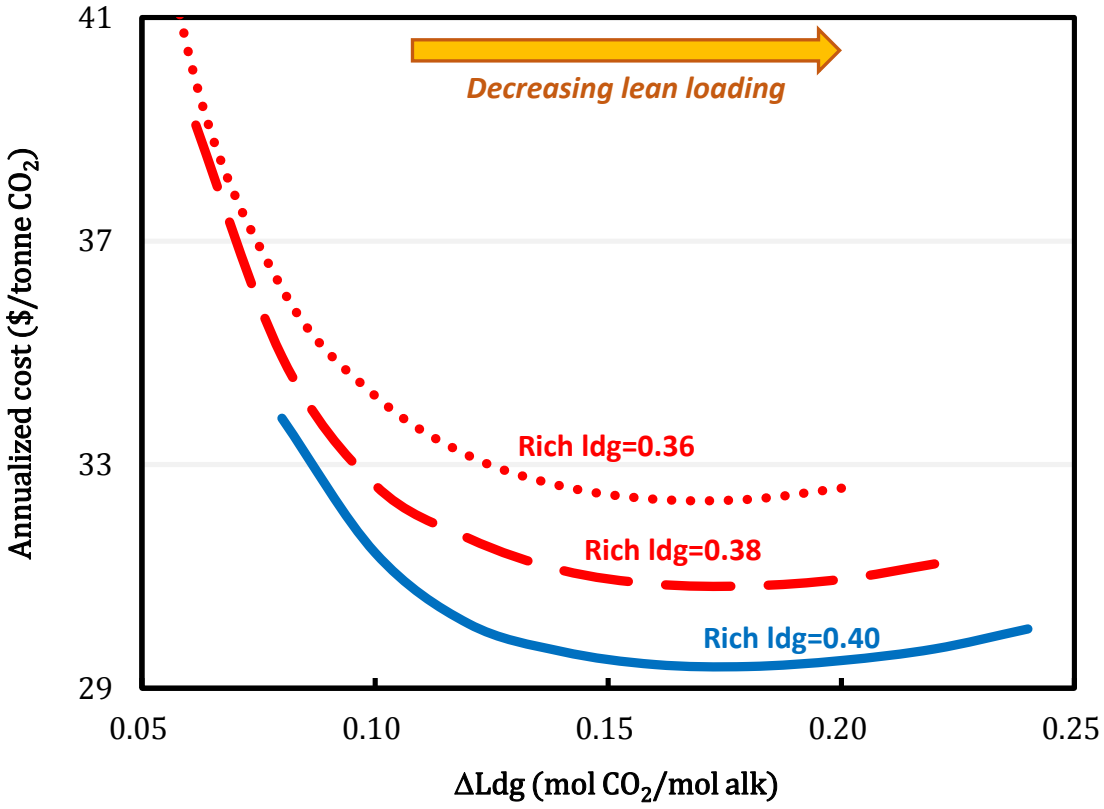

Figure 9.10: Effect of rich loading on annualized regeneration cost with varied ΔLdg.

9.3.4 Sensitivity of costing factors

The annualized regeneration cost depends on the capital scaling factor, annualizing factor, and COE, which not only affect the cost value but also the emphasis of CAPEX or OPEX. A sensitivity analysis was performed for the AFS by adjusting the αβ and the COE, which are 1 and $100/MWh, respectively for the base case.

Figures 9.11 and 9.12 show the annualized regeneration cost with ±50% change of αβ and ±20% change of COE, respectively. The change results in $4–5/tonne CO_2 systematic increase or decrease across the lean loading range. All the cases have similar trends and optimum lean loadings as the base case.

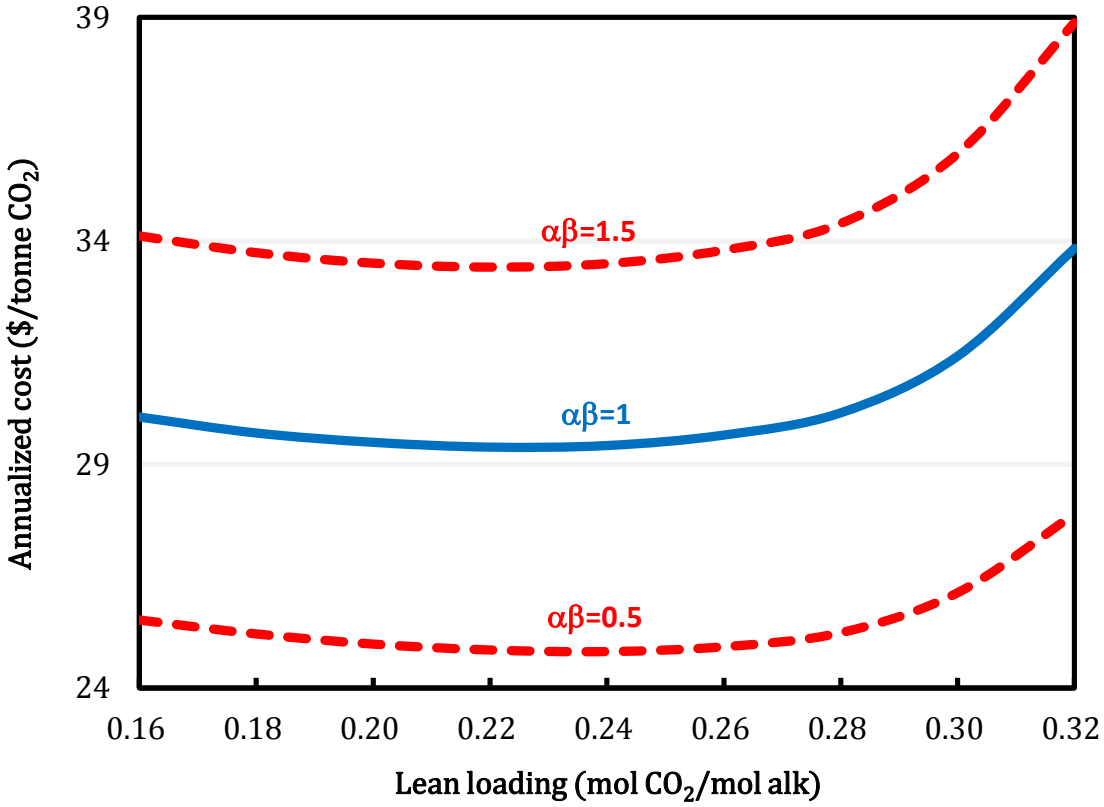

Figure 9.11: Sensitivity of capital costing factor on annualized regeneration cost; COE: $100/MWh.

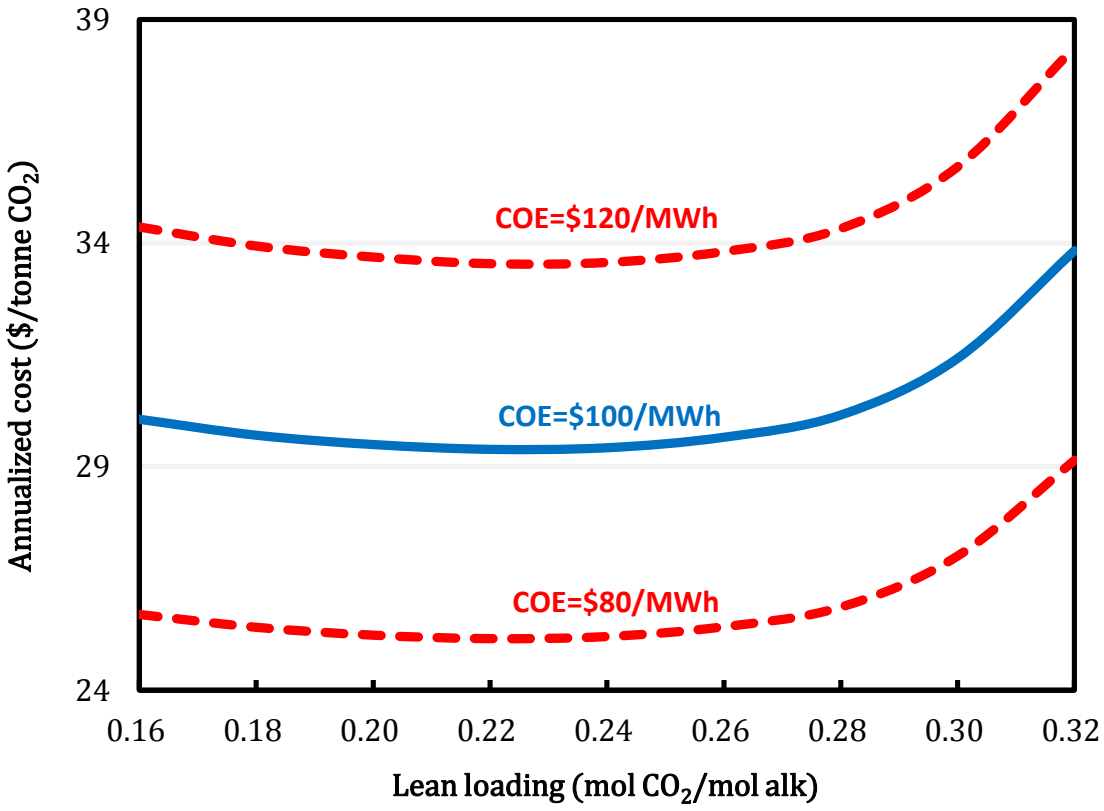

Figure 9.12: Sensitivity of COE on annualized regeneration cost; αβ=1.

Figure 9.13 shows an example of how the optimum design is adjusted to adapt to different emphasis on CAPEX and OPEX. The optimum cross exchanger LMTD decreases from 10 to 5 K when the ratio of COE to αβ increases from 50 to 240 (i.e., from 80 of COE and 1.5 of αβ to 120 of COE and 0.5 of αβ). Increasing the cross exchanger area is worthwhile to reduce steam consumption when the price of steam is high and the annualized capital cost is relatively cheaper.

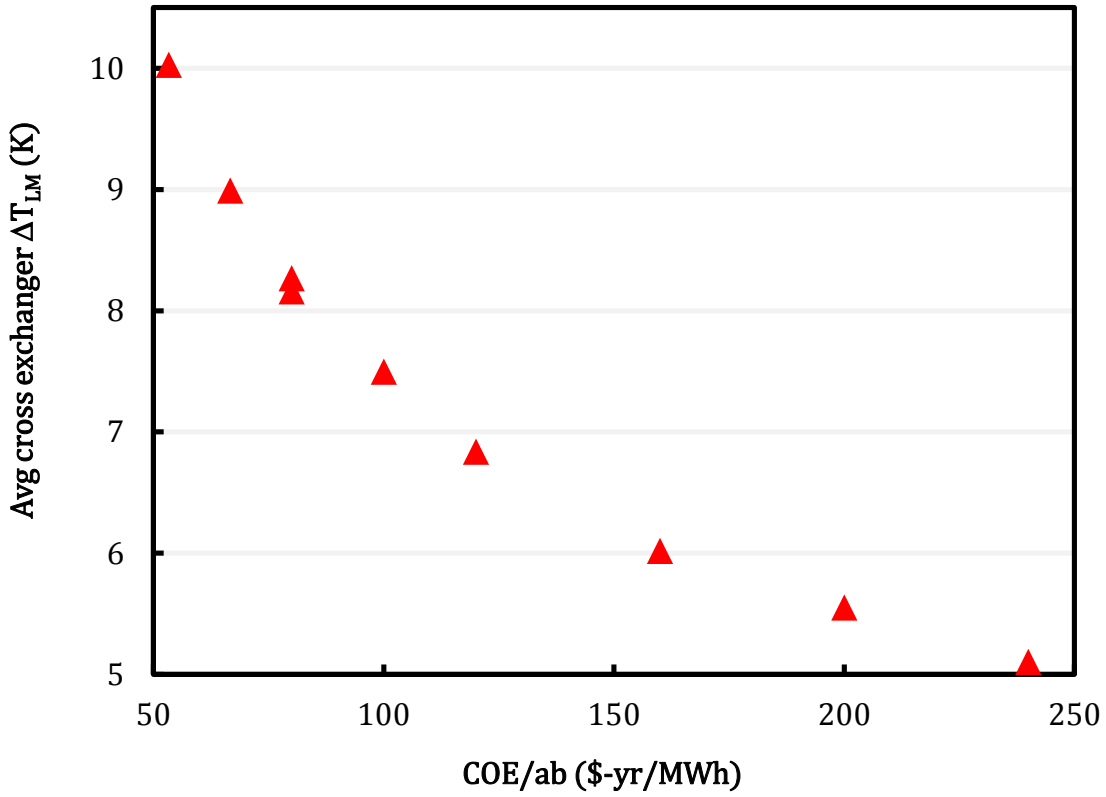

Figure 9.13: Optimum average cross exchanger LMTD with varied COE $80 to 120/MWh and αβ from 0.5 to 1.5.

9.3.5 5 m PZ vs. 8 m PZ

The optimum lean loading will be lower than 0.22 if the absorber CAPEX is included. However, lean loading of 0.22 for 8 m PZ may not be operationally attractive because of the potential precipitation of $PZ \cdot 6H_2O$ solid at upset conditions or during shutdown when the solvent cools below 40 °C. This possibility may require additional capital cost to heat trace lines and provide other means to recover from an upset. 5 m PZ is considered an option to extend the solid solubility window while still providing superior performance due to lower viscosity.

Figure 9.14 shows the transition temperature of precipitation for 5 m and 8 m PZ from prvious experimental measurement (Freeman, 2011; Li, 2015). By assuming the lowest temperature that the process would encounter, the solubility line corresponds to the lower limit of lean loading. The lower limit of lean loading is 0.19 for 5 m and 0.24 for 8 m PZ assuming 25 °C is the cooling water temperature that will be used in the trim cooler, which is the coldest spot in the process for the lean solvent. 5 m PZ also has no rich solubility limit unlike 8 m.

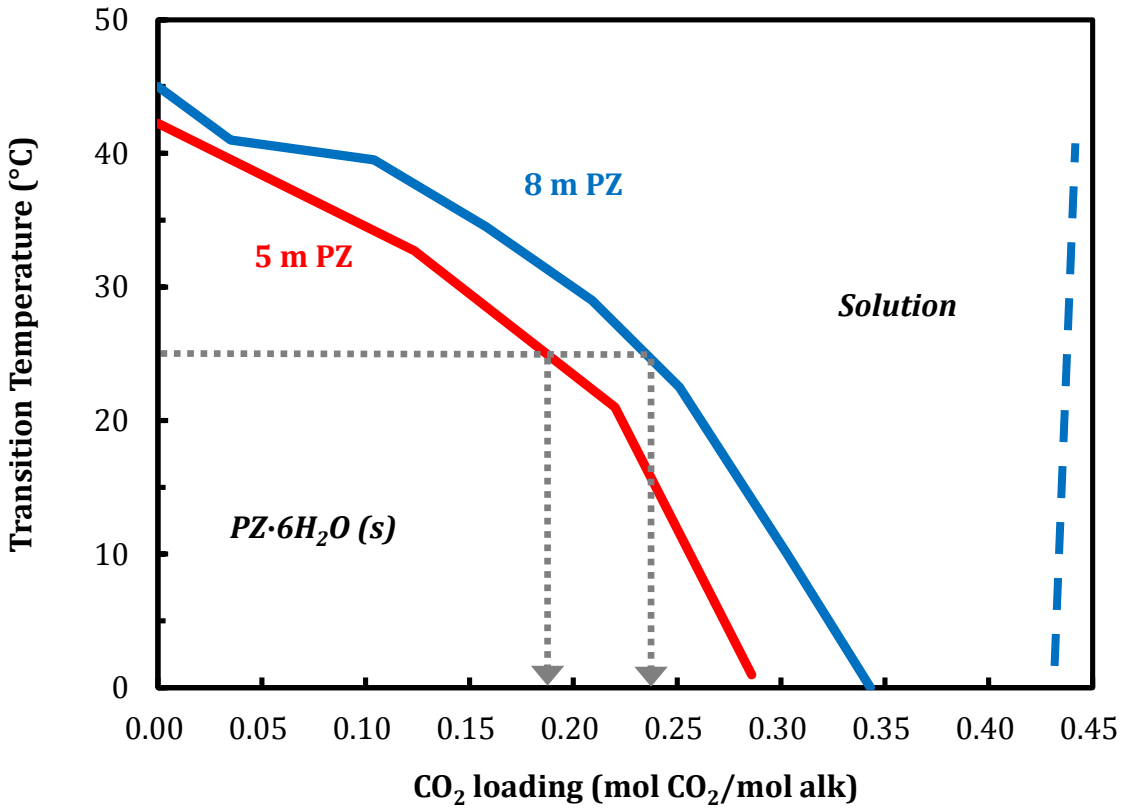

Figure 9.14: Comparison of 5 m and 8m PZ; rich loading: 0.40; stripper T: 150 °C (Freeman, 2011; Li, 2015).

Both 5 and 8 m PZ were tested in the 2015 SRP pilot plant campaign using an intercooled absorber and the AFS. Table 9.5 summarizes the absorber performance.

The comparisons show that at the same solvent to flue gas ratio (L/G) and lean loading 5 m PZ outperformed 8 m with a higher rich loading, which offsets the drawback in capacity due to lower amine concentration. The absorber performance will be taken into account in the economic analysis by assuming a higher rich loading for 5 m PZ. According to the pilot plant results, two sets of comparisons are made: 0.41/0.38 and 0.39/0.36 of rich loading for 5 m/8 m PZ.

Table 9.9: Comparison of absorber performance between 5 m and 8 m PZ in 2015 SRP pilot plant

	Comparison 1		**Comparison 2**	
PZ concentration (m)	5	8	5	8
Absorber L/G (kg/kg)	4.7	5	3.3	3.4
Lean loading (mol CO_2/mol alkalinity)	0.24	0.24	0.24	0.24
Rich loading (mol CO_2/mol alkalinity)	0.37	0.34	0.39	0.36

Figure 9.15 shows the annualized regeneration cost of 5 m and 8 m PZ at two sets of rich loading. 5 m PZ reduces the annualized regeneration cost by 6% compared to 8 m in both comparisons. The savings mainly come from higher rich loading and better heat transfer performance. As discussed in Section 9.3.3, higher rich loading benefits the stripper performance and result in less cold rich bypass required to recover the stripping steam heat. 5 m PZ also reduces the cross exchanger CAPEX by a greater heat transfer coefficient. The viscosity of 5 m PZ is 30–50% that of 8 m, which increases the transfer coefficient by around 40%.

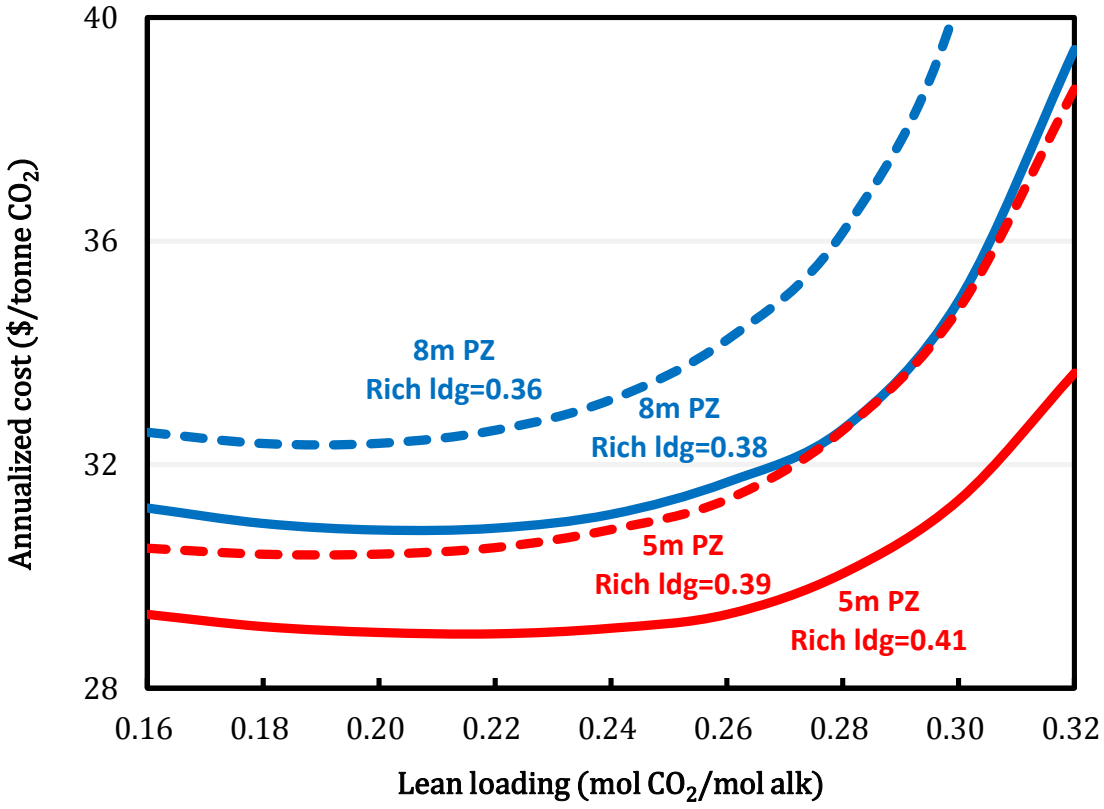

Figure 9.15: Comparing the annualized regeneration cost of 5 m and 8 m PZ.

Table 9.10: Summary of economic analysis for 5 m and 8 m PZ.

	5 m PZ	**8 m PZ**
Lean loading (mol CO_2/mol alkalinity)	0.22	0.22
Rich loading (mol CO_2/mol alkalinity)	0.39	0.36
Solvent rate (kg/s)	2482	2284
Cold rich BPS (%)	8	12
Warm rich BPS (%)	28	31
Cross exchanger U (W/K-m^2)	2358	1615
Avg cross exchanger ΔT_{LM} (K)	6.1	7.7

9.4. ALTERNATIVE SUPERSONIC COMPRESSOR

The Ramgen Company has been developing the Supersonic Shock Wave Compressor with a blade tip not limited by Mach number, so the pressure ratio can be up to 10 per stage (Lawlor et al., 2005). The physical size of the compressor is smaller and only 1–2 stages are required. It has been claimed that the Supersonic Shock Wave Compressor can save 40–50% of capital cost by reducing the physical size of the compressor and provide higher compression efficiency (Lupkes, 2012). Also, the higher discharge temperature makes heat recovery from the intercoolers easier to implement. The design allows the discharge temperature to be up to 260 °C compared to 120–140 °C for a conventional compressor. A single-stage supersonic compressor has been demonstrated with 7.7 pressure ratio, and a commercial size will be tested in the future (Lupkes, 2012).

This section will simulate the compressor with the same configuration as shown in Figure 9.3 except with a higher pressure ratio up to 10 per stage and a higher polytropic efficiency 90% claimed by Ramgen Company. With various inlet pressure, the overall pressure ratio will be distributed evenly to each stage. Table 9.11 shows the design specifications for the supersonic compressor.

Table 9.11: Design specifications of supersonic compressor.

Supersonic compressor	
Maximum pressure ratio/stage	10
Compressor polytropic efficiency (%)	90
Intercooling temperature (°C)	40
Aftercooling temperature (°C)	30
Supercritical pump efficiency (%)	65
Multi-stage compressor outlet P (bar)	76
Final target P (bar)	150
Supersonic compressor integrated with AFS	
Intercooler LMTD (K)	20
Cold rich bypass out T (°C)	150

A greater pressure ratio implies CO_2 will contain more enthalpy after each compressor stage. Recovering the waste heat by a heat integration with the AFS is proposed in this work. As shown in Figure 9.16, the heat in the CO_2 vapor will be used to heat the cold rich solvent bypass from 46 °C up to 150 °C, which is assumed to be limited by thermal degradation. The cold rich bypass rates are adjusted to meet the specified 20 K LMTD of the intercooler.

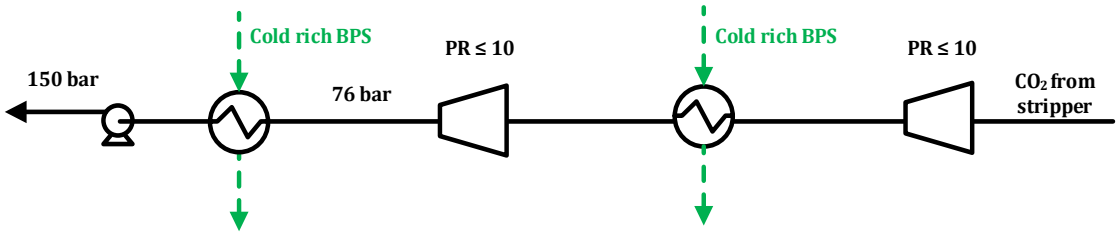

Figure 9.16: Supersonic compressor with heat integration.

Figure 9.17 compares the compression work of the conventional and the supersonic compressors. In the loading range from 0.20 to 0.34 (5–13 bar), only one or two stages are required for the supersonic compressor. A significant increase of compression work around 8 bar is due to the transition from two stages to one stage. The increase in pressure ratio causes the elevated discharge temperature and further departure from isothermal operation. Since the conventional compressor intercools more frequently, the more isothermal compression requires less work. The waste heat from the intercoolers of the supersonic compressor can be recovered by the process itself using the cold rich bypass.

The compression work of the supersonic compressor with heat integration is also presented. The total equivalent work is calculated with and without heat integration, and the difference is considered the reduction of compression work. With heat recovery, the supersonic compressor can have the same energy performance as the conventional compressor. This demonstrates that the supersonic compressor has potential to reduce the overall cost from the net savings of capital and installation costs due to the compact design.

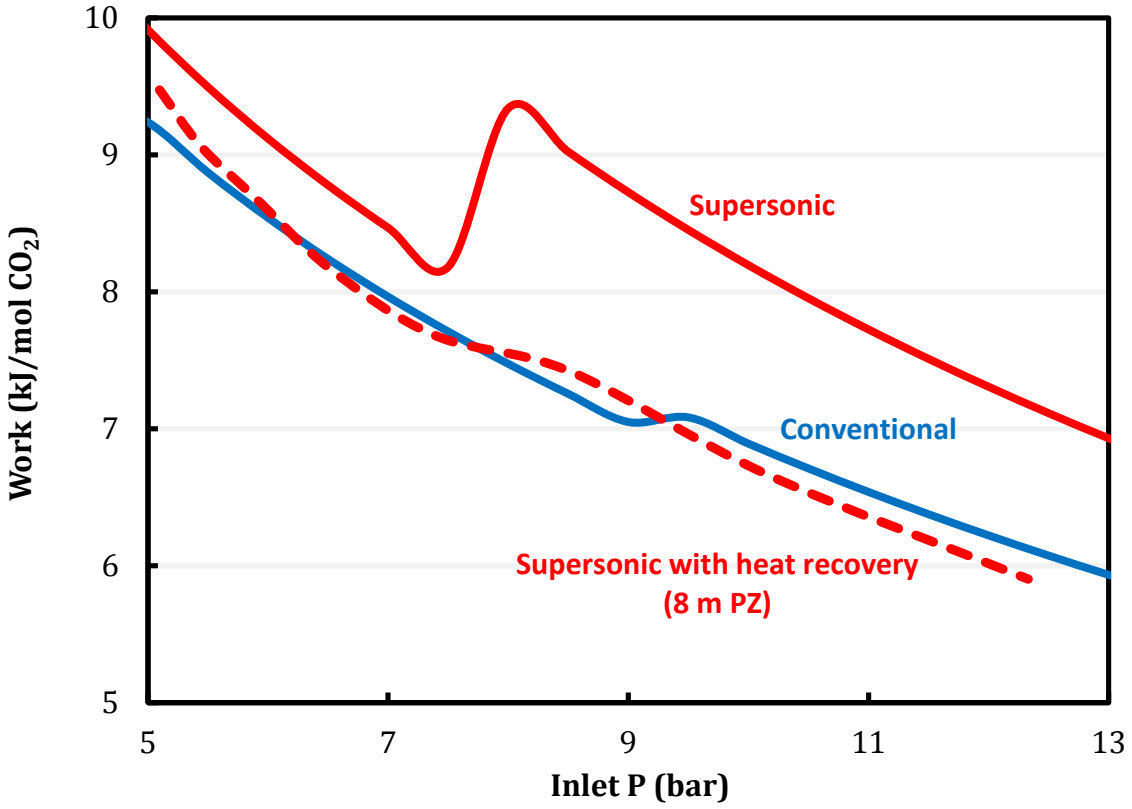

Figure 9.17: Comparison of supersonic and conventional multi-stage compressors.

9.5. CONCLUSIONS

- The annualized regeneration cost is \$33.7–33.9/tonne CO_2 and \$29.4–30.2/tonne CO_2 for the simple stripper and the AFS, respectively with lean loading from 0.16 to 0.0.28 using 8 m PZ.
- The AFS reduces the annualized regeneration cost by 13% and the major savings come from the reduction of the steam cost. The AFS has the same CAPEX as the simple stripper.
- The OPEX accounts for over 70% of the annualized regeneration cost. The compressor and the cross exchanger are the major components of the CAPEX.

- The annualized regeneration cost is flat between lean loadings 0.18 and 0.24 but increases 13% from 0.28 to 0.32 because the reduced solvent capacity increases the sensible heat requirement and the CAPEX of cross exchanger, which is the most sensitive cost when lean loading varies.
- Rich loading that reflects the absorption performance can affect the solvent capacity and the stripper performance, which dominate at higher and lower lean loadings, respectively.
- 5 m PZ not only extends the solid solubility window but also reduces the annualized regeneration cost by 6% when compared to 8 m because of better absorption performance and a higher heat transfer coefficient of the cross exchanger.
- The supersonic compressor with heat integration has the same energy performance as the conventional multi-stage compressor and potentially can reduce the capital cost due to the compact design.

Chapter 10: Conclusions and Recommendations

10.1 SUMMARY

10.1.1 Advanced flash stripper

- The lost work of the condenser and the cross exchanger were identified as the two major sources of lost work for the simple stripper.
- The AFS using cold and warm rich bypasses is proposed to reduce the lost work. The warm rich bypass reduces the work loss associated with condensing water vapor resulting from the stripping steam. The cold rich bypass recovers the rest of the stripping steam heat by providing a low temperature heat sink while avoiding CO_2 re-absorption.
- The rich bypasses also make the cross exchanger more reversible by balancing the flow heat capacity between the rich and lean streams.
- Compared to other alternative strippers that have been proposed to reduce the stripping steam heat, the advanced reboiled/flash stripper provides the best energy performance. It uses 11% less total equivalent work with 8 m PZ and 7% less with 9 m MEA compared to the simple stripper.
- The AFS reduces the reboiler duty by 16.1% and the total equivalent work by 11.2% compared to the simple stripper.
- The AFS reaches a remarkable thermodynamic efficiency at 55–74% over a range of operating lean loading.
- The optimum lean loading that minimizes the total equivalent work is 0.28–0.30 for 8 m PZ and 0.36–0.38 for 9 m MEA at constant rich loading. The energy improvement is more significant at lower lean loading where the stripping steam is excessive.

10.1.2 Demonstration of the AFS

10.1.2.1 Pilot plant test

- 17 runs have process heat duty 2.1–2.5 GJ/tonne CO_2 and 4 runs without adequate rich solvent bypass are 2.5–2.9 GJ/tonne CO_2. The lowest W_{eq} is 32.0 kJ/mol CO_2.
- The AFS shows over 25% heat duty reduction compared to previous SRP campaigns, and over 30% compared to the DOE base case.
- Cold and warm rich solvent bypass were manually controlled to recover the stripping steam heat by maintaining the stripper vapor outlet temperature and the cold rich exchanger vapor outlet temperature. Four runs that did not achieve the temperature target increased the process heat duty by 15%.
- 5 m PZ provides 20% greater number of heat transfer units than 8 m PZ on the cold cross exchanger and results in a lower process heat duty because of lower viscosity.
- The "Independence" model was validated using the pilot plant data and accurately represents the performance of the pilot plant. The modeled lean loading and rich loading show 5.4% and 3.6% average error compared to the density-predicted loading. The modeled and the measured process heat duty has 3% average error.
- The validated model was used to re-optimize the bypass rates. It confirmed that the bypass control strategy used during the test successfully minimized the heat duty.
- Increasing the stripper packing height has a more significant effect at low lean loading. The packing utilization efficiency can reach 88% using 5 m of RSR no. 0.3.
- The irreversibility analysis showed that the thermodynamic efficiency of the SRP pilot plant using the AFS is about 50%. The absorber and the cross exchanger are the two major sources of lost work and can only be addressed by greater absorption rate and solvent capacity, respectively.

10.1.2.2 Economic analysis

- The regeneration and compression costs are \$33.7–37/tonne CO_2 and \$29.4–33.8/tonne CO_2 for the simple stripper and the AFS, respectively with lean loading from 0.16 to 0.32 using 8 m PZ.
- The AFS reduces 13% of the annualized cost from the steam cost with the same CAPEX as the simple stripper.
- The OPEX accounts for over 70% of the regeneration and compression cost. The compressor and the cross exchanger are the major costs of the CAPEX.
- The annualized cost is flat between lean loadings 0.18 and 0.24 but increases 13% from 0.28 to 0.32 because the reduced solvent capacity increases the sensible heat requirement and the CAPEX of cross exchanger, which is the most sensitive cost when lean loading varies.
- Rich loading that reflects the absorption performance can affect the solvent capacity and the stripper performance, which dominate at higher and lower lean loadings, respectively.
- 5 m PZ not only extends the solid solubility window but also reduces the annualized cost by 6% when compared to 8 m because of better absorption performance and a higher heat transfer coefficient of the cross exchanger.
- The supersonic compressor with heat integration has the same energy performance as the conventional multi-stage compressor and potentially can reduce the capital cost due to the compact design.

10.1.3 Effect of solvent properties

- Approximate stripper model (ASM) were developed to predict the energy performance for the simple stripper and the AFS.
- The total equivalent work is sensitive to the predicted heat capacity of solvent especially when the cross exchanger has a large heat transfer unit. Generally the ASM showed a similar trend that was predicted by the rigorous Aspen Plus® model.
- As the rich loading varies from 3 to 7 kPa, a constant optimum ΔLdg was found and the energy savings by the AFS is not affected.
- Using solvents with high heat of absorption can increase the partial pressure of CO_2 and effectively reduce the stripping steam heat and the compression work. Optimum heat of absorption can be found when the energy reductions show diminishing returns and the increase in the pump work is dominant.
- The optimum heat of absorption ranges from 70 to 125 kJ/mol. The simple stripper and the operating conditions at low reboiler temperature and low lean loading will need a higher optimum heat of absorption to boost the partial pressure of CO_2.
- By increasing the heat of absorption, the total equivalent work can be reduced by 10% for the simple stripper and less than 1% for the AFS.
- The AFS always has a lower optimum heat of absorption than the simple stripper since the stripping steam heat is already eliminated by the rich solvent bypasses.
- The AFS is a flexible system that can be applied to a wide range of heat of absorption while still minimizing the energy requirement. Further reduction by increased heat of absorption is marginal.

- Increasing the partial pressure of CO_2 by reboiler temperature will not effectively reduce the total equivalent work. The savings of compression work is almost offset by the increase in the heat duty work.
- Improving the efficiency of the steam turbine and compressor will favor mechanical compression rather than thermal compression, and result in a heat of absorption as low as 70−85 kJ/mol, which is close to that of available solvents.

10.2 RECOMMENDATIONS FOR FUTURE WORK

10.2.1 Model improvement

1. This work concluded that over-stripping lean loading is more cost-efficient. The partial pressure of CO_2 at high temperature and low lean loading predicted by Independence model was extrapolated because of lacking data below 0.25 mol CO_2/mol alkalinity. More CO_2 solubility data at high temperature and over-stripping conditions should be measured and confirmed with model.
2. This work showed that the heat capacity can have significant impact on predicting the sensible heat especially for a cross exchanger with a large number of heat transfer units. The uncertainties of the predicted heat capacity come from the inconsistency of measurement data and a poor fit of the Independence model. These should be improved in the future in order to accurately predict the sensible heat.
3. The diffusion coefficient of amine predicted by Independence is overestimated by about 4 times. It should be fixed otherwise a 0.15 correction for packing area needs to be used.

10.2.2 Heat transfer measurement

1. Most literature that predicted the heat transfer coefficient for plate-and-frame exchanger used water as fluid. Viscous fluid should be considered in the future measurement in order to investigate the viscosity effect.
2. Pilot plant tests showed that the heat transfer coefficient is not sensitive to flow rate when the solvent starts flashes. The nucleate boiling heat transfer is inferred as the dominant mechanism. The operating regime should be confirmed by experiments.

10.2.3 Application of the AFS

1. At over-stripping lean loading, the AFS becomes less energy-efficient due to the excessive stripping steam. The ARS that has an additional hot rich bypass is recommended. The marginal effect of increasing number of bypasses should be investigated in the future.
2. 5 m PZ with lower viscosity was found more cost-efficient than 8 m since better absorber and cross exchanger performance. Other PZ concentrations should be explored in the future.
3. Besides coal-fired power plants, other major emission sources include steel/iron plant, cement plant, and olefin cracking. These CO_2 concentration of these industrial emissions is from 3% to 20%.
    - The performance of AFS should be re-evaluated at various rich loadings that are determined by the absorber performance. The optimum design and operating conditions of the applications should be determined.
    - The solvent performance will differ from applications because of the shifting VLE at various CO_2 concentration range. Solvent selections should be re-evaluated at a wider range of CO_2 concentration.

Appendix A: Theoretical minimum work

- **Enthalpy and entropy balance**

For a steady state flow system:

$$H_{in} - H_{out} + Q + W_s = 0 \tag{A.1}$$

$$S_{in} - S_{out} + \left(\frac{Q_{rev}}{T} + S_{irr}\right) = 0 \tag{A.2}$$

Minimum work occurs when process is reversible:

$$Q = Q_{rev} \tag{A.3}$$

$$S_{irr} = 0 \tag{A.4}$$

$$W_{min} = W_s = \Delta H - Q_{rev} = \Delta H - T\Delta S + TS_{irr} = \Delta G + TS_{irr} \tag{A.5}$$

$$W_{min} = \Delta G \tag{A.6}$$

- **Minimum work for CO_2 regeneration and compression**

The CO_2 regeneration and compression for minimum work calculation is simplified in Figure A.1. The minimum work accounts for compressing CO_2 from the equilibrium partial pressure of CO_2 in the lean/rich solvent to the final pressure 150 bar. The process is assumed isothermal at 40 °C.

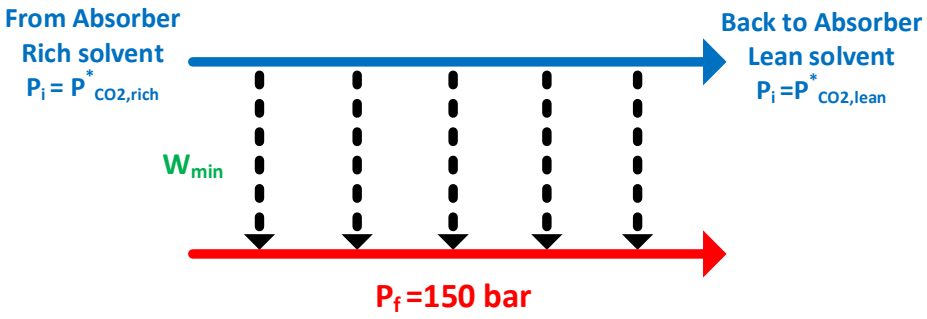

Figure A.1: Minimum work integration for CO_2 regeneration process.

Assuming ideal gas, the minimum work can be calculated by initial pressure and final pressure:

$$W_{min} = \Delta G = RTlnP_f - RTlnP_i = n_{CO2}RTln\frac{P_f}{P_i} \quad \text{(A.7)}$$

Since the partial pressure of CO_2 changers with CO_2 loading in the solvent. The equation is integration from rich to lean.

$$dW_{min} = d(\Delta G) = RTln\frac{P_f}{P_i}dn_{CO_2} \quad \text{(A.8)}$$

$$Total\ W_{min} = \int_{Rich}^{Lean} d(\Delta G) = \int_{Rich}^{Lean} RTln\frac{P_f}{P^*_{CO_2}}dn_{CO_2} \quad \text{(A.9)}$$

$$W_{min} = \frac{\int_{Rich}^{Lean} RTln\frac{P_f}{P^*_{CO2}}dn_{CO_2}}{\int_{Rich}^{Lean} dn_{CO_2}} = \frac{RT\int_{Rich}^{Lean} lnP_f dn_{CO_2}}{\int_{Rich}^{Lean} dn_{CO_2}} - \frac{RT\int_{Rich}^{Lean} lnP^*_{CO2}dn_{CO_2}}{\int_{Rich}^{Lean} dn_{CO_2}} \quad \text{(A.10)}$$

The CO_2 transferred is equal to the change of loading, α

$$dn_{CO2} = d\alpha \quad \text{(A.11)}$$

$$W_{min} = \frac{RT}{\int_{\alpha_{rich}}^{\alpha_{lean}} d\alpha}\left(\int_{\alpha_{rich}}^{\alpha_{lean}} lnP_f d\alpha - \int_{\alpha_{rich}}^{\alpha_{lean}} lnP^*_{CO2}d\alpha\right)$$

$$= \frac{RT}{(\alpha_{lean}-\alpha_{rich})}\left[lnP_f(\alpha_{lean} - \alpha_{rich}) - \int_{\alpha_{rich}}^{\alpha_{lean}} lnP^*_{CO2}d\alpha\right] \quad \text{(A.12)}$$

The equilibrium partial pressure of CO_2 can be expressed by the semi-empirical equation as a function of temperature and loading to get analytical solution.

Appendix B: Tabulated Simulation Data

Table B.1: Simple stripper using 8 m PZ; rich loading: 0.4; cross exchanger ΔT_{LM}: 5 K; 1 m Mellapak 250X packing; correction for interfacial area: 1; reboiler T: 150 °C.

Lean ldg (mol/mol)	0.20	0.22	0.24	0.26	0.28	0.30	0.32	0.34
P (bar)	5.1	5.4	5.9	6.5	7.4	8.6	10.1	12.3
Energy performance (kJ/mol CO_2)								
Q_{reb}	121.1	115.4	111.3	108.1	106.0	105.1	106.4	111.0
W_{heat}	29.28	27.90	26.90	26.14	25.63	25.41	25.73	26.84
W_{pump}	0.3	0.4	0.5	0.6	0.9	1.2	1.9	3.1
W_{comp}	9.2	9.0	8.7	8.3	7.9	7.4	6.8	6.1
W_{eq}	38.8	37.3	36.1	35.1	34.4	34.0	34.4	36.1

Table B.2: Simple stripper using 8 m PZ; rich loading: 0.4; cross exchanger ΔT_{LM}: 5 K; 2 m Mellapak 250X packing; correction for interfacial area: 1; reboiler T: 150 °C.

Lean ldg (mol/mol)	0.20	0.22	0.24	0.26	0.28	0.30	0.32	0.34
P (bar)	5.1	5.4	5.9	6.5	7.4	8.6	10.1	12.3
Energy performance (kJ/mol CO_2)								
Q_{reb}	114.9	112.1	109.7	107.6	106.0	105.1	106.0	110.9
W_{heat}	27.8	27.1	26.5	26.0	25.6	25.4	25.6	26.8
W_{pump}	0.3	0.4	0.5	0.6	0.9	1.2	1.9	3.1
W_{comp}	9.2	9.0	8.7	8.3	7.9	7.4	6.8	6.1
W_{eq}	37.3	36.5	35.7	35.0	34.4	34.0	34.3	36.0

Table B.3: Simple stripper using 8 m PZ; rich loading: 0.4; cross exchanger ΔT_{LM}: 5 K; 5 m Mellapak 250X packing; correction for interfacial area: 1; reboiler T: 150 °C.

Lean ldg (mol/mol)	0.20	0.22	0.24	0.26	0.28	0.30	0.32	0.34
P (bar)	5.1	5.4	5.9	6.5	7.4	8.6	10.1	12.3
Energy performance (kJ/mol CO_2)								
Q_{reb}	113.2	111.4	109.6	107.5	105.8	105.0	106.1	110.9
W_{heat}	27.4	26.9	26.5	25.0	25.6	25.4	25.7	26.8
W_{pump}	0.3	0.4	0.5	0.6	0.9	1.2	1.9	3.1
W_{comp}	9.2	9.0	8.7	8.3	7.9	7.4	6.8	6.1
W_{eq}	36.9	36.3	35.7	34.0	34.4	34.0	34.3	36.0

Table B.4: Cold rich bypass using 8 m PZ; rich loading: 0.4; cross exchanger ΔT_{LM}: 5 K; 2 m Mellapak 250X packing; correction for interfacial area: 1; reboiler T: 150 °C; optimum bypass rate.

Lean ldg (mol/mol)	0.20	0.22	0.24	0.26	0.28	0.30	0.32	0.34
P (bar)	5.1	5.4	5.9	6.5	7.4	8.6	10.1	12.3
Cold BPS (%)	18	14	11	9	7	5	3	2
Energy performance (kJ/mol CO_2)								
Q_{reb}	106.3	102.1	99.0	96.9	95.8	96.0	98.2	104.4
W_{heat}	25.7	24.7	23.9	23.4	23.2	23.2	23.7	25.2
W_{pump}	0.3	0.4	0.5	0.7	0.9	1.2	1.9	3.1
W_{comp}	9.2	9.0	8.7	8.3	7.9	7.4	6.8	6.1
W_{eq}	35.2	34.0	33.1	32.4	31.9	31.8	32.4	34.5

Table B.5: Rich exchanger bypass using 8 m PZ; rich loading: 0.4; cross exchanger ΔT_{LM}: 5 K; 2 m Mellapak 250X packing; correction for interfacial area: 1; reboiler T: 150 °C; optimum bypass rate.

Lean ldg (mol/mol)	0.20	0.22	0.24	0.26	0.28	0.30	0.32	0.34
P (bar)	5.1	5.4	5.9	6.5	7.4	8.6	10.1	12.3
Cold BPS (%)	25	21	17	13	10	7	5	3
Energy performance (kJ/mol CO_2)								
Q_{reb}	100.3	97.9	95.9	94.3	93.5	93.9	96.4	102.8
W_{heat}	24.2	23.7	23.2	22.8	22.6	22.7	23.3	24.8
W_{pump}	0.3	0.4	0.5	0.6	0.9	1.2	1.9	3.1
W_{comp}	9.2	9.0	8.7	8.3	7.9	7.4	6.8	6.1
W_{eq}	33.8	33.0	32.4	31.8	31.4	31.3	32.0	34.1

Table B.6: Interheated stripper using 8 m PZ; rich loading: 0.4; cross exchanger ΔT_{LM}: 5 K; 2 m Mellapak 250X packing; correction for interfacial area: 1; reboiler T: 150 °C.

Lean ldg (mol/mol)	0.20	0.22	0.24	0.26	0.28	0.30	0.32	0.34
P (bar)	5.1	5.4	5.9	6.5	7.4	8.6	10.1	12.3
Energy performance (kJ/mol CO_2)								
Q_{reb}	100.7	97.6	95.5	94.2	93.9	95.0	98.2	105.5
W_{heat}	24.3	23.6	23.1	22.8	22.7	23.0	23.7	25.5
W_{pump}	0.3	0.4	0.5	0.7	0.9	1.2	1.9	3.1
W_{comp}	9.2	9.0	8.7	8.3	7.9	7.4	6.8	6.1
W_{eq}	33.9	33.0	32.3	31.7	31.5	31.6	32.4	34.7

Table B.7: Lean vapor compression using 8 m PZ; rich loading: 0.4; cross exchanger ΔT_{LM}: 5 K; 2 m Mellapak 250X packing; correction for interfacial area: 1; reboiler T: 150 °C; optimum pressure ratio.

Lean ldg (mol/mol)	0.20	0.22	0.24	0.26	0.28	0.30	0.32	0.34
Stripper P (bar)	5.5	6.1	6.9	8.0	9.4	11.0	12.9	14.6
Flash P (bar)	3.2	3.6	4.1	4.7	5.5	6.9	8.6	11.2
Energy performance (kJ/mol CO_2)								
Q_{reb}	101.7	99.8	98.2	96.9	96.2	97.5	100.4	107.9
W_{heat}	24.6	24.1	23.7	23.4	23.3	23.6	24.3	26.1
W_{pump}	0.3	0.4	0.5	0.7	0.9	1.2	1.9	3.1
W_{comp}	8.9	8.6	8.1	7.6	7.0	6.5	6.0	5.5
$W_{LV\ comp}$	1.5	1.5	1.5	1.5	1.4	1.1	0.9	0.4
W_{eq}	35.4	34.6	33.9	33.2	32.6	32.5	33.0	35.1

Table B.8: Lean vapor compression using 8 m PZ; rich loading: 0.4; cross exchanger ΔT_{LM}: 5 K; 5 m packing; correction for interfacial area: 1; reboiler T: 150 °C; optimum pressure ratio.

Lean ldg (mol/mol)	0.20	0.22	0.24	0.26	0.28	0.30	0.32	0.34
Stripper P (bar)	5.5	6.1	6.9	8.0	9.4	11.0	12.4	13.8
Flash P (bar)	3.2	3.6	4.1	4.7	5.5	6.9	8.8	11.5
Energy performance (kJ/mol CO_2)								
Q_{reb}	100.5	99.3	98.0	96.9	96.2	97.5	101.4	108.9
W_{heat}	24.3	24.0	23.7	23.4	23.3	23.6	24.5	26.3
W_{pump}	0.4	0.5	0.6	0.8	1.2	1.6	2.3	3.5
W_{comp}	8.9	8.6	8.1	7.6	7.0	6.5	6.1	5.7
$W_{LV\ comp}$	1.5	1.5	1.5	1.5	1.4	1.1	0.6	0.2
W_{eq}	35.1	34.6	33.9	33.3	32.9	32.9	33.6	35.8

Table B.9: AFS using 8 m PZ; rich loading: 0.4; cross exchanger ΔT_{LM}: 5 K; 2 m Mellapak 250X packing; correction for interfacial area: 1; reboiler T: 150 °C; optimum bypass rates.

Lean ldg (mol/mol)	0.20	0.22	0.24	0.26	0.28	0.30	0.32	0.34
P (bar)	5.1	5.4	5.9	6.5	7.4	8.6	10.1	12.3
Cold BPS (%)	14	12	10	8	6	5	4	2
Warm BPS (%)	46	41	34	27	20	14	10	5
Energy performance (kJ/mol CO_2)								
Q_{reb}	93.8	91.6	90.1	89.3	89.4	90.7	94.1	101.2
W_{heat}	22.7	22.1	21.8	21.6	21.6	21.9	22.8	24.5
W_{pump}	0.3	0.4	0.5	0.7	0.9	1.2	1.9	3.1
W_{comp}	9.2	9.0	8.7	8.3	7.9	7.4	6.8	6.1
W_{eq}	32.2	31.5	31.0	30.6	30.4	30.6	31.4	33.7

Table B.10: AFS using 8 m PZ; rich loading: 0.4; cross exchanger ΔT_{LM}: 5 K; 5 m Mellapak 250X packing; correction for interfacial area: 1; reboiler T: 150 °C; optimum bypass rates.

Lean ldg (mol/mol)	0.20	0.22	0.24	0.26	0.28	0.30	0.32	0.34
P (bar)	5.1	5.4	5.9	6.5	7.4	8.6	10.1	12.3
Cold BPS (%)	11	10	9	7	6	4	3	2
Warm BPS (%)	44	36	28	22	16	12	8	6
Energy performance (kJ/mol CO_2)								
Q_{reb}	90.1	89.0	88.4	88.1	88.6	90.3	93.8	101.3
W_{heat}	21.8	21.5	21.4	21.3	21.4	21.8	22.7	24.5
W_{pump}	0.3	0.4	0.5	0.7	0.9	1.2	1.9	3.1
W_{comp}	9.2	9.0	8.7	8.3	7.9	7.4	6.8	6.1
W_{eq}	31.3	30.9	30.5	30.3	30.2	30.5	31.4	33.7

Table B.11: ARS using 8 m PZ; rich loading: 0.4; cross exchanger ΔT_{LM}: 5 K; 2 m Mellapak 250X packing; correction for interfacial area: 1; reboiler T: 150 °C; optimum bypass rates.

Lean ldg (mol/mol)	0.20	0.22	0.24	0.26	0.28	0.30	0.32	0.34
P (bar)	5.1	5.4	5.9	6.5	7.4	8.6	10.1	12.3
Cold BPS (%)	14	11	9	8	6	5	4	2
Warm BPS (%)	41	35	28	21	15	10	5	2
Energy performance (kJ/mol CO_2)								
Q_{reb}	92.2	90.4	89.2	88.6	88.9	90.3	93.8	100.9
W_{heat}	22.3	21.8	21.6	21.4	21.5	21.8	22.7	24.4
W_{pump}	0.3	0.4	0.5	0.7	0.9	1.2	1.9	3.1
W_{comp}	9.2	9.0	8.7	8.3	7.9	7.4	6.8	6.1
W_{eq}	31.8	31.2	30.7	30.4	30.3	30.4	31.3	33.6

Table B.12: Simple stripper using 9 m MEA; rich loading: 0.5; cross exchanger ΔT_{LM}: 5 K; 2 m Mellapak 250X packing; correction for interfacial area: 1; reboiler T: 120 °C.

Lean ldg (mol/mol)	0.30	0.32	0.34	0.36	0.38	0.40	0.42	0.44
P (bar)	2.3	2.4	2.6	2.8	3.0	3.3	3.8	4.5
Energy performance (kJ/mol CO_2)								
Q_{reb}	147.9	146.3	145.1	144.4	144.4	145.6	148.8	157.5
W_{heat}	28.4	28.1	27.9	27.7	27.7	28.0	28.6	30.3
W_{pump}	0.2	0.2	0.3	0.3	0.4	0.6	0.9	1.5
W_{comp}	11.9	11.8	11.6	11.3	11.0	10.7	10.2	9.6
W_{eq}	40.5	40.1	39.7	39.4	39.2	39.2	39.7	41.4

Table B.13: Rich exchanger bypass using 9 m MEA; rich loading: 0.5; cross exchanger ΔT_{LM}: 5 K; 2 m Mellapak 250X packing; correction for interfacial area: 1; reboiler T: 120 °C; optimum bypass rate.

Lean ldg (mol/mol)	0.30	0.32	0.34	0.36	0.38	0.40	0.42	0.44
P (bar)	2.3	2.4	2.6	2.8	3.0	3.3	3.8	4.5
Cold BPS (%)	22	19	16	13	10	8	5	3
Energy performance (kJ/mol CO_2)								
Q_{reb}	139.7	137.9	136.6	135.7	135.7	137.1	141.1	151.0
W_{heat}	26.8	26.5	26.2	26.1	26.1	26.4	27.1	29.0
W_{pump}	0.2	0.2	0.3	0.3	0.4	0.6	0.9	1.5
W_{comp}	11.9	11.8	11.6	11.3	11.0	10.7	10.2	9.6
W_{eq}	38.9	38.5	38.1	37.7	37.5	37.6	38.2	40.2

Table B.14: Interheated stripper using 9 m MEA; rich loading: 0.5; cross exchanger ΔT_{LM}: 5 K; 2 m Mellapak 250X packing; correction for interfacial area: 1; reboiler T: 120 °C.

Lean ldg (mol/mol)	0.30	0.32	0.34	0.36	0.38	0.40	0.42	0.44
P (bar)	2.3	2.4	2.6	2.8	3.0	3.3	3.8	4.5
Energy performance (kJ/mol CO_2)								
Q_{reb}	136.2	134.1	133.0	133.0	133.9	136.6	142.6	152.5
W_{heat}	26.2	25.8	25.6	25.6	25.7	26.2	27.4	29.3
W_{pump}	0.2	0.2	0.3	0.3	0.4	0.6	0.9	1.5
W_{comp}	11.9	11.8	11.6	11.3	11.0	10.7	10.2	9.6
W_{eq}	38.3	37.8	37.4	37.2	37.2	37.5	38.5	40.5

Table B.15: AFS using 9 m MEA; rich loading: 0.5; cross exchanger ΔT_{LM}: 5 K; 2 m Mellapak 250X packing; correction for interfacial area: 1; reboiler T: 120 °C; optimum bypass rates.

Lean ldg (mol/mol)	0.30	0.32	0.34	0.36	0.38	0.40	0.42	0.44
P (bar)	2.3	2.4	2.6	2.8	3.0	3.3	3.8	4.5
Cold BPS (%)	13	11	10	8	7	6	4	3
Warm BPS (%)	52	46	39	31	24	16	10	5
Energy performance (kJ/mol CO_2)								
Q_{reb}	131.4	129.9	129.3	129.4	130.6	133.2	138.3	149.1
W_{heat}	25.2	25.0	24.8	24.9	25.1	25.6	26.6	28.6
W_{pump}	0.2	0.2	0.3	0.3	0.4	0.6	0.9	1.5
W_{comp}	11.9	11.8	11.6	11.3	11.0	10.7	10.2	9.6
W_{eq}	37.3	36.9	36.7	36.5	36.6	36.9	37.7	39.8

Table B.16: ARS using 9 m MEA; rich loading: 0.5; cross exchanger ΔT_{LM}: 5 K; 2 m Mellapak 250X packing; correction for interfacial area: 1; reboiler T: 120 °C; optimum bypass rates.

Lean ldg (mol/mol)	0.30	0.32	0.34	0.36	0.38	0.40	0.42	0.44
P (bar)	2.3	2.4	2.6	2.8	3.0	3.3	3.8	4.5
Cold BPS (%)	13	11	10	8	7	6	4	3
Warm BPS (%)	46	39	32	24	16	9	4	1
Energy performance (kJ/mol CO_2)								
Q_{reb}	130.0	128.8	128.4	128.7	129.9	132.6	137.7	148.4
W_{heat}	25.0	24.7	24.7	24.7	25.0	25.5	26.5	28.5
W_{pump}	0.2	0.2	0.3	0.3	0.4	0.6	0.9	1.5
W_{comp}	11.9	11.8	11.6	11.3	11.0	10.7	10.2	9.6
W_{eq}	37.1	36.7	36.5	36.4	36.4	36.8	37.6	39.7

Appendix C: Approximate Stripper Model Equations

C.1 SIMPLE STRIPPER

- Equilibrium partial pressure of CO_2 For generic solvent

$$P^*_{CO_2}(T,\alpha) = exp\left[lnP^*_{CO_2,r}(T_r,\alpha_r) + \int_{\alpha_r}^{\alpha} k(T_r,\alpha)d\alpha + \int_{T_r}^{T} -\frac{\Delta H_{abs}(\alpha)}{R} d\left(\frac{1}{T}\right)\right] \quad \text{(C.1)}$$

- Stripper pressure calculation

$$P_{strp} = P^*_{CO_2}(T_{reb},\alpha_{lean}) + P^{sat}_{H_2O}(T_{reb})x_{H_2O,lean} \quad \text{(C.2)}$$

- Overall mass balance

$$m_{rich} = m_{lean} + m_{strpV} + m_{richhV} \quad \text{(C.3)}$$

$$m_{i,rich} = m_{i,lean} + m_{i,strpV} + m_{i,richhV} \qquad i = H_2O, CO_2, am \quad \text{(C.4)}$$

$$m_j = \sum_i m_{i,j} \qquad i = H_2O, CO_2, am \quad j = any\ stream \quad \text{(C.5)}$$

$$\sum_i y_{i,j} = 1 \qquad i = H_2O, CO_2, am \quad j = any\ vapor\ stream \quad \text{(C.6)}$$

$$\sum_i x_{i,j} = 1 \qquad i = H_2O, CO_2, am \quad j = any\ liquid\ stream \quad \text{(C.7)}$$

$$m_{am,j} = y_{i,j} = 0 \qquad j = any\ vapor\ stream \quad \text{(C.8)}$$

- Warm rich solvent flashing

$$P^*_{CO_2}(T_{richw},\alpha_{rich}) + P^{sat}_{H_2O}(T_{richw})x_{H_2O,rich} = P_{strp} \quad \text{(C.9)}$$

- Hot rich solvent flashing mass balance

$$m_{rich} = m_{richhV} + m_{richhL} \quad \text{(C.10)}$$

$$m_{i,rich} = m_{i,richhV} + m_{i,richhL} \qquad i = H_2O, CO_2, am \quad \text{(C.11)}$$

$$P^*_{CO_2}(T_{richh},\alpha_{richh}) + P^{sat}_{H_2O}(T_{richh})x_{H_2O,richhL} = P_{strp} \quad \text{(C.12)}$$

- Stripper mass balance

$$m_{i,strpL} = m_{i,richhL} \qquad i = H_2O, CO_2, am \quad \text{(C.13)}$$

$$m_{strptopL} + m_{strpbotV} = m_{strpbotL} + m_{strptopV} \quad \text{(C.14)}$$

$$m_{i,strptopL} + m_{i,strpbotV} = m_{i,strpbotL} + m_{i,strptopV} \quad \text{(C.15)}$$

- Stripper top liquid flashing

$$\alpha_{strptopL} = \alpha_{richh} \tag{C.16}$$

$$T_{strptopL} = T_{richh} \tag{C.17}$$

$$(T_{strptopL}, \alpha_{strptopL}) + P^{sat}_{H_2O}(T_{strptopL}) x_{H_2O,strptopL} = P_{strp} \tag{C.18}$$

$$y^{*}_{CO_2,strptopL} = \frac{P^{*}_{CO_2}(T_{strptopL}, \alpha_{strptopL})}{P_{strp}} \tag{C.19}$$

$$y^{*}_{H_2O,strptopL} = \frac{P^{sat}_{H_2O}(T_{strptopL}) x_{H_2O,strptopL}}{P_{strp}} \tag{C.20}$$

- Stripper bottom liquid flashing

$$P^{*}_{CO_2}(T_{strpbotL}, \alpha_{strpbotL}) + P^{sat}_{H_2O}(T_{strpbotL}) x_{H_2O,strpbotL} = P_{strp} \tag{C.21}$$

$$y^{*}_{CO_2,strpbotL} = \frac{P^{*}_{CO_2}(T_{strpbotL}, \alpha_{strptbotL})}{P_{strp}} \tag{C.22}$$

$$y^{*}_{H_2O,strpbotL} = \frac{P^{sat}_{H_2O}(T_{strpbotL}) x_{H_2O,strpbotL}}{P_{strp}} \tag{C.23}$$

- Stripper reboiler flashing

$$T_{strpbotV} = T_{reb} \tag{C.24}$$

$$y_{CO_2,strpbotV} = \frac{P^{*}_{CO_2}(T_{reb}, \alpha_{lean})}{P_{strp}} \tag{C.25}$$

$$y_{H_2O,strpbotV} = \frac{P^{sat}_{H_2O}(T_{reb}) x_{H_2O,lean}}{P_{strp}} \tag{C.26}$$

- Enthalpy balance around cross exchanger

$$\dot{H}_{richc}(T_{richc}) - \dot{H}_{richw}(T_{richw}) = \dot{H}_{leanc}(T_{leanc}) - \dot{H}_{leanw}(T_{leanw}) \tag{C.27}$$

$$\dot{H}_{richw}(T_{richw}) - \dot{H}_{richh}(T_{richh}) = \dot{H}_{leanw}(T_{leanw}) - \dot{H}_{leanh}(T_{leanh}) \tag{C.28}$$

- Enthalpy balance around stripper

$$\dot{H}_{strptopL}(T_{strptopL}) - \dot{H}_{strpbotL}(T_{strpbotL}) = \dot{H}_{strptopV}(T_{strptopV}) - \dot{H}_{strpbotV}(T_{strpbotV}) \tag{C.29}$$

- Cross LMTD calculation

$$Q_{crossX,1} = \dot{H}_{leanw} - \dot{H}_{leanc} \tag{C.30}$$

$$Q_{crossX,2} = \dot{H}_{leanh} - \dot{H}_{leanw} \tag{C.31}$$

$$\Delta T_{LM,crossX,1} = \frac{(T_{richc} - T_{leanc}) - (T_{richw} - T_{leanw})}{ln\left[\frac{(T_{richc} - T_{leanc})}{(T_{richw} - T_{leanw})}\right]} \tag{C.32}$$

$$\Delta T_{LM,crossX,2} = \frac{(T_{richh} - T_{leanh}) - (T_{richw} - T_{leanw})}{ln\left[\frac{(T_{richh} - T_{leanh})}{(T_{richw} - T_{leanw})}\right]} \tag{C.33}$$

$$\Delta T_{LM,crossX,avg} = \frac{Q_{crossX,1} + Q_{crossX,2}}{\frac{Q_{crossX,1}}{\Delta T_{LM,crossX,1}} + \frac{Q_{crossX,2}}{\Delta T_{LM,CrossX,2}}} \tag{C.34}$$

- Stripper temperature and concentration driving force

$$\Delta T_{strptop} = T_{strptopV} - T_{strptopL} \tag{C.35}$$

$$\Delta T_{strpbot} = T_{strpbotV} - T_{strpbotL} \tag{C.36}$$

$$\Delta y_{strptop} = y_{i,strptopV} - y^{*}_{i,strptopL} \tag{C.37}$$

$$\Delta y_{strpbot} = y_{i,strpbotV} - y^{*}_{i,strpbotL} \tag{C.38}$$

$$\Delta T_{LM,strp} = \frac{\Delta T_{strptop} - \Delta T_{strpbot}}{ln\left(\frac{\Delta T_{strptop}}{\Delta T_{strpbot}}\right)} \tag{C.39}$$

$$\Delta y_{LM,strp} = \frac{\Delta y_{strptop} - \Delta y_{strpbot}}{ln\left(\frac{\Delta y_{strptop}}{\Delta y_{strpbot}}\right)} \tag{C.40}$$

- Overall enthalpy balance

$$\dot{Q}_{reb} = \dot{H}_{leanc}(T_{leanc}) - \dot{H}_{rich}(T_{richc}) + \dot{H}_{strpV}(T_{strpV}) \tag{C.41}$$

C.2 ADVANCED FLASH STRIPPER

- Equilibrium partial pressure of CO_2 For generic solvent

$$P^*_{CO_2}(T,\alpha) = exp\left[lnP^*_{CO_2,r}(T_r,\alpha_r) + \int_{\alpha_r}^{\alpha} k(T_r,\alpha)d\alpha + \int_{T_r}^{T} -\frac{\Delta H_{abs}(\alpha)}{R} d\left(\frac{1}{T}\right)\right] \quad \text{(C.42)}$$

- Stripper pressure calculation

$$P_{strp} = P^*_{CO_2}(T_{reb},\alpha_{lean}) + P^{sat}_{H_2O}(T_{reb})x_{H_2O,lean} \quad \text{(C.43)}$$

- Overall mass balance

$$m_{rich} = m_{lean} + m_{strpV} \quad \text{(C.44)}$$

$$m_{i,rich} = m_{i,lean} + m_{i,strpV} + m_{i,richhV} \qquad i = H_2O, CO_2, am \quad \text{(C.45)}$$

$$m_j = \sum_i m_{i,j} \qquad i = H_2O, CO_2, am \quad j = any\ stream \quad \text{(C.46)}$$

$$\sum_i y_{i,j} = 1 \qquad i = H_2O, CO_2, am \quad j = any\ vapor\ stream \quad \text{(C.47)}$$

$$\sum_i x_{i,j} = 1 \qquad i = H_2O, CO_2, am \quad j = any\ liquid\ stream \quad \text{(C.48)}$$

$$m_{am,j} = y_{i,j} = 0 \qquad j = any\ vapor\ stream \quad \text{(C.49)}$$

- Rich solvent bypass mass balance

$$m_{rich} = m_{richc} + m_{cbps} \quad \text{(C.50)}$$

$$m_{richc} = m_{richw} + m_{wbps} \quad \text{(C.51)}$$

- Warm rich solvent flashing

$$P^*_{CO_2}(T_{richw},\alpha_{rich}) + P^{sat}_{H_2O}(T_{richw})x_{H_2O,rich} = P_{strp} \quad \text{(C.52)}$$

- Hot rich solvent flashing mass balance

$$m_{richw} = m_{richhV} + m_{richhL} \quad \text{(C.53)}$$

$$m_{i,richw} = m_{i,richhV} + m_{i,richhL} \qquad i = H_2O, CO_2, am \quad \text{(C.54)}$$

$$P^*_{CO_2}(T_{richh},\alpha_{richh}) + P^{sat}_{H_2O}(T_{richh})x_{H_2O,richhL} = P_{strp} \quad \text{(C.55)}$$

- Stripper mass balance

$$m_{i,strpL} = m_{i,wbps} \qquad i = H_2O, CO_2, am \quad \text{(C.56)}$$

$$m_{strptopL} + m_{strpbotV} = m_{strpbotL} + m_{strptopV} \quad \text{(C.57)}$$

$$m_{i,strptopL} + m_{i,strpbotV} = m_{i,strpbotL} + m_{i,strptopV} \quad \text{(C.58)}$$

- Cold rich exchanger mass balance

$$m_{strpV} = m_{crxV} + m_{crxL} \quad \text{(C.59)}$$

$$m_{i,strpV} = m_{i,crxV} + m_{i,crxL} \qquad i = H_2O, CO_2, am \quad \text{(C.60)}$$

- Stripper top liquid flashing

$$\alpha_{strptopL} = \alpha_{rich} \quad \text{(C.61)}$$

$$T_{strptopL} = T_{richw} \quad \text{(C.62)}$$

$$(T_{strptopL}, \alpha_{strptopL}) + P^{sat}_{H_2O}(T_{strptopL}) x_{H_2O,strptopL} = P_{strp} \quad \text{(C.63)}$$

$$y^*_{CO_2,strptopL} = \frac{P^*_{CO_2}(T_{strptopL}, \alpha_{strptopL})}{P_{strp}} \quad \text{(C.64)}$$

$$y^*_{H_2O,strptopL} = \frac{P^{sat}_{H_2O}(T_{strptopL}) x_{H_2O,strptopL}}{P_{strp}} \quad \text{(C.65)}$$

- Stripper bottom liquid flashing

$$P^*_{CO_2}\left(T_{strpbotL}, \alpha_{strpbotL}\right) + P^{sat}_{H_2O}\left(T_{strpbotL}\right) x_{H_2O,strpbotL} = P_{strp} \quad \text{(C.66)}$$

$$y^*_{CO_2,strpbotL} = \frac{P^*_{CO_2}(T_{strpbotL}, \alpha_{strptbotL})}{P_{strp}} \quad \text{(C.67)}$$

$$y^*_{H_2O,strpbotL} = \frac{P^{sat}_{H_2O}(T_{strpbotL}) x_{H_2O,strpbotL}}{P_{strp}} \quad \text{(C.68)}$$

- Stripper sump flashing

$$T_{strpbotV} = T_{reb} \quad \text{(C.69)}$$

$$y_{CO_2,strpbotV} = \frac{P^*_{CO_2}(T_{reb}, \alpha_{lean})}{P_{strp}} \quad \text{(C.70)}$$

$$y_{H_2O,strpbotV} = \frac{P^{sat}_{H_2O}(T_{reb}) x_{H_2O,lean}}{P_{strp}} \quad \text{(C.71)}$$

- Cold rich exchanger flashing

$$T_{cbps} = T_{richc} \quad \text{(C.72)}$$

$$P_{H_2O}^{sat}(T_{crx}) = P_{strp} \quad \text{(C.73)}$$

- Enthalpy balance around cross exchangers

$$\dot{H}_{richc}(T_{richc}) - \dot{H}_{richw}(T_{richw}) = \dot{H}_{leanc}(T_{leanc}) - \dot{H}_{leanw}(T_{leanw}) \quad \text{(C.74)}$$

$$\dot{H}_{richw}(T_{richw}) - \dot{H}_{richh}(T_{richh}) = \dot{H}_{leanw}(T_{leanw}) - \dot{H}_{leanh}(T_{leanh}) \quad \text{(C.75)}$$

- Enthalpy balance around stripper

$$\dot{H}_{strptopL}(T_{strptopL}) - \dot{H}_{strpbotL}(T_{strpbotL}) = \dot{H}_{strptopV}(T_{strptopV}) - \dot{H}_{strpbotV}(T_{strpbotV}) \quad \text{(C.76)}$$

- Enthalpy balance around cold rich exchanger

$$\dot{H}_{strpV}(T_{strptopV}) - \dot{H}_{crxV}(T_{crx}) - \dot{H}_{crxL}(T_{crx}) = \dot{H}_{cbps}(T_{cbps}) - \dot{H}_{cbpsout}(T_{cbpsout}) \quad \text{(C.77)}$$

- Cross LMTD calculation

$$Q_{crossX,1} = \dot{H}_{leanw} - \dot{H}_{leanc} \quad \text{(C.78)}$$

$$Q_{crossX,2} = \dot{H}_{leanh} - \dot{H}_{leanw} \quad \text{(C.79)}$$

$$\Delta T_{LM,crossX,1} = \frac{(T_{richc} - T_{leanc}) - (T_{richw} - T_{leanw})}{ln\left[\frac{(T_{richc} - T_{leanc})}{(T_{richw} - T_{leanw})}\right]} \quad \text{(C.80)}$$

$$\Delta T_{LM,crossX,2} = \frac{(T_{richh} - T_{leanh}) - (T_{richw} - T_{leanw})}{ln\left[\frac{(T_{richh} - T_{leanh})}{(T_{richw} - T_{leanw})}\right]} \quad \text{(C.81)}$$

$$\Delta T_{LM,crossX,avg} = \frac{Q_{crossX,1} + Q_{crossX,2}}{\frac{Q_{crossX,1}}{\Delta T_{LM,crossX,1}} + \frac{Q_{crossX,2}}{\Delta T_{LM,CrossX,2}}} \quad \text{(C.82)}$$

- Cold rich exchanger LMTD

$$Q_{crx} = \dot{H}_{cbpsout} - \dot{H}_{cbps} \quad \text{(C.83)}$$

$$\Delta T_{LM,crx} = \frac{(T_{cbps} - T_{crx}) - (T_{cbpsout} - T_{strpV})}{ln\left[\frac{(T_{cbps} - T_{crx})}{(T_{cbpsout} - T_{strpV})}\right]} \quad \text{(C.84)}$$

- Stripper temperature and concentration driving force

$$\Delta T_{strptop} = T_{strptopV} - T_{strptopL} \quad \text{(C.85)}$$

$$\Delta T_{strpbot} = T_{strpbotV} - T_{strpbotL} \quad \text{(C.86)}$$

$$\Delta y_{strptop} = y_{i,strptopV} - y^{*}_{i,strptopL} \quad \text{(C.87)}$$

$$\Delta y_{strpbot} = y_{i,strpbotV} - y^{*}_{i,strpbotL} \quad \text{(C.88)}$$

$$\Delta T_{LM,strp} = \frac{\Delta T_{strptop} - \Delta T_{strpbot}}{ln\left(\frac{\Delta T_{strptop}}{\Delta T_{strpbot}}\right)} \quad \text{(C.89)}$$

$$\Delta y_{LM,strp} = \frac{\Delta y_{strptop} - \Delta y_{strpbot}}{ln\left(\frac{\Delta y_{strptop}}{\Delta y_{strpbot}}\right)} \quad \text{(C.90)}$$

- Overall enthalpy balance

$$\dot{Q}_{reb} = \dot{H}_{leanc}(T_{leanc}) - \dot{H}_{rich}(T_{richc}) + \dot{H}_{crxV}(T_{crx}) + \dot{H}_{crxL}(T_{crx}) \quad \text{(C.91)}$$

NOMENCLATURE

$\dot{H}_j$: enthalpy of stream *j*

m_j: total mass flow rate of stream *j*

$m_{i,j}$: mass flow rate of component *i* in stream *j*

P_{strp}: stripper pressure

$P_{i,j}$: partial pressure of component *i* in vapor stream *j*

$P_{i,j}^{*}$: equilibrium partial pressure of component *i* in liquid stream *j*

$P_{H_2O}^{sat}(T)$: saturation pressure of water at temperature T

T_j: temperature of stream *j*

$x_{i,j}$: mole fraction of component *i* in liquid stream *j*

$y_{i,j}$: mole fraction of component *i* in vapor stream *j*

Greek letter:

α_j: CO_2 loading of stream *j*

$\Delta H_{abs}(\alpha)$: heat of absorption at CO_2 loading α

ΔT: temperature approach

ΔT_{LM}: log mean temperature difference

Δy: concentration difference between y and y*

Stream name j:

cbps: cold rich bypass

cbpsout: cold rich bypass at cold rich exchanger outlet

crxL: liquid phase at cold rich exchanger out

crxV: vapor phase at cold rich exchanger out

lean: lean solvent

leanc: cold lean solvent

leanh: hot lean solvent

leanw: warm lean solvent

rich: rich solvent

richc: cold rich solvent

richh: hot rich solvent

richhV: vapor in hot rich solvent

richhL: liquid in hot rich solvent

richw: warm rich solvent

strpbotL: liquid at bottom of stripper

strpbotV: vapor at bottom of stripper

strptopL: liquid at top of stripper

strptopV: vapor at top of stripper

strpV: total stripping vapor of stripping process

wbps: warm rich bypass

References

Abu-Zahra, M. R. M., Niederer, J. P. M., Feron, P. H. M., & Versteeg, G. F. (2007). CO2 capture from power plants. Part II. A parametric study of the economical performance based on mono-ethanolamine. *International Journal of Greenhouse Gas Control*, *1*(2), 135–142.

Ahn, H., Luberti, M., Liu, Z., & Brandani, S. (2013). Process configuration studies of the amine capture process for coal-fired power plants. *International Journal of Greenhouse Gas Control*, *16*, 29–40.

Amrollahi, Z., Ertesvåg, I. S., & Bolland, O. (2011). Thermodynamic analysis on post-combustion CO2 capture of natural-gas-fired power plant. *International Journal of Greenhouse Gas Control*, *5*(3), 422–426.

Amundsen, T. G., Øi, L. E., & Eimer, D. A. (2009). Density and viscosity of monoethanolamine + water + carbon dioxide from (25 to 80) °C. *Journal of Chemical and Engineering Data*, *54*(11), 3096–3100.

Aroonwilas, A., & Veawab, A. (2007). Integration of CO2 capture unit using single- and blended-amines into supercritical coal-fired power plants: Implications for emission and energy management. *International Journal of Greenhouse Gas Control*, *1*(2), 143–150.

Ayub, Z. H. (2003). Plate Heat Exchanger Literature Survey and New Heat Transfer and Pressure Drop Correlations for Refrigerant Evaporators. *Heat Transfer Engineering*, *24*(5), 3–16.

Benson, H., & Mccrea, D. (1979). Removal of acid gases from hot gas mixtures.

Bergamini, L., Vescovo, C., & Milone, F. (2011). Centrifugal pumps for CO2 applications. In *Proceedings of the Twenty-Seventh International Pump User Symposium* (pp. 45–49). Houston, TX, USA.

Bhatt, M. S. (2011). Enhancement of energy efficiency and loading of steam turbines through retrofitting 2-d designs with 3-d designs. *Journal of Scientific and Industrial Research*, *70*, 64–70.

Bhatt, M. S., & Rajkumar, N. (1999). Performance enhancement in coal fired thermal Power plants. Part II: steam turbines. *International Journal of Energy Research*, *23*, 489–515.

Bravo, J. L., Rocha, J. A., & Fair, J. R. (1985). Mass transfer in gauze packings. *Hydrocarbon Processing*, *64*(1), 91–95.

Bumb, P., Kumar, R., Khakharia, P., & Goetheer, E. (2014). Demonstration of Advanced APBS Solvent at TNO's CO2 Capture Pilot Plant. *Energy Procedia*, *63*, 1657–1666.

Chang, H., & Shih, C. M. (2005). Simulation and optimization for power plant flue gas CO2 absorption-stripping systems. *Separation Science and Technology*, *40*(4), 877–909.

Chen, C. C., Britt, H., Boston, J., & Evans, L. (1982). Local composition model for excess Gibbs energy of electrolyte systems. Part I: Single solvent, single completely dissociated electrolyte systems. *AIChE Journal*, *28*(4), 588–596.

Chen, C. C., & Song, Y. (2004). Generalized electrolyte-NRTL model for mixed-solvent electrolyte systems. *AIChE Journal*, *50*(8), 1928–1941.

Chen, E., Fulk, S. M., Sachde, D., Lin, Y. J., & Rochelle, G. T. (2014). Pilot Plant Activities with Concentrated Piperazine. *Energy Procedia*, *63*, 1376–1391.

Chen, E., Madan, T., Sachde, D., Walters, M. S., Nielsen, P. T., & Rochelle, G. T. (2013). Pilot Plant Results with Piperazine. *Energy Procedia*, *37*, 1572–1583.

Chowdhury, F. A., Yamada, H., Higashii, T., Goto, K., & Onoda, M. (2013). CO2 capture by tertiary amine absorbents: A performance comparison study. *Industrial & Engineering Chemistry Research*, *52*(24), 8323–8331.

Cousins, A., Huang, S., Cottrell, A., Feron, P. H. M., Chen, E., & Rochelle, G. T. (2015). Pilot-scale parametric evaluation of concentrated piperazine for CO2 caputre at an australian coal-fired power station. *Greenhouse Gases: Science and Technology*, *2*(6), 408–418.

Cousins, A., Wardhaugh, L. T., & Feron, P. H. M. (2011). Preliminary analysis of process flow sheet modifications for energy efficient CO2 capture from flue gases using chemical absorption. *Chemical Engineering Research and Design*, *89*(8), 1237–1251.

Davis, J. D. (2009). *Thermal Degradation of Aqueous Amines Used for Carbon Dioxide Capture. Ph.D. Dissertation*. The University of Texas at Austin.

Dittus, F., & Boelter, L. (1985). Heat transfer in automobile radiators of the tubular type. *International Communications in Heat and Mass …*, *12*, 3–22.

Dugas, R. E. (2009). *Carbon Dioxide Absorption, Desorption, and Diffusion in Aqueous Piperazine and Monoethanolamine. Ph.D. Dissertation*. The University of Texas at Austin.

Ebnson, H. E., & McCrea, D. H. (1979). Removal of acid gases from hot gas mixtures. US.

EIA. (2015). *Annual Energy Outlook 2015*.

Eisenberg, B., & Johnson, R. R. (1979). Amine regeneration process. US.

EPA. (2015a). *Clean Power Plan proposal*.

EPA. (2015b). *Inventory of U.S. Greenhouse Gas Emissions and Sinks 1990-2013*. Washington, DC.

Fang, M., Xiang, Q., Wang, T., Moullec, Y. Le, Lu, J., Jiang, W., Zhou, X., Zhang, J., & Chen, G. (2014). Experimental Study on the Novel Direct Steam Stripping Process for Postcombustion CO 2 Capture.

Fernandez, E. S., Bergsma, E. J., de Miguel Mercader, F., Goetheer, E. L. V., & Vlugt, T. J. H. (2012). Optimisation of lean vapour compression (LVC) as an option for post-combustion CO2 capture: Net present value maximisation. *International Journal of Greenhouse Gas Control*, *11*, S114–S121.

Fisher, K. S. (2007). Advanced Amine Solvent Formulations and Process Integration for Near-Term CO2 Capture Success. Grant No: DE-FG02-06ER84625.

Fitzmorris, R. E., & Mah, R. S. H. (1980). Improving distillation column design using thermodynamic availability analysis. *AIChE Journal*, *26*(2), 265–273.

Frailie, P. T. (2014). *Modeling of Carbon Dioxide Absorption/Stripping by Aqueous Methyldiethanolamine/Piperazine. Ph.D. Dissertation*. The University of Texas at Austin.

Freeman, S. A. (2011). *Thermal Degradation and Oxidation of Aqueous Piperazine for Carbon Dioxide Capture. Ph.D. Dissertation*. The University of Texas at Austin.

Freeman, S. A., & Rochelle, G. T. (2011). Density and viscosity of aqueous (piperazine + carbon dioxide) solutions. *Journal of Chemical and Engineering Data*, *56*, 574–581.

Geuzebroek, F. H., Schneiders, L. H. J. M., Kraaijveld, G. J. C., & Feron, P. H. M. (2004). Exergy analysis of alkanolamine-based CO2 removal unit with AspenPlus. *Energy*, *29*(9-10), 1241–1248.

Goto, K., Okabe, H., Shimizu, S., Onoda, M., & Fujioka, Y. (2009). Evaluation method of novel absorbents for CO2 capture. *Energy Procedia*, *1*(1), 1083–1089.

Hammond, G. P., Akwe, O., & Williams, S. (2011). Techno-economic appraisal of fossil-fuelled power generation systems with carbon dioxide capture and storage. *Energy*, *36*(2), 975–984.

Hanak, D. P., Biliyok, C., Yeung, H., & Białecki, R. (2014). Heat integration and exergy analysis for a supercritical high-ash coal-fired power plant integrated with a post-combustion carbon capture process. *Fuel*, *134*, 126–139.

Hasan, M., & Baliban, R. (2012). Modeling, simulation, and optimization of postcombustion CO2 capture for variable feed concentration and flow rate. 1. Chemical absorption and membrane processes. *Industrial & Engineering Chemistry Research*, *51*, 15642−15664.

Heavner, R. L., Kumar, H., & Wanniarachchi, A. S. (1993). Performance of an Industrial Heat Exchanger: Effect of Chevron Angle. *AIChE Symposium Series*, *89*, 262–267.

Heberlea, J. R., & Bhown, A. (2014). Absorption system modeling to identify desirable solvent properties. *Energy Procedia*, *63*, 1135–1143.

Herrin, J. P. (1989). Process sequencing for amine regeneration. United States.

Higgins, S. J., & Liu, Y. A. (2015). CO2 Capture Modeling, Energy Savings, and Heat Pump Integration. *Industrial & Engineering Chemistry Research*, *54*(9), 2526–2553.

Hilliard, M. D. (2008). *A Predictive Thermodynamic Model for an Aqueous Blend of Potassium Carbonate, Piperazine, and Monoethanolamine for Carbon Dioxide Capture from Flue Gas. Ph.D. Dissertation*. The University of Texas Austin.

Hirata, T., Nagayasu, H., Yonekawa, T., Inui, M., Kamijo, T., Kubota, Y., Tsujiuchi, T., Shimada, D., Wall, T., & Thomas, J. (2014). Current status of MHI CO2 capture plant technology, 500 TPD CCS demonstration of test results and reliable technologies applied to coal-fired flue gas. *Energy Procedia*, *63*, 6120–6128.

Huang, B., Xu, S., Gao, S., Liu, L., Tao, J., Niu, H., Cai, M., & Cheng, J. (2010). Industrial test and techno-economic analysis of CO2 capture in Huaneng Beijing coal-fired power station. *Applied Energy*, *87*(11), 3347–3354.

IEA. (2013). *Technology Roadmap- Carbon Capture and Storage*. France.

Iwakabe, K., Nakaiwa, M., Huang, K., Nakanishi, T., Røsjorde, A., Ohmori, T., Endo, A., & Yamamoto, T. (2006). Energy saving in multicomponent separation using an internally heat-integrated distillation column (HIDiC). *Applied Thermal Engineering*, *26*, 1362–1368.

Jassim, M., & Rochelle, G. T. (2006). Innovative absorber/stripper configurations for CO2 capture by aqueous monoethanolamine. *Industrial & Engineering Chemistry Research*, *45*(8), 2465–2472.

Jung, J., Jeong, Y. S., Lee, U., Lim, Y., & Han, C. (2015). New Configuration of the CO 2 Capture Process Using Aqueous Monoethanolamine for Coal-Fired Power Plants. *Industrial & Engineering Chemistry Research*, *54*(15), 3865–3878.

Karimi, M., Hillestad, M., & Svendsen, H. F. (2011). Capital costs and energy considerations of different alternative stripper configurations for post combustion CO2 capture. *Chemical Engineering Research and Design*, *89*(8), 1229–1236.

Khan, T. S., Khan, M. S., Chyu, M.-C., & Ayub, Z. H. (2010). Experimental investigation of single phase convective heat transfer coefficient in a corrugated plate heat exchanger for multiple plate configurations. *Applied Thermal Engineering*, *30*, 1058–1065.

Kim, H., Hwang, S. J., & Lee, K. S. (2015). Novel shortcut estimation method for regeneration energy of amine solvents in an absorption-based carbon capture process. *Environmental Science & Technology*, *49*(3), 1478–1485.

Kim, H., & Lee, K. S. (2016). Design guidance for an energy-thrift absorption process for carbon capture: Analysis of thermal energy consumption for a conventional process configuration. *International Journal of Greenhouse Gas Control*, *47*, 291–302.

Kim, I., & Svendsen, H. F. (2007). Heat of absorption of carbon dioxide (CO2) in monoethanolamine (MEA) and 2-(aminoethyl) ethanolamine (AEEA) solutions. *Industrial & Engineering Chemistry Research*, 5803–5809.

Kim, I., & Svendsen, H. F. (2011). Comparative study of the heats of absorption of post-combustion CO2 absorbents. *International Journal of Greenhouse Gas Control*, *5*(3), 390–395.

Kim, Y. H. (2012). Energy saving and thermodynamic efficiency of a double-effect distillation column using internal heat integration. *Korean Journal of Chemical Engineering*, *29*(12), 1680–1687.

Knudsen, J. N., Andersen, J., Jensen, J. N., & Biede, O. (2011). Evaluation of process upgrades and novel solvents for the post combustion CO2 capture process in pilot-scale. *Energy Procedia*, *4*, 1558–1565.

Knudsen, J. N., Jensen, J. N., Vilhelmsen, P. J., & Biede, O. (2009). Experience with CO2 capture from coal flue gas in pilot-scale: Testing of different amine solvents. *Energy Procedia*, *1*(1), 783–790.

Kumar, H. (1984). The Plate Heat Exchanger: Construction and Design. In *Institute of Chemical Engineering Symposium Series* (pp. 1275–1288).

Lawlor, S., & Baldwin, P. (2005). Conceptual design of a supersonic CO2 compressor. In *Proceedings of ASME Turbo Expo: Power for Land, Sea and Air*.

Le Moullec, Y., & Kanniche, M. (2011). Screening of flowsheet modifications for an efficient monoethanolamine (MEA) based post-combustion CO2 capture. *International Journal of Greenhouse Gas Control*, *5*(4), 727–740.

Leites, I. L., & Berchenko, V. M. (1993). Application of the Second Law of Thermodynamics for Optimization of Absorption Processes to Decrease the Energy Consumption. In *Energy Systems and Ecology Conference 93*. Cracow, Poland.

Lewis, G. N., & Randall, M. (1923). *Thermodynamics and the Free Energy of Chemical Substances* (1st ed.). McGraw-Hill Book Company, Inc. New York and London.

Li, L. (2015). *Carbon Dioxide Solubility and Mass Transfer in Aqueous Amines for Carbon Capture. Ph.D. Dissertation*. The Univerisity of Texas at Austin.

Li, L., & Rochelle, G. T. (2013). Absorption rate and CO2 solubility in new PZ blends. *Energy Procedia*, *37*, 370–385.

Li, L., Voice, A. K., Li, H., Namjoshi, O., & Nguyen, T. (2013). Amine blends using concentrated piperazine, *00*, 1–17.

Liang, Z., Gao, H., Rongwong, W., & Na, Y. (2015). Comparative studies of stripper overhead vapor integration-based configurations for post-combustion CO2 capture. *International Journal of Greenhouse Gas Control*, *34*, 75–84.

Lin, Y. J., Madan, T., & Rochelle, G. T. (2014). Regeneration with rich bypass of aqueous piperazine and monoethanolamine for CO2 capture. *Industrial and Engineering Chemistry Research*, *53*(10), 4067–4074.

Lin, Y. J., & Rochelle, G. T. (2014). Optimization of Advanced Flash Stripper for CO2 Capture using Piperazine. *Energy Procedia*, *63*, 1504–1513.

Lin, Y. J., & Rochelle, G. T. (2016). Approaching a reversible stripping process for CO2 capture. *Chemical Engineering Journal*, *283*, 1033–1043.

Lupkes, K. (2012). Ramgen Supersonic Shock Wave Compression and Engine Technology. Grant no: FE0000493.

Luyben, W. L. (1983). Comparison of Energy Consumption in Five Heat-Integrated Distillation Configurations. *Ind. Eng. Chem. Process Des. Dev.*, *22*, 175–179.

Madan, T. (2013). *Modeling of Stripper Configurations for CO2 Capture using Aqueous Piperazine. M.S. Thesis*. The University of Texas at Austin.

Madan, T., Van Wagener, D. H., Chen, E., & Rochelle, G. T. (2013). Modeling pilot plant results for CO2 stripping using piperazine in two stage flash. *Energy Procedia*, *37*, 386–399.

Mangalapally, H. P., Notz, R., Asprion, N., Sieder, G., Garcia, H., & Hasse, H. (2012). Pilot plant study of two new solvents for post combustion carbon dioxide capture by reactive absorption and comparison to MEA. *Chemical Engineering Science*, *8*(22), 205–216.

Manglik, R. M., & Muley, A. (1995). Thermal–hydraulic behavior of a mixed chevron single-pass plate-and-frame heat exchanger. In *Proceedings of the 30th National Heat Transfer Conference, ASME-Heat Transfer Division* (Vol. 314, pp. 89–96).

Martin, H. (1999). Economic optimization of compact exchangers. *EF-Conference on Compact Heat Exchangers and Enhancement Technology for the Process Industries*, *0*(1), 1–6.

Mathias, P. M., & O'Connell, J. P. (2012). The gibbs-helmholtz equation and the thermodynamic consistency of chemical absorption data. *Industrial and Engineering Chemistry Research*, *51*(13), 5090–5097.

McGlashan, N. R., & Marquis, A. J. (2007). Availability analysis of post-combustion carbon capture systems: Minimum work input. *Proceedings of the Institution of Mechanical Engineers, Part C: Journal of Mechanical Engineering Science*, *221*(9), 1057–1065.

Moore, J., & Nored, M. (2008). Novel concepts for the compression of large volumes of Carbon Dioxide. In *Proceedings of ASME Turbo Expo: Power for Land, Sea and Air*. Berlin,Germany.

Muley, A., & Manglik, R. (1999). Experimental study of turbulent flow heat transfer and pressure drop in plate heat exchanger with chevron plates. *Journal of Heat Transfer*, *121*, 110–117.

Nakaiwa, M., Huang, K., Endo, a., Ohmori, T., Akiya, T., & Takamatsu, T. (2003). Internally Heat-Integrated Distillation Columns: A Review. *Chemical Engineering Research and Design*, *81*, 162–177.

Nakamura, S., Yamanaka, Y., Matsuyama, T., Okuno, S., Sato, H., Iso, Y., & Huang, J. (2014). Effect of Combinations of Novel Amine Solvents, Processes and Packing at IHI's Aioi Pilot Plant. *Energy Procedia*, *63*, 687–692.

NETL. (2010). *Cost and Performance Baseline for Fossil Energy Plants Volume 1: Bituminous Coal and Natural Gas to Electricity*.

Nguyen, B.-T. N. (2013). *Amine Volatility in CO2 Capture. Ph.D Dissertation*. The Univerisity of Texas at Austin.

Notz, R., Tönnies, I., Mangalapally, H. P., Hoch, S., & Hasse, H. (2011). A short-cut method for assessing absorbents for post-combustion carbon dioxide capture. *International Journal of Greenhouse Gas Control*, *5*(3), 413–421.

Oexmann, J. (2011). *Post-Combustion CO2 Capture: Energetic Evaluation of Chemical Absorption Processes in Coal-Fired Steam Power Plants. Ph.D. Dissertation*. Technischen Universität Hamburg-Harburg.

Oexmann, J., & Kather, A. (2010). Minimising the regeneration heat duty of post-combustion CO2 capture by wet chemical absorption: The misguided focus on low heat of absorption solvents. *International Journal of Greenhouse Gas Control*, *4*(1), 36–43.

Ohashi, Y., Ogawa, T., & Egami, N. (2011). Development of carbon dioxide removal system from the flue gas of coal fired power plant. *Energy Procedia*, *4*, 29–34.

Okada, K., Ono, M., Tomimura, T., Okuma, T., Konno, H., & Ohtani, S. (1972). Design and Heat Transfer Characteristics of a New Plate Heat Exchanger. *Heat Transfer Japanese Research*, *1*, 90–95.

Oyenekan, B. A., & Rochelle, G. T. (2006). Energy performance of stripper configurations for CO2 capture by aqueous amines. *Industrial & Engineering Chemistry Research*, 2457–2464.

Oyenekan, B. A., & Rochelle, G. T. (2007). Alternative stripper configurations for CO2 capture by aqueous amines. *AIChE Journal*, *53*(12), 3144–3154.

Plaza, J. M. (2011). *Modeling of Carbon Dioxide Absorption using Aqueous Monoethanolamine, Piperazine and Promoted Potassium Carbonate. Ph.D. Dissertation*. The University of Texas at Austin.

Plaza, J. M., & Rochelle, G. T. (2013). Modeling of pilot plant results for CO2 capture by aqueous piperazine. *Energy Procedia*, *4*, 1593–1600.

Rabensteiner, M., Kinger, G., Koller, M., Gronald, G., & Hochenauer, C. (2015). Investigation of carbon dioxide capture with aqueous piperazine on a post combustion pilot plant–Part I: Energetic review of the process. *International Journal of Greenhouse Gas Control*, *39*, 79–90.

Rayer, A. V., Henni, A., & Tontiwachwuthikul, P. (2012). Molar heat capacities of solvents used in CO2 capture: A group additivity and molecular connectivity analysis. *The Canadian Journal of Chemical Engineering*, *90*(2), 367–376.

Reddy, S., Gillmartin, J., & Francuz, V. (2009). Integrated Compressor/Stripper Configurations and Methods. US.

Rochedo, P. R. R., & Szklo, A. (2013). Designing learning curves for carbon capture based on chemical absorption according to the minimum work of separation. *Applied Energy*, *108*, 383–391.

Rochelle, G. T. (2009). Amine scrubbing for CO2 capture. *Science (New York, N.Y.)*, *325*(5948), 1652–1654.

Rochelle, G. T., Chen, E., Freeman, S. A., Van Wagener, D. H., Xu, Q., & Voice, A. K. (2011). Aqueous piperazine as the new standard for CO2 capture technology. *Chemical Engineering Journal*, *171*(3), 725–733.

Roetzel, W., Das, S., & Luo, X. (1994). Measurement of the heat transfer coefficient in plate heat exchangers using a temperature oscillation technique. *International Journal of Heat and Mass Transfer*, *37*, 325–331.

Romeo, L. M., Espatolero, S., & Bolea, I. (2008). Designing a supercritical steam cycle to integrate the energy requirements of CO2 amine scrubbing. *International Journal of Greenhouse Gas Control*, *2*(4), 563–570.

Rosenblad, G., & Kullendorff, A. (1975). Estimating heat transfer rates from mass transfer studies on plate heat exchanger surfaces. *Wärme-Und Stoffübertragung*, *8*, 187–191.

Schach, M. O., Schneider, R., Schramm, H., & Repke, J. U. (2010). Techno-economic analysis of postcombustion processes for the capture of carbon dioxide from power plant flue gas. *Industrial and Engineering Chemistry Research*, *49*(5), 2363–2370.

Seider, W. D., Seader, J. D., & Lewin, D. R. (2003). *Product and proces design principles* (2nd ed.). Wiley.

Shenvi, A. a., Herron, D. M., & Agrawal, R. (2011). Energy efficiency limitations of the conventional heat integrated distillation column (HIDiC) configuration for binary distillation. *Industrial and Engineering Chemistry Research*, *50*, 119–130.

Sherman, B. (2016). *Thermodynamic and Mass Transfer Modeling of Aqueous Hindered Amines for Carbon Dioxide Capture*. The Univerisity of Texas at Austin.

Singh, A., & Stéphenne, K. (2014). Shell Cansolv CO2 capture technology: Achievement from first commercial plant. In *Energy Procedia* (Vol. 63, pp. 1678–1685). Austin, TX, USA.

Snijder, E. D., te Riele, M. J. M., Versteeg, G. F., & van Swaaij, W. P. M. (1993). Diffusion coefficients of several aqueous alkanolamine solutions. *Journal of Chemical & Engineering Data*, *38*(3), 475–480.

Soave, G., & Feliu, J. a. (2002). Saving energy in distillation towers by feed splitting. *Applied Thermal Engineering*, *22*(8), 889–896.

Spycher, N. F., & Reed, M. H. (1988). Fugacity coefficients of H2, CO2, CH4, H2O and of H2O-CO2-CH4 mixtures: a virial equation treatment for moderate pressures and temperatures applicable to calculations of hydrothermal boiling. *Geochimica et Cosmochimica Acta*, *52*(3), 739–749.

Stec, M., Tatarczuk, A., Więcław-Solny, L., Krótki, A., Ściążko, M., & Tokarski, S. (2015). Pilot plant results for advanced CO2 capture process using amine scrubbing at the Jaworzno II Power Plant in Poland. *Fuel*, *151*, 50–56.

Stéphenne, K. (2014). Start-up of world's first commercial post-combustion coal fired ccs project: Contribution of shell cansolv to saskpower boundary dam iccs project. *Energy Procedia*, *63*, 6106–6110.

Suri, R. (2007). *CO2 Compression for Capture-Enabled Power Systems*. University of Waterloo.

Talik, A. C., Fletcher, L. S., Anand, N. K., & Swanson, L. W. (1995). Heat Transfer and Pressure Drop Characteristics of a Plate Heat Exchanger. *Proceedings of the ASME/JSME Thermal Engineering Conference*, *4*, 321–329.

Thimsen, D., Maxson, A., Smith, V., Cents, T., Falk-Pedersen, O., Gorset, O., & Hamborg, E. (2014). Results from MEA testing at the CO2 Technology Centre Mongstad. Part I: Post-Combustion CO2 capture testing methodology. *Energy Procedia*, *63*, 5938–5958.

Thonon, B., Vidil, R., & Marvillet, C. (1995). Recent research and developments in plate heat exchangers. *Journal of Enhanced Heat Transfer*, *2*, 149–155.

Tobiesen, F. A., & Svendsen, H. F. (2006). Study of a Modified Amine-Based Regeneration Unit. *Industrial & Engineering Chemistry Research*, *45*(8), 2489–2496.

Tsai, R. E. (2010). *Mass Transfer Area of Structured Packing*. The University of Texas at Austin.

Turton, R., Bailie, R. C., Whiting, W. B., Shaeiwitz, J. A., & Bhattacharyya, D. (2012). *Analysis, Synthesis, and Design of Chemical Processes* (4th ed.). Prentice Hall.

Vaie, C. (1975). *The Performance of Plate Heat Exchanger. Ph.D. Dissertation*. University of Bradford.

Van Wagener, D. H. (2011). *Stripper Modeling for CO2 Removal Using Monoethanolamine and Piperazine Solvents. Ph.D. Dissertation*. The University of Texas at Austin.

Van Wagener, D. H., & Rochelle, G. T. (2011). Stripper configurations for CO2 capture by aqueous monoethanolamine. *Chemical Engineering Research and Design*, *89*(9), 1639–1646.

Van Wagener, D. H., & Rochelle, G. T. (2014). Cold Rich Bypass to Strippers for CO2 Capture by Concentrated Piperazine. *Chemical Engineering & Technology*, *37*(1), 149–156.

Van Wagener, D. H., Rochelle, G. T., & Chen, E. (2013). Modeling of pilot stripper results for CO2 capture by aqueous piperazine. *International Journal of Greenhouse Gas Control*, *12*, 280–287.

Versteeg, G. F., & Van Swaaij, W. P. M. (1988). Solubility and diffusivity of acid gases (carbon dioxide, nitrous oxide) in aqueous alkanolamine solutions. *Journal of Chemical and Engineering Data*, *33*(1), 29–34.

Wang, C. (2015). *Mass Transfer Coefficients and Effective Area of Packing. Ph.D. Dissertation*. The University of Texas at Austin.

Warnakulasuriya, F. S. K., & Worek, W. M. (2008). Heat transfer and pressure drop properties of high viscous solutions in plate heat exchangers. *International Journal of Heat and Mass Transfer*, *51*, 52–67.

Xu, Q. (2011). *Thermodynamics of CO2 Loaded Aqueous Amines. Ph.D Dissertation*. The Univerisity of Texas at Austin.

Yoo, K. P., Lee, K. S., Lee, W. H., & Park, H. S. (1988). Diagnosis of thermodynamic efficiency in heat integrated distillation. *Korean Journal of Chemical Engineering*, *5*(2), 123–130.

Zhang, Y., Chen, H., & Chen, C. (2009). Rate-based process modeling study of CO2 capture with aqueous monoethanolamine solution. *Industrial & Engineering Chemistry Research*, *48*, 9233–9246.

Vita

Yu-Jeng Lin was born in Taipei, Taiwan in 1987. After receiving a B.S in Chemical Engineering from National Taiwan University in May 2009, he entered National Tsing Hua University for graduate school. In May 2011, he received a M.S. in Chemical Engineering. After serving one year in Taiwan Army, he began his graduate studies in Chemical Engineering at the University of Texas at Austin in the fall of 2012. He has accepted a full-time position at Mitsubishi Heavy Industries in Yokohama, Japan upon graduation with his Ph.D. degree.

Permanent email: yjlin76@gmail.com

This dissertation was typed by Yu-Jeng Lin.